Neuronal Networks with Nonlinear Couplings

— Computing with Synchrony —

Dissertation

(Cumulative Thesis)

for the award of the degree
"Doctor rerum naturalium"
of the Georg-August-Universität Göttingen

submitted by

Sven Jahnke

from Pasewalk

Göttingen, 2014

Thesis committee

Prof. Dr. Marc Timme,
Network Dynamics, Max Planck Institut für Dynamik & Selbstorganisation, Göttingen, Germany

Prof. Dr. Ulrich Parlitz,
Complex Dynamical Systems, Max Planck Institut für Dynamik & Selbstorganisation, Göttingen, Germany

Dr. Oskar Hallatschek,
Evolutionary Dynamics, Max Planck Institut für Dynamik & Selbstorganisation, Göttingen, Germany
Department of Physics, University of California, Berkeley, USA

Members of the examination board

First Reviewer: **Prof. Dr. Marc Timme**,
Network Dynamics, Max Planck Institut für Dynamik und Selbstorganisation, Göttingen, Germany

Second Reviewer: **Prof. Dr. Florentin Wörgötter**,
Biophysics - III. Physikalisches Institut, Georg-August-Universität Göttingen, Germany

Third Reviewer: **Prof. Dr. Markus Diesmann**,
Institute of Neuroscience and Medicine (INM-6), Research Center Jülich, Germany
Institute for Advanced Simulation (IAS-6), Research Center Jülich, Germany

Further members of the examination board

Prof. Dr. Ulrich Parlitz,
Complex Dynamical Systems, Max Planck Institut für Dynamik & Selbstorganisation, Göttingen, Germany

Dr. Oskar Hallatschek,
Evolutionary Dynamics, Max Planck Institut für Dynamik & Selbstorganisation, Göttingen, Germany
Department of Physics, University of California, Berkeley, USA

Prof. Dr. Theo Geisel,
Department of Nonlinear Dynamics, Max Planck Institut für Dynamik und Selbstorganisation, Göttingen, Germany
Department of Theoretical Physics, Georg-August-Universität Göttingen, Germany

Prof. Dr. Jörg Enderlein,
Biophysics/Complex Systems - III. Physikalisches Institut, Georg-August-Universität Göttingen, Germany

Date of the oral examination: 22th of May, 2014

Affidavit

I comfirm that I have written this thesis independently and with no other sources and aids than quoted.

Göttingen, 31.03.2014
Place, Date

Sven Jahnke

Judith, Joanne
Eileen & Michelle,
I love you to pieces.

To you I dedicate
this thesis ...

List of Publications

[1] **Jahnke, S.**, Memmesheimer, R.-M. and Timme, M. (2008). Stable irregular dynamics in complex neural networks, *Phys. Rev. Lett.*, **100**, 048102.

[2]† **Jahnke, S.**, Memmesheimer, R.-M. and Timme, M. (2009). How chaotic is the balanced state?, *Front. Comp. Neurosci.*, **3**, 13.

[3]†* **Jahnke, S.**, Timme, M. and Memmesheimer, R.-M. (2012). Guiding synchrony through random networks, *Phys. Rev. X*, **2**, 041016.
(for reprint see Chapter 4)

[4]†* **Jahnke, S.**, Memmesheimer, R.-M. and Timme, M. (2013). Propagating synchrony in feed-forward networks, *Front. Comp. Neurosc.*, **7**, 153.
(for reprint see Chapter 3)

[5]†* **Jahnke, S.**, Memmesheimer, R.-M. and Timme, M. (2014). Hub-activated signal transmission in complex networks, *Phys. Rev. E (Rapid)*, **89**, 030701.
(for reprint see Chapter 5)

[6]†* **Jahnke, S.**, Memmesheimer, R.-M. and Timme, M. (2014). Oscillation-induced signal transmission and gating in neural circuits, *PLoS Comp. Biol.*, **10**, e1003940.
(for preprint see Chapter 6)

[7]†* **Jahnke, S.**, Timme, M. and Memmesheimer, R.-M. (2015). Towards a unified model for Sharp-Wave-Ripples and replay, *J. Neurosci.*, submitted.
(for preprint see Chapter 7)

[8]† Arnoldt, H., Chang, S., **Jahnke, S.**, Urmersbach, B., Taschenberger, H. and Timme, M. (2015). When less is more: Non-monotonic spike sequence processing in neurons, *PLoS Comp. Biol.*, **11**, e10004002.

† manuscripts finished within Ph.D. time-period

* manuscripts included in the main part of this thesis; a signed statement of own contribution is given in the beginning of the corresponding Chapters 3 - 7

Contents

Chapter 1

Introduction

The brain is the most flexible information processing and controlling device we know. It receives inputs from a broad range of sensors, including detectors for electro-magnetic radiation, pressure, temperature, and is equipped with acoustic and even chemical sensors. By processing the inputs from these different sources, it constructs an internal representation of the real world, stores information about the past, processes data about the present, interpolates into the future, enables us to interact with our environment, and — even more astonishing — is the source of something we call "consciousness".

The human brain itself is an assembly of more than 85 billion single information processing units (Azevedo et al., 2009; Herculano-Houzel, 2009), called neurons — cells that are highly specialized for generating electrical signals to communicate with. These neurons are accompanied by about the same number of non-neuronal glia cells (Azevedo et al., 2009) which are thought to not directly be involved in information processing, but fulfill a variety of supporting functions. It is a crucial, established assumption that the source of the complex dynamics of the brain arises from the high number of neurons and the complex interconnection scheme among them — the neural network (Kandel et al., 2000; Purves et al., 2008). This assumption suggests that it is possible to reveal basic properties and functions of cortical networks by studying (comparatively) simple neuron models and considering their interactions in large networks. Such studies may reveal general mechanisms underlying (neuronal) information processing which might be obscured by highly detailed description of single neurons otherwise.

Networked dynamical systems

Moreover, recognizing the brain as a network of interacting units opens the path to draw connections between different research areas, as the dynamics of a plethora of real world systems can be described as a networked dynamical system (Newman, 2010): Prominent examples include spreading of diseases (Hufnagel et al., 2004), rumor spreading in social networks (Moreno et al., 2004), chains of chemical reactions in biological cells (Johnson and Alberts, 2002), regulation

of gene activation and deactivation (Bornholdt, 2008), and energy transmission in power-grids (Rohden et al., 2012; Filatrella et al., 2008). Interestingly, sometimes not only the interaction topology but also the dynamics of single units are approximated by similar models for distinct systems. For instance, phase or pulse coupled oscillators have been successfully employed to describe dynamics of earthquakes (Herz and Hopfield, 1995), synchronization phenomena of flashing fireflies (Mirollo and Strogatz, 1990; Strogatz, 2003), neural network dynamics (Ernst et al., 1995; Timme, 2002; Jahnke et al., 2008) and properties of power grids (Filatrella et al., 2008; Rohden et al., 2012). Likewise, the underlying networks share features across different disciplines. For example, many real world networks have been shown to be small-world networks (i.e., networks are highly clustered, but the average distance between two nodes is small) and/or to contain a few number of highly connected nodes — called "Hubs" (Watts and Strogatz, 1998; Bornholdt and Ebel, 2001; Liljeros et al., 2001; Riley et al., 2003; Hagmann et al., 2008; Bonifazi et al., 2009; Newman, 2010; Varshney et al., 2011). Thus, studying neural network models — besides beeing helpful for understanding information processing in the brain itself — might yield some insights into general mechanisms of information processing, with potential applications to other research fields.

The neural code

How is information stored and represented in the brain? What are candidates for the neural code? Single neurons in the brain communicate with each other by exchanging electrical signals in the form of short, strong variations of their trans-membrane voltage — called action potentials or spikes. There is evidence that both the mean activity of neurons (or ensemble of neurons) averaged over longer time intervals (firing rate; rate-code) and the exact timing (or relative timing) of single spikes (temporal code) encode sensory information and represent memory.

In this thesis we concentrate on the latter, and investigate the emergence of precisely timed spike patterns in recurrent networks. Such patterns have been experimentally found in various neural systems: They indicate whisker position and movement in the rat (Panzeri et al., 2001; Jones et al., 2004), complex features of tactile stimuli (Johansson and Birznieks, 2004; Birznieks et al., 2010), and noise source position and auditory stimulus identity (Gutfreund et al., 2002; Schnupp et al., 2006; Engineer et al., 2008). Also in cortical regions where activity cannot be directly linked to external stimuli, precise spiking has been found: In songbirds, precise spike patterns are locked to the song generation process and are replayed during sleep (Yu and Margoliash, 1996; Dave and Margoliash, 2000; Leonardo and Fee, 2005). In the motor cortex of mammals, precisely synchronous spiking between neurons was found to be correlated with internal cognitive states and task performance (Riehle et al., 1997; Kilavik et al., 2009; Putrino et al., 2010). Despite the strong evidence that precise spike patterns are crucially involved in information processing, their dynamical origin, however, is not yet well understood.

Feed-forward networks

A possible explanation for the occurrence of such patterns is the existence of feed-forward structures, also known as "synfire chains" (Abeles, 1982, 1991). These are layered subnetworks (i.e., there are groups of neurons (layers) where each group has prominent excitatory connections to its subsequent group) embedded in a larger recurrent network. A synchronous signal (pulse-packet) may propagate from one layer to next by exciting a sufficiently large number of neurons to spike synchronously, and thereby generate the precise spike patterns observed in experiments. Moreover, this mechanism of propagating synchrony constitute a promising candidate to explain the transmission of information in cortical networks within or between brain regions (reviewed in Kumar et al., 2010).

Numerical and theoretical studies have shown that synfire chains indeed are capable of propagating synchronous signals, however, very prominent feed-forward anatomies have to be assumed: Either in the sense of dense (possibly all-to-all) coupling, or in form of very strong synaptic efficiencies (Diesmann et al., 1999; Gewaltig et al., 2001; Aviel et al., 2003; Mehring et al., 2003; Vogels and Abbott, 2005; Kumar et al., 2008a). Moreover, systematic computational studies have shown that the interaction between the embedded feed-forward structure and the embedding network might hinder meaningful signal propagation: On the one hand, synchronous signals tend to spread out over the whole network and cause pathological activity ("synfire-explosion" Aviel et al., 2003; Mehring et al., 2003). On the other hand, correlations in the spike times induced by the background activity might accumulate over the layers of the embedded feed-forward network and thus induce spontaneous propagation of synchronous signals (Litvak et al., 2003; Tetzlaff et al., 2002, 2003; Rosenbaum et al., 2010, 2011) which hinders a separation of the signal (induced propagating synchrony) and background activity.

Dendritic spikes

Neurons in cortical networks typically receive inputs from thousands of other neurons. The input sites of the neurons, often organized like a broad arborescent tree, are called dendrites. Traditionally, they are considered as a tree of passive cables that conduct the electrical signal from the contact sites with the presynaptic neurons (synapses) to the postsynaptic neurons' cell body — the soma (Bear et al., 2006). Here the signals are integrated over time, and the actual neuronal computation takes place. Yet, this view has changed over the last decades: It has been demonstrated that in addition to just conducting signals, dendrites can actively contribute to computational processes by generation of dendritic spikes (reviewed in, e.g., Häusser and Mel, 2003; London and Häusser, 2005; Spruston, 2008; Major et al., 2013): Some dendrites express a high density of voltage gated ion channels which can be activated by sufficiently strong and synchronous presynaptic inputs, and if so, cause a strong voltage transient — a regenerative, all-or-none event similar to somatic spikes. As a consequence the impact on the postsynaptic neuron (somatic depolarization) substantially exceed the responses expected from summation of single input responses. Thus dendritic spikes contribute a synchrony detection mechanism to the computing capabilities of single neurons (cf., e.g., Poirazi and Mel, 2001; Poirazi et al.,

2003b; Polsky et al., 2004; Rhodes, 2008). In particular, dendritic sodium spikes exhibit a remarkable sensitivity to input synchrony: Only inputs received within a time interval of less than a few milliseconds might elicit such dendritic spikes (Ariav et al., 2003; Gasparini et al., 2004; Gasparini and Magee, 2006).

Once generated a dendritic spike can trigger a somatic spike in the postsynaptic neuron, and if so, this output is can be highly precise with trial-to-trial jitter in the millisecond (or even sub-millisecond) range (Ariav et al., 2003; Losonczy et al., 2008; Müller et al., 2012; Makara and Magee, 2013). In particular, sodium spikes generated in the basal dendrite of hippocampal pyramidal neurons exhibit such a precise input-output relation.

Hippocampus

The hippocampus is one of the evolutionary oldest regions of the brain and crucially involved in episodic memory formation and consolidation (reviewed in, e.g., Girardeau and Zugaro, 2011). This involvement has been directly demonstrated experimentally (Girardeau et al., 2009; Ego-Stengel and Wilson, 2010): Selective suppression of short episodes of highly increased hippocampal activity (Sharp-Wave-Ripple complexes; SWR) during sleep, significantly reduces the day-by-day performances increase (learning) in solving spatial memory tasks (finding food rewards in a maze) in multi-day training episodes. This observation supports the "two-stage model" of memory (Marr, 1971; Buzsáki, 1989) which assumes that information is first preliminary stored (in the hippocampus) and later (e.g., during rest or sleep) recalled and consolidated (i.e., transferred to the neocortex for long-term memorization). The storage of spatial information is likely to be based on a temporal code: During SWRs previously experienced spatio-temporal spike patterns reflecting spatial properties of the environment (e.g., traversed paths in the maze) are replayed (Wilson and McNaughton, 1994; Nadasdy et al., 1999; Ji and Wilson, 2007). The replay is accompanied by a synchronous activation of $10-20\%$ of the hippocampal pyramidal neurons (Ylinen et al., 1995; Buzsáki and Silva, 2012). The occurrence of highly synchronous events (SWRs) in conjunction with precise spike patterns in a brain region where highly synchrony sensitive dendritic sodium spikes have been prominently found, might suggest that the observed activity patterns are based on exactly those spikes (cf., Memmesheimer, 2010).

Synopsis and structure of this thesis

In this thesis we study the impact of dendritic sodium spikes on the activity of recurrent (neural) networks. In particular, we investigate synchrony propagation in embedded feed-forward substructures. We study the signal transmission analytically, supported by numerical simulations and take the interactions between embedded structures and surrounding network into account. As a direct biological application, we demonstrate that hippocampal activity patterns may be generated by dendritic sodium spikes.

In Chapter 2 we provide information about the neurophysiological background as well as the computational and analytical tools used in this thesis. Moreover, this chapter serves as an extended introduction.

In Chapter 3 we consider synchrony propagation in *isolated* feed-forward networks, i.e., the embedding network is modeled by externally generated random input spike trains. We compare the propagation properties of networks with and without dendritic nonlinearities, derive an analytical description for the propagating (synchronous) pulse-packet, and identify linear and nonlinear propagation as qualitatively different phenomena.

In Chapter 4 we proceed by considering feed-forward networks which are natural part of a recurrent, sparsely connected, random network. We show that dendritic nonlinearities enable robust signal propagation in networks with biologically plausible topology, and synaptic efficiencies in the biologically observed range.

In Chapter 5 we consider the interaction between the embedding network and the embedded substructure in more detail. We show that for purely random networks, synchronous activity in the feed-forward subnetworks may either have only a small effect on the activity of the remaining network, or cause pathological activity by inducing global network synchrony. In contrast, in networks with long-tailed degree distribution (that contain some highly connected nodes — hubs), a propagating signal can induce moderate network oscillations (within the "hub-network") without causing pathological activity states, and these oscillations may in turn stabilize signal propagation. This phenomenon of hub-activated signal transmission further relaxes the requirement for a prominent feed-forward anatomy. The proposed function of hubs is fundamentally different to the function usually attributed to them: In our settings they do not spread the relevant signal, but act as an unspecific signal amplifier. We note that the underlying mechanism does not depend on single neuron properties, rather it is generic for networks of sharply nonlinear threshold units, and thus may be found in other networked dynamical systems as well.

In Chapter 6, motivated by the abundance of cortical oscillations observed in experiments, we study the interaction of (external) oscillations and signal propagation. In particular, we show the existence of resonances between oscillatory input and propagating synchronous signals. Such resonance are absent in linearly coupled networks. Thus the co-action of oscillations and dendritic nonlinearities, additionally to their support of signal transmission in general, can serve as mechanism to selectively activate different pathways in a recurrent network.

In Chapter 7 we develop a unified model for the storage and replay of spatial information in the hippocampus in conjunction with SWR-like spiking activity. We consider activity patterns observed during spatial exploration phases and show by simulations that they lead to a formation of a stripe-like feed-forward substructure. In a later resting phase, the imprinted information is recalled, i.e., previously learned spike patterns are replayed supported by dendritic spikes. We analyze the replay events and show that they resemble hippocampal activity observed during SWRs. We further discuss the plausibility of our model for SWR-generation and replay in the light of recent experiments.

In Chapter 8 we summarize and discuss the results achieved in this thesis.

Chapter 2

Fundamentals

The aim of the present chapter is to provide the basic concepts and methods used in the main part of this thesis. Although each chapter constitutes a self-contained publication and thus includes an introduction and model section, this presentation of fundamentals is meant to be more comprehensive than it is possible in a typical journal article due to length restrictions, and necessary due to the specialized readership. Besides explaining the fundamental concepts, we refer to further literature, in particular textbooks and review articles, which might serve as a starting point to gain a deeper understanding of the considered topics.

The main computing units of the brain are neurons which interact by sending and receiving electrical pulses. In Section 2.1, we briefly discuss the biological/chemical processes underlying signal generation and transmission in the brain and describe how neurons and their communication among each other can be modeled.Information processing in active dendrites (the input sites of neurons) is of particular interest for this thesis. In Section 2.2 we discuss different forms of active dendrites observed in neuroscientific experiments.

In Section 2.3 we consider the topology of cortical networks, and also discuss the highly irregular ground state dynamics of such networks. A central question in neuroscience (and this thesis) is the question of how information is represented and transmitted in the brain. In Section 2.4 we outline how signals might be encoded and transmitted in cortical networks in general, and by feed-forward sub-networks in particular.

The hippocampus is one of the evolutionary oldest brain regions which is crucially involved in, e.g., the formation of long-term memory. One of the main motivations of this thesis is to gain a deeper understanding of the activity patterns observed in the hippocampus and how information, in particular spatial information, is stored in that brain region. In Section 2.5 we briefly describe the anatomy and activity patterns of the hippocampus and refer to previous modeling studies.

Finally, in Section 2.6 we outline how the dynamics of neuronal networks can be numerically simulated, and comment on the techniques and algorithms employed in this thesis.

2.1. Neurons - Building blocks of the brain

Historical preface

Up to the end of the nineteenth century the brain and the spinal cord were believed to be a giant network of fusing elements (also known as "reticular theory", Gerlach, 1872; Glickstein, 2006). It was assumed that signals were carried from the skin to the brain and from the brain to the muscles by a hypothesized fluid (possibly "electrical fluid", Galvani and Aldini, 1792; Reeves and Taylor, 2004) which flows along hollow tubes (Van Leeuwenhoek, 1719; Glickstein, 2006, and Figure 2.1A). This (nowadays proved as wrong) belief was partly attributed to the fact that fresh brain tissue, as studied by early microscopists, is soft; clean cuts are difficult to make and the optical resolution was not sufficient to discriminate single cells in the cortex. Just subtle difference in the structure of different areas could be identified (Gennari, 1782; Vicq-d'Azur, 1786; Glickstein and Rizzolatti, 1984).

In the late 19^{th} century a paradigm change was facilitated by experimental techniques developed by Camillo Golgi. In 1873 he wrote in a letter to his friend Nicolo Manfredi:

> "I have found a new reaction to demonstrate, even to the blind, the structure of the interstitial stroma of the cerebral cortex. I let the silver nitrate react with pieces of brain hardened in potassium dichromate. I have obtained magnificent results and hope to do even better in the future." (reprinted in Mazarello, 1999).

This was the first record of the "black reaction" (nowadays known as Golgi staining), which allows to visualize single neurons (in fact a small set of randomly selected cells) and its attached dendritic trees and axons (cf. Figure 2.1B). Golgi himself, however, was still convinced to observe a giant communication network of fused axonal branches (he considered the dendrites just as a nutrition network, Golgi, 1873; Raviola and Mazzarello, 2011), and not single processing units.

It was Ramón y Cajal who used Golgis method to produce fascinating drawings of nerve cells (cf. Figure 2.1C) and came to the conclusion that the brain is made up of individual elements, which may touch each other but do not fuse (Ramón y Cajal, 1888a,b,c; Sotelo, 2003). Later, his ideas were put forward by – among others – H.W.G. Waldeyer-Hartz, who coined the term "neuron" for the single units of the brain (Waldeyer-Hartz, 1891; Glickstein, 2006).

The "neuron doctrine" is a fundament of modern neuroscience, however, it is worth mentioning, that in the end the idea of a fusing network – which was strongly promoted by Golgi – turned out to be partly true: While the most prevalent mechanism of communicating signals from one neuron to another is by chemical synapses, where the signals are transferred between two individual neurons by the usage of neurotransmitters (detailed description see below), it turned out that additionally, some neurons have the ability to communicate electrical signals (and even exchange cytoplasm, Payton et al., 1969; Dermietzel, 1998) directly via so called gap-junctions (see Connors and Long, 2004, for a recent review on this topic).

Recent studies suggest that gap-junctions and electrical coupling are much more ubiquitous than assumed in the last decades (Connors and Long, 2004, and references therein). However, we

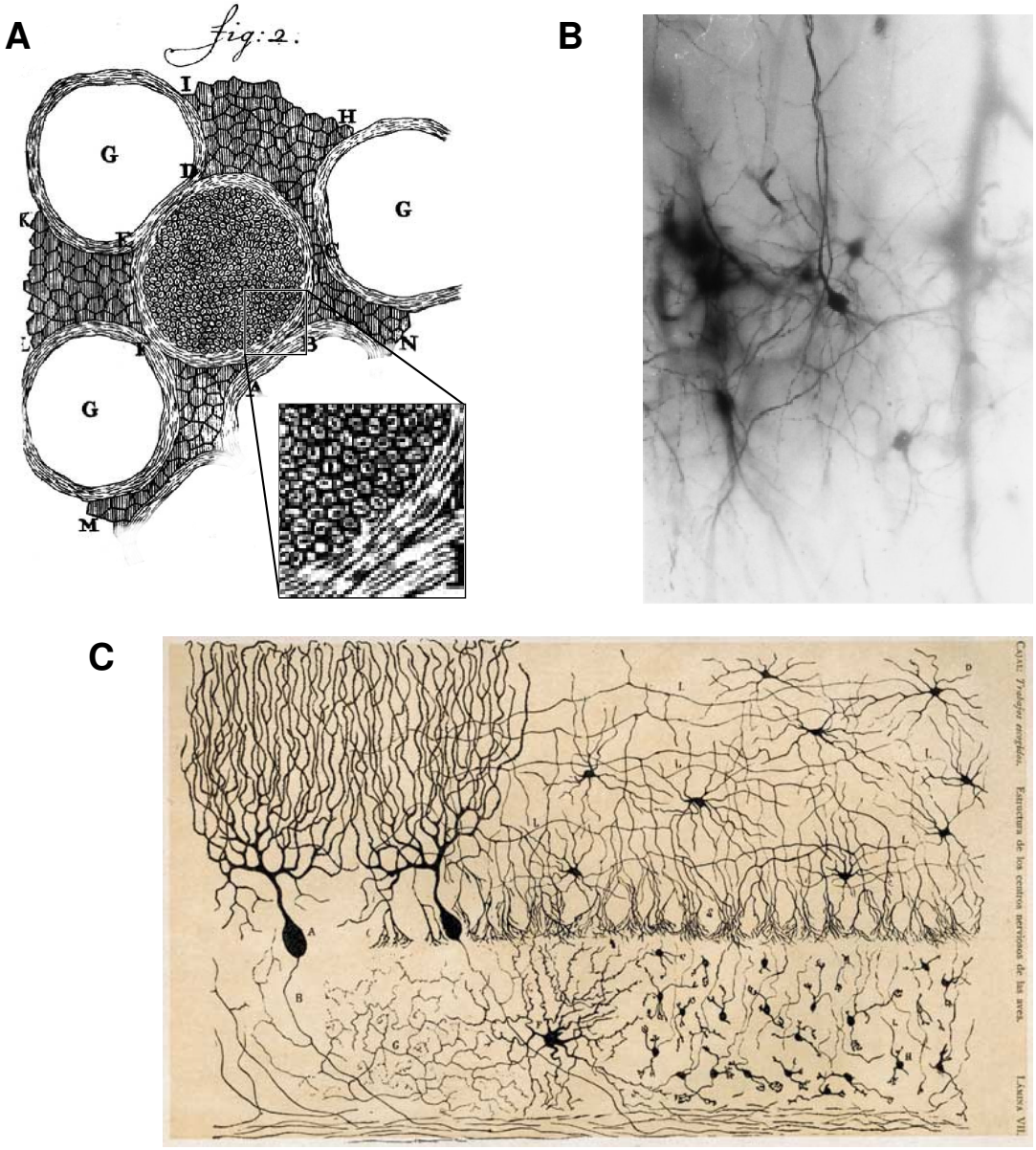

Figure 2.1: Historical pictures. (A) Drawing of a peripheral nerve by Leeuwenhoek (adapted from Van Leeuwenhoek, 1719, copyright expired) clearly showing single fibers containing (probably) myelinated axons. He depicted the axons in the centers of each fiber as small slits. He misinterpreted these as — due to the fast escape of a very liquid humour — collapsed tubes. This drawing is probably the first attempt to represent a cross section of a peripheral nerve in human history. (B) Cerebral cortex of the rabbit impregnated by the black reaction (Golgi staining). Photomicrograph of a preparation signed by C. Golgi, 1877 (reproduced with permission from Mazarello, 1999). (C) Illustration by Ramón y Cajal (Ramón y Cajal, 1888a) showing the five classes of neuron population that exist in the cerebellum (reproduced with permission from Sotelo, 2003).

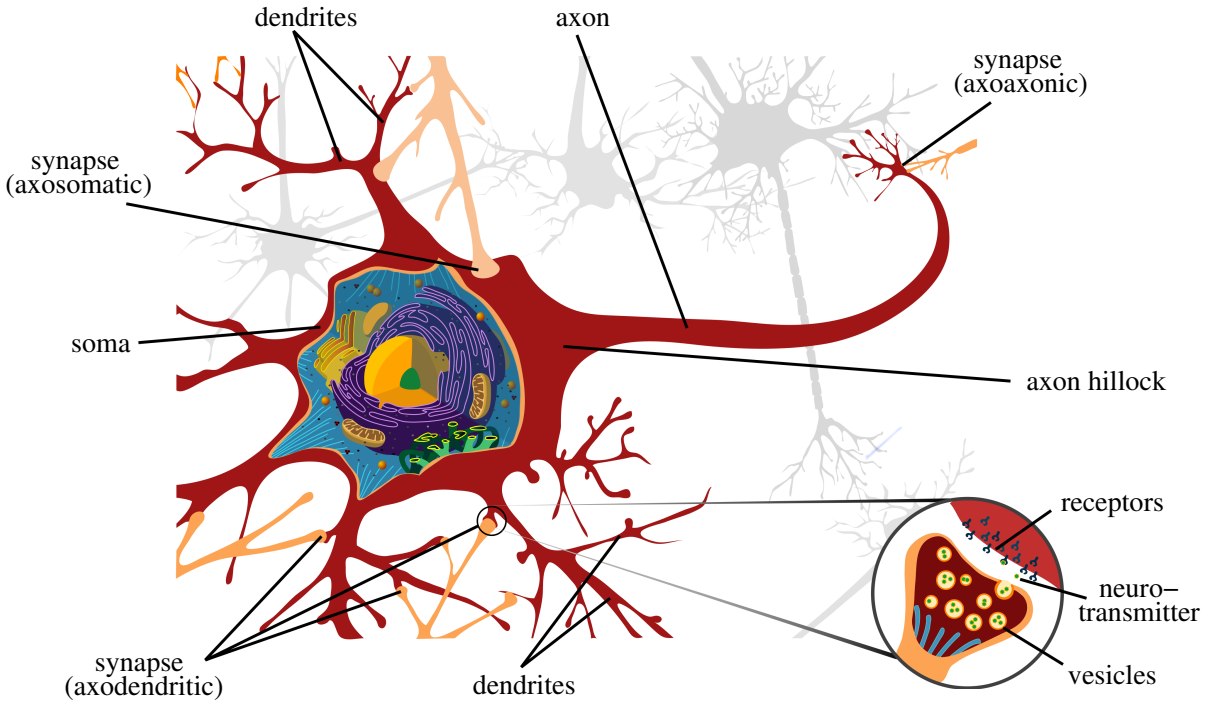

Figure 2.2: Anatomical overview of a neuron. The major morphological features of a typical neuron are the axon and the dendrites outgrowing from the soma. The axons form connections (synapses) to postsynaptic neurons and may target the soma, dendrites or even axons. Signals between two connected neurons are transmitted over the synaptic cleft (extracellular fluid) by releasing neurotransmitters (see zoomed view of a synapse in the lower right). For detailed explanation of signal transmission by chemical synapses see main text. Figure is modified from Wikimedia (2007) published under public domain.

will not go into details as this thesis (almost) exclusively deals with chemical synapses (but, cf. Section 2.5.3 and Chapter 7, where one of the models (Traub et al., 1999; Traub and Bibbig, 2000) proposed for the generation of Sharp-Wave-Ripple complexes crucially depends on axo-axonic gap-junctions).

2.1.1. Biological fundamentals

Signal generation

On a coarse scale, a typical neuron can be separated into cell body (soma), the axon which transfers signals to other neurons, and the dendrites which receive signals from other neurons (cf. Figure 2.2). The morphological features of a neuron, e.g., the number of dendritic and axonal branches or the length of these outgrowths varies strongly between different neuron types (cf. also Figure 2.1C). The axon of a neuron might form "connections" to other neurons (the contact points are called synapses) that allow the transfer of an electrical signal from one neuron to

another by the usage of chemical messengers (neurotransmitters). If two neurons are coupled, the cell receiving inputs is called postsynaptic to the sending neuron, and the sending neuron is termed presynaptic with respect to the neuron receiving signals.

Neurons are cells that are highly specialized to generate and transfer electrical signals. In particular, the membrane (separating the neuron from the extracellular fluid) contains a wide variety of ion-channels. These channels control the flow of ions, predominantly sodium (Na^+), potassium (K^+), calcium (Ca^{2+}) and chloride (Cl^-), between inside and outside the cell. The channels may open and close in response to voltage changes or due to other external or internal signals.

Under resting conditions, there is a difference in the electrical potential between the interior of a neuron and the extracellular medium of about -70mV (by convention the potential of the surrounding of the cell is defined as 0mV). This difference is termed membrane potential and is maintained by "ion pumps", integral membrane proteins, that actively transport charged particles over the membrane. For example, there is typically much more potassium (K^+) inside a cell than outside, and much more sodium (Na^+) outside the cell than inside. The electrical as well as concentration gradients cause a flow of charged particles, if the channels (which may be permeable for only a subset of ions) open. If the membrane potential inside the neuron is reduced in response to opening of some channels (e.g., by the outflux of positively charged ions or the influx of negatively charged ions), the neuron is said to be hyperpolarized. Likewise the increase of the membrane potential is called depolarization.

Communication between neurons is mainly mediated by the generation of action potential (also called "spikes", "nerve impulses" or "neuronal discharges"). This is a brief, but large depolarization of the membrane potential of roughly 100mV (cf. Figure 2.3). It is generated in the axon initial segment (adjacent to the axon hillock where the axon leaves the soma; cf. Figure 2.2), if the membrane potential becomes sufficiently strong depolarized (i.e., exceeding a "threshold potential"). Sub-threshold depolarization does not elicit an action potential and thus such (sub-threshold) fluctuations in the membrane potential are typically not transmitted to subsequent neurons.

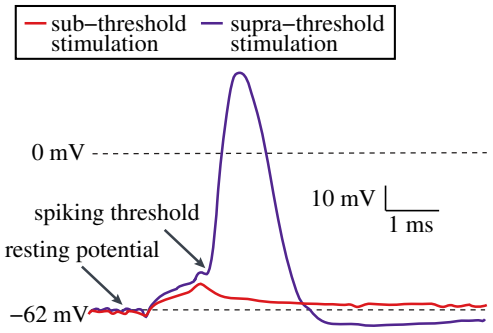

Figure 2.3: Anatomy of an action potential recorded from a pyramidal neuron in CA1 (modified with permission from Bean, 2007).

Action potentials result from a complex interplay of different voltage-gated ion channels (Bear et al., 2006; Bean, 2007; Dayan and Abbott, 2001): Neuronal discharges are initiated, if the membrane potential is sufficiently depolarized by, e.g., the influx of sodium ions in response to a presynaptic action potential. If the depolarization exceeds a threshold potential (typically ≈ -55mV), more and more voltage gated sodium channels open in a positive feed-back cascade (the opening of channels results in an influx of sodium ions that depolarizes the neuron even more

and thus opens more sodium channels, etc.). The opening (activation) of the channels is typically very fast (hundreds of microseconds) and thus cause a very rapid rise of the membrane potential up to a value close to the reversal potential of sodium ($E_{\mathrm{Na}} \approx 55\mathrm{mV}$). The sodium channels typically stay open for up to one millisecond and become impermeable to sodium afterwards. Simultaneously to the opening of sodium channels, other voltage-gated channels, in particular potassium channels, open. When the maximal permeability for sodium is achieved and the ion channels are closing, the dynamics of the flow of potassium ions start to govern the change of the membrane potential. The strong depolarization of the neuron cause a strong driving force on (positively charged) potassium ions to leave the neuron. The membrane potential decreases towards the reversal potential of potassium ($E_{\mathrm{K}} \approx -80\mathrm{mV}$) causing a hyperpolarization relative to the resting potential. Finally, also the voltage gated potassium channels close and the neuron reverses to the resting potential. After generation of an action potential, the ion channels are in an "inactivated" state that makes it impossible to elicit another action potential. The time period for which no further spikes can be generated or require a substantially larger depolarization to elicit a spike is called (absolute/relative) refractory period.

We note that the above description of action potential generation is very basic, e.g., we consider only two type of ion channels. Neurons in the brain might express a plethora of such channels, thus generating action potentials with widely varying amplitudes and timescales. However, the basic mechanism as outlined above still holds. More detailed descriptions of action potential generation can be found in recent textbooks or review articles (e.g., Bear et al., 2006; Bean, 2007; Dayan and Abbott, 2001).

Axonal transmission

Once an action potential is initiated, it is actively transmitted along the axonal tree. The depolarization caused by an action potential activates the voltage gated ion channels downstream the axon and thereby "refresh" the signal.

In vertebrates most axons are myelinated, which drastically increases the speed and decreases the energetic cost of signal transmission. Parts of the axon are sheath by myelin cells that isolate the axon from the surrounding intercellular plasma and therefore allow the direct electromagnetical transmission of an action potential (which would not be possible in uninsulated axons due to the leak over the membrane and the resulting strong attenuation). The myelin sheaths are interrupted by so called "nodes of Ranvier", where the membrane contains a large amount of voltage gated ion channels that refresh the action potential (see also description of generation of action potentials above).

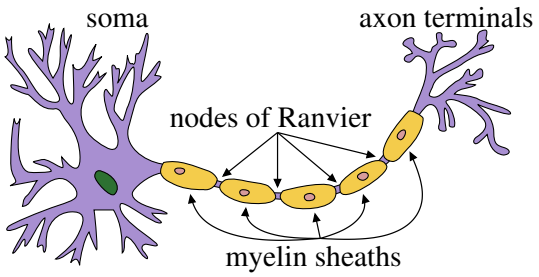

Figure 2.4: Sketch of a myelinated axon (modified from Wikimedia, 2009, published under CC-BY-SA-3.0).

Chemical transmission

At the axonal terminals (the synapses) the chemical signal transmission to other neurons takes place. These terminals contain synaptic vesicles filled with neurotransmitters (cf. Figure 2.2). The neurotransmitters are amino acids, amines or peptides which are synthesized in specialized fabrication units and/or by the support of enzymes in the soma or directly at the axonal terminal (see, e.g., Bear et al., 2006, for detailed description). An arriving action potential causes opening of voltage-gated calcium channels that are found within the membrane in the "active zones" of the axonic terminal. At resting conditions the concentration of calcium within the cell is very low such that an opening of the calcium channels causes an influx of calcium to the cell.

In a process termed exocytosis, the calcium influx triggers a fusion of the vesicles with the membrane and thus causes the release of the contained neurotransmitters. The exocytosis can happen remarkably rapid within tens of microseconds after the onset of the calcium influx (Sabatini and Regehr, 1996) allowing for a fast signal transmission. After the release of the neurotransmitters, the vesicle membrane is recovered in a process called endocytosis (Sudhof, 2004; Bear et al., 2006). The precise mechanism by which calcium stimulates exocytosis and the cellular mechanisms underlying endocytosis are not completely understood, but are currently under intensive investigation (see, e.g., Sudhof, 2004; Jahn and Fasshauer, 2012, for recent reviews).

After being released, the neurotransmitters diffuse across the synaptic cleft (separating the pre- and postsynaptic terminal) and bind to specific receptor proteins embedded in the postsynaptic membrane. The binding causes conformational changes in the receptor protein and induce a signal either by the opening of ion channels (cf. Figure 2.5) or by triggering the release of secondary messengers to the cytosol of the postsynaptic neuron (Bear et al., 2006). In the final step of synaptic transmission, the released neurotransmitters are removed from the synaptic cleft. This removal may happen by re-uptake through specialized proteins (neurotransmitter pumps) in the membrane of the presynaptic terminal (or other surrounding non-neural cells, called glia cells), simple diffusion away from the synapse or enzymatic destruction of the transmitter.

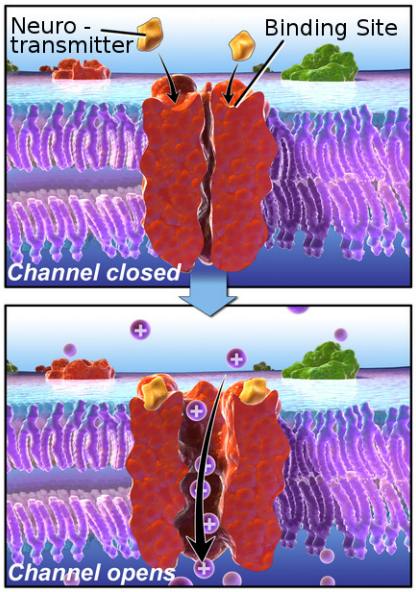

Figure 2.5: Chemically gated ion channel (modified from Wikimedia, 2013, published under CC-BY-3.0).

On the postsynaptic side the opening of channels cause an influx or efflux of ions. Depending whether the membrane potential is depolarized or hyperpolarised (postsynaptic potential), the effect of the synaptic transmission is called excitatory or inhibitory. There is a wide variety of neurotransmitters and -receptors present in

the nervous system. However, the most abundant receptors mediating (fast) excitatory signals in the mammalian brain are α-amino-3-hydroxy-5-methyl-4-isocazoleprpionic acid receptors (AMPA receptors) which open channels permeable to potassium and sodium. Inhibitory signals are mainly mediated by receptors responding to gamma-aminobutric acid (GABA receptors) that allow an influx of chloride to the cell. We note that depending on the concentration of the single ions within the cell and in the intercellular medium a synapse might act excitatory or inhibitory. For example it has been shown that the chloride level inside a cell decreases during development of the brain and thus GABA acts excitatory in the immature brain and inhibitory in later development stages (Ben-Ari et al., 1997).

Dendritic transmission and signal integration

The induced (excitatory or inhibitory) postsynaptic potential is transmitted from the synaptic terminal to the soma of the postsynaptic cell by the dendrites (cf. Figure 2.2). The dendritic tree gathers signals from thousands of presynaptic inputs and this bombardment causes fluctuations of the membrane potential of the postsynaptic cell, and if the cell is sufficiently depolarized an action potential might be elicited. The transfer of signals by the dendrites is typically passive, i.e., the electrical signal is conducted like in a (dendritic) cable. The amplitude decays over distance and the contribution of a single presynaptic input to the total depolarization/hyperpolarization at the soma is comparably weak. In this thesis, we refer to this type of dendritic signal transmission and integration as "linear", appreciating the fact that multiple presynaptic inputs are summed approximately linearly. This, however, does not mean that all postsynaptic quantities are just a linear summation of single responses: For example, a second identical presynaptic input might double the (total) amount of presynaptic transmitter release and thus double the number of open ion channels (i.e., the total conductance change is a linear superposition of single responses). Yet, the depolarization at the soma is not the arithmetic sum of the single responses as it also depends on the reversal potential of involved ion channels (cf. also Section 2.1.2 below), and thus single postsynaptic potentials are typically summed sublinearly.

However, recent neurophysiological experiments have shown that neuronal dendrites are capable of actively integrating synchronous presynaptic inputs (e.g., Ariav et al., 2003; Gasparini et al., 2004; Gasparini and Magee, 2006; Nevian et al., 2007; Losonczy et al., 2008; Remy et al., 2009; Branco et al., 2010; Müller et al., 2012; Makara and Magee, 2013). Temporally and spatially simultaneous presynaptic stimulation might elicit dendritic spikes (similiar to somatic spikes described above), that are actively (by voltage gated channels along the dendrite) or passively transmitted to the soma, and cause somatic depolarizations of the postsynaptic neuron much stronger than expected from linear transmission of signals. In this thesis, we study the impact of such nonlinear amplification on the dynamics of neuronal networks. Appreciating the great importance of active dendrites to this thesis, we discuss them separately in Section 2.2.

Synaptic plasticity

The connections between neurons, i.e., the underlying network that gives birth to the fascinating computing capabilities of our brain, are far from being static. Our brain restructures permanently by creating new neurons (which was recently shown to happen even in adult mammals, cf. Kempermann et al., 2004; Lledo et al., 2006, for reviews), building new connections between them or abolishing existing ones (Bear et al., 2006). Additionally, also existing synapses undergo changes of their efficiencies in an activity dependent manner on different timescales (Tetzlaff et al., 2012).

On a short time scale (up to some minutes) the repetitive activation of a synapse, might lead to a facilitation or depression of consecutive postsynaptic responses (see, e.g., Zucker and Regehr, 2002, for a comprehensive review on underlying biochemical mechanisms): Facilitation is mostly attributed to enhanced calcium influx or an increased residual level of calcium concentration inside the presynaptic terminal after multiple stimulation. Depression might arise from depletion of release-ready pool of vesicles, release of modulatory messengers from presynaptic, postsynaptic or glia cells, and/or a desensitization of postsynaptic receptors. However, after short recovery periods postsynaptic responses return to the initial amplitude.

In contrast, a coordinated pre- and postsynaptic activity might induce changes that are "permanent", i.e., lasting for days, weeks or even months (Sjöström et al., 2008, and references therein). Synaptic efficiencies might be enhanced ("long term potentiation"; LTP) or decreased ("long term depression"; LTD) and this adaptation is assumed to be controlled by calcium influx to the postsynaptic terminal (Bear et al., 2006): A high calcium concentration may activate different protein kinases which then enhance the efficiency of AMPA receptors by phosphorylation or — on a longer time scale — trigger the insertion of entirely new AMPA receptors in the postsynaptic membrane. In contrast, modest and prolonged elevations in calcium concentration activate protein phosphatases, which by dephosphorylasation weaken the efficiency of AMPA receptors.

The level of calcium influx itself is dominantly controlled by N-methyl-D-aspartate (NMDA) receptors (cf. Figure 2.6) which are integrated in the postsynaptic membrane. These work as coincidence detectors between pre- and postsynaptic stimulation (see also Section 2.2): The channel opens by binding of presynaptic released glutamate, however, ion conduction is minimized by a Mg^{2+} ion blocking the channel and only moderate amounts of ions (mainly calcium and sodium) pass through the channel. Yet, a sufficient postsynaptic depolarization removes the Mg^{2+} block, thus opens the channel completely and causes strong calcium fluxes. The depolarization might arise from

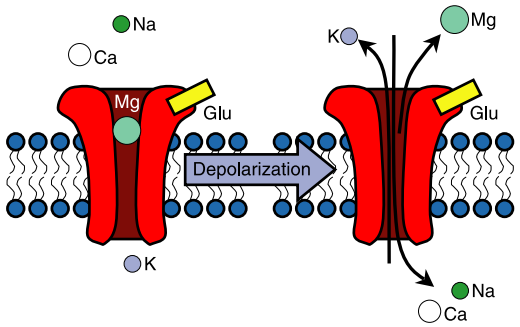

Figure 2.6: NMDA receptors are opened by binding of presynaptic glutamate and removal of Mg^{2+}-block by postsynaptic depolarization (modified from Sjöström et al., 2008, with permission).

back propagating action potentials (originating from the soma) and thus provide a mechanism for coincidence detection of pre- and postsynaptic activity. Thus the timing of the action potentials of pre- and postsynaptic neurons intimately control the depression or potentiation of the synaptic efficiencies (more detailed description, additional mechanisms are discussed in Sjöström et al., 2008).

We note that the above description of the biophysical foundations of signal generation, transmission and processing outlines some of the basic principles, but is by no means complete. Further informations can be found in recent textbooks (e.g., Dayan and Abbott, 2001; Bear et al., 2006; Purves et al., 2008).

2.1.2. Neuron models

Neuron models exists on a large scale of abstraction levels. There are attempts to simulate cortical networks with highly detailed neuron models which include a large number of compartments and precise distribution of ion channels (e.g., the "Blue Brain Project", Markram, 2006). Simulation of such systems can yield a good picture of the neural dynamics, but might be far too complex to gain insight about the mechanisms underlying neuronal information processing. In the other extreme, neurons can be simplified to threshold units with only two active states ("firing" or "not firing", e.g., Hopfield, 1982) and allow an analytical treatment of the dynamics of networks of such units. Of course, simplification bears the risk of studying model artifacts which cannot be generalized; thus it might be reasonable to verify prediction with more complex neuron models and experiments.

In this thesis we employ single compartment models, i.e., we neglect the spatial extend of the neurons. Thus the membrane potential of each neuron can be described by a single variable V and the influence of spikes on postsynaptic neurons is described by its effective action on the action potential initiation zone of the postsynaptic neurons.

Leaky integrate-and-fire neurons

In most parts of the thesis we deal with neurons of the leaky integrate-and-fire (LIF) type (Lapicque, 1907; Dayan and Abbott, 2001; Tuckwell, 1988). These models have a reasonable degree of accuracy, but are often still analytically tractable (for an extensive review of current research see Burkitt, 2006a,b).

For small fluctuations around the resting potential, the neuronal conductances are approximately constant. The LIF model omits the voltage dependency of the ion channels (and thus the mechanism of generation of action potentials) completely and models subthreshold dynamics only. All membrane conductances are lumped togethet into one single term g_{L} (leak conductance).

The model behaves like an electrical circuit (cf. Figure 2.7) consisting of (1) a capacitor with capacity C_m (representing the charge separating membrane), (2) a resistor with leak conductance g_L parallel to the capacitor (representing the leak current over the passive ion channels) and (3) a battery generating the potential difference equal to the leak (or resting) potential E_L (representing the ion pumps charging the neuron). The capacitor (neuron) might be charged by an additionally (time varying) current $I(t)$, arising from presynaptic stimulation (or direct injections by electrodes). Taken together, the subthreshold dynamics is governed by

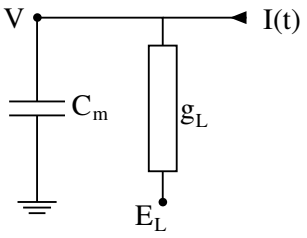

Figure 2.7: Equivalent circuit for the LIF model.

$$C_\mathrm{m}\frac{dV}{dt} = -g_\mathrm{L}\left(V - E_\mathrm{L}\right) + I(t). \tag{2.1}$$

It is convenient to multiply Equation (2.1) by the membrane resistance $R = 1/g_\mathrm{L}$ which yields

$$\tau_\mathrm{m}\frac{dV}{dt} = E_\mathrm{L} - V + RI(t) \tag{2.2}$$

where $\tau_\mathrm{m} = RC_\mathrm{m}$ is the membrane time constant.

When the potential difference (at the capacitor) reaches a certain threshold (spiking threshold) Θ it is assumed that an action potential is generated. The membrane potential is reset to the reset potential $V_\mathrm{reset} < \Theta$ and the action of the generated spike on the postsynaptic neurons is considered in form of injected currents to the postsynaptic cell (cf. Section 2.1.3).

Despite its simplicity, the LIF model reproduces several aspects of the response properties of real neurons to constant and fluctuating input with not too high frequencies fairly well (Dayan and Abbott, 2001; Rauch et al., 2003; Naundorf et al., 2005; Burkitt, 2006b).

Hodgkin-Huxley type neurons

Although the main results in this thesis are derived for networks of LIF neurons, we verified some of the analytical predictions by simulations employing the biophysically more plausible Hodgkin-Huxley model (Hodgkin and Huxley, 1952). This model was established in 1952 to describe the giant axon of the squid and takes three different types of ion currents (leak current, potassium current and sodium current) into account. In contrast to the LIF model, it explicitly models the generation of action potentials.

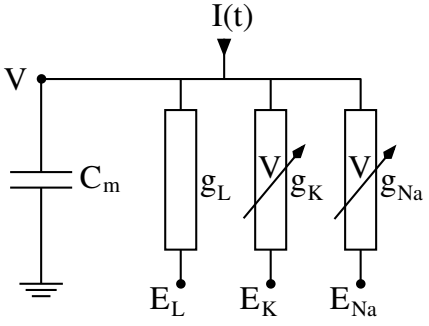

Figure 2.8: Equivalent circuit for the Hodgkin-Huxley model.

The potassium and sodium currents, $I_{\mathrm{K}}(V)$ and $I_{\mathrm{Na}}(V)$, are assumed to be voltage dependent (see also Section 2.1.1), the leak current I_{L} (gathering all other channels which are not explicitly described) is not. Figure 2.8 shows the equivalent electrical circuit. According to Kirchoff's Law the membrane potential obeys

$$C_{\mathrm{m}}\frac{dV}{dt} = -I_{\mathrm{L}} - I_{\mathrm{Na}}(V) - I_{\mathrm{K}}(V) + I(t), \tag{2.3}$$

where $I(t)$ is a temporally varying stimulation current as before (cf. Equation 2.1). We denote the reversal potentials of the single currents by E_{L}, E_{Na}, E_{K} and the (maximal) conductance for each considered channel by g_{L}, g_{Na} and g_{K}. Hodgkin and Huxley found that the voltage dependence of the channels can be described by three gating variables, $m(V)$, $h(V)$ and $n(V)$,

$$C_{\mathrm{m}}\frac{dV}{dt} = -g_{\mathrm{L}}\left(V - E_{\mathrm{L}}\right) - g_{\mathrm{Na}}m^3h\left(V - E_{\mathrm{Na}}\right) - g_{\mathrm{K}}n^4\left(V - E_{\mathrm{Na}}\right) + I(t). \tag{2.4}$$

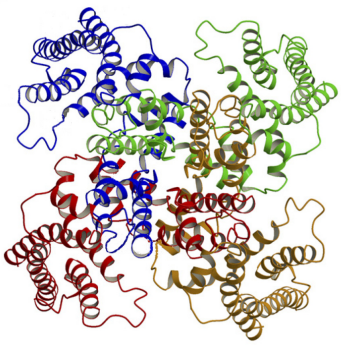

Figure 2.9: View of the ribbon representation of the Kv1.2 (potassium) channel from the extracellular side of the membrane. All four subunits are colored individually (modified from Pathak et al., 2007, with permission).

The gating variables can be interpreted as the probability that a subunit of a specific ion channel gate has undergone a conformal change which is necessary to open the gate (Dayan and Abbott, 2001). The exponents in Equation (2.4) arise from the fact that for some channels more than one of this subunits are involved in the opening of the channel: For example to open the potassium channel, the gate has four identical subunits (cf. Figure 2.9) that have to undergo a structural change to open the channel. We note that the sodium current involves two different gates, an activating gate (described by m) and an inactivating gate (described by h), which is responsible for the deactivation of the channel for strong depolarizations (cf. also Section 2.1.1).

Denoting the voltage dependent opening rate of a subunit gate by $\alpha(V)$ and the closing rate by $\beta(V)$, the temporal dynamics of the probability that a subunit gate is open obeys

$$\frac{dm}{dt} = \alpha_m(V)(1-m) - m\beta_m(V) \quad \text{(sodium activation)} \tag{2.5}$$

$$\frac{dn}{dt} = \alpha_n(V)(1-n) - n\beta_n(V) \quad \text{(potassium activation)} \tag{2.6}$$

$$\frac{dh}{dt} = \alpha_h(V)(1-h) - h\beta_h(V) \quad \text{(sodium deactivation)} \tag{2.7}$$

Here, the probability that a gate is opened (in a short time interval) is the product of the probability to find the gate closed times the opening rate, $(1-n)\alpha(V)$, minus the probability to find the gate open times the closing rate, $n\beta(V)$.

The voltage dependent opening and closing rates have to be determined experimentally and can be found elsewhere (e.g., Hodgkin and Huxley, 1952; Dayan and Abbott, 2001 or in the supplement of Chapter 3). We note that the original model considers only two types of channels as described above, however, other channels can easily be added to the model with the same approach.

The Hodgkin-Huxley model has been proven to reproduce the dynamics of real neurons quite well. However, despite its complexity it fails to describe some features of the initiation dynamics of cortical action potentials (rapid initiation and variable onset potential) accurately (Naundorf et al., 2006).

2.1.3. Modelling synaptic interactions

Analogous to the formulation of an appropriate neuron model, there are different level of abstractions for modeling the impact of presynaptic spikes on the membrane potential of the post synaptic neurons.

Conductance based models

When neurotransmitters are released to the synaptic cleft and there is a large portion of this transmitters available, the postsynaptic receptor gated ion channels open at a high rate. After the neurotransmitters are removed, the channel closes with a time constant typically substantially larger than the time constant for opening the channels.

To account for the two different timescales (for opening and closing the channels), the temporal development of the conductance (for the currents across one channel type) might be described by the difference of two exponentials (Dayan and Abbott, 2001). The transient conductance change in response to one single input (received at $t = 0$) is then

$$g(t) = g_{\max} A \left(e^{-t/\tau_1} - e^{-t/\tau_2} \right) \tag{2.8}$$

with time constants $\tau_1 > \tau_2$ and normalization factor A that assures that the peak value of the conductance equals $g_{\max}$,

$$A = \left[\left(\frac{\tau_2}{\tau_1} \right)^{\frac{\tau_2}{\tau_1 - \tau_2}} - \left(\frac{\tau_2}{\tau_1} \right)^{\frac{\tau_1}{\tau_1 - \tau_2}} \right]^{-1} . \tag{2.9}$$

The rise time of the synaptic conductances is determined by $\tau_{\text{rise}} = \tau_1 \tau_2 / (\tau_1 - \tau_2)$ and the decay time is set by τ_1. The peak conductance $g_{\max}$ measures the strength (determined by, e.g., the density of postsynaptic ion channels and the amount of presynaptic transmitter release) of the synaptic connection.

If a neuron receives multiple inputs at times $t \in \{t_1, t_2, \ldots\}$, the temporal development of the induced conductance change obeys

$$g(t) = g_{\max} A \sum_i \Theta(t - t_i) \left(e^{-(t-t_i)/\tau_1} - e^{-(t-t_i)/\tau_2} \right), \tag{2.10}$$

where $\Theta(\cdot)$ is the Heaviside step function. Accordingly, the induced current in the postsynaptic neuron is

$$I(t) = [E - V(t)]\, g_{\max} A \sum_i \Theta(t - t_i) \left(e^{-(t-t_i)/\tau_1} - e^{-(t-t_i)/\tau_2} \right) \tag{2.11}$$

where E is the reversal potential of the considered ion channel and $V(t)$ the membrane potential.

The input zones to neurons typically express more than one channel type (cf. Section 2.1.1) and the contribution of each of these channels has to be described separately. In this thesis we consider AMPA and $\mathrm{GABA_A}$ receptor channels which are the main excitatory and inhibitory channels in the adult brain. The synaptic time constants τ_1 and τ_2 for each of these channels have to be measured experimentally and are available in the literature (e.g., Jonas et al., 1993; Pearce, 1993; Liu and Tsien, 1995; Hájos and Mody, 1997, and others).

We note that the choice to describe the time course of the conductances by the difference of two exponential functions is attributed to the types of channels we describe and the level of accuracy we want to achieve. For other types it might be reasonable to consider different interaction functions (interaction kernels) $K(t)$ which might be more or less complex, and describe the postsynaptic current by

$$I(t) = [E - V(t)]\, g_{\max} \sum_i \Theta(t - t_i) K\left(t - t_i\right). \tag{2.12}$$

Current based models

By neglecting the voltage dependency in Equation (2.12) one derives the so-called current based synapse models. Replacing $V(t)$ by the resting potential V_{rest} yields,

$$I(t) = [E - V_{\mathrm{rest}}]\, g_{\max} \sum_i \Theta(t - t_i) K\left(t - t_i\right). \tag{2.13}$$

Each presynaptic input causes a stereotypical current pulse (equivalent to a current pulse obtained by clamping the membrane potential to the resting potential).

Networks of neurons with either conductance based or current based synapses can generate quite different dynamics (e.g., Kuhn et al., 2004; Vogels and Abbott, 2005; Kumar et al., 2008a). For example, for conductance based synapses, the amplitude and also the width of postsynaptic potentials are influenced by external constant currents, and even by balanced (i.e., equal average amount of presynaptic excitatory and inhibitory input) synaptic bombardments (cf. Figure 2.10). Besides the general decrease of postsynaptic responses for membrane potentials closer to the reversal potential of the considered ion channel (cf. Equation 2.12), this is attributed to the decrease of the effective membrane time constant in the high-conductance state (Kuhn et al., 2004, and Figure 2.10C). Due to the negligence of the voltage dependence of the synaptic interactions, such an alteration of the postsynaptic response is not found in current based models (cf. Figure 2.10B,D). Therefore, in networks, current based models have a higher tendency to cause epileptic-like pathological activity by amplifying strong synchronous signals (Mehring

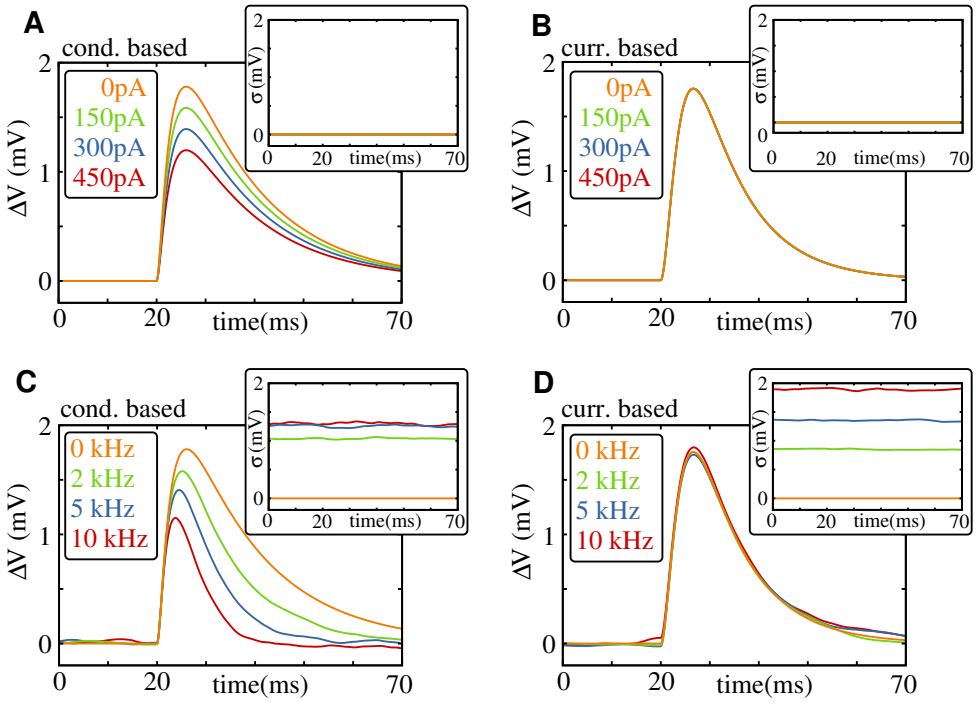

Figure 2.10: Current based versus conductance based synapses. For models with current based synapses the amplitude and width of the postsynaptic potential is decreased by the injection of a constant input current (A) and also by bombardment with balanced excitatory and inhibitory inputs (C). Neurons with current based synapses do not show such a dependency (B,D). The panels show simulations of LIF neurons (cf. Equation 2.2) with double exponential conductances (A,C; Equation 2.13) and alpha-function shaped input currents (B,D; $K(t) = e\frac{t}{\tau_1}\exp(-t/\tau_1)$). The main panels show the average postsynaptic potentials, the insets their standard deviations.

et al., 2003), whereas conductance based synapses might hinder this behavior by extenuating too strong synchronous activity (Kumar et al., 2008a and Chapter 6).

Nonetheless, current based models have been proven to be very useful to describe and understand activity states of neural networks, e.g., its irregular ground state, and their simplicity often allows even an analytical treatment (e.g., v. Vreeswijk and Sompolinsky, 1996; Brunel and Hakim, 1999; Timme et al., 2002; Denker et al., 2004; Goedeke and Diesmann, 2008; Jahnke et al., 2008; Memmesheimer, 2010; Helias et al., 2010, and many others).

In this thesis, we employ the leaky integrate-and-fire model in conjunction with the assumption of ultra-fast current responses to obtain analytical predictions (Chapter 3 and 4). Single presynaptic inputs are assumed to induce an instantaneous jump in the membrane potential (of size ϵ), and the model equation can be written — in abuse of mathematical notation — as (cf. Equation 2.2 and 2.13)

$$\tau_\mathrm{m}\frac{dV}{dt} = E_\mathrm{L} - V + \epsilon\sum_i \delta\left(t - t_i\right), \tag{2.14}$$

where $\delta(\cdot)$ is the Dirac delta function.

2.1.4. Models of Spike Time Dependent Plasticity (STDP)

In Chapter 7 we consider the (unsupervised) learning of network substructures (feed-forward subnetworks) in the presence of behavior-reflecting spiking patterns (place cell activity during exploration of space; cf. also Section 2.5). The formation of feed-forward anatomy is based on long-term potentiation and depression (LTP; LTD). In this thesis, we do not consider the impact of short term plasticity which is a source of additional computing capabilities for single neurons and networks, but its plasticity effects are restricted to short times (up to some seconds) and does not induce permanent changes (cf. Section 2.1.1). Models of short-term plasticity and their biological basis have been recently reviewed by Hennig (2013).

Pair based STDP

Although he had very limited knowledge about the cellular mechanism underlying the modification of synaptic weights (cf. Section 2.1.1), in 1949 Hebb postulated how synaptic connections might modify during activity:

> When an axon of cell A is near enough to excite a cell B and repeatedly or persistently takes part in firing it, some growth process or metabolic change takes place in one or both cells such that A's efficiency, as one of the cells firing B, is increased. (Hebb, 1949)

This statement has become famous in the more catchy formulation: *Fire together wire together.*

In classical Hebbian models modification of synaptic efficiencies is driven by correlations in the firing rate of pre- and postsynaptic neurons. The activity is expressed in terms of rates — a continuous description — and the fine temporal structure between pre- and postsynaptic spikes is neglected (e.g., Oja, 1982; Bienenstock et al., 1982).

However, it has been shown that the timing of single spikes is important: Using a pair-based stimulation protocol Bi and Poo (1998) have demonstrated that the strength of a synaptic connection increases, if the postsynaptic cell fires after the presynaptic one, and that the strength decreases if the spiking order is reversed. The amplitude of weight change decreases with the temporal difference between the spikes (cf. Figure 2.11) and the potentiation/depression is stronger for initially weak synapse than for strong ones (cf. Figure 2.12).

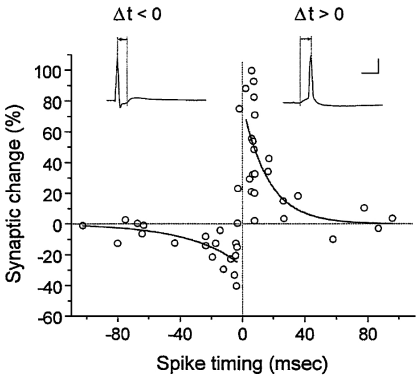

Figure 2.11: Time window of STDP for pair-based stimulation protocol (modified from Bi and Poo, 2001, with permission).

More formal, the change of the synaptic strength w induced by one spike pairing of a pre- and postsynaptic spike, can be written as

$$\Delta w = \begin{cases} F_+(w) \cdot \exp\left(-\frac{|\Delta t|}{\tau_+}\right) & \text{if} \quad \Delta t > 0 \\ F_-(w) \cdot \exp\left(-\frac{|\Delta t|}{\tau_-}\right) & \text{if} \quad \Delta t \leq 0 \end{cases} \tag{2.15}$$

where Δw is the amplitude of the positive/negative weight change (potentiation/depression), $F_\pm(w)$ describe the weight dependence on the current weight w, and Δt is the time difference between the post- and presynaptic spike. To completely define the model, one has to additionally specify which spike pairings are taken into account: For updating the weights one could pair only temporally neighbored spikes (nearest neighbors) or all spikes (for a discussion of the single approaches see, e.g., Morrison et al., 2008).

For the weight dependence, different functions have been proposed. In the simplest case they might be purely additive (the update does not depend on the weight at all),

$$F_+(w) = \lambda \tag{2.16}$$

$$F_-(w) = \alpha\lambda, \tag{2.17}$$

where λ is the learning rate and α the asymmetry factor (relating potentiation to depression). However, additive learning rules tend to develop bimodal weight distributions, where the peaks are placed at the extrema of the possible weights, i.e., $w = 0$ or $w = w_{\max}$ assuming that a synapse cannot become infinitly strong (Rubin et al., 2001).

For multiplicative update rules where

$$F_\pm(w) \propto w, \tag{2.18}$$

and also for rules placed somewhere between additive and multiplicative, i.e., $F_\pm(w) \propto w^\mu$ with $0 < \mu < 1$, it has been shown that they typically yield an unimodal weight distribution for uncorrelated Poissonian spiking activity (Rubin et al., 2001; Gütig et al., 2003; Morrison et al., 2007). Experiments analyzing the weight distribution of cortical networks suggest that such an unimodal distribution is more realistic than a bimodal one (Song et al., 2005).

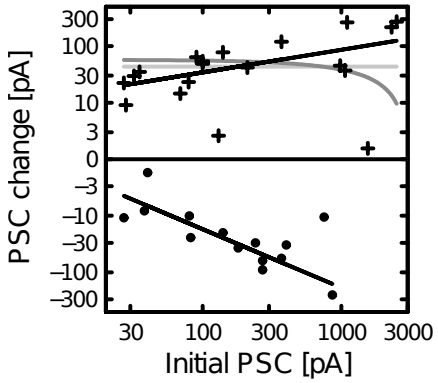

Figure 2.12: Weight dependence of synaptic potentiation and depression; data from (Bi and Poo, 1998) together with predictions from different update rules (black: powerlaw, pale gray: additive, dark gray: multiplicative). Figure reproduced from Morrison et al. (2007) with permission.

In Chapter 7 we employ the "powerlaw-update-rule",

$$F_+(w) \propto \lambda w^\mu \tag{2.19}$$

$$F_-(w) \propto \lambda\alpha w \tag{2.20}$$

which has been shown to yield an unimodal weight distribution in large balanced random networks with plastic couplings (Morrison et al., 2007). Moreover, it resembles the experimental

data of Bi and Poo (1998) better than additive or purely multiplicative update rules (cf. Figure 2.12, black curves).

We remark that reported STDP curves may vary for different areas and neuron types (Abbott and Nelson, 2000; Caporale and Dan, 2008) and also higher order correlation (triplet-stimulation) may change the properties of synaptic plasticity (Wang et al., 2005; Gjorgjieva et al., 2011). More information can be found in recent reviews on mechanism and modelling of STDP(Morrison et al., 2008; Caporale and Dan, 2008; Tetzlaff et al., 2012).

2.2. Active dendrites

2.2.1. Dendritic democracy

In classical view, signals arriving at the synapses are chemically transmitted to the postsynaptic terminal (see Section 2.1 above) and passively conducted along the dendrites down to the soma. Yet, the signal is strongly attenuated while spreading along the dendrites (especially within thin dendritic branches with high ohmic resistance) and thus the contribution of single inputs, in particular at distal synapses, to the de-/hyperpolarization of the soma is very weak (cf. Figure 2.13 illustrating the widespread morphological structure of a pyramidal neuron). This raises the question, why neurons are equipped with such long dendrites, extending up to several hundreds of micrometers (Andersen et al., 2007; Cutsuridis et al., 2010) away from the soma, if the inputs do not affect the somatic output at all?

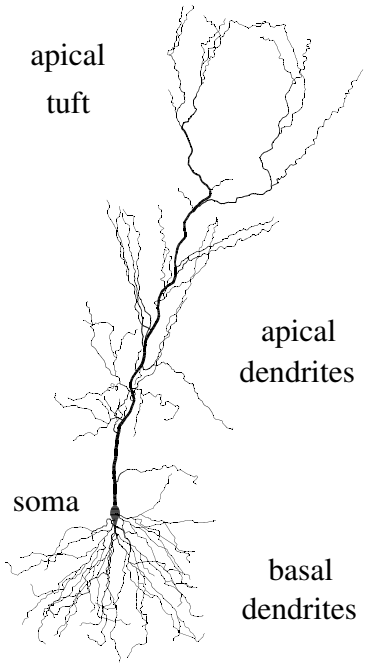

Figure 2.13: Morphology of the dendritic tree of a pyramidal CA1 neuron (modified from Golding et al., 2005, with permission)

Different mechanisms have been proposed — and experimentally verified – to counterbalance this discrimination of distal inputs: Remote synapse might be stronger to overcome the distance dependent attenuation ("synaptic scaling", Iansek and Redman, 1973; Magee and Cook, 2000; Häusser, 2001), and/or the leak currents are counterbalanced by (gradually) opening of voltage gated ion channels along the dendrite causing inward directed currents ("subthreshold boosting", Cook and Johnston, 1997, 1999; Migliore and Shepherd, 2002), and/or dendritic spikes — all-or-none events — might be elicited in distal locations and thus provide a (nonlinear) amplification of presynaptic inputs (see, e.g., numerous recent reviews on different aspects and variants of dendritic spikes, Häusser et al., 2000; Häusser and Mel, 2003; London and Häusser, 2005; Spruston, 2008; Major et al., 2013). Whereas the first both effects ensure that the remote signal can contribute to the voltage changes of the soma (also known as "dendritic democracy"), the latter one adds additional

computing power to the dendrites: Dendritic spikes are elicited by sufficiently strong and synchronous stimulation only and might require back propagating action potentials in addition; thus the dendrite itself carries out some part of the neural computation (cf. also Section 2.2.3).

2.2.2. Dendritic spikes

The term "dendritic spike" describes strong, often stereotypical, voltage transient in the dendrite; they have some kind of threshold (voltage or other input variables, e.g., concentration of neurotransmitter in the synaptic cleft) and the response to suprathreshold input qualitatively differs from subthreshold responses, and finally the event is regenerative (see also definition in Major et al., 2013). So far three different types of dendritic spikes have been reported and they can be classified depending on the main underlying class of conductances/ion channels, i.e., there are NDMA- (based on NMDA gated ion channels; cf. also Figure 2.6), Ca^{2+}-spikes (based on voltage gated calcium channels) and Na^{+}-spikes (based on voltage gated sodium channels).

Na^{+}-spikes

In this thesis, we consider the influence of fast (compared to other types of dendritic spikes, see below) dendritic sodium spikes on the dynamics of recurrent networks. These spikes have been found prominently in hippocampal regions CA1 in basal (Ariav et al., 2003; Losonczy et al., 2008; Remy et al., 2009; Müller et al., 2012) and apical dendrites (Golding and Spruston, 1998; Gasparini et al., 2004; Jarsky et al., 2005; Losonczy and Magee, 2006; Gasparini and Magee, 2006; Makara et al., 2009), recently in CA3 (Kim et al., 2012; Makara and Magee, 2013) and also in the neocortex (Stuart et al., 1997; Larkum et al., 2001; Nevian et al., 2007).

The dendritic Na^{+}-spike is initiated by voltage gated sodium channels, causing a sharp rise of the voltage transient, and shaped by concurrent activation of NMDA receptors, voltage gated Ca^{2+}- and A-type K^{+}-currents (cf. Figure 2.14; Ariav et al., 2003; Losonczy and Magee, 2006; Remy et al., 2009; Kim et al., 2012). The generation of dendritic spikes requires sufficiently strong, or — if elicited by multiple presynaptic inputs — highly synchronized (in time and space) inputs (Ariav et al., 2003; Gasparini et al., 2004; Gasparini and Magee, 2006). This synchrony detection is remarkably sensitive, probably due to the small membrane time constant in thin dendrites; only sufficiently strong inputs within a very short time interval of up to roughly 3ms may generate dendritic sodium spikes (cf. also Figure 2.14).

Dendritic spikes may cause depolarizations at the soma, which substantially exceed the depolarizations expected from summation of the effect of single inputs. Interestingly, it has been shown that this increased depolarization may even trigger somatic spikes (e.g., Ariav et al., 2003; Losonczy et al., 2008; Müller et al., 2012; Makara and Magee, 2013): The triggering of somatic action potentials by dendritic spikes generated in the apical dendrite (in particular in the apical tuft) has been shown to be highly variable; the dendritic spike is attenuated during transmission down the dendrite, but can be modulated (in particular reinforced) by additional inputs to the apical dendrite, which establishes a kind of gating mechanism for the remotely

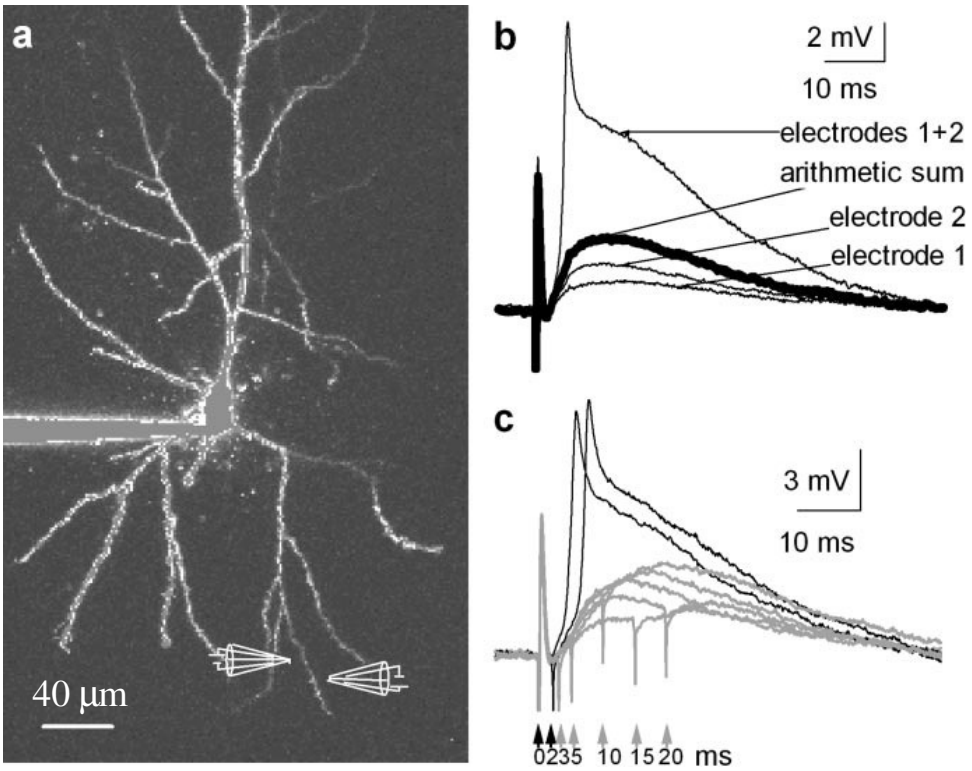

Figure 2.14: Nonlinear amplification of synchronous inputs. (a) Fluorescent image of a CA1 pyramidal neuron. Two stimulating electrodes were placed in close proximity to a basal dendrite. (b) Traces showing the individual excitatory postsynaptic potentials (EPSPs) evoked by each of the synaptic stimulating electrodes, the summed synaptic potential during coincident activation of the two synaptic stimulating electrodes, and the arithmetic sum of the two individual responses (bold line). Note the large supralinear amplification and sharpening of the summed synaptic potential, as compared with the expected arithmetic sum response. The fast component is attributed to voltage gated sodium channels, followed by a longer lasting component mediated by subsequent opening of NMDA receptors. (c) Voltage traces obtained in response to coincident activation of two closely spaced electrodes at various time delays ($0 - 20$ms). Black traces represent voltage responses to activation of the electrodes at time delays of 0 and 2ms. Gray traces show the responses for activation at time delays of $\{3, 5, 10, 15, 20\}$ms. Note that, in this experiment, the time window for coincident detection was < 3ms. Figure and caption modified from Ariav et al. (2003) with permission.

generated signal (Golding and Spruston, 1998; Gasparini et al., 2004; Jarsky et al., 2005; Makara and Magee, 2013). Dendritic sodium spikes generated in basal (or radial oblique) dendrites are much more reliable in triggering somatic spikes (Ariav et al., 2003; Losonczy et al., 2008; Müller et al., 2012; Makara and Magee, 2013). The timing of the evoked somatic action potential can be surprisingly precise; the temporal jitter is in the sub-millisecond range (Ariav et al., 2003; Losonczy et al., 2008).

The strength of sodium spikes (both the amplitude ΔV and rate of rise dV/dt) is relatively invariant between different trials, but there is remarkable variance between the branches (Losonczy et al., 2008; Makara et al., 2009; Müller et al., 2012). They can be classified in strong and weak dendritic branches (cf. Figure 2.15). The propagation of weak dendritic spikes is strongly attenuated until they reach the soma, and the timing of subsequent action potentials — probably elicited by the slow, longer lasting spike component following the initial sodium spike, cf. Figure 2.14 and 2.15 — is relatively unreliable; thus the temporal jitter between trials is high (Gasparini et al., 2004; Losonczy et al., 2008; Müller et al., 2012). In contrast, dendritic spikes generated in strong branches require less presynaptic stimulation, are transmitted essentially without attenuation, are very reliable in triggering of somatic action potentials — probably due to the fast sodium spike — with sub-millisecond precision (Ariav et al., 2003; Losonczy and Magee, 2006; Losonczy et al., 2008; Müller et al., 2012; Makara and Magee, 2013).

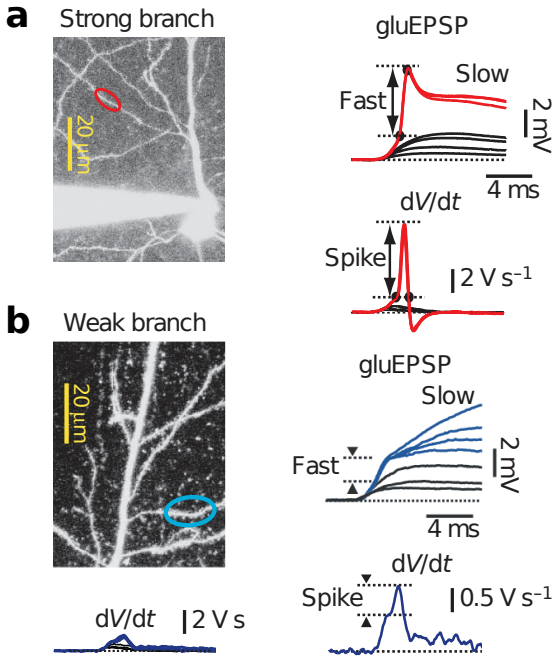

Figure 2.15: Characteristics of dendritic spikes evoked by optically stimulated glutamate uncaging in strong (red) and weak (blue) dendritic branches (modified from Losonczy et al., 2008, with permission).

Interestingly, it has been shown that weak branches can be transformed into strong branches by suitable stimulation protocols — e.g., by mimicking the presynaptic stimulation on hippocampal pyramidal cells during exploration of space, cf. also Section 2.5.3 — and/or by the application of neuromodulators (Losonczy et al., 2008; Müller et al., 2012). This suggests that single branches may act as sub-processing units which can be turned on and off in an experience-based manner, e.g., during phases of spatial exploration.

Finally, it is noteworthy that strong dendritic sodium spikes cannot be suppressed by (both recurrent or locally applied) inhibition, whereas weak dendritic spikes are completely attenuated (Müller et al., 2012; though the inhibition decreases the probability that the dendritic spike can elicit a somatic spike). Interestingly, this mechanism further increases the output precision of

somatic spikes: All somatic action potentials, but the highly precise ones caused by strong dendritic spikes, are suppressed.

Taken together, (strong) dendritic sodium spikes act as powerful coincidence detectors with remarkable precision, regarding both the detection of input synchrony and the generation of output spikes. They are prominently found in the basal dendrites of hippcampal pyramidal neurons. In this dendritical region most of the recurrent excitatory inputs (from other pyramidal of the same region) in hippocampal area CA1/CA3 arrive (Andersen et al., 2007; Cutsuridis et al., 2010). Thus, the available data suggest that dendritic sodium spikes are crucially involved in processing synchronous inputs in the hippocampus (e.g., during Sharp-Wave-Ripple events; cf. Sections 2.5.3, 2.5.4 and Chapter 7).

NMDA- and Ca^{2+}-spikes

As mentioned above, additionally to dendritic sodium spikes, dendritic NMDA-spikes and calcium-spikes have been reported in the hippocampus and neocortical areas (cf., e.g., Major et al., 2013, for a review). These spike also nonlinearly amplify presynaptic inputs, but are far less sensitive to input synchrony. For example, Polsky et al. (2004) reported that two stimuli on the same dendritic branch cause somatic responses exceeding the level expected from linear summation of inputs up to time intervals of more than 40 ms between the stimuli. This insensibility (compared to sodium spikes) is attributed to the fact that, in particular NMDA receptors (cf. also Figure 2.6 and describing text), typically deactivate only slowly (Paoletti, 2011, and references therein). As a consequence, the caused somatic depolarization is long lasting or "plateau-like" (Major et al., 2013, and references therein), and NMDA-spikes and calcium spikes are often associated with the generation of bursts of action potentials (Traub and Wong, 1982; Williams and Stuart, 1999; Larkum and Zhu, 2002; Milojkovic et al., 2004; Polsky et al., 2009; Long et al., 2010).

2.2.3. Previous work on dendritic computation

The first indications of dendritic nonlinearities (spikes) have been measured more than 50 years ago (Spencer and Kandel, 1961, measured small pre-potential (spikelets) and proposed the existence of dendritic nonlinearities). During the last decades a wealth of experimental data accumulated clearly showing the existence (and measuring the properties) of dendritic spikes (see Section 2.2.2). Nonetheless, there are astonishing few theoretical/modelling studies so far aiming to an understanding of the impact of these dendritic spikes on computational properties on the network level.

Single neuron level

Theoretical studies on active dendrites mainly focused on single neurons. Simulations of neuron models with detailed channel density and morphology showed dendritic spike generation and its

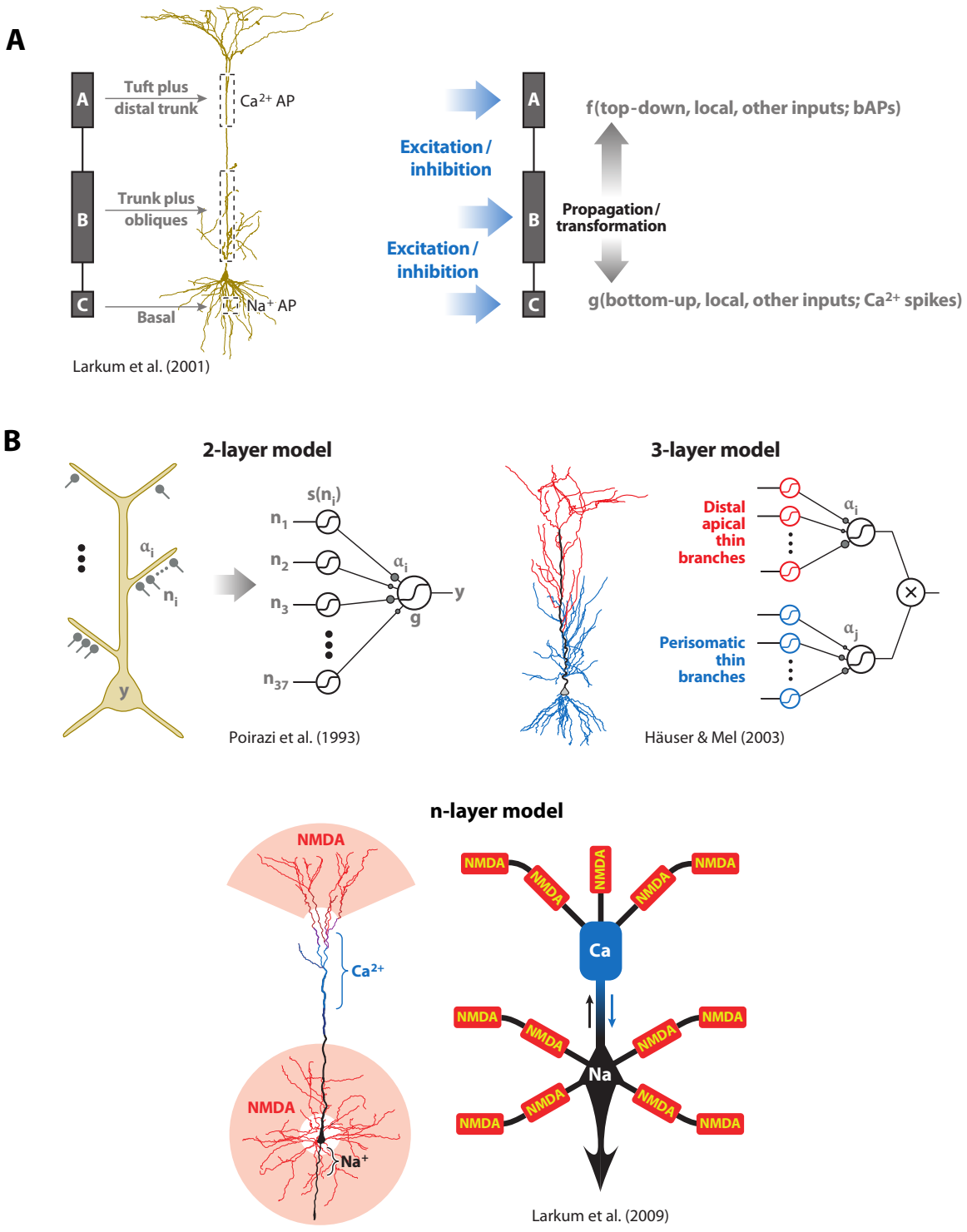

Figure 2.16: Computing by single neurons with active dendrites. (A) Inputs to the apical dendrite control whether dendritic spikes generated in the apical tuft are transmitted to the soma, and whether somatic action potentials may propagate back from the soma to the apical tuft. (B) Single neurons as multilayer networks: Each dendritic compartment can act as a single computing unit with sigmoidal transfer function. Figure modified from Major et al. (2013) with permission.

sensitivity to synchronous stimulations (coincidence detection) in agreement with neurobiological experiments (Stuart and Häusser, 2001; Ariav et al., 2003; Gasparini et al., 2004; Poirazi et al., 2003a,b; Nevian et al., 2007). It has been shown that, e.g., presynaptic inputs to the apical dendrite might function as a gating mechanism for signal propagation from the apical tuft to the soma and back (Larkum et al., 2001; Jarsky et al., 2005; Katz et al., 2007, and Figure 2.16A).

On the basis of these detailed modelling studies more abstract rate models have been developed (Poirazi and Mel, 2001; Poirazi et al., 2003a,b; Häusser and Mel, 2003; Polsky et al., 2004; Larkum et al., 2009): Single dendrites are considered as independent computational units with a sigmoidal input-output relation, and neurons equipped with such dendrites effectively act like multi-layer feed-forward networks (cf. Figure 2.16B). Thus nonlinear dendrites improve the ability of single neurons and ensembles of single neurons to discriminate and learn different input patterns (Mel, 1992; Poirazi and Mel, 2001; Rhodes, 2008; Branco et al., 2010; Schiess et al., 2012). The propagation of dendritic spikes in branched dendrites with step-like activation functions (i.e. without analogous signal transmission) has been studied by Gollo et al. (2012, 2013) where the authors derived a statistical description of the input-output relations.

Network level

So far, only few studies considered the impact of nonlinear dendrites on network dynamics. Dendrites equipped with voltage gated calcium channels and NMDA receptors have been shown to provide a bursting mechanism, which may synchronize network activity (and serve as a model for epilepsy, Traub and Wong, 1982), or explain the emergence and propagation of burst in the high vocal center (HVC) of songbirds (Long et al., 2010). Further, it has been proposed that NMDA-receptor dependent dendritic nonlinearities play a crucial role in working memory (Lisman et al., 1998; Wang, 1999, 2001): Here the dynamical system is bistable (high- and low-activity attractor) and the activation of NMDA receptors with slow time constant enables to shift between the both states.

Recently, it has been shown that fast dendritic sodium spikes may explain the occurrence of intermittent or persistent high-frequency oscillations in sparse recurrent random networks (Memmesheimer, 2010; Memmesheimer and Timme, 2012). Spontaneous or induced synchronous activity is amplified by local dendritic spikes, and thus might spread over moderate fractions of a recurrent network.

2.3. Networks and dynamics

2.3.1. Some notations from graph theory

We describe the structure of a neural network by a directed graph, also called digraph (Chartrand and Lesniak, 2000; Bang-Jensen and Gutin, 2002). The neurons are the nodes, the synaptic connections are the directed edges of the graph and the weights of the edges are the coupling strengths.

A graph $G = (V, E)$ is a pair of two finite sets: The nonempty set V which is the set of nodes or vertices and the set of edges E. The elements of V (the nodes or neurons) are labeled by a natural number (index),

$$V = \{1, \ldots, N\} \text{ with } N = |V| \,. \tag{2.21}$$

For a directed graph, the set E contains ordered pairs of elements of the set of nodes V. These edges are often called arcs to distinguish between directed and undirected graphs. Additionally one can define a weighting function c on the edges of graph G,

$$c : E \to \mathbb{R}, \tag{2.22}$$

which assigns a weight (coupling strength) to every arc. The triple (V, E, c) is called weighted graph. In this thesis, we describe the coupling structure of our networks by a coupling matrix ϵ with

$$\epsilon_{ji} = \begin{cases} c(i,j) & \text{if } (i,j) \in E \\ 0 & \text{if } (i,j) \notin E. \end{cases} \tag{2.23}$$

We further denote the set of neurons which have a connection to a given node j,

$$\mathrm{Pre}(j) = \{i | \epsilon_{ji} \neq 0\} \,, \tag{2.24}$$

as the presynaptic neurons to neuron j. Likewise the set of neurons

$$\mathrm{Post}(j) = \{i | \epsilon_{ij} \neq 0\} \,, \tag{2.25}$$

which receives connections from neuron j are called postsynaptic neurons to neuron j.

2.3.2. Connectivity between neurons

Dale's Law

It has been found that neurons in the brain typically release the same set of neurotransmitters at all their axonal terminals — an observation which is nowadays known as "Dale's Law" (Dale, 1935; Eccles et al., 1954). In particular, neurons can be classified as either excitatory or inhibitory, depending on their main effect on postsynaptic cells. The most abundant excitatory cell type in mammalian cortical structures are so called pyramidal neurons which received their name due to the pyramidal shape of their cell body, and constitute around 80% of cortical neurons (Braitenberg and Schüz, 1998).

Connection probabilities

In general, the local connectivity between pyramidal neurons, estimated from dual cell recordings, is low (e.g., Deuchars and Thomson, 1996; Thomson et al., 2002; Holmgren et al., 2003, and references therein). It varies between different areas and usually decays with the distance between two neurons: For example, the connection probability between two neocortical pyramidal

neurons in Layer 2/3 has been estimated to be approximately 10% for adjacent cells and decays to approximately 2.5% in a distance of 130μm (Holmgren et al., 2003). In the hippocampal region CA3, the connectivity has been estimated to be between $2-6\%$ (Amaral et al., 1990; Ascoli and Atkeson, 2005), and in the CA1, a very sparse region, it is approximately 1% in a distance of 200μm (Deuchars and Thomson, 1996; Ascoli and Atkeson, 2005).

As a starting point we model local recurrent networks as classical (Erdös-Renyi) random graphs (cf. Chapter 4 - 7). In such networks each possible edge is realized with a fixed probability p, and thus the indegree (number of incoming connections) and outdegree (number of outgoing connections) distribution follows a Binomial distribution (Newman, 2010): Denoting the number of neurons by N the probability that a single neuron has exactly k presynaptic neurons is

$$p\left(|\mathrm{Pre}(i)|=k\right)=\binom{N-1}{k}(p)^k\,(1-p)^{N-1-k}, \tag{2.26}$$

and equals the probability to have exactly k postsynaptic partners,

$$p\left(|\mathrm{Post}(i)|=k\right)=p\left(|\mathrm{Pre}(i)|=k\right). \tag{2.27}$$

We assume a pure random graph as the basis connectivity attributing the fact that the actual degree distribution in cortical networks is unknown (due to experimental difficulties). However, simultaneous measurements of a small number of cells (up to 12, Perin et al., 2011), have shown small, but significant deviations from random graphs even if the distance dependency is taken into account (Song et al., 2005; Perin et al., 2011): Certain sub-patterns (called motifs, cf. Figure 2.17) are significantly more often detected than expected. Moreover, Bonifazi et al., 2009 provided direct experimental evidence that so called "hubs", highly-connected nodes, are found in developing hippocampal networks. This observations inspired us to also consider scale-free networks (cf. Chapter 5) where the degree distribution obeys a power-law, e.g.,

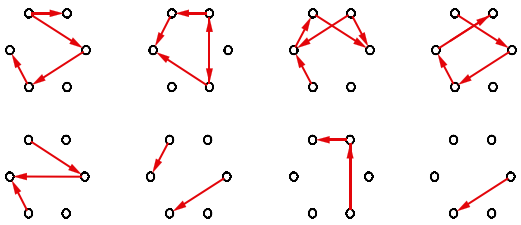

Figure 2.17: Example of network motifs in clusters of six cells (modified from Perin et al., 2011, with permission).

$$p\left(|\mathrm{Pre}(i)|=k\right)\propto k^{-\gamma}. \tag{2.28}$$

Here super-connected nodes are relatively common due to the "fat-tail" of the distribution (Newman, 2010).

In Chapter 5 we demonstrate that these hubs alter the network response properties: Whereas in simple random networks synchronous activity might spread out over the whole network or decay fastly, in the same class of networks, but containing hubs, synchrony might spread to only a fraction of neurons. Thus, moderate-amplitude — non-pathological — network oscillations are excited which interestigly may foster signal transmission (cf. also Section 2.4.2 and Chapter 6).

2.3.3. The ground state of cortical networks

The ground state activity of cortical networks is characterized by highly irregular activity with low spiking rates of several Hz per neuron (Softky and Koch, 1993; Rieke et al., 1997; Shadlen and Newsome, 1998). The spike train statistics resemble that of a Poissonian spike train, where inter-spike-intervals (ISIs) are exponentially distributed,

$$p(\mathrm{ISI} = \Delta t) = \nu \exp\left(-\nu \Delta t\right). \tag{2.29}$$

Although the cortical networks are sparse, they are large (the brain contains more than 85 billion neurons in total; Herculano-Houzel, 2009), and each neuron in the brain receives inputs from ten thousands of presynaptic neurons. Yet, an ongoing bombardment with random (Poissonian) spike trains is expected to cause a much more regular spiking activity than the one observed (Softky and Koch, 1993): According to the central limit theorem (Rice, 2007), the summed inputs can be approximated by a normal distribution and the standard deviation is expected to be small with respect to the mean input. As a consequence the neurons would receive an almost constant input which would lead to a regular spiking activity.

Balance of excitation and inhibition

This apparent paradoxical situation might be resolved by considering balanced excitatory and inhibitory inputs (Shadlen and Newsome, 1994, 1998). Although there are far less inhibitory neurons than excitatory neurons in the brain (Braitenberg and Schüz, 1998; Ascoli and Atkeson, 2005), many types of the inhibitory acting neurons are more active and densely coupled to surrounding excitatory cells (Ascoli and Atkeson, 2005; Jonas et al., 2004; Klausberger, 2009), and thus they may counterbalance the excitatory input on average.

If the average excitatory and inhibitory inputs are of the same order of magnitude, the membrane potential fluctuates (below the spiking thresholds) and spikes are elicited by random fluctuations in the input — also called "fluctuation driven regime" (cf. Figure 2.18). Theoretical studies have shown that such balance between excitation and inhibition naturally emerge in sparsely coupled networks and indeed generates highly irregular spiking dynamics as observed in experiments (v. Vreeswijk and Sompolinsky, 1996, 1998; Brunel, 2000; Jahnke et al., 2008; Renart et al., 2010). Indeed, a detailed balance between excitation and inhibition has been shown to exist during spontaneous as well as sensory evoked activity (Haider et al., 2006; Okun and Lampl, 2008; Atallah and Scanziani, 2009) allowing single neurons (in this fluctuation driven

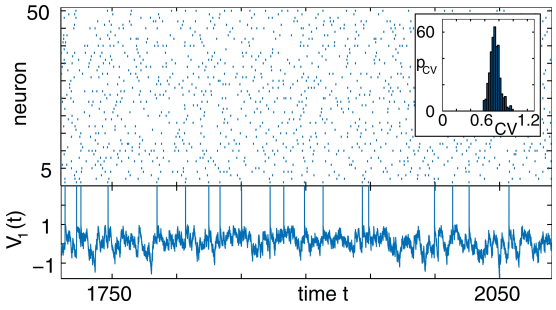

Figure 2.18: Example dynamics of highly irregular activity in balanced state networks (modified from Jahnke et al., 2008, with permission).

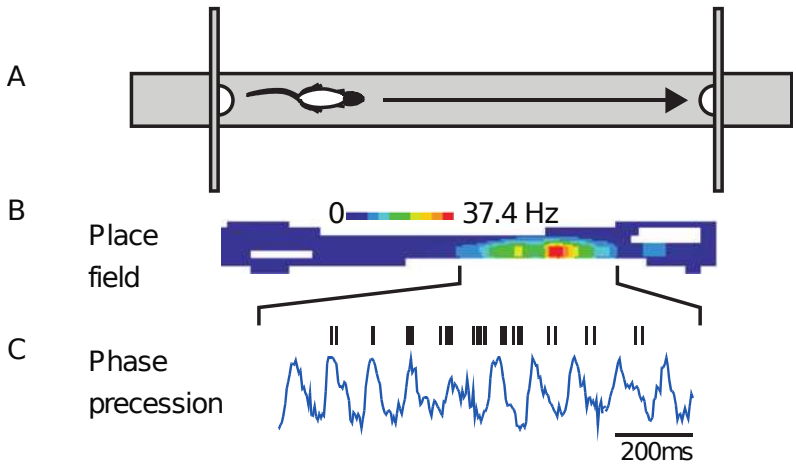

Figure 2.19: Rate and temporal coding in hippocampal place cells. (A) As a rat runs on a track, a place cell in the hippocampus fires as the animal passes through a specific region (the "place field", B). This firing rate code for location is also a temporal code (C): spikes (ticks) are fired at successively earlier phases of the theta rhythm of the local field potential (blue trace), referred to as "theta-phase precession". Figure and caption modified from Burgess and O'Keefe (2011) with permission.

regime) to respond very fast to changes in presynaptic stimulations (Tchumatchenko et al., 2011, and references therein).

2.4. Information representation and transmission in recurrent networks

2.4.1. Rate code vs. temporal code

Our brain encodes, decodes and processes information about our environment. The underlying neural code must serve four key functions: stimulus representation, interpretation, transformation and transmission (Perkel and Bullock, 1968; Kumar et al., 2010). In this thesis we consider two of these aspects, representation (Chapter 7) and transmission (Chapter 3-6) of information.

How is a stimulus (or a previously processed and stored information; memory) represented in the brain? It is somewhere hidden in the spiking activity, the spike trains of neurons or populations of neurons. Traditionally, it is assumed that most of the information is contained in the firing rate of neurons ("rate code"; reviewed in standard textbooks, e.g., Rieke et al., 1997; Gerstner and Kistler, 2002): For example, single "place cells" (cf. also Section 2.5.2) in the hippocampus encode the current position in space partly by a rate code — when an animal traverses the receptive field of a particular neuron its firing rate increases (O'Keefe, 1976; Wilson and McNaughton, 1993; Kjelstrup et al., 2008 and Figure 2.19B).

The rate approach neglects information that may be contained in precise spike times. However, the responses of neurons to repeated stimuli can be rather reliable (Mainen and Sejnowski, 1995; Nowak et al., 1997), and thus may lead to precisely timed spike patterns where the information is encoded in the timing — or relative timing — of the spikes (temporal code). Indeed, such patterns have been experimentally found in various neural systems and can be related to information representation and processing of stimuli: They indicate whisker position and movement in the rat (Panzeri et al., 2001; Jones et al., 2004), complex features of tactile stimuli in humans and monkeys (Johansson and Birznieks, 2004; Birznieks et al., 2010), noise source position and auditory stimulus identity (Gutfreund et al., 2002; Schnupp et al., 2006; Engineer et al., 2008). In the motor cortex of mammals, precisely synchronous spiking among neurons has been observed which is correlated with internal cognitive states and task performance (Riehle et al., 1997; Kilavik et al., 2009; Putrino et al., 2010).

Information provided by precise spike patterns can be complementary to that of spike rates over longer time windows (O'Keefe and Recce, 1993; Skaggs and McNaughton, 1996; Maurer and McNaughton, 2007; Kayser et al., 2009; Panzeri et al., 2010): For example place cells encode the current position in space by a rate code (see above) and, additionally, by precisely timed spikes — occurring spikes are locked to the oscillations of the LFP and indicate the position within the traversed place field (O'Keefe and Recce, 1993; Skaggs and McNaughton, 1996; Maurer and McNaughton, 2007, and Figure 2.19C).

2.4.2. Signal transmission in feed-forward networks

A common hypothesis states that such precise spike patterns are generated by synchronous activity propagating in specific sub-populations of neurons, so-called "synfire chains", which are embedded in a larger recurrent network. This concept was introduced by Abeles (1982) as feed-forward chains of groups of neurons (layers) with dense anatomical connections between subsequent groups (cf. Figure 2.20). Synchronous activity may spread from layer to layer by exciting a sufficiently large number of neurons to spike synchronously in every layer, and thus generate precise spike patterns (as observed in experiments; see above) reflecting the transmitted synchronous pulse. In an alternative view, by this mechanism information in the form of synchronous activity can be transmitted through recurrent networks (Kumar et al., 2010).

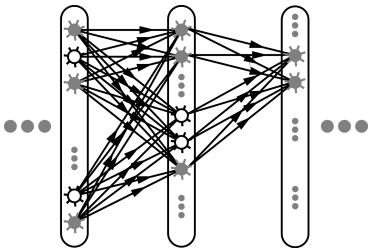

Figure 2.20: Schematic illustration of synfire anatomy (modified from Diesmann et al., 1999, with permission).

During the last decades a large number of theoretical and modelling studies have elaborated on this idea (Aertsen et al., 1996; Diesmann et al., 1999; Gewaltig et al., 2001; Kistler and Gerstner, 2002; Aviel et al., 2003; Mehring et al., 2003; Vogels and Abbott, 2005; Kumar et al., 2008a; Goedeke and Diesmann, 2008; Kumar et al., 2010; Kremkow et al., 2010) and looked for conditions for (and properties of) robust propagation of synchrony in synfire chains.

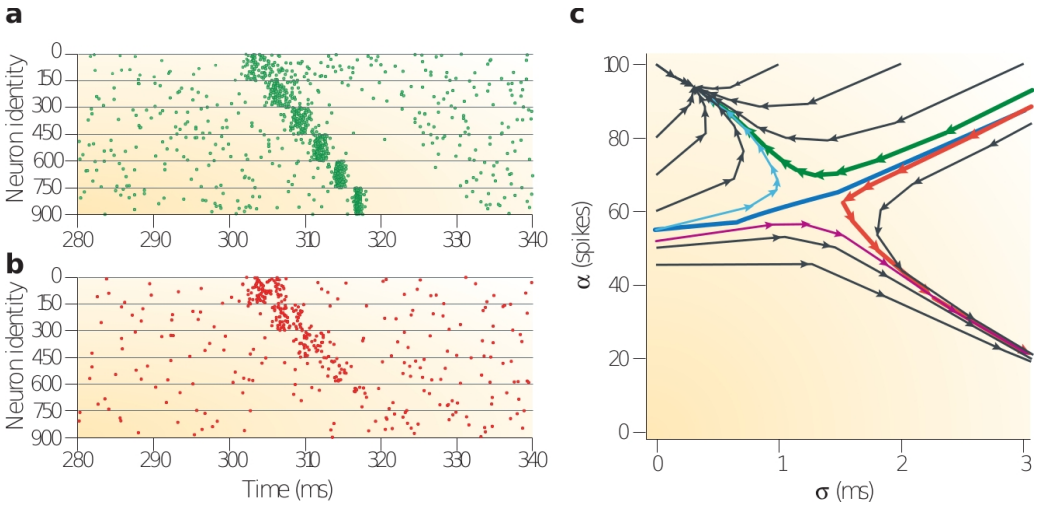

Figure 2.21: Illustration of the synfire attractor. Pulse packets (a) may or (b) may not propagate along a synfire chain, depending on the initial conditions. (c) Temporal development of synchronous pulses in the (α, σ)-space (size and width of pulse packet). The blue line (seperatrix) separates the basin of attraction of persistent propagation (green) and the region where synchronous activity decays (red). Figure modified from Kumar et al. (2010) with permission.

Isolated synfire chains

To describe and quantify the propagation of synchrony, it is useful to introduce the notion of a "pulse packet"(Aertsen et al., 1996; Diesmann et al., 1999): This is a volleys of α spikes that are drawn from a Gaussian distribution with standard deviation σ. By computer simulations it has been demonstrated that such pulse packets can propagate robustly along isolated synfire chains (where the embedding network is emulated by Poissonian spike trains) provided that the initial pulse is sufficiently large and synchronized (Aertsen et al., 1996; Diesmann et al., 1999; Gewaltig et al., 2001, and Figure 2.21).

The location of the seperatrix (separating regimes of successful and unsuccessful propagation) depends on the synfire architecture (e.g., the size of the layers, Diesmann et al., 1999), synaptic and background noise (Câteau and Fukai, 2001; Gewaltig et al., 2001), the input-output transfer function of the neurons (Goedeke and Diesmann, 2008), and refractory properties of single units (Kistler and Gerstner, 2002).

Embedded synfire chains

Further computational studies revealed that it is not straight forward to actually embed feed-forward chains into recurrent networks and still keep the capability to robustly propagate synchrony (Aviel et al., 2003; Mehring et al., 2003; Vogels and Abbott, 2005; Kumar et al., 2008a,

2010): Synchronous activity tend to spread out over the whole network and cause pathological, epileptic-like activity ("synfire explosions", Aviel et al., 2003; Mehring et al., 2003). To counterbalance this pathological activity either very large networks and/or very prominent feed-forward structures with respect to the remaining (i.e., embedding) network have to be assumed (Aviel et al., 2003; Vogels and Abbott, 2005). However, considering a local connectivity and conductance based synapses with sufficiently long time-scales (cf. Section 2.1.2) may also prevent synfire explosions (Kumar et al., 2008a), partly because of the reduced membrane time constants in the high-conductance state (Kuhn et al., 2004; Kumar et al., 2008b). Yet, also in this study the authors assumed an all-to-all coupling between successive layers.

Alternatively to densely connected layers, one may consider "diluted" synfire chains with sparse connectivity that naturally occur as part of a random neuronal circuit. In this scenario, the low connection probability between neurons of successive layers may be compensated by strengthening synapses (Vogels and Abbott, 2005). Following this "pathway" approach, a propagation of synchrony over a certain number of groups can be enabled if synaptic efficiencies are strongly (about a factor of ten) enhanced and a negative gain modulation is added (i.e., weakening all synapses onto pathway neurons).

However, for both types of embedding, highly prominent feed-forward structures are assumed — either in the sense of dense, possibly all-to-all coupling or in the sense of strongly, selectively modified local features — that are not experimentally observed. Additionally, prominent feed-forward structures hinder the signal separation from background activity: Correlations in the spike times induced by (even random) background activity, can accumulate over the layers and lead to spontaneous synchronous spiking activity (Litvak et al., 2003; Rosenbaum et al., 2010, 2011). Such spontaneous propagation of synchrony may happen even in isolated synfire chains with large layer sizes or too strong connection strengths (Tetzlaff et al., 2002, 2003; Mehring et al., 2003).

Fast dendritic spikes and synfire chains

In this thesis, we study the impact of fast dendritic spikes (cf. Section 2.2.2) on propagation of synchrony in diluted feed-forward networks, and demonstrate that they lessen the problems raised above: We show that these spikes relax the requirement of prominent feed-forward structures by selectively amplifying synchronous inputs, and therefore enabling signal propagation in isolated as well embedded feed-forward networks with biological plausible topology (Chapter 3 and 4). Moreover, due to the sensitivity of dendritic spike generation to only highly synchronous activity, spontaneous propagation of synchrony is hindered (Chapter 4). This sensitivity also opens the possibility to stabilize signal propagation by oscillatory inputs of suitable frequencies which further relax the requirement for prominent feed-forward anatomy (Chapter 5 and 6).

2.5. The Hippocampus

The hippocampus is one of the evolutionary oldest regions of the brain and crucially involved in episodic memory formation and consolidation (reviewed in, e.g., Girardeau and Zugaro, 2011). According to the "two-stage model" of memory (Marr, 1971; Buzsáki, 1989) information is first preliminary stored (in the hippocampus) and later (e.g., during rest or sleep) recalled and consolidated (i.e., transferred to the neocortex for long-term memorization). As discussed in Section 2.2.2, fast dendritic sodium spikes have been prominently found in hippocampal area CA1 (and to a lesser extent in CA3). In the very same regions, high-frequency oscillations (i.e., highly synchronized population activity) in conjunction with re-occurrence (replay) of previously learned spatio-temporal patterns occur during sleep and resting phases ("Sharp-Wave-Ripple complexes"; see Section 2.5.3 below). This might suggest a connection between dendritic nonlinearities and the observed activity patterns. In Chapter 7 we derive a model for learning and replay of spike patterns in the hippocampus based on fast dendritic spikes. As a basis for the results presented in Chapter 7, we provide a short overview of the anatomy of the hippocampus and observed activity patterns below.

2.5.1. Brief anatomical overview

The hippocampus derived its name from the Greek words *hippos* (horse) and *kampos* (sea monster) because it resembles the form of a seahorse (cf. Figure 2.22). The hippocampus is part of the limbic system, and its size generally increase in higher species (Stephan, 1983; although there are some highly developed species like dolphins and whales which do not follow this law Jacobs et al., 1979; Stephan and Manolescu, 1980). For example, the volume is ten times larger in monkeys than in rats, and even hundred times larger in humans. Nonetheless the *basic* anatomy is similar in all three species (Andersen et al., 2007), and therefore it is assumed that also the general functions (including the behavioral functions it subserves) are similar. The following description, and also the studies of hippocampal activity described afterwards, refer to rat experiments, because this species has become the main target of experimentalist.

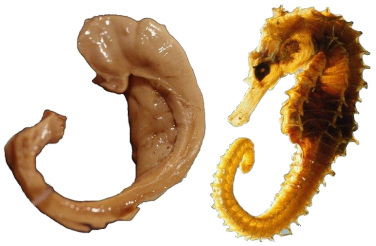

Figure 2.22: Preparation of a human hippocampus alongside a sea horse (from Wikimedia, 2010, published under CC-BY-3.0).

The hippocampus consists of three subregions: The dentate gyrus (DG), the hippocampus proper (HP; subdivided into CA1,CA2 and CA3) and the subiculum (Andersen et al., 2007; van Strien et al., 2009; Cutsuridis et al., 2010, and Figure 2.23).

It has a laminar structure with three main sublayers: The deepest layer contains a mixture of afferent and efferent fibers and interneurons. It is called hillus in the DG and stratum oriens in the CA regions. Superficial to this polymorph layer there is the cell layer that contains principal cells (mainly pyramidal neurons) and interneurons This layer is named granule layer in the DG,

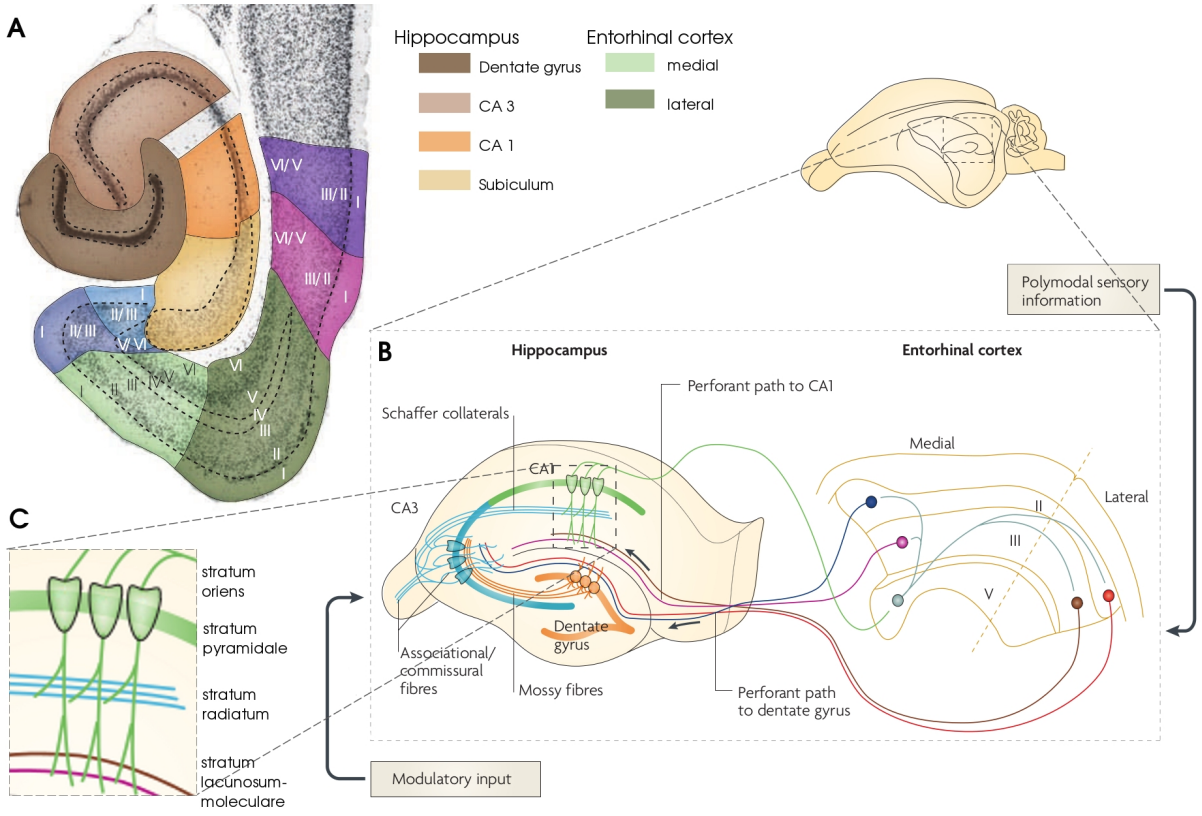

Figure 2.23: Basic anatomy of the hippocampus. (A) Nissl-stained crossection of the hippocampal formation and the parahippocampal region in the rat brain (Figure modified from van Strien et al., 2009, with permission). (B,C) The wiring diagram of the hippocampus is traditionally presented as a trisynaptic loop. The major input is carried by axons of the perforant path, which convey polymodal sensory information from neurons in layer II of the entorhinal cortex to the dentate gyrus. Perforant path axons make excitatory synaptic contact with the dendrites of granule cells: axons from the lateral and medial entorhinal cortices innervate the outer and middle third of the dendritic tree, respectively. Granule cells project, through their axons (the mossy fibers), to the proximal apical dendrites of CA3 pyramidal cells which, in turn, project to ipsilateral CA1 pyramidal cells through Schaffer collaterals and to contralateral CA3 and CA1 pyramidal cells through commissural connections. In addition to the sequential trisynaptic circuit, there is also a dense associative network interconnecting CA3 cells on the same side. CA3 pyramidal cells are also innervated by a direct input from layer II cells of the entorhinal cortex. The distal apical dendrites of CA1 pyramidal neurons receive a direct input from layer III cells of the entorhinal cortex. There is also substantial modulatory input to hippocampal neurons. The three major subfields have an elegant laminar organization (see also zoomed view in C) in which the cell bodies of principal cells are tightly packed in an interlocking C-shaped arrangement (granule layer/stratum pyramidale), with afferent fibers terminating on selective regions of the dendritic tree. The hippocampus is also home to a rich diversity of inhibitory neurons that are not shown in the figure. Figure and caption modified from Neves et al. (2008) with permission.

and stratium pyramidale in the HP. The most superficial layer is referred to as the molecular layer (stratum moleculare) in the DG and the subiculum; in the HP it can be further subdivided into stratum lucidum (only in CA3), stratum radiatum and stratum lacunosum-moleculare (cf. zoomed view of CA1 in Figure 2.23C).

The most prominent connection pathways to and within the hippocampus are summarized in Figure 2.23 (for a more complete description see, e.g., Witter and Amaral, 2004; Andersen et al., 2007; van Strien et al., 2009; Cutsuridis et al., 2010): The main input to the hippocampus arises from the entorhinal cortex (EC) via the so called perforant pathway and terminates at the dendrites of granule cells in the DG. These cells project forward via the mossy fibers to the pyramidal neurons in CA3, which in turn project to the CA1 pyramidal neurons via the Shaffer collaterals. This feed-forward projection (EC→DG→CA3→CA1) is referred to as the trisynaptic loop, or in an extended version polysynaptic pathway, where the subsequent projection from CA1 to the subiculum is also considered. In fact the projection from CA1 to the subiculum has turned out to be even more prominent than the CA1→EC projection, the classical termination of the trisynaptic loop (Andersen et al., 2007; Cenquizca and Swanson, 2007; van Strien et al., 2009). The output from the hippocampus formation arises (mainly) from CA1 and subiculum and targets, in particular, the deeper layers of the entorhinal cortex.

Besides this feed-forward pathway, recurrent connections within the areas of the hippocampus, and back projections (i.e., in the reverse direction of the polysynaptic pathway) have been described (reviewed in, e.g., Witter and Amaral, 2004; Andersen et al., 2007; van Strien et al., 2009). Recurrent connection (also referred to as associational projections) are most prominent in area CA3, but they are also found — although less prominent — in the other regions of the hippocampal formation (Witter and Amaral, 2004; van Strien et al., 2009, and references therein).

In Chapter 7 we consider the representation of spatial information (location) by the principal cells, i.e., the pyramidal neurons, in area CA1 and CA3. These cells (cell bodies) are placed in the stratum pyramidale, with the basal dendritic tree located in the stratum oriens and the apical tree extending to the superficial layers (cf. Figure 2.13 and 2.23C). The pyramidal cells are surrounded by a very heterogeneous group of GABAergic interneurons (at least 12 types of interneurons differing in single cell properties, formation and extent of axonal and dendritic trees have been reported so far, Witter and Amaral, 2004; Klausberger, 2009). These interneurons form mainly (but not exclusively) local recurrent connections to both the soma (in particular the axonal initial segment) and the dendrites of the pyramidal neurons, and therefore provide a feed-back loop which dampens excitatory input, but might be also involved in dendritic computation (see Section 2.2).

More information about the anatomy and the properties of single cells can be found in textbooks and review articles (e.g., Paxinos, 2004; Duvernoy, 2005; Andersen et al., 2007; van Strien et al., 2009; Klausberger, 2009; Cutsuridis et al., 2010)

2.5.2. Place cells

In a given environment a large fraction of pyramidal neurons in CA1 and CA3 display sensitivity to the current position (O'Keefe and Dostrovsky, 1971; O'Keefe, 1976; Ekstrom et al., 2003; Mizuseki et al., 2012). The receptive fields are referred to as "place fields"; and the same neurons encode for different positions in different environments, i.e., the place fields are environment specific and the place field in one environment does not predict the place field in another (Muller and Kubie, 1987; Colgin et al., 2008).

Additionally to such "global remapping" (or total remapping) where the firing rate as well as firing fields are altered, more subtle remapping, "rate remapping" are reported (relevant literature is reviewed in Leutgeb et al., 2005b; Colgin et al., 2008). In rate remappings substantial changes in the firing rates are observed, but place field locations are little shifted. They are more likely to be observed when the environmental changes are small (e.g., changing the wall color of a room, cf. Figure 2.24A). Global remapping is more likely to be induced by larger changes (like complete replacement to a new room, cf. Figure 2.24B). In new environments place fields emerge on the time-scale of minutes (Bostock et al., 1991; Wilson and McNaughton, 1993), but can be stable in a non-changing environment for long time periods up to months (Thompson and Best, 1990; Agnihotri et al., 2004).

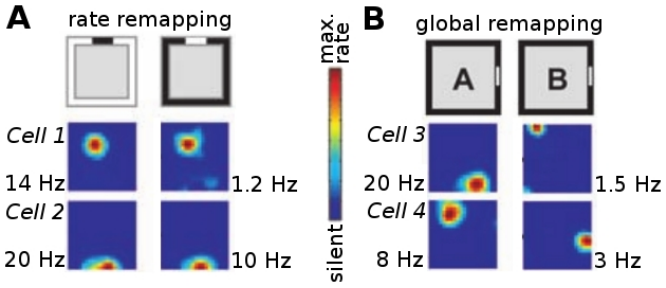

Figure 2.24: Global vs. rate remapping. The panels show the location depend firing rate of four cells (in a square box) and the remapping of the receptive field due (A) to changes of the wall color or (B) replacement to another box. The maximal firing rate (corresponding to red color) is given next to each rate map. Figure modified from Leutgeb et al. (2005a) with permission.

We remark that additionally to the key role in spatial representation, there is evidence that position is only one of the — although very important — facets stored in the hippocampal network (cf. reviews Eichenbaum et al., 1999; Leutgeb et al., 2005b; Colgin et al., 2008; Moser et al., 2008, and references therein): For example single place cells might have different place fields in the same environment while different tasks are performed, or for different running directions (e.g., Markus et al., 1995; Wood et al., 2000). Place-fields might also be altered by other non-spatial influences (e.g., presentation of odors or fear conditioning, Wood et al., 1999; Moita et al., 2004).

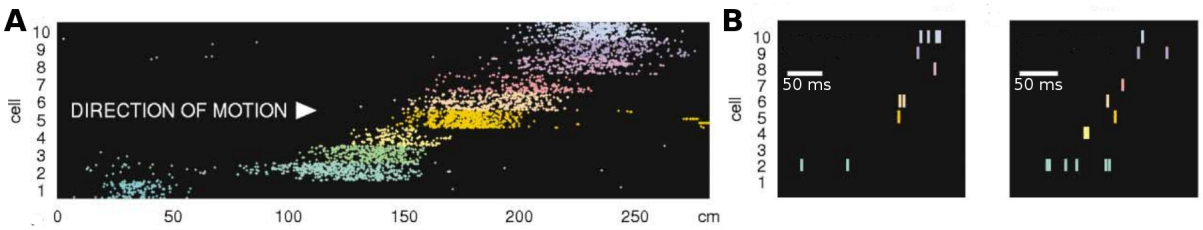

Figure 2.25: Replay of experienced spike sequences. (A) Spike raster plot from 10 CA1 cells (different colors) from 30 runs along a linear track (for each cell the recordings from every trial are placed one over each other). (B) Activity of the same cells during slow-wave sleep following the exploration. Modified from Lee and Wilson (2002) with permission.

2.5.3. Activity patterns in the hippocampus

Movement on a linear track

We now consider the run along a linear track (cf. also Figure 2.19). During the traversal of the track, neurons which encode a position in this particular environment are activated in the same order as the the place fields are traversed, and thus define a spike pattern (sequence) that corresponds to that specific track. Interestingly, this sequence is replayed during sleep or resting phases following the exploration in a highly compressed manner (Wilson and McNaughton, 1994; Nadasdy et al., 1999; Lee and Wilson, 2002; Ji and Wilson, 2007; Davidson et al., 2009, and cf. also Figure 2.25).

Theta phase precession

The learning of spike patterns taking places during exploration is most likely based on the phenomenon of phase precession, a form of temporal coding of position complementing the rate coding discussed above (cf. also Section 2.4.1 and Figure 2.19).

While exploration of space prominent rhythmic modulations of the local field potential (LFP) in the frequency range $4 - 10$Hz, called theta oscillations, are observed, and the timing of single spikes of place cells reflects the position within the corresponding place field (O'Keefe and Recce, 1993; Skaggs et al., 1996; Mehta et al., 2002; Maurer and McNaughton, 2007; Gupta et al., 2012): When entering the place field spikes occur preferentially late in the theta-cycle and move to earlier and earlier times while the place field is traversed (cf. Figure 2.26).

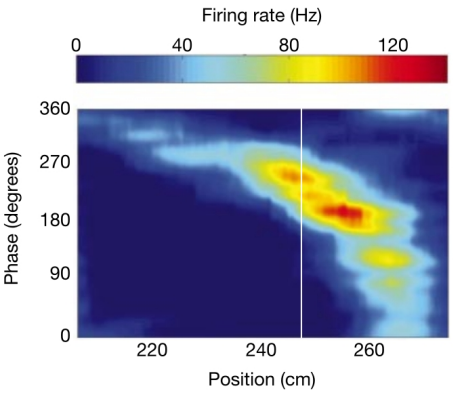

Figure 2.26: Hippocampal spatio-temporal field. The firing rate of a hippocampal neuron as a function of position and phase. Modified from Mehta et al. (2002) with permission.

Neurons with overlapping place fields are activated during one theta-cycle, and the phenomenon of phase precession yields a compressed representation of recently traversed, present and future locations in space: Neurons representing positions already passed, spike (on average) early in each theta cycle (i.e., at lower phases with respect to the theta rhythm), followed by neurons representing the present position and neurons corresponding to places that will be passed in the future. The average time difference between spikes of place cells with nearby place field centers is in the order of tens of milliseconds and therefore perfectly suited for inducing spike time dependent plasticity (cf. Section 2.1.4). Thus, the combination of the compressed representation of the sequence of locations by phase precession favors the emergence of feed-forward structures (Skaggs et al., 1996; Buzsáki, 2006; Mehta et al., 1997; Bush et al., 2010). These structures are candidates for the later replay of the spike sequences during sleep (cf. also "Spatial exploration phase" in Chapter 7).

Sharp-Wave-Ripples

The replay of experienced spike patterns occurs in sleep (slow-wave sleep) or resting phases after exploration during short phases of strongly enhanced network activity, called "sharp waves", superimposed by high-frequency oscillations, called "ripples" (Buzsáki et al., 1992; Ylinen et al., 1995; Maier et al., 2003, 2011; Buzsáki and Silva, 2012). The sharp-wave-ripple complex (SWR) has a duration of approximately $50 - 150$ms and the ripple frequency is in the range of $100 - 200$Hz (cf. Figure 2.27). SWRs are reported all over the hippocampus and in parts of the entorhinal cortex, however, the superimposed oscillations are most prominent and have the highest frequency (up to 200Hz) in the CA1 region (Chrobak and Buzsáki, 1996; Csicsvari et al., 1999a; Andersen et al., 2007; Sullivan et al., 2011).

A moderate fraction of approximately $10 - 20\%$ of pyramidal neurons (Ylinen et al., 1995; Buzsáki and Silva, 2012) contribute only a single spike or single burst (Buzsáki et al., 1992) to the SWR event, nonetheless, the coordination of single neuronal discharges over the whole CA3-CA1-subicular complex-EC region makes them the most synchronous event observed in the mammalian brain (Chrobak and Buzsáki, 1996; Csicsvari et al., 1999a,b, 2000; Buzsáki and Silva, 2012). Although, the sharp-wave is highly coordinated over all participating areas via the polysynaptic loop, the high-frequency oscillations (ripples), in particular in CA1, are generated locally (Ylinen et al., 1995; Csicsvari et al., 1999a; Maier et al., 2011; Sullivan et al., 2011).

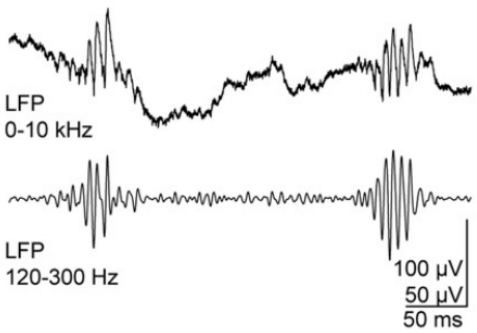

Figure 2.27: Unfiltered extracellular local field potential (LFP) recording of SWRs in CA1 (top) and $120 - 300$Hz bandpassed-filtered version (below). Figure reproduced from Maier et al. (2011) with permission.

Models of Sharp-Wave-Ripples

Experiments show that the pyramidal neurons fire action potentials synchronized to the local field potential oscillations (ripples) during the SWRs (Buzsáki et al., 1992; Csicsvari et al., 1999b; Maier et al., 2011). Likewise the spiking probability of various types of interneurons change during the SWR events (Klausberger et al., 2003, 2004, 2005; Klausberger, 2009). In particular, basket cells (targeting the soma of pyramidal neurons — and therefore having a powerful direct inhibitory control) and bi-stratified cells (targeting the dendrites in stratum radiatum and stratum oriens) show increased spiking activity in SWR episodes (Klausberger et al., 2003, 2004).

This observations lead to the idea that transiently increased excitatory input (e.g., from CA3 to CA1 via the Schaffer collaterals) during sharp-waves excites oscillations in the interneuron network of basket cells (Ylinen et al., 1995; Buzsáki and Chrobak, 1995; Brunel and Wang, 2003; Geisler et al., 2005). The induced oscillations in the sharp-wave ripple frequency range then entrain the phasic spiking of the pyramidal cells (Ylinen et al., 1995; Buzsáki and Chrobak, 1995; Brunel and Wang, 2003; Geisler et al., 2005). Alternatively, it was proposed that the high-frequency oscillations are based on axo-axonal gap junctions (Traub et al., 1999; Traub and Bibbig, 2000; Maex and Schutter, 2007). Here, it is assumed that the axons of the pyramidal neurons form a sparse (electrically coupled) network, where spikes may propagate and multiply in the presence of transiently increased depolarizing input. This yields rhythmic generation of bursts of axonal spiking, which excites the pyramidal cell somata to spike after antidromic and orthodromic propagation.

The third model (considered in Chapter 7) is based on fast dendritic spikes (Memmesheimer, 2010): Spontaneous fluctuations (or appropriate stimulations) cause (weakly) synchronized firing of a subset of pyramidal neurons. The impact of this synchronized pulse on postsynaptic neurons is amplified by synchrony sensitive dendritic spikes (cf. also Section 2.2.2), and thus generates an even more synchronized pulse which in turn may cause synchronous spiking in the subset of postsynaptic neurons, etc. By this mechanism larger and larger groups of neurons spike synchronously and establish neuronal oscillations resembling an SWR events. The oscillation frequency (time difference between subsequent groups) is determined by the conductance delays and the initiation time of dendritic sodium spikes. For sparsely and locally coupled networks (like CA1) and plausible parameters for dendritic spike generation (cf. Ariav et al., 2003; Müller et al., 2012) the oscillation frequency is in the range of approximately 200Hz, for more globally coupled networks (and thus larger average conductance delays; like CA3) it decreases (Memmesheimer, 2010), consistent with experimental findings (Chrobak and Buzsáki, 1996; Ylinen et al., 1995; Csicsvari et al., 1999a; Sullivan et al., 2011). This may also explain, why the ripple frequency in *in vitro* slice is generally higher than those detected *in vivo* (Maier et al., 2003; Nimmrich et al., 2005; Both et al., 2008), since long-range connections are decreased during the preparation. We remark that we discuss the plausibility of this model comprehensively in the light of recent experimental findings in Chapter 7.

Replay

Replay of experienced spike sequences during sleep has been demonstrated in a wealth of experimental studies (Wilson and McNaughton, 1994; Nadasdy et al., 1999; Lee and Wilson, 2002; Ji and Wilson, 2007; Davidson et al., 2009, and others) and is thought be initiated in CA3 (Chrobak and Buzsáki, 1996; Csicsvari et al., 1999a, 2000; O'Neill et al., 2008). In this comparatively densely coupled region an initial coincident activation (spontaneously or induced) of a subgroub of cells ("initiator cells" Buzsáki, 1989) is assumed to trigger the activation of the whole previously stored sequence (cf. also Section 2.4.2 about signal transmission in feed-forward networks). Then the activity is projected to region CA1 via the Shaffer Collaterals, where the high-frequency oscillations are superimposed by a local network mechanism (see subsections above).

A replay in CA1 itself based on recurrent connections is assumed to be unlikely because of the sparse recurrent connectivity. However, recent *in vivo* experiments with mutants having a projection from CA3 to CA1 (Shaffer collaterals) that can be temporally deactivated (Nakashiba et al., 2008, 2009), have shown that replay during SWRs in CA1 still persists if CA1 is deafferented from CA3 (Nakashiba et al., 2009).

2.5.4. A unified model of sharp-wave-ripple events and replay

In this thesis we demonstrate that fast dendritic spikes (as found in CA regions), allow a replay in very sparse networks (Chapter 3 and 4). In particular, in Chapter 7 we argue that even the sparse recurrent connectivity in CA1 is indeed sufficient to induce dendritic sodium spikes in the basal dendrites of pyramidal neurons during SWR events in the absence of input from CA3. Similiarly, a replay in CA3 based on recurrent connections is possible, however, the oscillation frequency is reduced by long-ranging connections (cf. also Memmesheimer, 2010). Whereas usually studied as separated effects, in our approach the replay, the sharp-wave and the superimposed high-frequency oscillations are intimately interrelated with each other (Chapter 7). Furthermore, we show that high-frequency oscillations itself may foster replay of previously learned spike patterns (Chapter 6), and that such network oscillations naturally emerge in networks with heavy-tailed degree distribution (Chapter 5).

2.6. Remark on simulation strategies

2.6.1. Hybrid systems

In favor of an efficient numerical simulations of neural networks, it is reasonable to rewrite the model equations defining the dynamics of the membrane potential (e.g., Equations 2.2 and 2.4) and the synaptic currents (cf. Equations 2.12 and 2.13) to a hybrid system (Brette et al., 2007): Let the vector $\vec{X}(t)$ define the state of a single neuron: the membrane potential and other state variable, e.g., the state of activated currents, gates or conductances. The state $\vec{X}$

evolves *continuously* according to some function $f(\vec{X})$, and spikes received by synapses cause *non-continous* changes in some of the state variables,

$$\frac{d\vec{X}}{dt} = f(\vec{X}) \tag{2.30}$$

$$\vec{X} \leftarrow h_n(\vec{X}) \quad \text{upon spike arrival from synapse } n. \tag{2.31}$$

To be more specific, we consider the leaky integrate-and-fire neuron with one single exponential conductance-based synapse (cf. Section 2.1.2 and 2.1.3),

$$C_\mathrm{m}\frac{dV}{dt} = g_\mathrm{L}\left(E_\mathrm{L} - V\right) + \left(E - V\right) g_\mathrm{max} \sum_i \Theta(t - t_i)\left(e^{-(t-t_i)/\tau_1}\right), \tag{2.32}$$

where C_m is the membrane capacity, g_L the leak conductance, E_L the leak potential, g_max the maximal conductance induced by a single presynaptic spike, τ_1 the decay time constant of the postsynaptic conductance transient, and t_i the arrival time of the ith presynaptic input. The state $\vec{X}$ of the neuron is given by the membrane potential $X_1 = V$ and the actual value of the synaptic conductance $X_2 = g$; the system evolves according to

$$\frac{d\vec{X}}{dt} = f(\vec{X}) = \begin{pmatrix} \frac{1}{C_\mathrm{m}}\left[g_\mathrm{L}\left(E_\mathrm{L} - X_1\right) + \left(E - X_1\right)\left(X_2\right)\right] \\ -\frac{1}{\tau_1}X_2 \end{pmatrix} \tag{2.33}$$

$$h_n(\vec{X}) = \begin{pmatrix} X_1 \\ X_2 + g_\mathrm{max} \end{pmatrix}. \tag{2.34}$$

The advantage of this formalism is that the temporal development of the state of a neuron does not explicitly depend on the former spike times t_i, and thus spike times need not to be stored. For Hodgkin-Huxley type neurons the state vector $\vec{X}$ has to be extended by the gating variables (cf. Equations 2.5 - 2.7). Likewise the extension to double exponential or α-function shaped kernels is straightforward. Spike time dependent synaptic plasticity (STDP; cf. Section 2.1.4) can also be included into this formalism by keeping track of previous spikes by an additional variable which decays according to the temporal interaction window (Song et al., 2000; Morrison et al., 2007, 2008).

Spikes are emitted and transferred to postsynaptic neurons when the threshold condition is satisfied, e.g., for integrate-and-fire neurons when the $V = X_1 \geq \Theta_\mathrm{V}$. The membrane potential is reset $V = X_1 \leftarrow V_\mathrm{reset}$ (if applicable), and an absolute refractory time can be introduced by holding the membrane potential to the reset value for the refractory time period.

2.6.2. Simulation strategies

There are two different approaches to simulate the dynamics of neural networks (Brette et al., 2007): Synchronous ("clock-driven") simulation strategies, where the neuronal dynamics of all units is updated simultaneously; and asynchronous ("event-driven") simulation strategies, where the state of a unit is updated only when it sends or receives a spike.

Both approaches have its advantages and disadvantages: Clock-driven algorithms can be implemented comparatively easily independent of the complexity of the neuron model. However, spike times are bound to a discrete grid and thus the precision of the simulation results might be an issue. Event-driven algorithms are "more precise", ideally exact, in the sense that at each point in time the next event (sending or receiving of spikes) is determined and the system is updated accordingly. However, for complex neuron models this determination might become arbitrary difficult and time consuming (consider, e.g., the complex dynamics of Hodgkin-Huxley type neurons) and an event-driven algorithm might not be affordable.

Clock-driven algorithms

For numerical simulations of networks of leaky integrate-and-fire neurons with temporal extended interactions (Chapter 3 – 7) and Hodgkin-Huxley type neurons (Chapter 3), we employ a clock-driven algorithm. We use the "NEural Simulation Tool" (NEST; Gewaltig and Diesmann, 2007), a software developed for clock-driven simulations of spiking neural networks. It is optimized to scope with large networks with a high number of synaptic connections and supports parallel computing. Some standard neuron models are available in the NEST release, and it is comparatively simple to extend the simulation engine by own models: One has to define a new model as an C++-class, provide methods for initialization and update of neuronal dynamics, and handlers for spiking events (more in formation can be found in Gewaltig and Diesmann, 2007).

In clock-driven simulations the state variables are updated in time intervals dt. After each update the neurons are tested if the threshold condition is satisfied, and if so, the relevant neurons are reset and spikes are generated. Spikes are stored in circular array (spike list), where each element corresponds to a future time bin and specifies the arrival of the spikes at the postsynaptic neurons (Morrison et al., 2005). A pseudo-code representation of the algorithm is shown in Figure 2.28. It is straight forward to include external random input spike trains in the formalism by inserting the arriving spikes in the spike list or handle them in a separate circular array.

The drawback of this approach is that spikes are aligned to a grid, thus the simulation results are approximate even when the state update is computed exactly. Additionally, there is small probability that spikes are missed because the threshold condition is checked only in intervals of dt. However, both approximation errors generally decrease with decreasing time bin dt, appear to have only minor effects on the statistical measures of network dynamics and are less serious for models with continuous postsynaptic responses. Yet, the errors can become a serious for systems with instantaneous postsynaptic responses. Here the strong, jump-like nonlinearity in the membrane potential (cf. Equation 2.14), particularly in combination with highly synchronized network events, might cause delay, cancellation and generation of such synchronous pulses (Brette et al., 2007; Rudolph and Destexhe, 2007).

```
time = 0
while ( time < total time )
  for every neuron
    advance neuron dynamics by dt
    process incomming spikes from spike list
  end

  for every neuron
    if ( threshold condition satisfied )
      reset neuron (if applicable)
      for every outgoing connection
        insert spike in spike list
      end
    end
  end

  time = time + dt
end
```

Figure 2.28: Pseudo-code of simple clock-driven simulation scheme.

Event-driven algorithms

In Chapter 3 and 4 we verified some of the analytical results by network simulations of leaky integrate-and-fire neurons with jump-like postsynaptic potentials (i.e., currents with infinitesimal fast rise and decay, cf. Equation 2.14). Here we took advantage of the very simple single neuronal dynamics and implemented a standard event-driven algorithm (cf. pseudo-code in Figure 2.29).

In an initialization phase for every neuron the next spike times are computed (which might be $+\infty$) and stored in an ordered list (NextSpikeList). Spikes which have been already emitted but not reached the postsynaptic neurons are stored in a second ordered list (ArrivalSpikeList), which might be empty or not initially. External random spikes might be stored in an additional list or inserted in the list of arrival spikes (not explicitly considered in the simple pseudo-code in Figure 2.29).

Each iteration starts with evaluating the next event, which can be sending of a spike or receiving of a spike. Then the state of the relevant neuron (sender or receiver) is updated and the action (sending and reset, or receiving of spike) is computed and the spike lists are updated accordingly. For systems with homogenous delays, one might store each spiking event only once in the ArrivalSpikeList and consider the complete set of postsynaptic neurons at spike arrival.

In our example (Equation 2.14) the state vector of each neuron is one-dimensional (just the membrane potential) and spikes simply induce jumps in the membrane potential,

$$\frac{dV}{dt} = \frac{1}{\tau_{\mathrm{m}}} \left(E_{\mathrm{L}} - V \right) \tag{2.35}$$

$$h_n = (V + \epsilon), \tag{2.36}$$

```
for every neuron
  compute time to next spike
  insert event in NextSpikeList
end

time = 0
while (NextSpikeList not empty) or (ArrivalSpikeList not empty)
  (NextArrivalTime, postsynaptic neuron j, weight )
                <- extract event with lowest timing from ArrivalSpikeList
  (NextSpikeTime,   spiking neuron i )
                <- extract event with lowest timing from NextSpikeList


  if NextSpikeTime < NextArrivalTime
    t <- NextSpikeTime
    compute state of neuron i at time t
    reset neuron
    compute timing of next spike of neuron i
    insert event in NextSpikeList

    for every outgoing connection of neuron i
      insert event (Arrival time, postsynaptic neuron, strength) in ArrivalSpikeList
    end
  else
    t <- NextArrivalTime
    compute state of neuron j at time t
    change state of neuron j according to weight
    compute timing of next spike of neuron j
    insert/change/suppress event in NextSpikeList
  end

  if t > maximal simulation
    finish simulation
  end

end
```

Figure 2.29: Pseudo-code of simple event-driven simulation scheme.

where τ_{m} is the membrane time, E_{L} the leak potential (which might be shifted by additional constant currents) and ϵ the interaction strength. The solution of Equation (2.35) is an exponential function and thus the update of a neurons' state is given by

$$V(t + \Delta T) = E_{\mathrm{L}} - e^{-\frac{\Delta T}{\tau_{\mathrm{m}}}} \left(E_{\mathrm{L}} - V(t)\right), \tag{2.37}$$

and the time interval to the next spike of a neuron is

$$\Delta t = \begin{cases} \tau_{\mathrm{m}} \log\left(\frac{E_{\mathrm{L}} - V(t)}{E_{\mathrm{L}} - \Theta}\right) & \text{if } E_{\mathrm{L}} > \Theta \\ +\infty & \text{if } E_{\mathrm{L}} \leq \Theta \end{cases}. \tag{2.38}$$

If all external currents are sub-threshold ($E_{\mathrm{L}} \leq \Theta$) the NextSpikeList list has not to be considered, because neurons may generate spikes only in response to arriving spikes (from the network or from external sources).

Chapter 3

Original Manuscript: Propagating sychrony in feed-forward networks

Citation

Jahnke, S., Memmesheimer, R.-M. and Timme, M. (2013), Propagating synchrony in feed-forward networks, *Front. Comp. Neurosc.*, **7**, 153, DOI:10.3389/fncom.2013.00153

Original contribution

Conception and design of the study together with R.-M. Memmesheimer and M. Timme. I performed the analytical calculations and numerical simulations. For the simulations I wrote own code (C++ and python modules) and implementated neuron models within the NEST simulation environment (www.nest-initiative.org). I analyzed the data and prepared all figures. I wrote main parts of the manuscript supported by R.-M. Memmesheimer and M. Timme.

Göttingen, 31.03.2014
Place, Date

Sven Jahnke

frontiers in
COMPUTATIONAL NEUROSCIENCE

ORIGINAL RESEARCH ARTICLE
published: 15 November 2013
doi: 10.3389/fncom.2013.00153

Propagating synchrony in feed-forward networks

***Sven Jahnke*[1,2,3]*, *Raoul-Martin Memmesheimer*[4] *and Marc Timme*[1,2,3]**

[1] *Network Dynamics, Max Planck Institute for Dynamics and Self-Organization (MPIDS), Göttingen, Germany*
[2] *Bernstein Center for Computational Neuroscience (BCCN), Göttingen, Germany*
[3] *Fakultät für Physik, Georg-August-Universität Göttingen, Göttingen, Germany*
[4] *Department for Neuroinformatics, Donders Institute, Radboud University, Nijmegen, Netherlands*

Edited by:
Tatjana Tchumatchenko, Max Planck Institute for Brain Research, Germany

Reviewed by:
Robert Rosenbaum, University of Pittsburgh, USA
Arvind Kumar, University of Freiburg, Germany
Raul C. Muresan, Romanian Institute of Science and Tehnology, Romania

****Correspondence:***
Sven Jahnke, Network Dynamics, Max Planck Institute for Dynamics and Self-Organization (MPIDS), Am Faßberg 17, 37077 Göttingen, Germany
e-mail: sjahnke@nld.ds.mpg.de

Coordinated patterns of precisely timed action potentials (spikes) emerge in a variety of neural circuits but their dynamical origin is still not well understood. One hypothesis states that synchronous activity propagating through feed-forward chains of groups of neurons (synfire chains) may dynamically generate such spike patterns. Additionally, synfire chains offer the possibility to enable reliable signal transmission. So far, mostly densely connected chains, often with all-to-all connectivity between groups, have been theoretically and computationally studied. Yet, such prominent feed-forward structures have not been observed experimentally. Here we analytically and numerically investigate under which conditions diluted feed-forward chains may exhibit synchrony propagation. In addition to conventional linear input summation, we study the impact of non-linear, non-additive summation accounting for the effect of fast dendritic spikes. The non-linearities promote synchronous inputs to generate precisely timed spikes. We identify how non-additive coupling relaxes the conditions on connectivity such that it enables synchrony propagation at connectivities substantially lower than required for linearly coupled chains. Although the analytical treatment is based on a simple leaky integrate-and-fire neuron model, we show how to generalize our methods to biologically more detailed neuron models and verify our results by numerical simulations with, e.g., Hodgkin Huxley type neurons.

Keywords: synchrony, networks, synfire chains, spike pattern, mathematical neuroscience, non-additive coupling, non-linear dendrites

1. SPIKE PATTERNS AND SIGNAL TRANSMISSION IN NEURONAL CIRCUITS

Reliable signal transmission is a core part of neuronal processing. A common hypothesis states that activity propagating along neuronal sub-populations that are connected in a feed-forward manner may support such signal transmission. Indeed, there is strong indication that activity propagation along feed-forward structures drives the generation of bird songs (Long et al., 2010) and experiments have shown propagation of synchronous and rate activity in feed-forward networks (FFNs) *in vitro* (Reyes, 2003; Feinerman et al., 2005; Feinerman and Moses, 2006). Sequential replay in the hippocampus and in neocortical networks also suggest underlying feed-forward mechanisms (August and Levy, 1999; Nadasdy et al., 1999; Lee and Wilson, 2002; Leibold and Kempter, 2006; Xu et al., 2011; Eagleman and Dragoi, 2012; Jahnke et al., 2012) and propagation of synchronous activity along feed-forward chains is a possible explanation for experimentally observed precise spike timing in the cortex (Riehle et al., 1997; Kilavik et al., 2009; Putrino et al., 2010). Further, the modular, hierarchical structure of many sensory and motor systems suggests propagation over sequences of areas in feed-forward manner, e.g., in bottom-up signal transfer (Felleman and Van Essen, 1991; Scannell et al., 1999; Bullmore and Sporns, 2009; Kumar et al., 2010).

Feed-forward structures which support the propagation of synchronous activity are termed synfire chains. The concept was introduced by Abeles (1982) as groups of neurons (layers) with dense anatomical connections between subsequent groups that are embedded in otherwise roughly randomly connected local neural circuits. Two major questions regarding the dynamical options for synfire activity include a) how synchrony may actively propagate and b) how such spatio-temporally coordinated spike timing may be robust against irregular background activity, because the synfire chains are part of a cortical network with dynamics defined by the so-called irregular balanced state (van Vreeswijk and Sompolinsky, 1996, 1998).

Addressing these points, theoretical studies have established conditions for stable propagation of synchrony in synfire chains (Diesmann et al., 1999; Gewaltig et al., 2001). Most synfire chain models assume functionally relevant FFNs that exhibit a very dense, often all-to-all connectivity between subsequent layers (Aviel et al., 2003; Mehring et al., 2003; Kumar et al., 2008) (see also a recent review on this topic Kumar et al., 2010). Such highly prominent feed-forward-structures, however, have not been found experimentally. Since cortical neural networks are overall sparse (e.g., Braitenberg and Schüz, 1998; Holmgren et al., 2003), we may also expect some level of dilution for embedded feed-forward chains. So far, computational model studies assumed that such chains created from existing connections in sparse recurrent networks exhibit strong synaptic efficiencies and specifically modified neuron properties to enable synchrony propagation (Vogels and Abbott, 2005).

Recently, we have shown that non-additive dendritic interactions promote propagation of synchrony (Jahnke et al., 2012). The non-additive dendritic interactions considered are mediated by fast dendritic spikes (Ariav et al., 2003; Gasparini et al., 2004; Polsky et al., 2004; Gasparini and Magee, 2006): upon stimulation within a time interval less than a few milliseconds, dendrites are capable of generating sodium spikes. These induce a strong, short and stereotypical depolarization in the soma. If this depolarization elicits a somatic spike, the spike occurs a fixed time interval after stimulation with sub-millisecond precision. This dendritic non-linearities relax the requirement of dense feed-forward anatomy and thereby allow for robust propagation of synchrony even in *diluted* FFNs with synapses of moderate strength within the biologically observed range.

In the present article, we analytically and numerically investigate in detail under which conditions synchronous activity may reliably propagate along the layers of an FFN where the inter-group connectivity is diluted, as may be expected when they are part of a sparse cortical network. An embedding network is mimicked by external, noisy input. We study the influence of the network setup, including the influence of the emulated embedding network, and of different types of standard linearly additive as well as non-additive dendritic interactions.

We derive analytical estimates for the critical connectivity—the minimal connectivity that allows robust propagation of synchrony. Some fundamental analytical results, in particular the ansatz for deriving a critical connectivity in the first place, have been briefly reported before (Jahnke et al., 2012). Here, we extend the approach and show how the bifurcation point, i.e., the transition point from the non-propagating to the propagating regime, can be estimated quantitatively from the neurons' ground state properties. We investigate the validity range of the analytical predictions and check them via direct numerical simulations. Furthermore, we discuss the applicability of our results to biologically more detailed neuron models and network setups. In particular, we argue that the assumptions underlying the analytical approach are met by a wide class of neuron models, including, e.g., conductance based leaky integrate-and-fire and Hodgkin–Huxley-type neurons.

The article is structured as follows: After introducing the neuron model and network setup in section 2, we study in the main part the propagation of synchrony in linearly coupled FFNs (section 3.1) and in FFNs incorporating dendritic non-linearities (section 3.2). In particular, we derive tools to study the system analytically, compare the results to computer simulations and elaborate differences of the dynamics of FFNs with and without non-additive dendritic interactions. In the final part (section 3.3), we discuss the application of our analytical results to biologically more detailed neuron models.

2. METHODS AND MODELS

2.1. NEURON MODEL

2.1.1. Linear model

Consider networks of leaky integrate-and-fire neurons that interact by sending and receiving spikes via directed connections. The state of neuron k at time t is described by its membrane potential $V_k(t)$ and its dynamics satisfy

$$\frac{dV_k(t)}{dt} = -\frac{V_k(t)}{\tau_k^{\mathrm{m}}} + I_k^{\mathrm{const}} + I_k^{\mathrm{net}}(t) + I_k^{\mathrm{ext}}(t), \tag{1}$$

where τ_k^{m} is the membrane time constant of neuron k, $I_k^{\mathrm{const}} := I_k^0/\tau_k^{\mathrm{m}}$ a constant input current, $I_k^{\mathrm{net}}(t)$ the input current caused by spikes within the network and $I_k^{\mathrm{ext}}(t)$ the input current arising from spikes from external sources. When the neuron's membrane potential reaches or exceeds the threshold Θ_k its membrane potential is reset to V_k^{reset} and a spike is sent to the postsynaptic neurons n, where it changes the postsynaptic potential after a delay τ_{nk}. After emitting a spike at $t = t_0$ the neuron becomes refractory for a time period t^{ref}, i.e., $V_k(t) = V_k^{\mathrm{reset}}$ for $t \in \left[t_0, t_0 + t^{\mathrm{ref}}\right]$.

To keep the model analytically tractable, we model the fast rise of the membrane potential upon the arrival of presynaptic spikes by instantaneous jumps of the membrane potential, such that the resulting input current reads

$$I_k^{\mathrm{net}}(t) = \sum_l \sum_m \epsilon_{kl} \delta\left(t - t_{lm}^f - \tau_{kl}\right). \tag{2}$$

Here ϵ_{kl} denotes the coupling strength from neuron l to neuron k, t_{lm}^f is the mth spike time of neuron l and τ_{kl} specifies the synaptic delay. In addition to spikes from the network each neuron receives excitatory and inhibitory random inputs that emulate an embedding network. These external inputs are modeled as random Poisson spike trains with rate ν^{exc} and ν^{inh}, respectively. The resulting input current is given by

$$I_k^{\mathrm{ext}}(t) = \sum_m \epsilon^{\mathrm{exc}} \delta\left(t - t_{km}^{\mathrm{ext,\,exc}}\right) + \sum_m \epsilon^{\mathrm{inh}} \delta\left(t - t_{km}^{\mathrm{ext,\,inh}}\right), \tag{3}$$

where $t_{km}^{\mathrm{ext,\,exc}}$ ($t_{km}^{\mathrm{ext,\,inh}}$) is the arrival time of the mth excitatory (inhibitory) spike to neuron k and $\epsilon^{\mathrm{exc}} > 0$ ($\epsilon^{\mathrm{inh}} < 0$) denote the corresponding coupling strength.

2.1.2. Non-linear model

In the above model all input currents are summed up linearly. To also investigate the effect of dendritic spikes we modulate the sum of synchronously arriving excitatory inputs by a non-linear dendritic modulation function $\sigma_{NL}(\cdot)$. This can be directly read off from experimental data (Ariav et al., 2003; Gasparini et al., 2004; Polsky et al., 2004; Gasparini and Magee, 2006): If the sum of excitatory inputs is below the dendritic threshold Θ_b, the single inputs are processed linearly ($\sigma_{NL}(\cdot)$ equals the identity). If the sum of inputs exceeds the dendritic threshold Θ_b, the depolarization is strongly non-linearly enhanced compared to that expected from linear summation. This is, in biological terms, due to a dendritic spike elicited. Larger inputs have been experimentally found to not further increase the somatic peak depolarization. The dendritic modulation function may then be modeled as

$$\sigma_{NL}(\epsilon) = \begin{cases} \epsilon & \text{for } \epsilon < \Theta_b \\ \kappa & \text{otherwise} \end{cases}. \tag{4}$$

The dendrites process synchronous inputs non-additively: inputs below the dendritic threshold are summed linear, inputs above this threshold are summed supra-linear and, due to the saturation, very large inputs are summed sub-linear.

If not stated otherwise, we consider only exactly simultaneous arriving spikes as sufficiently synchronous; to allow for exactly simultaneous arrivals, the synaptic delays are chosen as homogeneous $\tau_{kl} \equiv \tau$. The input currents caused by spikes that are received from the network are then given by

$$I_k^{\text{net}}(t) = \sum_{t^f} \left[\sigma_{NL} \left(\sum_{l \in M_{\text{exc}}(t^f)} \epsilon_{kl} \right) + \sum_{l \in M_{\text{inh}}(t^f)} \epsilon_{kl} \right] \delta\left(t - t^f - \tau\right). \quad (5)$$

Here, the sum over t^f denotes the sum over all times at which spike(s) are sent in the network, irrespective of which neuron(s) is (are) spiking. The sets $M_{\text{exc}}\left(t^f\right)$ and $M_{\text{inh}}\left(t^f\right)$ specify the set of neurons that send an excitatory or inhibitory spike at time t^f, respectively. (To describe a network with linear dendrites $\sigma_{NL}(\epsilon)$ is replaced by ϵ).

In section 3.3.1 we consider inhomogeneous delay distributions and finite dendritic integration window Δt (i.e., non-linear amplification of inputs received within finite time interval Δt) and discuss how the results achieved for homogeneous systems can be generalized.

2.2. NETWORK TOPOLOGY

We consider the propagation of synchrony in diluted Feed-Forward-Networks (FFNs, synfire-chains). They consist of a sequence of m layers, each composed of ω neurons. Neurons of one layer form excitatory projections to the neurons of the subsequent layer with probability p; the strength of an existing connection from neuron l to neuron k is denoted by ϵ_{kl}.

For simplicity of presentation, we consider homogeneous neuronal populations, i.e., all neurons have identical properties ($\tau_k^{\text{m}} = \tau^{\text{m}}$, $\Theta_k = \Theta$ and $V_k^{\text{reset}} = V^{\text{reset}}$ for all i), as well as homogeneous coupling strengths, i.e., $\epsilon_{kl} = \epsilon$ if a connection is realized, throughout this article. If not stated otherwise, we use $\tau^{\text{m}} = 14\,\text{ms}$ and $\Theta = 15\,\text{mV}$ as standard values for the membrane time constant and the neuron threshold.

2.3. GROUND STATE DYNAMICS

We consider networks, where the single neurons are placed in a "fluctuation driven regime," i.e., in the ground state the average input to each neuron is sub-threshold and spiking of neurons is caused by fluctuations of the inputs. This setup allows to emulate the dynamics of neurons which are part of a balanced network (van Vreeswijk and Sompolinsky, 1996, 1998). The neurons fire asynchronously and irregularly with low firing rate ν; the spike trains resemble Poissonian spike trains (Tuckwell, 1988; Brunel and Hakim, 1999; Brunel, 2000; Burkitt, 2006). Thus, the inputs to the neurons may be described by three Poissonian spike trains with rates ν^{exc} (external, excitatory), ν^{inh} (external, inhibitory) and $\nu^{\text{int}} = \nu p \omega$ (inputs from the preceding layer). Since the number of inputs N_T^X, $X \in \{\text{exc}, \text{inh}, \text{int}\}$, in a time interval T is Poisson distributed, the expected number of inputs $\langle N_T^X \rangle$ and the variance $\left\langle \left(N_T^X - \langle N_T^X \rangle\right)^2 \right\rangle$, equal $\nu^X T = \langle N_T^X \rangle = \left\langle \left(N_T^X - \langle N_T^X \rangle\right)^2 \right\rangle$. Then

$$\mu = I_0 + \tau^{\text{m}} \nu^{\text{exc}} \epsilon^{\text{exc}} + \tau^{\text{m}} \nu^{\text{inh}} \epsilon^{\text{inh}} + \tau^{\text{m}} p \omega \nu \epsilon \quad (6)$$

is the mean of the total input to the neurons in an interval of the size of the membrane time constant, $T = \tau^{\text{m}}$, and

$$\sigma^2 = \tau^{\text{m}} \nu^{\text{exc}} \left(\epsilon^{\text{exc}}\right)^2 + \tau^{\text{m}} \nu^{\text{inh}} \left(\epsilon^{\text{inh}}\right)^2 + \tau^{\text{m}} p \omega \nu \epsilon^2 \quad (7)$$

is its variance. In diffusion approximation, the distribution of membrane potentials $P_V(V)$ and the mean firing rate ν can be derived analytically (Brunel and Hakim, 1999; Brunel, 2000; Helias et al., 2010). In particular, for networks with low firing rates the probability density of membrane potentials (see, e.g., Tuckwell, 1988)

$$P_V(V) = \frac{1}{\sqrt{\pi \sigma^2}} \exp\left[-\left(\frac{V - \mu}{\sigma} \right)^2 \right] \quad (8)$$

is Gaussian and can be expressed in terms of the input current. In this approximation the average firing rate is

$$\nu = \frac{1}{\sqrt{\pi} \tau^{\text{m}}} \frac{\Theta - \mu}{\sigma} \exp\left[-\left(\frac{\Theta - \mu}{\sigma} \right)^2 \right] \quad (9)$$

and depends on μ and σ only via the quotient

$$\alpha := \frac{\Theta - \mu}{\sigma}, \quad (10)$$

which is the distance of the average input μ from the neurons' threshold Θ normalized by the standard deviation σ of the input. For the analytical derivations throughout this article we focus on the regime of low spiking rates ($\alpha \gtrapprox 2$; $\nu \lessapprox 1.5\text{Hz}$).

In the absence of synchronous activity each neuron receives a large number of inputs from the external network and only a few inputs from the previous layer of the FFN, such that the ground state dynamics of the network is mainly established by the external inputs. To keep the input balanced we choose $\nu^{\text{exc}} = \nu^{\text{inh}} =: \nu^{\text{ext}}$ and $\epsilon^{\text{exc}} = -\epsilon^{\text{inh}} =: \epsilon^{\text{ext}}$ throughout the article.

2.4. PROPAGATION OF SYNCHRONY

To initiate propagating synchronous activity along the considered diluted FFN, we excite in the first layer a subgroup of $g_0 \leq \omega$ neurons to spike synchronously. This causes a synchronous input to the following layer after the synaptic delay τ and may therefore initiate synchronous spiking of a subgroup of neurons in that layer. These may again excite synchronous spiking in the next layer and so on. Depending on the ground state, i.e., the layout of the external network, on the layer size ω, and on the coupling strength ϵ, a synchronous pulse may or may not propagate along the FFN (cf. **Figures 1A,B,D,E**).

In addition to the triggered propagation, one might generally also expect the occurrence of spontaneous propagation of synchronous activity: Neurons of a particular layer share inputs from the previous layer and this causes correlations in their spiking

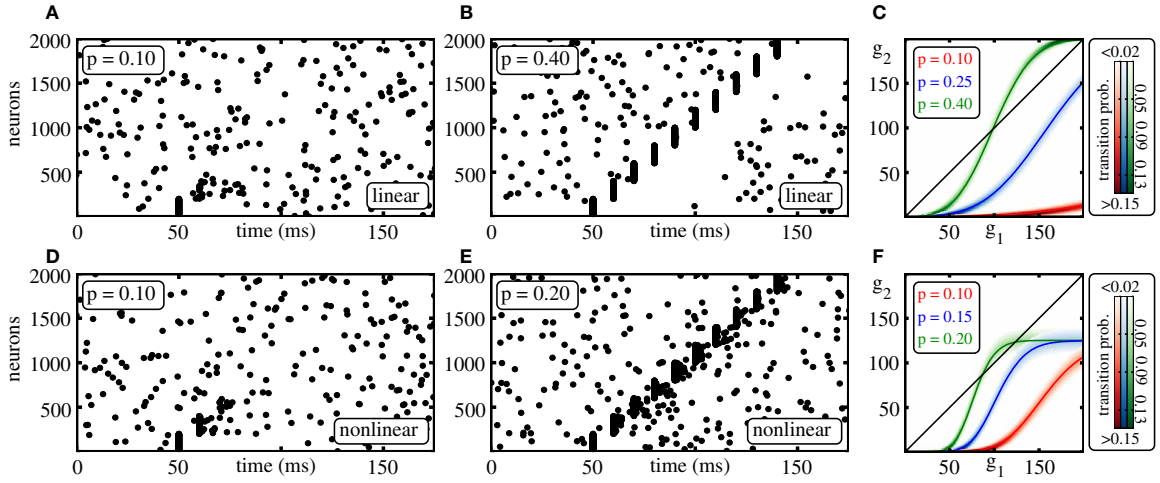

FIGURE 1 | Propagation of synchrony in diluted FFNs. (A,B,D,E) Raster plots of diluted feed-forward networks ($m = 10$, $\omega = 200$, $\epsilon = 0.25$ mV). With increasing connection probability p propagation of synchrony can be enabled **(A,B)** in networks with additive (linear) and **(D,E)** in networks with non-additive (non-linear) dendritic interactions ($\Theta_b = 4$ mV, $\kappa = 11$ mV). **(C,F)** Average number of synchronously active neurons in the second layer, g_2, vs. the number of synchronously active neurons in the initial layer, g_1; panel **(C)** linear, panel **(F)** non-additive dendritic interactions (average over $n = 10,000$ trials: solid line, transition probability: shading). Note that non-linear dendrites allow for sparser connectivity, **(E)** vs. **(B)** and for a sparser code, i.e., for smaller numbers of spiking neurons in an activated group, **(F)** vs. **(C)**.

activity. Over the layers these correlations can accumulate and lead to synchronous spiking (Aviel et al., 2003; Rosenbaum et al., 2010, 2011; Litvak et al., 2013). However, in the setups considered in this article, the effect is negligible due to two reasons: (1) each neuron receives a large number of external (uncorrelated) inputs and this background noise has a decorrelating effect, (2) we study the system near the critical point, i.e., for parameters where even synchronized spiking of all neurons of a particular layer is just sufficient to initiate a propagation of synchrony. Thus, spontaneous propagation of synchrony effectively does not occur.

We study the transition from the non-propagating to the propagating regime by means of a iterated map that yields the expectation value of the number of synchronously spiking neurons g_{i+1} in layer $i+1$ if g_i neurons are synchronously active in layer i. There is always one trivial fixed point, G_0, of this iterated map with $0 = G_0 = g_{i+1} = g_i$, which corresponds to absent activity. If $g_{i+1} < g_i$ for all $g_i > G_0$, synchronous activity will die out after a small number of layers. If $g_{i+1} \geq g_i$ for some substantial group size, $g_i > G_0$, a stable propagation of synchrony may be enabled (cf. **Figures 1C,F**). More precisely, we will show in this article that with increasing connectivity p the system undergoes a tangent bifurcation and two fixed points G_1 and $G_2 \geq G_1$ appear. If existing, G_1 is always unstable (the diagonal is crossed from below; the slope of the iterated map needs to be larger than one) and G_2 is always stable [all connections within the FFN are excitatory such that the iterated map is monotonically increasing (slope larger than zero, in particular larger than -1)]; further at G_2 there is an intersection with the diagonal from above thus the slope is smaller than one and stationary propagation with group sizes around G_2 is enabled.

In computer simulations, we determine for each given network setup by the following procedure whether a propagation is possible: after some initial time t^{init} we excite all neurons of the first layer to spike synchronously and measure the number of active neurons g_i in the ith layer at the expected spiking time $t_i^{\text{exp}} = t^{\text{init}} + i\tau$. If g_i is substantially larger than the number of active neurons arising from spontaneous activity in more than 50% of n trials (i.e., n repetition of the same simulation with different initial conditions), we denote the propagation of synchrony as successful. The critical connectivity p^*, that marks the transition from a regime where propagation of synchrony is not possible to a regime where propagation of synchrony is enabled, is found by determining the lowest connection probability p for which an initial synchronous pulse propagates successfully.

As the connections within the FFN are all excitatory, it is sufficient to check whether propagation of synchrony can be initiated by inducing synchronized spiking of all ω neurons of the first layer: Stationary propagation of synchrony can be enabled if there is a non-trivial stable fixed point (G_2) of the iterated map for the average group size. For purely excitatory connections the basin of attraction of this fixed point is bounded from the left by an unstable fixed point (G_1) and from the right by the maximum group size given by the layer size ω.

3. RESULTS AND DISCUSSION

Under which conditions can synchronous signals propagate robustly along diluted FFNs? To answer this question in detail, we first focus on networks with linear dendrites. Afterwards we study the propagation of synchrony in networks incorporating non-additive dendritic interactions and compare with the linear

case. Finally, we show that the derived results are directly applicable in biologically more detailed neuron models and network configurations.

3.1. FFNs WITH LINEAR DENDRITES

In this section, we consider linearly coupled FFNs. In the first part, we derive analytical estimates for the critical connectivity p_L^* that marks the transition from the non-propagating to the propagating regime; the initial steps follow the lines of Jahnke et al. (2012); Memmesheimer and Timme (2012). In the second part we investigate the influence of the external network on the propagation of synchrony and determine the parameter-region for which the analytical estimates are applicable. In particular, we show that the derived estimates are applicable in the biologically relevant parameter-region, where the spontaneous firing rate is low and the distribution of membrane potentials is sufficiently broad. Finally, we study how the properties of propagating synchronous pulses depend on different system parameters.

3.1.1. Analytical derivation of critical connectivity

To access the properties of propagation of synchrony we consider average numbers of active neurons in the different layers of an FFN: for this, we derive a iterated map which yields the expected number of neurons that will spike synchronously in one layer given that in the preceding layer a certain number of neurons was synchronously active.

If in the ith layer, g_i neurons spike synchronously, the number of synchronous inputs h a single neuron in layer $i+1$ receives follows a binomial distribution $h \sim B\left(g_i, p\right)$. We denote the spiking probability of a single neuron due to an input of strength x by $p_f\left(x\right)$. The average or expected spiking probability $p^{\mathrm{sp}}\left(g_i\right)$ of a single neuron in layer $i+1$ is then given by

$$p^{\mathrm{sp}}\left(g_i\right) = \mathrm{E}\left[p_f\left(h\epsilon\right)\middle|\, g_i\right] = \sum_{h=0}^{g_i} \binom{g_i}{h} p^h \left(1-p\right)^{g_i-h} p_f\left(h\epsilon\right). \quad (11)$$

Here and in the following we denote the expectation value of a function $f(X)$ of a random variable X by $\mathrm{E}[f(X)]$; conditional expectations are denoted by $\mathrm{E}[f(X)|Y]$. The expected number of spiking neurons in layer $i+1$ is then simply

$$\mathrm{E}\left[g_{i+1}\middle|\, g_i\right] = \omega p^{\mathrm{sp}}\left(g_i\right) \quad (12)$$

$$= \omega \sum_{h=0}^{g_i} \binom{g_i}{h} p^h \left(1-p\right)^{g_i-h} p_f\left(h\epsilon\right). \quad (13)$$

If the connection probability p is low and/or the connection strengths ϵ are small, the spontaneous spiking activity in the absence of synchrony is only weakly influenced by the spiking activity within the FFN. Thus as a starting point, we assume that the ground state is exclusively governed by external inputs (effectively setting $\epsilon_{ij} \equiv 0$). Then, the mean input to the neurons in an interval of length τ^{m} is $\mu = I_0$ with standard deviation $\sigma = \epsilon^{\mathrm{ext}}\sqrt{2\tau^{\mathrm{m}}\nu^{\mathrm{ext}}}$ (cf. section 2.3). Using the probability density (Equation 8), we calculate the spiking probability of a single neuron, $p_f\left(x\right)$, due to an input of strength x;

$$p_f\left(x\right) = \int_{\Theta-x}^{\Theta} P_V\left(V\right) dV \quad (14)$$

$$= \frac{1}{2}\left(\mathrm{Erf}\left[\frac{\Theta-\mu}{\sigma}\right] - \mathrm{Erf}\left[\frac{\Theta-\mu+x}{\sigma}\right]\right) \quad (15)$$

equals the probability of finding a neuron's membrane potential in the interval $[\Theta - x, \Theta]$. To derive a iterated map for the average number of active neurons (which maps $E[g_i] \to E[g_{i+1}]$), we interpolate $\mathrm{E}\left[g_{i+1}\middle|\, g_i\right]$ for continuous g_i and in the second step replace g_i by its expectation value $\mathrm{E}\left[g_i\right]$. The fixed points, $\mathrm{E}\left[g_{i+1}\middle|\, \mathrm{E}\left[g_i\right]\right] = \mathrm{E}\left[g_i\right]$, qualitatively determine the propagation properties of synchronous activity. In the rest of the manuscript we are dealing with the average number of active neurons in a given layer. Therefore, for simplicity we denote the expectation value of the average number of active neurons in a given layer i by g_i instead of $\mathrm{E}\left[g_i\right]$.

For sufficiently small connection probabilities p the map (Equation 12) has only one (trivial) fixed point $G_0 = g_{i+1} = g_i = 0$. Any initial synchronous pulse will die out after a small number of layers (see also **Figure 1**). With increasing connectivity two additional fixed points G_1 (unstable) and $G_2 \geq G_1$ (stable) appear via a tangent bifurcation.

For FFNs with purely excitatory couplings between the layers, the second fixed point G_2 (if it exists) is always stable: The spiking probability $p_f(x)$ is monotonically increasing with input x and thus also the iterated map (Equation 13) is monotonically increasing (i.e., the slope is larger than 0). Moreover, if G_2 exists the slope of the iterated map at this intersection point with the diagonal is smaller than 1. This implies that G_2 is stable and synchronous pulses of size $g_i \geq G_1$ typically initiate a propagation of synchrony with an average number of active neurons around G_2. The critical connectivity p_L^* at the bifurcation point marks the minimal connectivity that allows for stable propagation of synchrony.

Although the distribution of inputs from one layer to the subsequent one and the spiking probability of a single neuron $p_f(\cdot)$ are known, there is no analytic closed form solution to the fixed point equation $g_{i+1} = g_i = g_i^*$. In other words, we can compute the firing probability $p_f\left(x_0\right)$ for any x_0, and therefore also $\mathrm{E}\left[g_{i+1}\middle|\, g_i\right]$ for any g_i, but $g_i^* = \mathrm{E}\left[g_{i+1}\middle|\, g_i^*\right]$ is transcendental. We thus derive an approximate solution. We choose some expansion point g_i (see section 3.1.2 for details), and approximate the function $\mathrm{E}\left[g_{i+1}\middle|\, g_i^*\right]$ by a polynomial $g_i + S(g_i^* - g_i)$ in second order in $(g_i^* - g_i)$ near g_i. The arising quadratic fixed point equation $g_i^* = g_i + S(g_i^* - g_i)$ is then analytically solvable in g_i^*. This also allows to analytically compute the critical connectivity p_L^*: it is the parameter value at which the iterated map undergoes a tangent bifurcation, i.e., at which the two solutions of the fixed point equation become equal upon changing from complex-conjugate to real. Since the right hand side of Equation (13) does not offer itself for a direct series expansion in g_i^*, we derive $g_i + S(g_i^* - g_i)$ from an appropriate expansion of $p_f\left(h\epsilon\right)$ and a subsequent computation the arising expectation values.

In biologically relevant scenarios, the neurons usually receive a large number of synaptic inputs and thus the distribution of

membrane potentials $P_V(V)$ is broad, $P_V(V)$ changes slowly with V. Then, $P_V(V)$ around some $V = V_0$ can be approximated by considering a series expansion with a small order and it is possible to derive an approximation for the critical connectivity p_L^* based on an expansion of $p_f(\cdot)$. Expanding $p_f(x)$ into a Taylor series around some x_0 and using Equation (12) yields

$$g_{i+1} = \omega \mathrm{E}\left[\sum_{n=0}^{\infty} \frac{p_f^{(n)}(x_0)}{n!} (h\epsilon - x_0)^n \middle| g_i \right] \tag{16}$$

$$= \omega \sum_{n=0}^{\infty} \frac{p_f^{(n)}(x_0)}{n!} \mathrm{E}\left[(h\epsilon - x_0)^n \middle| g_i \right]. \tag{17}$$

Here and in the following we denote the nth derivative of a function $f(x)$ at $x = x_0$ by

$$f^{(n)}(x_0) = \frac{d}{d^n x} f(x) \bigg|_{x=x_0}. \tag{18}$$

Replacing the derivatives of $p_f(\cdot)$ by the (one order lower) derivatives of probability density of membrane potentials $P_V(V)$ according to Equation (14) yields

$$g_{i+1} = \omega p_f(x_0) + \omega \sum_{n=1}^{\infty} \frac{P_V^{(n-1)}(V_0)}{(-1)^{n-1} n!} \mathrm{E}\left[(h\epsilon - x_0)^n \middle| g_i \right], \tag{19}$$

where we defined

$$V_0 := \Theta - x_0 \tag{20}$$

for better readability.

We have recently shown (Jahnke et al., 2012) that it is possible to derive a scaling law for the critical connectivity using

$$x_0 = g_i p \epsilon, \tag{21}$$

the (unknown) average input from one layer to the next during stationary synchrony propagation, as expansion point. For this choice the expectation value $\mathrm{E}\left[(h\epsilon - x_0)^n \middle| g_i \right]$ in Equation (19) simplifies to

$$\mathrm{E}\left[(h\epsilon - x_0)^n \middle| g_i \right] = \epsilon^n \mathrm{E}\left[(h - \mathrm{E}[h])^n \middle| g_i \right] = \epsilon^n m_n, \tag{22}$$

where we denote by m_n the nth central moment of the Binomial distribution $B(g_i, p)$, specifying the distribution of inputs to the $(i+1)$th layer. In the limit of large layer sizes ω and small coupling strengths ϵ keeping the maximal input $\epsilon\omega$ to each layer constant (to preserve the network state), all summands for $n \geq 2$ vanish, and Equation (19) simplifies to

$$g_{i+1} = \omega p_f\left(g_i p \epsilon\right). \tag{23}$$

Using the implicit function theorem one can show that this implies the scaling law

$$p_L^* = \frac{1}{\lambda \epsilon \omega} \tag{24}$$

where λ is a constant independent of ϵ and ω (Jahnke et al., 2012). We note that for the derivation of the scaling law (Equation 24) we did not use the actual functional form of the distribution of membrane potentials $P_V(V)$. Therefore this estimate holds if $P_V(V)$ is sufficiently slow changing with V such that the Taylor expansion (cf. Equation 16) is applicable, but its validity is not restricted to the low-rate approximation.

However, the dependence of the prefactor $1/\lambda$ on the layout of the external network remained unknown. Here, we present an approach that enables us to derive an approximate value for λ. We consider the expansion (Equation 19) around x_0 up to second order,

$$g_{i+1} \approx \omega p_f(x_0) + \omega P_V(V_0) \cdot \left(\epsilon g_i p - x_0\right) - \frac{\omega P_V^{(1)}(V_0)}{2} \left[\left(\epsilon g_i p - x_0\right)^2 + \epsilon^2 g_i p \left(1 - p\right) \right] \tag{25}$$

The truncated series (Equation 25) is quadratic in g_i such that the fixed points $g_{1/2}^* = g_{i+1} = g_i$ can be obtained analytically,

$$g_{1,2}^* = \gamma_L \pm \sqrt{\gamma_L^2 - \frac{x_0 \left(2P_V(V_0) + x_0 P_V^{(1)}(V_0)\right) - 2p_f(x_0)}{p^2 P_V^{(1)}(V_0) \epsilon^2}}, \tag{26}$$

where we defined

$$\gamma_L := \frac{p\epsilon\omega \left(2\left(P_V(V_0) + x_0 P_V^{(1)}(V_0)\right) + \left(p-1\right) P_V^{(1)}(V_0)\epsilon\right) - 2}{2p^2 P_V^{(1)}(V_0)\epsilon^2\omega}. \tag{27}$$

At the bifurcation point, the root in Equation (26) vanishes such that both fixed points agree ($g_1^* = g_2^*$) and $\gamma_L = g_1^* = g_2^*$ specifies the average size of a propagating synchronous pulse. Consequently, the critical connectivity is obtained by choosing p such that

$$\gamma_L^2 = \frac{x_0 \left(2P_V(V_0) + x_0 P_V^{(1)}(V_0)\right) - 2p_f(x_0)}{p^2 P_V^{(1)}(V_0)\epsilon^2} \tag{28}$$

which yields

$$p_L^* = \frac{1}{2} - \frac{1}{\epsilon} \left[\frac{\lambda^*}{P_V^{(1)}(V_0)} - \sqrt{\frac{2}{P_V^{(1)}(V_0)\omega} + \frac{\left(\epsilon P_V^{(1)}(V_0) - 2\lambda^*\right)^2}{4\left(P_V^{(1)}(V_0)\right)^2}} \right] \tag{29}$$

where we defined

$$\lambda^* := P_V(V_0) + x_0 P_V^{(1)}(V_0) - \sqrt{P_V^{(1)}(V_0)\left(x_0\left(2P_V(V_0) + x_0 P_V^{(1)}(V_0)\right) - 2p_f(x_0)\right)} \tag{30}$$

which is independent of the setup of the FFN and completely determined by the layout of the external network and the choice of the expansion point x_0.

As before we consider the limit of large layer sizes ω and small coupling strengths ϵ, i.e., we replace $\omega \to \frac{\text{const}}{\epsilon}$ and consider the leading terms of a series expansion of Equation (29). The expansion of the square bracket in Equation (29) yields

$$\frac{\lambda^*}{P_V^{(1)}(V_0)} - \sqrt{\frac{2}{P_V^{(1)}(V_0)}\frac{\epsilon}{\text{const}} + \frac{\left(\epsilon P_V^{(1)}(V_0) - 2\lambda^*\right)^2}{4\left(P_V^{(1)}(V_0)\right)^2}}$$

$$= \left[\frac{\lambda^*}{P_V^{(1)}(V_0)} - \frac{\lambda^*}{P_V^{(1)}(V_0)}\right] - \epsilon\left(\frac{1}{\lambda^* \cdot \text{const}} - \frac{1}{2}\right) + O\left(\epsilon^2\right), \quad (31)$$

such that the critical connectivity assumes the functional form given by Equation (24),

$$p_L^* \approx \frac{1}{\lambda^* \epsilon \omega}. \quad (32)$$

Thus $\lambda = \lambda^*$ defined by Equation (30) provides an approximation of the constant λ fully specifying the critical connectivity p_L^*.

3.1.2. Optimal expansion point

To derive Equation (30) we assumed that it is sufficient to consider the second order expansion of $p_f(x)$. It is thus necessary to choose an appropriate expansion point that results in fast convergence. In particular for the choice $x_0 = x_0^*$, that we will now derive, Equation (37) below, the bifurcation diagram near the bifurcation point is well approximated already for $k = 2$ (cf. **Figure 2**).

The size of a propagating group at the critical connectivity is γ_L (cf. Equation 27) and thus the resulting average input is $p_L^* \gamma_L \epsilon$. Our expansion point x_0 should lie near to this value, which is, of course, unknown prior to solving the fixed point equation. We will thus compute a range in which $p_L^* \gamma_L \epsilon$ has to lie and choose the expansion point appropriately within. We assume that ω is large and employ Equation (23) which allows an direct estimate of this range as we know the functional form explicitly. Equation (23) with $g_{i+1} = g_i$ is just another transcendental equation for the fixed points and it has zero, one, or two non-trivial fixed point solutions points g_1^* and g_2^*, which are then also solutions of Equation (19) with $g_{i+1} = g_i$. At the bifurcation point ($g^* = g_1^* = g_2^*$) where the diagonal is touched, the function $p_f(g p \epsilon)$ has to be concave and monotonic increasing with respect to g. The definition (Equation 14) of $p_f(x)$ implies that it is monotonic increasing for all $x \geq 0$. Moreover, it is concave for all $x \geq \Theta - \mu$,

$$p_f^{(1)}(x) = P_V(\Theta - x) \geq 0 \quad \text{for } x \geq 0 \quad (33)$$

$$p_f^{(2)}(x) = -P_V^{(1)}(\Theta - x) \leq 0 \quad \text{for } x \geq \Theta - \mu, \quad (34)$$

such that the bifurcation point satisfies

$$x_0 \geq \Theta - \mu. \quad (35)$$

The condition Equation (33) holds because $P_V(V) \geq 0$ is a probability density and Equation (34) is derived directly from differentiating Equation (8). To maximize the quality of the second order approximation Equation (25), we choose $x_0 = x_0^*$ such that the contribution to the expansion (Equation 19) of the $k = 3$rd order term equals zero. According to Equation (19), all 3rd order terms are proportional to $P_V^{(2)}(\Theta - x_0)$; so we determine the expansion point x_0^* as a deflection point of $P_V(\cdot)$, requiring that the second derivative of $P_V(V)$ vanishes for $V = \Theta - x_0^*$,

$$p_f^{(3)}(x_0^*) = \left.\frac{d^2 P_V(V)}{dV^2}\right|_{V=\Theta - x_0^*} \stackrel{!}{=} 0. \quad (36)$$

In the considered regime of low spiking rates, we find $x_0^* = \Theta - \mu \pm \frac{\sigma}{\sqrt{2}}$, cf. Equation (8). Due to Equation (35)

$$x_0^* = \Theta - \mu + \frac{\sigma}{\sqrt{2}}. \quad (37)$$

For $x_0 = x_0^*$ the bifurcation diagram near the bifurcation point is well approximated already for $k = 2$ (cf. **Figure 2**) and Equation (30) provides a good estimate of the critical connectivity p_L^* (cf. **Figure 3**).

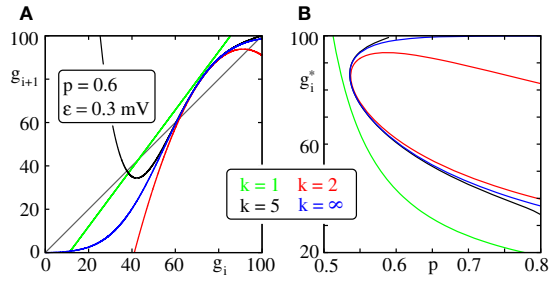

FIGURE 2 | Iterated map and bifurcation diagram for the average group size of a propagating synchronous pulse. (A) Iterated map (Equation 19) truncated after expansion order k (color code) with $x_0 = x_0^*$ (cf. Equation 37). **(B)** Fixed points of the iterated maps shown in **(A)**; with increasing connectivity two fixed points appear by a saddle node bifurcation. We note that already a second order expansion (red), i.e., the lowest order at which a saddle node bifurcation can occur, approximates the bifurcation diagram (blue) near the bifurcation point well.

3.1.3. Influence of external network

In the previous section we derived an iterated map for the average group size (cf. Equation 13) and an approximation for the critical connectivity p_L^* (cf. Equations 30 and 32) that marks the transition from FFNs which do not support propagation of synchrony to FFNs that do. In this section we focus on the robustness of our results. How does the critical connectivity change with the layout of the external network? For which parameter range does the estimate of the critical connectivity (given by Equations 30 and 32) yield reasonable results?

The derivation was based on the assumption that the ground state dynamics of the neurons of the FFN is completely determined by the external inputs. This assumption holds if the spontaneous firing rate ν of the neurons and/or the coupling strengths

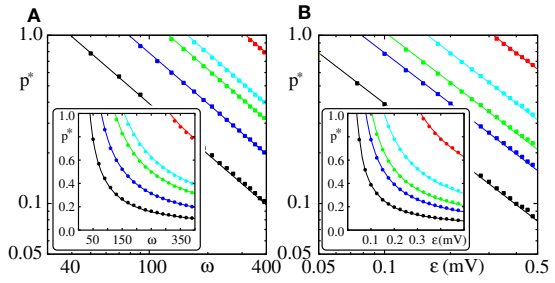

FIGURE 3 | Critical connectivity p_L^* in FFNs with linear dendrites decays algebraically with coupling strength ϵ and layer size ω. The parameters of the external inputs (emulated embedding network) are fixed ($I_0 = 5$ mV, $\nu^{\text{ext}} = 3$ kHz, $\epsilon^{\text{ext}} = 0.5$ mV). Panel **(A)** shows the critical connectivity p_L^* vs. the layer size ω for different coupling strengths ($\epsilon = \{0.05$ mV (red), 0.1 mV (cyan), 0.125 mV (green), 0.2 mV (blue), and 0.4 mV (black)$\}$) and panel **(B)** shows p_L^* vs. the coupling strength ϵ for different layer sizes ($\omega = \{50$ (red), 100 (cyan), 150 (green), 200 (blue), and 400 (black)$\}$). In the main panels we use a logarithmic scale, the insets have a linear scale. The squares indicate the connectivity above which a synchronous pulse propagates from the 1st to the 20th layer of a FFN in at least 50% of $n = 30$ trials. The critical connectivity given by Equation (32) (solid lines) with $x_0 = x_0^*$ (cf. Equation 37) is in good agreement with computer simulations. As predicted $p_L^* \propto (\epsilon\omega)^{-1}$ and the proportionality factor $1/\lambda$ is well approximated by the estimate $1/\lambda^*$ derived in Equation (30).

ϵ and/or the connectivity p are sufficiently small. We will generalize our approach and show how the impact of preceding layers on a layer's ground state can be taken into account. Thereafter we will compare the results with computer simulations, identify the regions in parameter space for which the derived approximations hold and discuss deviations between direct numerical simulations and analytics.

The first layer of an FFN receives inputs only from the external network and according to Equations (6, 7) the mean μ_1 and standard deviation σ_1 of its input is

$$\mu_1 = I_0 \tag{38}$$

$$\sigma_1 = \epsilon^{\text{ext}}\sqrt{2\tau^{\text{m}}\nu^{\text{ext}}}, \tag{39}$$

as assumed in the previous section. All following layers receive external inputs and spikes from their preceding layer(s). The mean μ_n and standard deviation σ_n of the input to neurons of the nth layer (with $n \geq 2$) reads (cf. Equations 6 and 7)

$$\mu_n = I_0 + \tau^{\text{m}} p\omega\nu_{n-1}\epsilon \tag{40}$$

$$\sigma_n = \sqrt{2\nu^{\text{ext}}\tau^{\text{m}}\left(\epsilon^{\text{ext}}\right)^2 + p\omega\nu_{n-1}\tau^{\text{m}}\epsilon^2}. \tag{41}$$

Here we denote the spontaneous firing rate (in the absence of synchrony) of neurons of the $(n-1)$th layer by ν_{n-1}. It is given by Equation (9) as

$$\nu_{n-1} = \frac{1}{\sqrt{\pi}\tau^{\text{m}}}\frac{\Theta - \mu_{n-1}}{\sigma_{n-1}}\exp\left[-\left(\frac{\Theta - \mu_{n-1}}{\sigma_{n-1}}\right)^2\right]. \tag{42}$$

From layer to layer, the mean input, the standard deviation as well as the firing rate increase. For setups, where the ground state of the FFN is non-pathological, i.e., the firing rates of all layers are bounded, the additional corrections $\Delta X_n := X_n - X_{n-1}$ for $X \in \{\mu, \sigma, \nu\}$ decrease with n, and μ_n, σ_n and ν_n saturate for sufficiently large n. Thus, μ_∞ and σ_∞ describe the input to the neurons of an infinitely long FFN and the single neurons of such an FFN spike with an average rate ν_∞. Accordingly, replacing μ and σ by μ_∞ and σ_∞ in Equation (13) [where they appear as parameters of $p_f(\cdot)$] yields an iterated map for the average group size.

In **Figure 4**, we compare the critical connectivity found by numerically determining the bifurcation point of the iterated map (Equation 13) (i.e., we determined the connectivity p for which the iterated map touches the diagonal; solid lines) with computer simulations of propagating synchrony (markers). To also cover scenarios, where the input from the preceding layer is not negligible, we consider infinitely long FFNs (then, the distribution of membrane potentials is equal in all layers). In computer simulations this can be approximated by a sufficiently long FFN with periodic boundary conditions, i.e., an FFN where the last layer connects to the first layer. For moderate external inputs, i.e., moderate I_0 and ϵ^{ext}, already the analytical results neglecting the influence of the preceding layers (using μ_1 and σ_1) agree well with computer simulations (cf. **Figure 4A**, solid lines). However, for large external inputs, i.e., large I_0 and ϵ^{ext}, the critical connectivity is overestimated. Here, the assumption that the distribution of membrane potentials is not influenced by the connectivity of the FFN does not hold. The additional input shifts the membrane potentials to higher values and consequently a lower connectivity is required for a propagation of a synchronous pulse. The corrections given by Equations (38–42) account for these deviations to some extent (cf. **Figures 4B,C**; solid lines), in particular for setups where the spontaneous firing rate is low. However, for very large I_0 and ϵ^{ext}, the critical connectivity is under-estimated. Here, the spontaneous firing rate is too high and the low-rate approximation, Equations (8–9), is not adequate to describe the system; the firing rate and thus the mean input from the previous layer are over-estimated. This becomes particularly clear in **Figure 4C**, where we show the critical connectivity as a function of the strength of the external inputs ϵ^{ext}. For any given I_0 (different colors), the critical connectivity for small ϵ^{ext} is well approximated; with increasing ϵ^{ext} the firing rate increases [α decreases and thus ν increases; cf. Equations (9 and 10)] and when the coupling strengths ϵ^{ext} exceed a I_0-dependent threshold, the low-rate approximation becomes inapplicable.

Applying the methods in Brunel and Hakim (1999); Brunel (2000), the firing rate and the distribution of membrane potentials can be derived in diffusion approximation for states with higher spontaneous firing rates. Although most of the analytical considerations above are also applicable within this approximation, the determination of an optimal expansion point (cf. Equations 36 and 37) becomes more difficult and a closed form expression does not exist. However, the critical connectivity can be obtained by numerically determining the fixed points of the iterated map (Equation 13) and we find that it agrees with

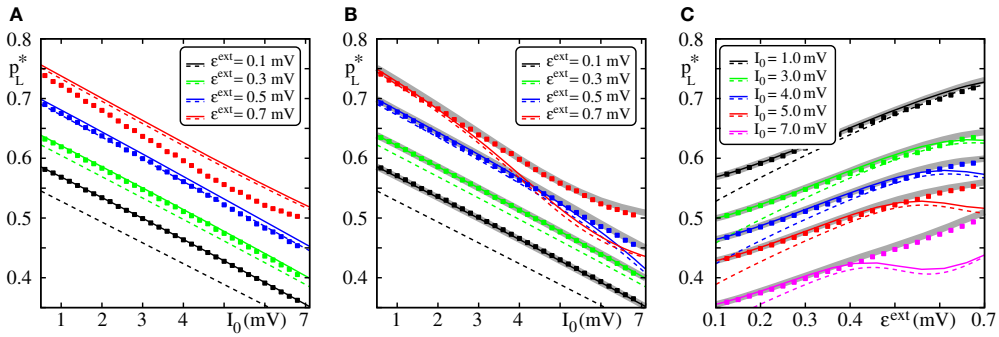

FIGURE 4 | Robustness of analytical estimates of the critical connectivity. (A–C) We consider the critical connectivity p_L^* of infinitely long FFNs, that are approximated by an FFN ($m = 20$, $\omega = 150$, $\epsilon = 0.2$ mV) with periodic boundary conditions in direct numerical simulations (markers), for different layouts of the external network. Panels **(A,B)** show p_L^* vs. I_0 for fixed ϵ^{ext} and panel **(C)** shows p_L^* vs. ϵ^{ext} for fixed I_0. The solid (colored) lines indicate the critical connectivity found by numerically determining the bifurcation point of the iterated map (Equation 13). In panel **(A)** we neglect the influence of previous layers on the ground state of a considered layer in the analytical computations [i.e., we use μ_1 and σ_1, cf. Equations (38) and (39)]. In **(B,C)** we employ corrections to account for their influence, cf. Equations (38–42). We show the third order correction, higher orders add only small modifications to the curves, but the numerical computations get more costly. The thick gray lines in **(B,C)** indicate the bifurcation point of the iterated map (Equation 13) with $P_V(V)$ derived from the diffusion approximation of leaky integrate-and-fire neuron dynamics with Poissonian input (Brunel and Hakim, 1999; Brunel, 2000). The dashed lines are the estimates of the critical connectivity given by Equations (30 and 32). Again, in panel **(A)** we neglect the influence of previous groups on the ground state, in panels **(B,C)** we use the third order correction. The estimates agree with the data from numerical simulations within the biologically relevant parameter range, where (1) the spontaneous spiking activity is low and (2) the distribution of membrane potentials is sufficiently broad. For further explanations see text (section 3.1.3).

computer simulations for the entire considered range of I_0 and ϵ^{ext}, (cf. **Figures 4B,C**; gray lines).

Analogous to the approach presented above, corrections for the influence of preceding layers can be taken into account for the analytical estimate of the critical connectivity derived in the previous section (Equations 30 and 32). Replacing the connectivity p by the approximation $p_L^* = (\lambda^* \epsilon \omega)^{-1}$ in Equations (40, 41) yields

$$\mu_n = I_0 + \tau^m / \lambda^*_{n-1} \nu_{n-1} \tag{43}$$

$$\sigma_n = \sqrt{2\nu^{ext}\tau^m (\epsilon^{ext})^2 + \epsilon \nu_{n-1} \tau^m / \lambda^*_{n-1}} \tag{44}$$

where $\lambda^*_{n-1} := \lambda^*(\mu_{n-1}, \sigma_{n-1})$ is given by Equation (30) and $\nu_{n-1} = \nu(\mu_{n-1}, \sigma_{n-1})$ is given by Equation (42). In **Figure 4** we show the estimate of the critical connectivity $p_L^* = \left(\lambda_n^* \epsilon \omega\right)^{-1}$ (cf. Equation 32) using λ_1^* (panel a; dashed line), i.e., neglecting the influence of the preceding layers, and using a higher correction order (panel b,c; dashed line: third order). For sufficiently large ϵ^{ext} the critical connectivity found by numerically determining the bifurcation point agrees with the analytical estimate given by Equation (32). As discussed above, the corrections Equations (43, 44) account for the deviations from the simulated data as long as the total spontaneous firing rate is sufficiently low. However, for small ϵ^{ext} the critical connectivity is under-estimated. Here, the standard deviation of the inputs (cf. Equation 7) is low, such that the distribution of membrane potentials $P_V(V)$ is narrow [for $\epsilon^{ext} \to 0$: $P_V(V) \to \delta(V - \mu)$; cf. Equation (8)], the spiking probability of one neuron, $p_f(\cdot)$, increases steeply in a small interval [for $\epsilon^{ext} \to 0$: $p_f(x) \to \Theta(x - \mu)$; cf. Equation (8)] and thus the approximation of $p_f(\cdot)$ by the leading terms of a Taylor expansion is not sufficiently accurate.

However, in the biologically plausible parameter regime, where the firing rates are small and the distribution of membrane potentials is broad, the critical connectivity is approximated well by Equation (32) together with Equation (30) (defining λ^*), Equation (37) (defining x_0^*) and the corrections that account for the influence of the preceding layers, Equations (43, 44).

3.1.4. Characteristics of propagating synchronous pulses

In the previous sections, we have shown that a synchronous pulse may propagate along a diluted FFN. In this section we study the characteristics and properties of a propagating synchronous signal. We consider them at the transition to stable propagation, p_L^*, because there they depend only weakly on the network setup. How large is the fraction of neurons that participate in propagating synchrony? How does this fraction depend on the network setup?

To answer such questions, we consider the effect of a propagation synchronous pulse on the single layers in the network, as a measure for the effective pulse size. In other words, we consider the mean input μ_L a neuron receives from the preceding layer if a synchronous pulse propagates along the FFN at the critical connectivity p_L^*. It is given by the product of the connection probability p_L^*, the connection strength ϵ and the average size of a propagating synchronous signal γ_L; using Equations (27) and (29) yields

$$\mu_L = \gamma_L p_L^* \epsilon = \frac{P_V(\Theta - x_0^*) + P_V^{(1)}(\Theta - x_0^*) x_0^* - \lambda^*}{P_V^{(1)}(\Theta - x_0^*)} \tag{45}$$

and after inserting λ^* as given by Equation (30),

$$\mu_L = \sqrt{\frac{x_0^* \left(2P_V(\Theta - x_0^*) + x_0^* P_V^{(1)}\left(\Theta - x_0^*\right)\right) - 2p_f\left(x_0^*\right)}{P_V^{(1)}\left(\Theta - x_0^*\right)}}. \quad (46)$$

According to Equation (46) the average input μ_L to the neurons due to a propagation of a synchronous pulse is independent of the layer size ω and coupling strength ϵ. For setups with moderate external inputs (i.e., inputs of the preceding layer influence the neurons' ground state only weakly; see also section 3.1.3) the distribution of membrane potentials $P_V(\cdot)$ (cf. Equation 8), the firing probability of single neurons $p_f(\cdot)$ (cf. Equation 14) as well as the expansion point (deflection point of $P_V(\cdot)$; cf. Equation 37)

$$x_0^* = \Theta - I_0 + \epsilon^{\text{ext}}\sqrt{\tau^{\text{m}}\nu^{\text{ext}}} \quad (47)$$

are fully determined by the external inputs (I_0, ν^{ext} and ϵ^{ext}). **Figures 5A,B** illustrates the dependence of μ_L on the layout of the external network and the FFN: as expected from our analytical considerations, the dependence on the layer size and coupling strength is weak when I_0 and ϵ^{ext} are kept fixed. With increasing mean of the external input (I_0) the distribution of membrane potentials $P_V(V)$ is shifted toward the threshold Θ, such that it is more likely to find the membrane potential of the neurons near the threshold and the critical connectivity decreases (cf. also **Figures 4A,B**). Naturally this implies a decreasing average input μ_L at p_L^*, which is shown in **Figure 5A** for different external couplings ϵ^{ext} and parameters of the FFN. Increasing the external coupling strength ϵ^{ext} (and with it the variance of the external input) causes a broadening of the distribution of membrane potentials; the membrane potentials of some neurons are shifted toward the threshold and the membrane potentials of other neurons are shifted away from it. If the fraction of neurons that participate in the propagation of the synchronous pulse is large, this implies an increasing critical connectivity (**Figure 5B**; cf. also **Figure 4C**).

The spiking probability of a single neuron due to the mean input μ_L equals the average fraction p^{frac} of neurons of one layer that participate in a propagating synchronous pulse,

$$p^{\text{frac}} = \frac{\gamma_L}{\omega} = p_f(\mu_L). \quad (48)$$

Interestingly, in the considered regime of low spiking rates and sufficiently broad distribution of membrane potentials, where the approximations given in section 3.1.1 are applicable, p^{frac} depends on the setup of the external inputs only via the quotient $\alpha = \frac{\Theta - \mu}{\sigma}$ (cf. Equation 10), or, equivalently, on the spontaneous firing rate ν of the neurons (cf. Equation 9). This can be shown by combining Equations (8, 37) and (Equation 46),

$$\mu_L = \sigma\left(\frac{e\pi}{2}\right)^{1/4}\left[\frac{\left(\sqrt{2}+2\alpha\right)\left(3+\sqrt{2}\alpha\right)}{2\sqrt{e\pi}} - \text{Erf}\left(\frac{1}{\sqrt{2}}\right) - \text{Erf}(\alpha)\right]^{1/2} \quad (49)$$

$$=: \sigma f_\mu(\alpha) \quad (50)$$

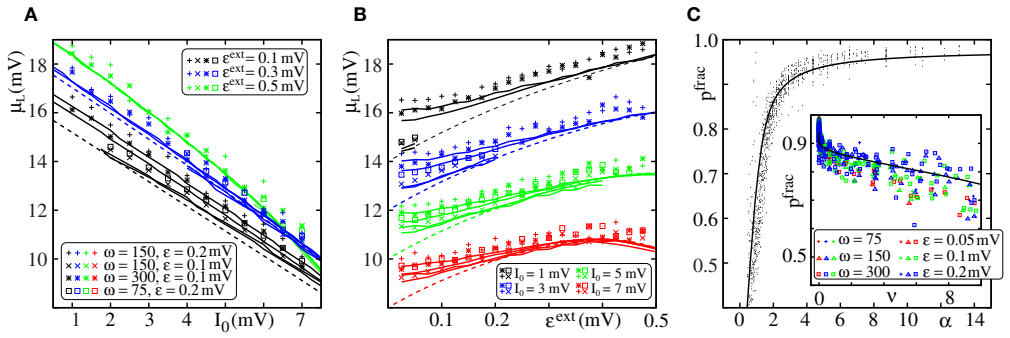

FIGURE 5 | Properties of propagating synchronous pulses at the transition from the no-propagation to the propagation regime. Panels **(A,B)** show the mean input μ_L that a layer receives due to a propagating synchronous pulse in the preceding layer. μ_L measures the effective pulse size (the impact of a propagating synchronous pulse) and is mainly determined by the external inputs rather than by the setup of the FFN. In **(A)** the variance of the external input (measured by ϵ^{ext}) is fixed and μ_L is plotted vs. I_0; in **(B)** the mean external input I_0 is fixed and μ_L is plotted vs. ϵ^{ext}. The markers indicate μ_L for FFNs of different sizes [ω and ϵ are given by the legend in **(A)**] obtained by numerical simulations of propagating synchrony. The dashed lines shows the approximation of μ_L given by Equation (46) (which is independent of ω and ϵ); the solid lines indicate $\mu_L = p_L^* G_2 \epsilon$; values of p_L^* and G_2 are found semi-analytically, by numerically identifying the bifurcation point of the analytically derived iterated map (Equation 13) for the different network setups (both analytical estimates are corrected for the influence of inputs from the preceding layer up to the first order). Panel **(C)** shows the fraction p^{frac} of neurons in a layer that participate in the propagation of a synchronous signal vs. α [(Equation 10); main panel] and vs. the spontaneous firing rate ν (inset). Data from different network setups are plotted without distinction as black dots in the main panel and with distinction by different colors and symbols in the inset (see legend); Simulations are repeated for different layouts of the external network ($I_0 \in \{1, 3, \ldots, 11\}$ mV; $\epsilon^{\text{ext}} \in \{0.1, 0.125, \ldots, 1.0\}$ mV). The solid lines indicate $p_f(\mu_L) = f_p(\alpha)$ as given by Equation (53). The layer size ω as well as the coupling strength ϵ influence p^{frac} only weakly. p^{frac} depends on the network setup mainly through α or, equivalently, through ν (cf. Equation 9): Measurement values from different network setups largely collapse to the graph of the function $p_f(\mu_L) = f_p(\alpha)$. For further explanations see text (section 3.1.4).

such that

$$p_f(\mu_L) = \frac{1}{2}\left[\mathrm{Erf}\left(\frac{\Theta-\mu}{\sigma}\right) + \mathrm{Erf}\left(\frac{\mu_L-\Theta+\mu}{\sigma}\right)\right] \quad (51)$$

$$= \frac{1}{2}\left[\mathrm{Erf}(\alpha) + \mathrm{Erf}\left(\frac{\mu_L}{\sigma}-\alpha\right)\right] \quad (52)$$

$$= \frac{1}{2}\left[\mathrm{Erf}(\alpha) + \mathrm{Erf}\left(f_\mu(\alpha)-\alpha\right)\right] =: f_p(\alpha). \quad (53)$$

In **Figure 5C** we compare the above predictions with direct numerical simulations: For different layer sizes ω, coupling strengths ϵ and layouts of the external networks (i.e., different values of I_0 and ϵ^{ext}), we detect whether propagation of a synchronous pulse is possible and if so, we numerically determine the average fraction of participating neurons as well as the spontaneous firing frequency. We find that indeed the size of the synchronous pulse is determined essentially by the quotient $\alpha = \frac{\Theta-\mu}{\sigma}$ and Equation (53) is a reasonable estimate of the average fraction of neurons spiking in each layer. With increasing α the fraction of participating neurons increases, it thus decreases with spontaneous firing rate ν see **Figure 5C**. For FFNs with low spontaneous spiking frequency almost all neurons of a layer participate in the propagation of a synchronous pulse.

3.2. FFNs WITH NON-LINEAR DENDRITES

In this section, we investigate propagation of synchrony mediated by dendritic non-linearities. Although the mechanism underlying the propagation is generally related to that in linear networks, the discontinuities introduced by non-additive dendritic interactions prevent a similar analytical approach. In the first part of this section, we thus derive analytical estimates for the critical connectivity p^*_{NL} in non-linearly coupled networks based on a self-consistency approach (see also Jahnke et al., 2012). In the second part, we study the transition from propagation of synchrony mediated by linear dendrites to propagation of synchrony mediated by non-additive dendritic interactions upon increasing the degree of non-linearity in the networks. In the last part, we evaluate the robustness of the analytical estimates with respect to the layout of the external network.

3.2.1. Analytical derivation of critical connectivity

Neurons with non-additive dendritic interaction process excitatory input by a non-linear dendritic modulation function σ_{NL} (see section 2.1), i.e., synchronous inputs that exceed the dendritic threshold Θ_b are amplified to an effective input of size κ (cf. Equation 4). Therefore the spiking probability of a single neuron due to a synchronous input of strength x, $p_f(\sigma_{NL}(x))$, is discontinuous and an approach based on expansion of $p_f(\cdot)$ is inappropriate. To derive an analytical expression for the critical connectivity p^*_{NL} in FFNs incorporating dendritic non-linearities, we consider the (average) fraction of neurons of one layer, p_γ, that receive an input x larger than the dendritic threshold, $x \geq \Theta_b$, due to the propagating synchronous pulse. If there is a stable (stationary) propagation of synchrony established, p_γ is constant throughout the layers, which allows us to formulate a self-consistency equation. The basic derivations have been published recently (Jahnke et al., 2012) and will be briefly reviewed in the following for the readers convenience.

For sufficiently small dendritic thresholds Θ_b and sufficiently large κ, the spiking probability of a neuron due to a sub-threshold input is small compared to the spiking probability of a supra-threshold input. Therefore, we approximate the spiking probability of a single neuron in response to a synchronous input of strength x by

$$p_f(\sigma_{NL}(x)) = \begin{cases} p_f(\kappa) & \text{if} \quad x \geq \Theta_b \\ 0 & \text{otherwise} \end{cases}, \quad (54)$$

i.e., we assume that somatic spikes due to the synchronous pulse are exclusively generated by dendritically enhanced inputs. We denote the fraction of neurons that receive a dendritic spike by p_γ. This may be considered as constant throughout the different layers if stable propagation of synchrony is enabled. Then the probability that a neuron receives exactly k inputs from the preceding layer follows a binomial distribution $k \sim B\left(\omega, p_\gamma p_f(\kappa)\, p\right)$, where $p_\gamma p_f(\kappa)\, p$ is the probability that (1) a neuron of the preceding layer receives a supra-threshold input (p_γ), (2) a somatic spike is elicited by that input $\left(p_f(\kappa)\right)$ and there is a connection from this spiking neuron to the considered neuron of the following layer (p). So we can formulate the self-consistency equation for p_γ,

$$p_\gamma = \sum_{k=\lceil\Theta_b/\epsilon\rceil}^{\omega} \binom{\omega}{k} \left(p_\gamma p_f(\kappa)\, p\right)^k \left(1 - p_\gamma p_f(\kappa)\, p\right)^{\omega-k}. \quad (55)$$

To solve Equation (55) we approximate the binomial distribution by a Gaussian distribution with mean $\delta := \omega p_\gamma p p_f(\kappa)$ and standard deviation $\sigma_\delta := \sqrt{\delta(1 - p_\gamma p p_f(\kappa))}$, which yields

$$p_\gamma = \frac{1}{2}\left[1 + \mathrm{Erf}\left(\frac{n}{\sqrt{2}}\right)\right], \quad (56)$$

where we defined

$$n := \frac{\delta - \Theta_b/\epsilon}{\sigma_\delta} \quad (57)$$

$$= \frac{\omega p_\gamma p p_f(\kappa) - \Theta_b/\epsilon}{\sqrt{\omega p_\gamma p p_f(\kappa)\left(1 - p_\gamma p p_f(\kappa)\right)}} \quad (58)$$

as the difference between the average number of inputs (δ) and the number of inputs needed to reach the dendritic threshold (Θ_b/ϵ) normalized by the standard deviation of the number of inputs (σ_δ). Solving definition (Equation 58) for p and replacing p_γ by Equation (56) yields

$$p_{NL} = \frac{n^2\epsilon + 2\Theta_b + n\sqrt{n^2\epsilon^2 + 4\Theta_b\left(\epsilon - \frac{\Theta_b}{\omega}\right)}}{p_f(\kappa)\epsilon(n^2+\omega)\left(1 + \mathrm{Erf}\left(\frac{n}{\sqrt{2}}\right)\right)}, \quad (59)$$

which is the connectivity p_{NL} where stable propagation of synchrony with some given n (or, equivalently, some given p_γ;

cf. Equation 56) is established. We note that a propagation of synchrony mediated by dendritic spikes requires

$$\epsilon\omega > \Theta_b \tag{60}$$

(otherwise even the input caused by a synchronized spiking of all neurons of a layer in a fully connected FFN ($p = 1$) is not sufficient to reach the dendritic threshold Θ_b).

For parameters fulfilling the inequality (Equation 60), $p_{NL}(n)$ has a global minimum (see Appendix) and the critical connectivity p^*_{NL}, again defined as the smallest connectivity that allows for a stable propagation of synchrony, matches that global minimum: any connectivity p_{NL} above the minimal connectivity p^*_{NL} has two preimages n_1 and n_2 corresponding to the both non-trivial fixed points G_1 and G_2 of the iterated map for the average group size (cf. **Figure 1** and section 2.4). However, there exists smaller connectivities for which a stationary propagation can be established. At the global minima p^*_{NL} both preimages n_1 and n_2 collapse to $n^* = n_1 = n_2$ and correspond to the fixed point $G = G_1 = G_2$ of the iterated map at the bifurcation point of the tangent bifurcation. Here the transition from the regime where no propagation of synchrony is possible to the regime where a propagation of synchrony is enabled takes place. For p_{NL} smaller than p^*_{NL} there are no preimages (i.e., a stationary propagation of synchrony mediated by non-additive dendritic interactions cannot be established); this scenario correspond to the absence of the non-trivial fixed points of the iterated map for connectivities below the tangent bifurcation.

In the following we will obtain the minima of p_{NL} (i.e., the critical connectivity p^*_{NL}) in the limit of large layer sizes ω and small coupling strength ϵ. We first derive an approximation of Equation (59) (cf. Equation 62), determine the validity range of this approximation (cf. Equation 69) and finally obtain an estimate for the critical connectivity (cf. Equation 71). As before, we fix the maximal input $\epsilon\omega$ to each neuron to preserve the network state and expand Equation (59) in a power series around $\epsilon \to 0$ and $\omega \to \infty$. Considering the leading terms yields

$$p_{NL} \approx p_{NL,\,a} := \frac{2\Theta_b}{p_f(\kappa)\,\epsilon\omega}\,\frac{1 + n\sqrt{\frac{\epsilon}{\Theta_b} - \frac{1}{\omega}}}{1 + \mathrm{Erf}\left(\frac{n}{\sqrt{2}}\right)}. \tag{61}$$

Further a propagation mediated by dendritic spikes (as introduced above) requires that the layer size ω and the coupling strength ϵ are sufficiently large such that a sufficiently large fraction of neurons of each layer receive a total input larger than the dendritic threshold Θ_b. In particular for diluted FFNs, this requirement translates to $\epsilon\omega \gg \Theta_b$ and Equation (61) simplifies further to

$$p_{NL,\,b} := \frac{2\Theta_b}{p_f(\kappa)\,\epsilon\omega}\,\frac{1 + n\sqrt{\frac{\epsilon}{\Theta_b}}}{1 + \mathrm{Erf}\left(\frac{n}{\sqrt{2}}\right)}. \tag{62}$$

Whereas p_{NL} has always a global minimum for $\epsilon\omega > \Theta_b$, this does not hold for the approximation $p_{NL,\,b}$, e.g., (cf. also **Figure 6C**)

$$\lim_{n\to-\infty}\left(p_{NL,\,b}\right) = -\infty. \tag{63}$$

However, we will now show that $p_{NL,\,b}$ has a (local) minimum if (and only if) $\epsilon \in \left(0, \frac{2\Theta_b}{\pi}\right]$ which approximates the global minimum of p_{NL} and therefore serve as an estimate for the critical connectivity. Starting with $\left.\frac{dp_{NL,\,b}(n)}{dn}\right|_{n=n^*} = 0$ yields

$$\sqrt{\frac{\Theta_b}{\epsilon}} = \sqrt{\frac{\pi}{2}}\exp\left(\frac{n^{*2}}{2}\right)\left(1 + \mathrm{Erf}\left(\frac{n^*}{\sqrt{2}}\right)\right) - n^* =: f\left(n^*\right), \tag{64}$$

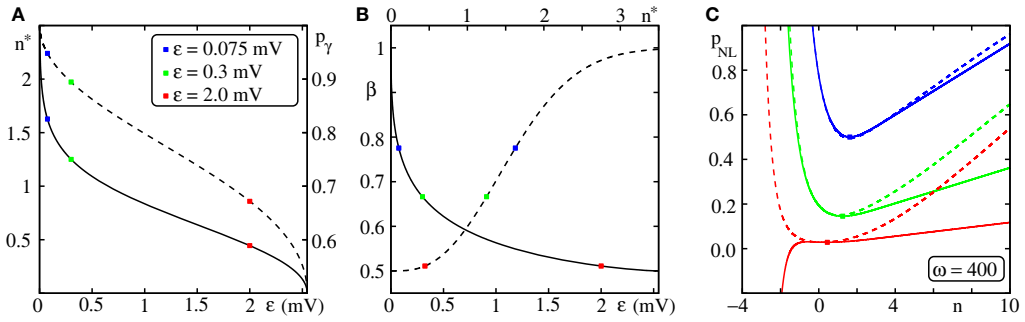

FIGURE 6 | Determining the critical connectivity in FFNs with non-additive dendritic interactions. (A) For a given setup, i.e., for a given dendritic threshold Θ_b and coupling strength $\epsilon < \frac{2\Theta_b}{\pi}$, the corresponding n^* (or equivalently p_γ; cf. Equation 56) is found by Equation (64). The solid line indicates n^* vs. ϵ (left vertical scale), the dashed line p_γ vs. ϵ (right vertical scale) and the markers $n^*(\epsilon)$ for $\epsilon = \{0.075, 0.3, 2.0\}$ mV (see legend). [Here, the dendritic threshold is $\Theta_b = 4$ mV, such that the estimate (Equation 64) is valid within the range $\epsilon \in (0, 2.55]$ mV; Equation (69)] **(B)** Knowing n^* allows to evaluate $\beta\left(\frac{\Theta_b}{\epsilon}\right) \in \left[\frac{1}{2}, 1\right]$ according to Equation (70). Panel **(B)** shows β (cf. Equation 70) vs. ϵ (solid line, lower horizontal axis) and β vs. n^* (dashed line, upper horizontal axis), respectively. **(C)** Finally, the critical connectivity p^*_{NL} is obtained by Equation (71) which depends on $\beta\left(\frac{\Theta_b}{\epsilon}\right)$. Panel **(C)** shows the connectivity p_{NL}[dashed; Equation (59)] and its approximation $p_{NL,\,b}$ [solid; Equation (62)] vs. n; for $\epsilon \in \left(0, \epsilon^{max}\right]$, $p_{NL,\,b}$ has a local minimum which agrees with the global minimum of p_{NL}. The markers indicate the critical connectivity p^*_{NL} obtained by the procedure described in **(A)** and **(B)**. For further explanations see text (section 3.2.1).

and n^* specifies the extremum of $p_{NL,\,b}(n)$. The second derivative of $p_{NL,\,b}(n)$ at the extremum n^* given by Equation (64) satisfies

$$\left.\frac{dp^2_{NL,\,b}}{dn^2}\right|_{n=n^*} = \frac{2n^*\sqrt{\frac{\Theta_b}{\epsilon}}}{p_f(\kappa)\,\omega\left(1+\mathrm{Erf}\left[\frac{n^*}{\sqrt{2}}\right]\right)} > 0 \tag{65}$$

if $n^* > 0$ such that the extremum actually is a minimum. Taken together, for a given setup, i.e., for given dendritic threshold Θ_b and coupling strength ϵ, the transcendent Equation (64) defines n^* which maximizes or minimize $p_{NL,\,b}(n)$ and if additionally $n^* > 0$ the extremum $p_{NL,\,b}(n^*)$ is a minimum.

Differentiating the right hand side of Equation (64),

$$\frac{df(n^*)}{dn^*} = n^* \cdot e^{\frac{n^{*2}}{2}}\sqrt{\frac{\pi}{2}}\left(1+\mathrm{Erf}\left[\frac{n^*}{\sqrt{2}}\right]\right) \tag{66}$$

$$\frac{d^2f(n^*)}{dn^{*2}} = n^* + \left(1+n^{*2}\right)e^{\frac{n^{*2}}{2}}\sqrt{\frac{\pi}{2}}\left(1+\mathrm{Erf}\left[\frac{n^*}{\sqrt{2}}\right]\right), \tag{67}$$

shows that $f(n^*)$ (as defined in Equation 64) is (1) minimal for $n^* = 0$ and (2) monotonically increasing for $n^* > 0$; according to Equation (64) the minimum $n^* = 0$ corresponds to

$$\epsilon^{\max} := \frac{\Theta_b}{\left[f(0)\right]^2} = \frac{2\Theta_b}{\pi} \approx 0.64\Theta_b. \tag{68}$$

The left hand side of Equation (64), i.e., $\sqrt{\Theta_b/\epsilon}$, is monotonically decreasing with ϵ from infinity to zero. Thus Equation (64) has a solution for any

$$\epsilon \in \left(0, \epsilon^{\max}\right] = \left(0, \frac{2\Theta_b}{\pi}\right] \tag{69}$$

and $p^*_{NL} := p^*_{NL,\,b}(n^*)$ is the (local) minimum of Equation (62) and provides an estimate for the critical connectivity, the (global) minimum of Equation (59).

For better readability we define the function $\beta(\cdot)$,

$$\beta\left(\frac{\Theta_b}{\epsilon}\right) := \frac{1}{2}\left(1+\mathrm{Erf}\left[\frac{n^*}{\sqrt{2}}\right]\right) - n^*\frac{e^{-\frac{n^{*2}}{2}}}{\sqrt{2\pi}}, \tag{70}$$

where $n^* = n^*\left(\frac{\Theta_b}{\epsilon}\right)$ as given by Equation (64). We note that $\beta\left(\frac{\Theta_b}{\epsilon}\right)$ can also be considered as a function of n^*. By combining Equations (62), (64), and (70) we obtain the critical connectivity

$$p^*_{NL} = \frac{\Theta_b}{p_f(\kappa)\,\epsilon\omega}\cdot\frac{1}{\beta\left(\frac{\Theta_b}{\epsilon}\right)}. \tag{71}$$

The function $\beta(\cdot)$ itself is monotonically decreasing with ϵ in the validity range $\epsilon \in (0, \epsilon^{\max}]$ of the above approximation: within this interval $n^* > 0$ and $\frac{d}{dn^*}f(n^*) > 0$ and thus the derivative

$$\frac{d\beta}{d\epsilon} = \frac{d\beta}{dn^*}\cdot\frac{dn^*}{d\sqrt{\Theta_b/\epsilon}}\cdot\frac{d\sqrt{\Theta_b/\epsilon}}{d\epsilon} \tag{72}$$

$$= -\frac{e^{-\frac{n^{*2}}{2}}n^{*2}}{\sqrt{2\pi}}\cdot\left(\frac{df(n^*)}{dn^*}\right)^{-1}\cdot\sqrt{\frac{\Theta_b}{4\epsilon^3}} \tag{73}$$

$$< 0. \tag{74}$$

Consequently β assumes its minimum

$$\beta^{\min} = \beta\left(n^* = 0\right) = \frac{1}{2} \tag{75}$$

for $\epsilon = \epsilon^{\max} = \frac{2\Theta_b}{\pi}$ and increases monotonically with decreasing ϵ against its asymptotic value

$$\beta^{\max} = \lim_{n^*\to\infty}\left[\frac{1}{2}\left(1+\mathrm{Erf}\left[\frac{n^*}{\sqrt{2}}\right]\right) - n^*\frac{e^{-\frac{n^{*2}}{2}}}{\sqrt{2\pi}}\right] = 1. \tag{76}$$

Thus the critical connectivity is bounded by

$$p^0 := \frac{\Theta_b}{p_f(\kappa)\,\epsilon\omega} \le p^*_{NL} \le 2\cdot\frac{\Theta_b}{p_f(\kappa)\,\epsilon\omega} = 2\cdot p^0 \tag{77}$$

and converges to the lower bound p^0 for small ϵ and to its upper bound $2p^0$ for large ϵ.

In **Figure 6** we visualize the determination of the critical connectivity (Equations 64, 70) and Equation (71). The critical connectivity obtained with the approach presented above agrees well with simulation data (cf. **Figure 7**).

3.2.2. Transition from linear to non-linear propagation

In the previous section we derived analytical estimates for the critical connectivity p^*_{NL} in FFNs with non-additive dendritic interactions; p^*_{NL} is determined by (1) the setup of the FFN (i.e., the layer size ω and coupling strength ϵ; cf. **Figure 7**), (2) the parameters of the non-linear modulation function (i.e., the dendritic threshold Θ_b and enhancement level κ) and (3) the layout of the external network (i.e., the mean external input I_0 and its variance, which is proportional to ϵ^{ext}). In this section, we discuss the influence of the parameters of the non-linear modulation function and study the transition from a regime where propagation of synchrony is mediated by dendritically enhanced inputs to a regime where the majority of inputs is processed linearly.

In general, with increasing threshold Θ_b more and more inputs are needed to reach this threshold and consequently the critical connectivity p^*_{NL} increases. If Θ_b exceeds μ_L, which is the average input to the neurons if a synchronous pulse propagates in linearly coupled FFNs (cf. Equation 45 and **Figure 5**), propagation mediated by linearly processed spikes is enabled for lower connectivities than propagation mediated by dendritic non-linearities. In this regime the linearly summed inputs (for $p = p^*_L$) are sufficient to maintain propagation of synchrony, but are not sufficient to cross the dendritic threshold. Increasing Θ_b even further has no

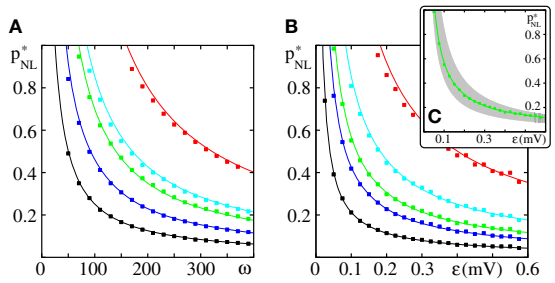

FIGURE 7 | Critical connectivity in FFNs with non-linear dendrites. The panels show **(A)** the critical connectivity p^*_{NL} vs. the layer size ω for different coupling strengths (ϵ = {0.05 mV (red), 0.1 mV (cyan), 0.125 mV (green), 0.2 mV (blue), and 0.4 mV (black)}) and **(B)** p^*_{NL} vs. the coupling strength ϵ for different layer sizes (ω = {50 (red), 100 (cyan), 150 (green), 200 (blue), and 400 (black)}). The points indicate the minimal connectivity for which a synchronous pulse propagates from the first to the last layer in an FFN with $m = 20$ layers in at least 50% of $n = 30$ trials. The critical connectivity given by Equation (71) (solid lines) is in good agreement with the computer simulations. **(C)** The critical connectivity is confined to the interval $p^*_{NL} \in [p^0, 2p^0]$ [indicated by the gray area for ω = 150 (green), cf. Equation (77)] and approaches its lower bound for small ϵ and its upper bound for large ϵ. Like in linearly coupled networks the critical connectivity decays inversely proportional to layer size, $p^*_{NL} \propto \omega^{-1}$, (cf. also **Figure 3**), but the scaling with coupling strength is more complicated, $p^*_{NL} \propto \epsilon^{-1} \cdot 1/\beta\left(\frac{\Theta_b}{\epsilon}\right)$; the factor $\beta\left(\frac{\Theta_b}{\epsilon}\right) \in [0.5, 1]$ [cf. Equation (70) and **Figure 6**] measures the deviation from the algebraic decay (as found in linearly coupled networks). In this figure the parameters of the external network are fixed to $I_0 = 5$ mV, $\nu^{\text{ext}} = 3$ kHz, $\epsilon^{\text{ext}} = 0.5$ mV.

influence on the critical connectivity p^*_{NL}, here a propagation of synchrony is possible for $p \geq p^*_L$ as discussed in section 3.1.

We illustrate this transition from non-linear to linear propagation in **Figure 8A**: We start with large $\Theta_b = \mu_L$ such that propagation is enabled for $p \approx p^*_L$ and also set $\kappa = \mu_L$. In fact, the linear critical connectivity p^*_L slightly under-estimates the observed critical connectivity p^*_{NL} as it does not account for the saturation of the non-linear modulation function, i.e., for the cutoff $\sigma_{NL}(x) = \kappa$ of inputs $x \geq \kappa$. With decreasing Θ_b the critical connectivity is substantially reduced and well approximated by Equation (71). Propagation of synchrony is now mainly mediated by dendritically enhanced inputs as described in section 3.2.1. The inset illustrates the impact of decreasing the dendritic threshold Θ_b on the iterated map. Initially, for $\Theta_b = \mu_L = \kappa$, the iterated map for linearly coupled and non-linearly coupled FFNs is similar; with decreasing Θ_b the jump like rise in the iterated map is shifted to lower group sizes and consequently the bifurcation point is shifted to lower connectivities.

The non-linear modulation function $\sigma_{NL}(\cdot)$ (cf. Equation 4) saturates for strong inputs, thus the enhancement level κ defines the maximal (effective) input to a neuron and $p_f(\kappa)$ is an upper bound for the spiking probability of any neuron in response to incoming inputs. This implies that in contrast to linearly coupled FFNs, the average size of a propagating synchronous pulse, γ_{NL}, given by the product of the probability of a neuron receiving sufficiently strong input to reach the dendritic threshold (p_γ; cf. Equation 56), the spiking probability due to that input [$p_f(\kappa)$] and the layer size ω, is bounded from above by

$$\gamma_{NL} = p_\gamma p_f(\kappa)\,\omega \leq \omega p_f(\kappa) =: \gamma^{\max}. \tag{78}$$

This bound decrease with decreasing κ as illustrated by **Figure 8B** (inset), where we compare the iterated maps for different values of κ. $p_f(\kappa)$ also influences the critical connectivity p^*_{NL} (cf. Equation 71): For small κ the spiking probability $p_f(\kappa)$ is low and thus p^*_{NL} is large (it may even exceed p^*_L). With increasing κ also $p_f(\kappa)$ increases and consequently the critical connectivity p^*_{NL} decreases; for very large κ the spiking probability $p_f(\kappa)$ approaches 1 (cf. Equation 14) and p^*_{NL} saturates (cf. **Figure 8B**).

In **Figure 8C** we show the critical connectivity for an additive enhancement by a constant Δ, i.e., inputs exceeding the dendritic threshold Θ_b are increased by the constant value $\Delta = \kappa - \Theta_b$. For small κ the critical connectivity p^*_{NL} is relatively large and may exceed p^*_L due to the low saturation level of the non-linear modulation function $\sigma_{NL}(\cdot)$ (cf. also **Figure 8B**). As mentioned above, with increasing κ, also $p_f(\kappa)$ increases and the critical connectivity p^*_{NL} decreases. However, for large κ and thus large dendritic threshold Θ_b propagation of synchrony mediated by linearly processed spikes is possible for lower connectivities than propagation mediated by dendritic non-linearities. Consequently, p^*_{NL} converges toward p^*_L (cf. also **Figure 8A**).

3.2.3. *Influence of external network*

In section 3.2.1 we derived an estimate of the critical connectivity p^*_{NL} for FFNs with non-additive dendritic interactions. So far we discussed the influence of the setup of the FFN (layer size ω and coupling strength ϵ) as well as the parameters of the non-linear modulation function σ_{NL} (dendritic threshold Θ_b and enhancement level κ). In the current section, we focus on the remaining determining factor, the layout of the external network. How does the critical connectivity change with the mean external input I_0 and external coupling strength ϵ^{ext} and how well are these changes covered by our analytics?

For the derivation of p^*_{NL} we assumed that somatic spikes are elicited exclusively by dendritically enhanced inputs (cf. Equation 54) and thus the critical connectivity depends on the layout of the external network only via $p_f(\kappa)$ (cf. also Equation 71), i.e., on the average spiking probability of a neuron receiving an input larger than the dendritic threshold $x \geq \Theta_b$. For sufficiently small $p_f(\kappa)$, $p^*_{NL} > 1$ and propagation of synchrony is not possible. With increasing $p_f(\kappa)$ the critical connectivity decreases and for $p_f(\kappa) \to 1$ it converges to $\Theta_b\,(\epsilon\omega\beta\,[\Theta_b/\epsilon])^{-1}$, independent of the external network.

In the regime of low spiking rates, changing the mean external input I_0 simply shifts the distribution of membrane potentials $P_V(V)$ (which is a Gaussian distribution centered at I_0; cf. Equation 8). Thus, with increasing I_0, $p_f(\kappa)$ increases and the critical connectivity p^*_{NL} decreases.

In **Figure 9A** we show the critical connectivity for different ϵ^{ext} [which determines the width of $P_V(V)$] vs. the mean external input I_0. For $I_0 = \Theta - \kappa$ (such that the sum of a dendritically enhanced input and the center of the distribution of membrane

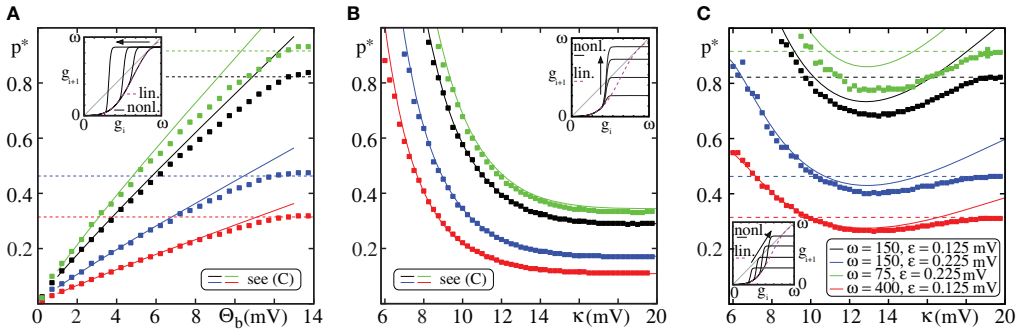

FIGURE 8 | Transition from linear to non-linear propagation. The figure shows the critical connectivity p^*_{NL} vs. the parameters of the non-linear modulation function σ_{NL} (cf. Equation 4) for different network setups (color code, see **(C)**). The lines are the theoretical predictions for p^*_{NL} [solid, Equation (71)] and p^*_L [dashed, Equation (32)]. The markers indicate the minimal connectivity for which a synchronous pulse propagates from the first to the last layer in an FFN ($I_0 = 5$ mV, $\nu^{ext} = 3$ kHz, $\epsilon^{ext} = 0.5$ mV) with $m = 20$ layers in at least 50% of $n = 30$ trials. The insets illustrate the effect of changing Θ_b and κ on the iterated map, cf. Equation (13), where connectivity is kept constant. **(A)** Critical connectivity vs. dendritic threshold Θ_b for constant enhancement level $\kappa = \mu_L \approx 13.7$ mV (cf. Equation 50). If the dendritic threshold Θ_b is sufficiently small such that $p_f(\Theta_b) \ll p_f(\kappa)$ (cf. Equation 54), the propagation of synchrony is mainly mediated by non-linear enhanced inputs and the critical connectivity can be estimated by Equation (71). For large Θ_b the probability that an input from the preceding layer exceeds the dendritic threshold is very low, propagation of synchrony is mainly mediated by linearly processed inputs and the critical connectivity is given by Equation (32). Between these scenarios (for moderate Θ_b) there is a "transition regime," where linear and non-linear propagation mix [similarly in **(C)**]. **(B)** Critical connectivity vs. enhancement level κ for constant threshold $\Theta_b = 4$ mV. For small enhancement levels κ the (maximal) spiking probability of a single neuron, $p_f(\kappa)$, is small and thus the critical connectivity p^*_{NL} is large. With increasing κ, $p_f(\kappa)$ increases and thus p^*_{NL} decreases; for large κ, $p_f(\kappa) \to 1$ (a neuron will almost surely spike upon the receipt of a non-linearly enhanced pre-synaptic input) and the critical connectivity saturates. **(C)** Critical connectivity vs. enhancement level κ for an additive enhancement by a constant $\Delta = \kappa - \Theta_b = 4$ mV. For further explanations see text (section 3.2.2).

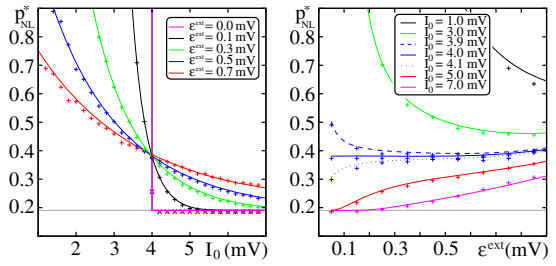

FIGURE 9 | Dependence of the critical connectivity p^*_{NL} on the layout of the external network. (A,B) The lines indicate the theoretical prediction for p^*_{NL} given by Equation (71) and agree well with the data from direct numerical simulations (markers; FFN with $\omega = 150$, $\epsilon = 0.2$ mV, $\Theta_b = 4$ mV, $\kappa = 11$ mV, $m = 20$). Panel **(A)** shows the critical connectivity vs. the mean external input I_0 for fixed ϵ^{ext} and panel **(B)** shows the critical connectivity vs. ϵ^{ext} for fixed mean external input I_0. The gray line indicates the minimal critical connectivity obtained for $p_f(\kappa) = 1$. With increasing mean (external) input I_0 the distribution of membrane potentials $P_V(V)$ is shifted toward the somatic threshold Θ, thus the spiking probability $p_f(\kappa)$ upon the reception of a non-linear enhanced input increases and the critical connectivity p^*_{NL} decreases. For $I_0 = \Theta - \kappa$, $p_f(\kappa) \approx 0.5$ (cf. Equation 80) and p^*_{NL} is largely independent of the layout of the external network [blue solid line in **(B)**; cf. also **(A)** where all curves coincide]. Further explanations see text (section 3.2.3).

potentials equals the somatic threshold Θ), $p_f(\kappa)$ simplifies to

$$p_f(\kappa) = \frac{1}{2}\left(\mathrm{Erf}\left[\frac{\Theta - I_0}{\sigma}\right] + \mathrm{Erf}\left[\frac{\kappa - \Theta + I_0}{\sigma}\right]\right) \quad (79)$$

$$= \frac{1}{2}\mathrm{Erf}\left(\frac{\Theta - I_0}{\sigma}\right) \quad (80)$$

and thus in the regime of low spiking rates, i.e., $(\Theta - I_0)/\sigma \gg 1$, $p_f(\kappa) \approx 0.5$ independent of the width of the distribution of membrane potentials. Consequently, all curves for different ϵ^{ext} coincide at this point. For $I_0 > \Theta - \kappa$ the majority of neurons (>50%) would spike upon receipt of a dendritically enhanced input. Thus $p_f(\kappa)$ increases and therewith the critical connectivity decreases upon decreasing ϵ^{ext} . In the limit of $\epsilon \to 0$, $P_V(V)$ converges toward a δ-distribution centered at I_0 and p_f becomes a step-function

$$p_f(\kappa) = \begin{cases} 0 & \kappa < \Theta - I_0 \\ 1 & \kappa \geq \Theta - I_0 \end{cases} \quad (81)$$

such that the critical connectivity is either constant and minimal for $I_0 \geq \Theta - \kappa$ or it diverges (no propagation possible) for $I_0 < \Theta - \kappa$ (cf. **Figure 9A**; magenta curve).

In **Figure 9B** we illustrate the effect of changing ϵ^{ext} on the critical connectivity for constant I_0. As discussed above for $I_0 = \Theta - \kappa$, $p_f(\kappa)$ and thus p^*_{NL} are rather independent of ϵ^{ext} and for $I_0 > \Theta - \kappa$ the critical connectivity increases with ϵ^{ext}. For $I_0 < \Theta - \kappa$ an increase of the width of the distribution of membrane potentials shifts the membrane potential of more and more neurons toward the relevant interval $[\Theta - \kappa, \Theta]$ and thus $p_f(\kappa)$ increases and the critical connectivity p^*_{NL} decreases.

For the derivation of p^*_{NL} we have assumed that the ground state dynamics is essentially not influenced by the spontaneous activity of the FFN itself (i.e., $\mu = I_0$ and $\sigma = \epsilon^{ext}\sqrt{2\tau^m \nu^{ext}}$). As

discussed in section 3.1.3, we can correct the results for such influences. However, since in non-linearly coupled FFNs the impact of (non-linearly enhanced) synchronous activity is much stronger than the impact of spontaneous activity (which is irregular and not amplified by non-additive dendritic interactions), we find that the deviations between the corrected and uncorrected version of p^*_{NL} is negligible.

Finally, we compare the critical connectivity for networks with and without non-additive dendritic interactions: The factor

$$c^{\text{rat}} := \frac{p^*_L}{p^*_{NL}} = \frac{p_f(\kappa)}{\lambda\Theta_b}\beta\left(\frac{\Theta_b}{\epsilon}\right) \tag{82}$$

measures how much the connectivity within the FFN can be reduced by introducing non-additive dendritic interactions. It is independent of the layer size ω and becomes maximal in the limit of small coupling strengths ϵ as $\beta(\Theta_b/\epsilon) \to \beta^{\max} = 1$ for $\epsilon \to 0$ (cf. Equation 76). It increases with decreasing Θ_b and increasing κ (see discussion in section 3.2.2). In **Figure 10** we show the influence of the external network. As discussed above, for small I_0, propagation of synchrony is not possible (the non-linear enhanced input is insufficient to elicit sufficiently many spikes in the layers of the FFN; white areas in **Figure 10**). With increasing I_0, p^*_{NL} decreases and c^{rat} increases.

3.3. GENERALIZATIONS

In the final section we discuss generalizations of the methods and results we derived. Compared to biological neurons, our models have simplifications which enable the analytical treatment, but might be suspected to be influential on the final result. These simplifications are the homogeneous delay distribution, the simplified initiation and impact of dendritic spikes, the limit of short synaptic currents and the sub-threshold leaky integrate-and-fire dynamics. Here, we verify that our results generalize to biologically more detailed neurons without these simplifications. In particular, we show that the estimates for the critical connectivity hold. Further, we consider a qualitatively different dendritic interaction function which assumes that the saturation is incomplete, i.e., beyond a region of saturation the impact of larger inputs increases. We show that the tools developed in the article are still applicable and reveal a new phenomenon, the coexistence of linear and non-linear propagation of synchrony.

In the first part (section 3.3.1), we discuss the influence of inhomogeneous delay distribution and finite dendritic integration windows. In the second part (section 3.3.2), we consider the non-linear modulation function with incomplete saturation. Finally, we consider biologically more detailed neuron models (section 3.3.3).

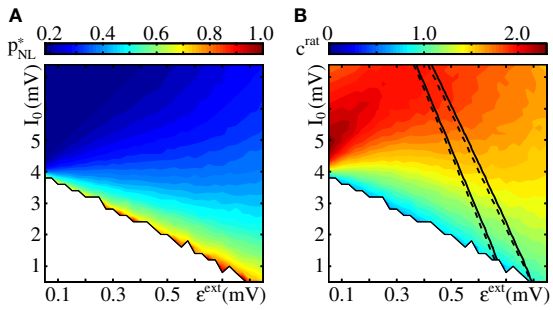

FIGURE 10 | Critical connectivity and reduction factor. Panel **(A)** shows the critical connectivity obtained from simulations of an FFN ($\omega = 150$, $\epsilon = 0.2$ mV, $m = 20$) incorporating non-additive dendritic interactions ($\Theta_b = 4$ mV, $\kappa = 11$ mV; see also **Figure 9**). Within the white area, propagation of synchrony is impossible because even for a fully coupled chain the input to the next layer (limited by the saturation of the non-linear modulation function and the layer size) is insufficient. Panel **(B)** shows the reduction factor c^{rat} (cf. Equation 82), the quotient between the critical connectivity in FFNs without and with non-additive dendritic interactions. The lines enclose the area for which the spontaneous firing is between $\nu \in [0.5, 1.5]$ Hz obtained from simulations (solid) and low-rate approximation (cf. Equation 9; dashed).

3.3.1. Heterogeneous delays

So far we considered FFNs with homogeneous delay distribution and dendritic modulation functions with integration window of zero length, i.e., only exactly synchronized inputs were possibly non-linearly amplified. Are these assumptions crucial for the obtained results? How does the critical connectivity change in the presence of heterogeneous delay distributions?

To answer this question, we consider synaptic delays τ_{kl} (specifying the synaptic delay between neuron l and k) uniformly drawn from

$$\tau_{kl} \in \left[\tau - \frac{\Delta T}{2}, \tau + \frac{\Delta T}{2}\right], \tag{83}$$

where τ is the mean delay. A direct consequence of heterogeneous delay distribution is that the spikes of the propagating synchronous signal are not simultaneous (i.e., exactly synchronized) anymore. To describe the system accurately one has to consider additionally to the size (g_i) also the temporal jitter (s_i) of the synchronous pulse in the ith layer and investigate the two-dimensional iterated map for (g_i, s_i) (e.g., Diesmann et al., 1999; Gewaltig et al., 2001; Goedeke and Diesmann, 2008). However, even if the synchronous pulse is blurred out to a pulse packet with finite width, for sufficiently large connectivity stable propagation still can be obtained (see e.g., Gewaltig et al., 2001).

For linearly coupled FFNs, with increasing width of the delay distribution, ΔT, the propagating pulse becomes broader and thus the critical connectivity p^*_L increases (cf. **Figures 11A,B**; squares). However, the scaling with layer size (cf. **Figure 11A**) and coupling strength (data not shown) is the same.

Under the assumption that the width of the pulse packet stays bounded, one can derive a lower bound for the critical connectivity. We assume that a pulse in layer i is perfectly synchronized and calculate the effective peak of the depolarization in the $(i+1)$th layer. Replacing the coupling strength ϵ by the effective depolarization ϵ' (derived below, cf. Equation 89) in the estimate of the critical connectivity (cf. Equation 32) one gains an estimate of the critical connectivity for systems with heterogeneous delays [Equation (90); shown in **Figure 11**]. Consider a perfectly synchronized pulse in layer i. Due to inhomogeneities in the delay, the inputs arriving at the $(i+1)$th layer are distributed uniformly in an interval of size ΔT (Equation 83). We assume that all inputs

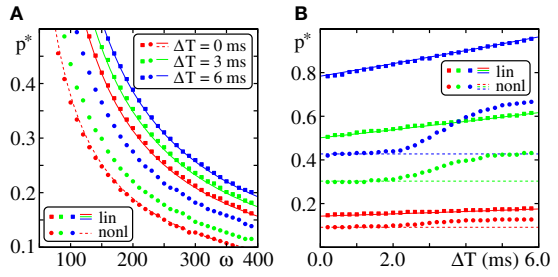

FIGURE 11 | Robustness against heterogeneities in the response delays. (A) Critical connectivity vs. layer size for FFNs ($m = 20$, $\epsilon = 0.25$ mV, $I_0 = 5$ mV, $\epsilon^{\text{ext}} = 0.5$ mV) with additive (squares) and non-additive ($\Theta_b = 4$ mV, $\kappa = 11$ mV, $\Delta t = 2.5$ ms; circles) dendritic interactions. Different colors indicate different widths of the delay distribution (cf. Equation 84). The solid lines indicate the critical connectivity p_L^* corrected for inhomogeneous delay distribution (cf. Equation 90), the dashed line p_{NL}^* for $\Delta T = 0$ ms. **(B)** Critical connectivity vs. width of delay distribution ΔT. Different colors indicate different setups of the FFN (red: $\omega = 275$, $\epsilon = 0.4$ mV; green: $\omega = 125$, $\epsilon = 0.25$ mV; blue: $\omega = 200$, $\epsilon = 0.1$ mV). Solid and dashed lines are p_L^* and p_{NL}^* as before.

arriving at a neuron of layer $i+1$ are equidistantly distributed over $[-\Delta T/2, \Delta T/2]$, i.e., the arrival time of the lth of a total number of k inputs is

$$t_l^{\text{arr}} = \tau - \frac{\Delta T}{2} + \frac{\Delta T}{k-1} \cdot (l-1)\,. \tag{84}$$

We consider the subthreshold dynamics only. Each single input depolarizes the neuron by an amount ϵ and afterwards the membrane potential $V(t)$ decays exponentially toward its asymptotic value (I_0) with the membrane time constant τ^{m} (cf. Equations 1, 2) until the next input arrives after a time interval $\frac{\Delta T}{k-1}$ (cf. Equation 84). Thus the total (effective) depolarization caused by the sum of these k inputs at the end of the considered time interval $\left(\tau + \frac{\Delta T}{2}\right)$ is

$$\Delta\epsilon_k = \sum_{l=1}^{k} \epsilon \exp\left(-\frac{1}{\tau^{\text{m}}}\frac{\Delta T}{k-1}(l-1)\right) \tag{85}$$

$$= \epsilon \frac{\exp\left(-\frac{\Delta T}{\tau^{\text{m}}}\frac{k}{k-1}\right) - 1}{\exp\left(-\frac{\Delta T}{\tau^{\text{m}}}\frac{1}{k-1}\right) - 1}. \tag{86}$$

We consider the effective depolarization per input, ϵ', in the limit of a large number of inputs k ($k \to \infty$),

$$\epsilon' = \lim_{k\to\infty}\left(\frac{\Delta\epsilon_k}{k}\right) \tag{87}$$

$$= \frac{\tau^{\text{m}}}{\Delta T}\left(1 - \exp\left[-\frac{\Delta T}{\tau^{\text{m}}}\right]\right)\epsilon \tag{88}$$

$$=: C(\Delta T)\,\epsilon. \tag{89}$$

Thus the correction factor $C(\Delta T) \leq 1$ defined in Equation (89) relates the coupling strength ϵ to the effective coupling strength ϵ' in the presence of inhomogeneous delays. The critical connectivity is then given by (cf. Equation 32)

$$p_L^* = \frac{1}{C(\Delta T)} \cdot \frac{1}{\lambda^* \epsilon \omega} \tag{90}$$

and this estimate agrees well with direct numerical simulations (cf. **Figure 11**).

For FFNs with dendritic non-linearities and inhomogeneous delays τ_{kl}, one has to consider a finite dendritic integration window Δt^{d}. Instead of amplifying only simultaneously received spikes (cf. Equation 5), the sum of spikes within the time interval Δt is considered. We denote the sum of inputs to a neuron within the time interval $[t - \Delta t, t]$ by

$$S_k^{\Delta t}(t) = \sum_l \sum_m \epsilon \chi_{[t-\Delta t,\, t]}\left(t_{lm}^f + \tau_{kl}\right), \tag{91}$$

where

$$\chi_A(x) = \begin{cases} 1 & \text{if } x \in A \\ 0 & \text{if } x \notin A \end{cases} \tag{92}$$

is the indicator function and t_{lm}^f is the mth firing time of neuron l as before. If $S_k^{\Delta t}(t)$ exceeds the dendritic threshold Θ_b for some $t = t_0$, neuron k is depolarized additionally (to the depolarization arising from linear spike summation) by

$$\epsilon_\kappa^{\text{add}}(t_0) = \kappa - S_k^{\Delta t}(t_0) \tag{93}$$

such that the total (effective) depolarization caused by an input $x \geq \Theta_b$ equals κ, modeling the effect of a dendritic spike; cf. also section 3.3.3. After such an additional depolarization the dendrite becomes refractory for a time $t^{\text{ref,ds}}$ and does not transfer additional spikes within the interval $\left[t_0, t_0 + t^{\text{ref,ds}}\right]$. For $\Delta t = 0$ we recover the non-linear modulation function $\sigma_{NL}(\cdot)$ given by Equation (4). Due to the finite dendritic interaction window, a delay distribution with $\Delta T \leq \Delta t$ affects the critical connectivity only weakly (cf. **Figure 11B**). For $\Delta T > \Delta t$, some of the inputs received from the preceding layer upon a propagation of synchrony fall out of the dendritic interaction window ΔT and thus the critical connectivity increases. However, the scaling with layer size ω (cf. **Figure 11B**) and coupling strength ϵ (data not shown) is practically identical with the scenario $\Delta T = 0$.

Before we discuss propagation of synchrony in biologically more plausible neuron models in section 3.3.3, we consider generalization of the non-linear modulation function in the following section.

3.3.2. Coexistence of linear and non-linear propagation

In this article, we employed a non-linear modulation function $\sigma_{NL}(\epsilon)$ that is linear for dendritic stimulation smaller than the dendritic threshold, $\epsilon < \Theta_b$, and constant (i.e., saturates) for supra-threshold stimulation, $\epsilon \geq \Theta_b$ (cf. Equation 4).

Biologically, if the linear inputs are transmitted despite the dendritic sodium spike and are not shadowed by, e.g., an NMDA spike, they may lead to a second, later peak depolarization after the one generated by the sodium spike. Since our models replace depolarizations by jumps to the peak depolarization, we have to account for the later peak as soon as it exceeds the earlier one. In this part, we thus assume that if the synchronous input is so large that the depolarization it generates upon linear summation exceeds the depolarization κ generated by the dendritic spike, this former is considered as the effect of the input. In other words, we assume that the dendritic modulation function continues linearly beyond κ, i.e., we define

$$\sigma'_{NL}(\epsilon) = \begin{cases} \epsilon & \text{for} \quad \epsilon \leq \Theta_b \\ \kappa & \text{for} \quad \Theta_b \leq \epsilon \leq \kappa \\ \epsilon & \text{for} \quad \epsilon \geq \kappa \end{cases} \tag{94}$$

(cf. inset of **Figure 12A**).

The iterated map, mapping the number of active neurons in layer i to the average number of active neurons in layer $i+1$ may now have (depending on the system parameters) between one and five fixed points (cf. **Figure 12**). As before, $G_0 = 0$ is a trivial fixed point corresponding to the level of absent activity and the only fixed point of the iterated map for small connectivity p. With increasing connectivity p, two additional pairs of fixed points $G_1 \leq G_2$ and $G_3 \leq G_4$ appear via tangent bifurcations. The first pair of fixed points, G_1 and G_2, correspond to the propagation of synchrony mediated by non-additive dendritic interactions (as discussed in section 3.1), the second pair, G_3 and G_4, correspond to propagation of synchrony mediated by linearly processed inputs (as discussed in section 3.2). By further increasing the connectivity p, the fixed points G_2 and G_3 disappear via a tangent bifurcation (cf. **Figure 12A**). Within the region, where five fixed points exists, both types of propagation of synchrony coexists (illustrated in **Figures 12B–D**): Synchronized pulses of size $g_0 < G_1$ typically decay to zero after a small number of layers. Pulse sizes with $G_1 < g_0 < G_3$ typically initiate propagation of synchrony with an average pulse size around G_2 (where the propagation is mediated by non-additive dendritic interactions) and synchronous pulses of size $g_0 > G_3$ typically initiate propagation of synchrony with average pulse sizes around G_4 (linear propagation). For sufficiently large p, i.e., the fixed points G_2 and G_3 disappeared, a synchronized pulse of size $g_0 \geq G_1$ will initiate propagation of synchrony with pulse sizes around G_4; in this parameter region the non-additive dendritic interactions essentially increase the basin of attraction of G_4.

Within the framework of our analytical tractable model, we neglect, e.g., the initiation time of a dendritic spike (in our model non-linear amplifications are instantaneous) or the different shapes of potential deflections caused by linearly and non-linearly processed inputs. Therefore, propagating synchronous signals mediated either by linear or non-linear dendrites differ only in their size. In biological more detailed models (briefly discussed in section 3.3.3 below) both propagation types will be more distinct, e.g., the propagation frequency (speed) and the quality of synchrony of the propagating pulses are different (see also Jahnke et al., 2012).

3.3.3. Biological more detailed models

The model we mainly consider in this article has the advantage of being analytically tractable. Here we ask whether it over-simplifies the considered systems. More precisely, we study whether the results derived above, in particular the analytical estimates for the critical connectivity, generalize to biologically more detailed models.

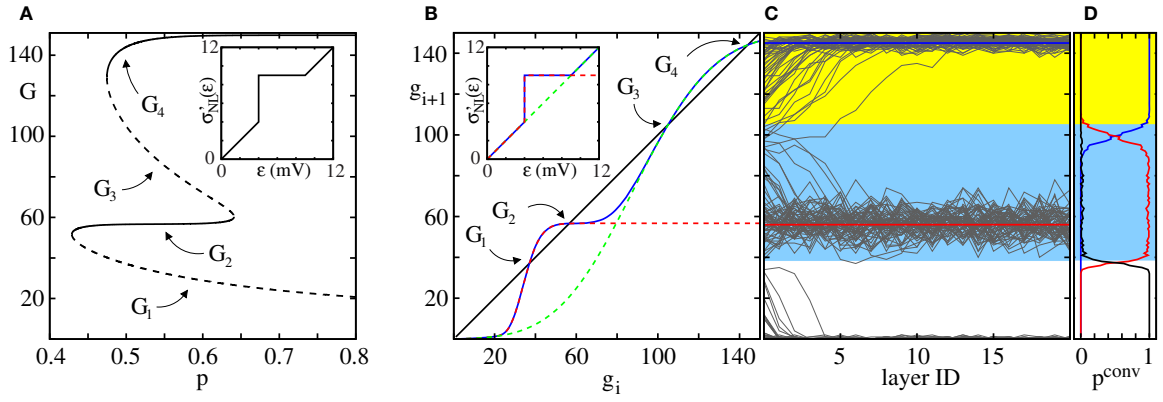

FIGURE 12 | Coexistence of linear and non-linear propagation. **(A)** Bifurcation diagram obtained from Equation (13) for an FFN ($\omega = 150$, $\epsilon = 0.225$ mV) with a non-linear modulation function σ'_{NL} with incomplete saturation [cf. Equation (94) and inset]. Panel **(B)** shows the iterated maps (Equation 13) for $p = 0.5$ with the different non-linear modulation functions considered in this article (linear coupling: green,dashed; non-linear coupling σ_{NL}: red, dashed; modified non-linear coupling σ'_{NL}: blue). Panel **(C)** depicts the development of the size of the synchronous pulse along the layers of the FFN (single trials). The blue and yellow regions are the basins of attraction of G_2 and G_4, respectively, derived from the data in panel **(B)**. Panel **(D)** shows the probability p^{conv} of converging to the linear propagation regime (yellow area, blue line) and the non-linear propagation regime (blue area, red line) after $m = 20$ layers (p^{conv} is obtained from $n = 150$ runs with different networks and initial conditions).

The main assumption underlying our analysis of linearly coupled networks is a very general one, namely that synchronous single inputs sum up linearly: we assumed that the spiking probability $p_f(\cdot)$ of a neuron due to the reception of x synchronous inputs of size ϵ equals the spiking probability due to the reception of one single input of size $y = x\epsilon$. Therefore, the results will hold also for more complex neuron models, as long as the effect of a synchronous input pulse is approximately the sum of the effects of single inputs. In particular, if the spiking probability due to an input of strength x, $p_f(x)$, is sufficiently slowly changing with x, according to Equation (24) the critical connectivity scales like $p_L^* \propto (\epsilon\omega)^{-1}$ for sufficiently large layer sizes and small coupling strengths. To fully compute the critical connectivity, the actual form of $p_f(\cdot)$ has to be known. Our leaky integrate-and-fire neuron with infinitesimally short current pulses approximates the behavior of a wide class of neuron models for which an analytical derivation of $p_f(\cdot)$ is impossible. Still even for more detailed models, $p_f(\cdot)$ is accessible for measurements in single neuron (computer) experiments.

In **Figure 13** we verify our predictions exemplary for two types of neuron models: We employ a model of conductance based leaky integrate-and-fire-type neurons with exponential input conductances (CB-type; see Appendix) and a Hodgkin-Huxley-type neuron model with alpha-function shaped input currents (HH-type; see Appendix). The post-synaptic potential induced by single excitatory inputs is shown in panels (a) and (b) and the scaling of the critical connectivity p_L^* with $\epsilon\omega$ in panel (c): the scaling of p_L^* is well described by $p_L^* \propto (\epsilon\omega)^{-1}$.

The main assumptions underlying our analysis of non-linearly coupled networks are (1) that the maximal spiking probability due to inputs which are subthreshold relative to the dendritic threshold, $p_f(\Theta_b)$, is significantly smaller than the spiking probability due to a suprathreshold input, $p_f(\kappa)$, and (2) that the temporal jitter of somatic spikes evoked by suprathreshold inputs is small such that synchronized inputs stay synchronized. Both conditions have been found to be satisfied in biological neurons (e.g., Ariav et al., 2003). Therefore, Equation (71) specifying the critical connectivity p_{NL}^* also holds for more detailed neuron models if these models incorporate biologically plausible features of fast dendritic spikes. To obtain a quantitative prediction of p_{NL}^*, it is sufficient to estimate (a) the number of inputs needed to elicit a dendritic spike, Θ_b/ϵ, (b) the layer size ω, and (c) the spiking probability due to the reception of a total input that is sufficiently strong to elicit a dendritic spike.

To investigate the scaling of the critical connectivity p_{NL}^* in direct numerical simulations, we account for the effects of dendritic spikes in the CB-type and HH-type: When the total excitatory input within the dendritic integration window exceeds the dendritic threshold level, a current pulse modeling the effect of a dendritic spike is initiated and causes an additional

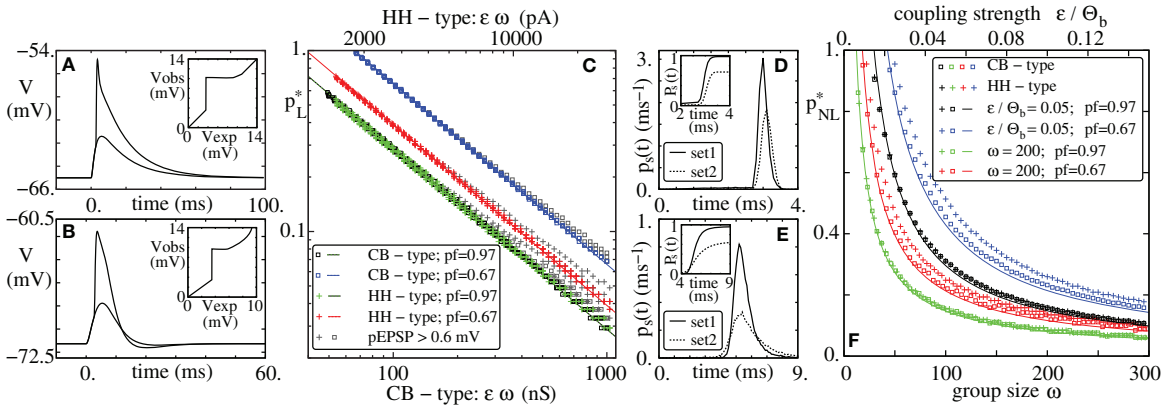

FIGURE 13 | Same scaling of propagating regime for networks of biologically more detailed neuron models. (A,B) Time course of the membrane potential of single neurons receiving inputs that are sufficiently strong to elicit a dendritic spike, with (non-linear model) and without (linear model) dendritic spike generation mechanism, for **(A)** a conductance based LIF-type neuron (henceforth: CB-type), and **(B)** a Hodgkin–Huxley-type neuron (HH-type). The insets show the observed peak of the induced postsynaptic potential (pEPSP) vs. the pEPSP expected from linear input summation (equivalent to the dendritic modulation function in the analytically tractable model). **(C)** Critical connectivity p_L^* vs. $\epsilon\omega$ in linearly coupled networks. For each value $\epsilon\omega$, we evaluated the critical connectivity for four different group sizes $\omega = 100, 300, 500, 700$ and four different coupling strengths $\epsilon = 0.3$, 0.6, 0.9, 1.2 nS (CB-type; squares; lower horizontal axis) and $\epsilon = 9$, 18, 27, 36 pA (HH-type; crosses; upper horizontal axis), respectively. The lines are fitted functions of the form $(\lambda\epsilon\omega)^{-1}$. The analytical estimate given by Equation (24) holds in the limit of large layer sizes ω and small couplings ϵ, therefore we exclude data points from the fitting where a single input yields an EPSP larger than 0.6 mV (CB-type: $\epsilon \geq 1.4$ nS; HH-type: $\epsilon \geq 46$ pA; these points are marked in gray). **(D,E)** Probability distribution of somatic spike times after stimulation of the neuron by an input which is sufficiently strong to generate a dendritic spike (**D**: CB-type, **E**: HH-type). We show exemplary two different configurations for the external inputs, which result in a total somatic spiking probability after dendritic spike generation of $p^f \approx 0.97$ (solid lines; set 1) and $p^f \approx 0.67$ (dashed lines; set 2). p^f equals the saturation level of the corresponding cumulative distribution function (shown in the insets). **(F)** Critical connectivity p_{NL}^* vs. group size ω (lower horizontal scale) and coupling strength ϵ normalized by threshold Θ_b (upper horizontal scale), respectively. The theoretical estimate of p_{NL}^* (cf. Equation 71) is a function of ω, Θ_b/ϵ and p^f, therefore the predictions agree for both models and the data from direct numerical simulations are consistent with the theoretical predictions. [All simulations of FFNs in this figure are obtained for inhomogeneous delay distribution with $\Delta T = 1$ ms (cf. Equation 83)].

depolarization of the soma of the post-synaptic neuron (see Appendix for details; cf. also section 3.3.1). In **Figure 13** we compare the results of direct numerical simulations with the estimate given by Equation (71). The post-synaptic potential induced by single excitatory inputs is shown in panels (A) and (B). Panel (D) and (E) shows the spiking probability of a single neuron (in the ground state of the FFN), p^f, due to an input exceeding the dendritic threshold level; as examples we present two different setups with $p^f = \{0.67, 0.97\}$. Panel (F) shows the scaling of p^*_{NL} with layer size and coupling strength and the good agreement of the analytical estimate with direct numerical simulations.

4. SUMMARY AND CONCLUSIONS

Propagation of synchrony in feed-forward sub-structures that are embedded in randomly connected recurrent networks has been a research topic for more than two decades now [see, e.g., review on this topic (Kumar et al., 2010)] and it is hypothesized that such propagation possibly explain the emergence of spatio-temporal spike patterns and information transmission.

In this article, we have analyzed diluted FFNs and investigated their capability to propagate synchrony. In addition to conventional additive (linear) input processing at single neurons, we considered non-additive dendritic interactions modeling the impact of fast dendritic spikes (Ariav et al., 2003; Gasparini et al., 2004; Polsky et al., 2004; Gasparini and Magee, 2006). We emulated the influence of the embedding recurrent network which establishes the irregular ground state in the FFN, by random Poissonian inputs (van Vreeswijk and Sompolinsky, 1996, 1998; Brunel, 2000). This approach does not account for back-reactions of activity within the FFN on the embedding network. It is justified as long as the connectivity and connection strength between the neurons of the FFN and the embedding network is low and weak compared to the feed-forward connectivity and connection strength. The back-reaction then influences the activity of the embedding network only weakly and a robust propagation of synchrony can be achieved (Vogels and Abbott, 2005; Kumar et al., 2008; Jahnke et al., 2012). Yet, if the condition is not met, synchronous activity within the FFN may spread out over the embedding network and potentially cause pathological activity ("synfire-explosions") (Mehring et al., 2003). For specifically structured networks also more complex interactions are possible, such as an enhancement of propagating synchrony (manuscript in preparation).

In the main part of the article, we studied the propagation of synchrony employing leaky integrate-and-fire neurons in the limit of temporally short synaptic inputs and homogeneous synaptic delays. Synchronous pulses consist of exactly synchronized (simultaneous) spikes. This allows to investigate propagation of synchrony by considering the size of a synchronized pulse only, so that the analysis becomes analytically tractable. Nevertheless, in the second part of our article we also consider systems with heterogeneous coupling delays and temporally extended interactions. In agreement with the literature (e.g., Diesmann et al., 1999; Gewaltig et al., 2001; Goedeke and Diesmann, 2008), we observe that pulse packets tend to synchronize along the layers of the FFN so that the results of our simplified description are directly applicable.

We derived scaling laws as well as quantitative estimates for the critical connectivity marking the bifurcation point between the regime where robust propagation of synchrony is possible and where it is not. In particular, based on a suitable series expansion we have shown that for linearly coupled FFNs the critical connectivity decays inversely proportional to layer size and coupling strength. Moreover, the proportionality factor can be estimated from the ground state properties of the single neurons. The estimate agrees with direct numerical simulations within the biologically relevant parameter regime where (a) the spontaneous firing rate of the neurons is low and (b) the distribution of membrane potentials is broad (each neuron receives a huge number of almost random presynaptic inputs). If a synchronous pulse propagates along the layers of a linearly coupled FFN, most of the neurons of each layer participate in the propagation of synchrony, independent of the actual layer size, coupling strength or layout of the external network.

For neurons incorporating non-additive dendritic interactions, the spiking probability as a function of the dendritic stimulation becomes discontinuous. Therefore, the analytical estimation of the critical connectivity in non-linearly coupled FFNs required a different approach than the treatment of linearly coupled FFNs. We have shown that the critical connectivity decays inversely proportional to the layer size (as in linearly coupled FFNs), and we have derived the dependence on the coupling strength which is more complicated. The critical connectivity is completely determined by layer size, spiking probability of the single neuron upon the reception of a non-linearly enhanced presynaptic input and the number of inputs required to reach the dendritic threshold. Our results indicate that in presence of non-linear dendrites, neurons process synchronous inputs similar to threshold units. Such units have been previously used as simplified rate neuron models to study activity propagation in discrete time, e.g., in Nowotny and Huerta (2003); Leibold and Kempter (2006); Cayco-Gajic and Shea-Brown (2013). Because the non-linear modulation function saturates, FFNs with non-additive dendritic interactions allow for a sparser coding, i.e., only a sub-fraction of each layer (the actual size depends on the non-linear enhancement level) participates in the propagation of synchrony. Whereas stable propagation of synchrony is possible in systems with and without dendritic non-linearities, it occurs in non-linearly coupled FFNs with substantially reduced feed-forward anatomy (reduced connectivity or reduced coupling strength) compared to linearly coupled FFNs.

The analytic derivation of the critical connectivity is based on rather general assumptions: (a) the effect of a synchronous input pulse is approximately the sum of the effects of single inputs and (b) for networks with non-additive dendritic interactions the spiking probability due to non-linearly enhanced input is substantially larger than due to a non-enhanced input. Therefore the predictions and estimates are directly applicable to networks of biologically more detailed neuron models.

In our article we have shown that even highly diluted feed-forward structures are suitable to reliably support the directed and constrained propagation of synchronous activity. Such structures occur naturally in sparse, random recurrent networks which are typical for the cortex. These structures might be enhanced

by simple synaptic plasticity to enable synchrony propagation. Fast dendritic spikes promote this propagation, as they selectively amplify synchronous inputs and are only weakly influenced by irregular background activity.

Indeed, important candidate regions for the generation of propagating synchrony such as the hippocampus and other, neocortical regions exhibiting replay of activity (Nadasdy et al., 1999; Lee and Wilson, 2002; Ji and Wilson, 2007; Xu et al., 2011; Eagleman and Dragoi, 2012) are sparse and show synaptic plasticity (Debanne et al., 1998; Kobayashi and Poo, 2004). Dendritic spikes as prominently found in, e.g., the hippocampus (Ariav et al., 2003; Gasparini et al., 2004; Polsky et al., 2004; Gasparini and Magee, 2006) trigger depolarizations and calcium influx sufficient to change synaptic strengths (Golding et al., 2002; Remy and Spruston, 2007) and the dendrites itself exhibit branch "strength potentiation," i.e., the strength of a dendritic spike on a dendritic branch exhibits experience- and activity-dependent plasticity (Losonczy et al., 2008; Makara et al., 2009; Müller et al., 2012).

Our work indicates that fast dendritic spikes reduce the required synaptic strength and connection density for replay of spike patterns. Moreover, their saturation and the resulting sparse coding might explain the observed variability during replay. Thus, in particular, our understanding of propagation along diluted feed-forward chains may now be combined with knowledge on synaptic plasticity and generation of activity accompanying replay (e.g., sharp wave/ripples) to gain an integrated mechanistic understanding for encoding, replay and memory transfer.

ACKNOWLEDGMENTS

This work was supported by the BMBF (Grant No. 01GQ1005B) [Sven Jahnke, Marc Timme], the DFG (Grant No. TI 629/3-1) [Sven Jahnke], the Swartz Foundation [Raoul-Martin Memmesheimer], and the Max Planck Society [Marc Timme]. Simulation results of networks with biologically more complex neuron models were obtained using the simulation software NEST (Gewaltig and Diesmann, 2007). Sven Jahnke thanks Harold Gutch, Elian Moritz, and Jonna Jahnke for stimulating discussions.

REFERENCES

Abeles, M. (1982). *Local Cortical Circuits: An Electrophysiological Study*. Berlin: Springer. doi: 10.1007/978-3-642-81708-3

Ariav, G., Polsky, A., and Schiller, J. (2003). Submillisecond precision of the input-output transformation function mediated by fast sodium dendritic spikes in basal dendrites of CA1 pyramidal neurons. *J. Neurosci.* 23, 7750–7758.

August, D. A., and Levy, W. B. (1999). Temporal sequence compression by an integrate-and-fire model of hippocampal area CA3. *J. Comput. Neurosci.* 6, 71–90. doi: 10.1023/A:1008861001091

Aviel, Y., Mehring, C., Abeles, M., and Horn, D. (2003). On embedding synfire chains in a balanced network. *Neural Comp.* 15, 1321–1340. doi: 10.1162/089976603321780290

Braitenberg, V., and Schüz, A. (1998). *Cortex: Statistics and Geometry of Neuronal Connectivity*. Berlin: Springer. doi: 10.1007/978-3-662-03733-1

Brunel, N. (2000). Dynamics of sparsely connected networks of excitatory and inhibitory spiking neurons. *J. Comp. Neurosci.* 8, 183–208. doi: 10.1023/A:1008925309027

Brunel, N., and Hakim, V. (1999). Fast global oscillations in networks of integrate-and-fire neurons with low firing rates. *Neural Comp.* 11, 1621–1671. doi: 10.1162/089976699300016179

Bullmore, E., and Sporns, O. (2009). Complex brain networks: graph theoretical analysis of structural and functional systems. *Nat. Rev. Neurosci.* 10, 186–198. doi: 10.1038/nrn2618

Burkitt, A. (2006). A review of the integrate-and-fire neuron model: I. Homogeneous synaptic input. *Biol. Cybern.* 95, 1–19. doi: 10.1007/s00422-006-0082-8

Cayco-Gajic, N. A., and Shea-Brown, E. (2013). Neutral stability, rate propagation, and critical branching in feedforward networks. *Neural Comput.* 25, 1768–1806. doi: 10.1162/NECO_a_00461

Dayan, P., and Abbott, L. (2001). *Theoretical Neuroscience: Computational and Mathematical Modeling of Neural Systems*. Cambridge: MIT Press.

Debanne, D., Gähwiler, B. H., and Thompson, S. M. (1998). Long-term synaptic plasticity between pairs of individual CA3 pyramidal cells in rat hippocampal slice cultures. *J. Physiol.* 507, 237–247. doi: 10.1111/j.1469-7793.1998.237bu.x

Diesmann, M., Gewaltig, M. O., and Aertsen, A. (1999). Stable propagation of synchronous spiking in cortical neural networks. *Nature* 402, 529–533. doi: 10.1038/990101

Eagleman, S. L., and Dragoi, V. (2012). Image sequence reactivation in awake V4 networks. *Proc. Natl. Acad. Sci. U.S.A.* 109, 19450–19455. doi: 10.1073/pnas.1212059109

Feinerman, O., and Moses, E. (2006). Transport of information along unidimensional layered networks of dissociated hippocampal neurons and implications for rate coding. *J. Neurosci.* 26, 4526–4534. doi: 10.1523/JNEUROSCI.4692-05.2006

Feinerman, O., Segal, M., and Moses, E. (2005). Signal propagation along unidimensional neuronal networks. *J. Neurophysiol.* 94, 3406–3416. doi: 10.1152/jn.00264.2005

Felleman, D. J., and Van Essen, D. V. C. (1991). Distributed hierarchical processing in the primate cerebral cortex. *Cereb. Cortex* 1, 1–47. doi: 10.1093/cercor/1.1.1

Gasparini, S., and Magee, J. C. (2006). State-dependent dendritic computation in hippocampal CA1 pyramidal neurons. *J. Neurosci.* 26, 2088–2100. doi: 10.1523/JNEUROSCI.4428-05.2006

Gasparini, S., Migliore, M., and Magee, J. C. (2004). On the initiation and propagation of dendritic spikes in CA1 pyramidal neurons. *J. Neurosci.* 24, 11046–11056. doi: 10.1523/JNEUROSCI.2520-04.2004

Gewaltig, M. O., and Diesmann, M. (2007). NEST (NEural Simulation Tool). *Scholarpedia* 2:1430. doi: 10.4249/scholarpedia.1430

Gewaltig, M. O., Diesmann, M., and Aertsen, A. (2001). Propagation of cortical synfire activity: survival probability in single trials and stability in the mean. *Neural Netw.* 14, 657–673. doi: 10.1016/S0893-6080(01)00070-3

Goedeke, S., and Diesmann, M. (2008). The mechanism of synchronization in feed-forward neuronal networks. *New J. Phys.* 10:015007. doi: 10.1088/1367-2630/10/1/015007

Golding, N. L., Staff, N. P., and Spruston, N. (2002). Dendritic spikes as a mechanism for cooperative long-term potentiation. *Nature* 418, 326–331. doi: 10.1038/nature00854

Helias, M., Deger, M., Rotter, S., and Diesmann, M. (2010). Instantaneous non-linear processing by pulse-coupled threshold units. *PLoS Comput. Biol.* 6:e1000929. doi: 10.1371/journal.pcbi.1000929

Holmgren, C., Harkany, T., Svennenfors, B., and Zilberter, Y. (2003). Pyramidal cell communication within local networks in layer 2/3 of rat neocortex. *J. Physiol.* 551, 139–153. doi: 10.1113/jphysiol.2003.044784

Jahnke, S., Timme, M., and Memmesheimer, R.-M. (2012). Guiding synchrony through random networks. *Phys. Rev. X* 2:041016. doi: 10.1103/PhysRevX.2.041016

Ji, D., and Wilson, M. A. (2007). Coordinated memory replay in the visual cortex and hippocampus during sleep. *Nat. Neurosci.* 10, 100–107. doi: 10.1038/nn1825

Kilavik, B. E., Roux, S., Ponce-Alvarez, A., Confais, J., Grün, S., and Riehle, A. (2009). Long-term modifications in motor cortical dynamics induced by intensive practice. *J. Neurosci.* 29, 12653–126563. doi: 10.1523/JNEUROSCI.1554-09.2009

Kobayashi, K., and Poo, M.-M. (2004). Spike train timing-dependent associative modification of Hippocampal CA3 recurrent synapses by mossy fibers. *Neuron* 41, 445–454. doi: 10.1016/S0896-6273(03)00873-0

Kumar, A., Rotter, S., and Aertsen, A. (2008). Conditions for propagating synchronous spiking and asynchronous firing rates in a cortical network model. *J. Neurosci.* 28, 5268–5280. doi: 10.1523/JNEUROSCI.2542-07.2008

Kumar, A., Rotter, S., and Aertsen, A. (2010). Spiking activity propagation in neuronal networks: reconciling differentperspectives on neural coding. *Nat. Rev. Neurosci.* 11, 615–627. doi: 10.1038/nrn2886

Lee, A. K., and Wilson, M. A. (2002). Memory of sequential experience in the Hippocampus during slow wave sleep. *Neuron* 36, 1183–1194. doi: 10.1016/S0896-6273(02)01096-6

Leibold, C., and Kempter, R. (2006). Memory capacity for sequences in a recurrent network with biological constraints. *Neural Compt.* 18, 904–941. doi: 10.1162/neco.2006.18.4.904

Litvak, V., Sompolinsky, H., Segev, I., and Abeles, M. (2013). On the transmission of rate code in long feedforward networks with excitatory-inhibitory balance. *J. Neurosci.* 23, 3006–3015.

Long, M. A., Jin, D. Z., and Fee, M. S. (2010). Support for a synaptic chain model of neuronal sequence generation. *Nature* 468, 394–399. doi: 10.1038/nature09514

Losonczy, A., Makara, J. K., and Magee, J. C. (2008). Compartmentalized dendritic plasticity and input feature storage in neurons. *Nature* 452, 436–441. doi: 10.1038/nature06725

Makara, J. K., Losonczy, A., Wen, Q., and Magee, J. C. (2009). Experience-dependent compartmentalized dendritic plasticity in rat hippocampal CA1 pyramidal neurons. *Nat. Neurosci.* 12, 1485–1487. doi: 10.1038/nn.2428

Mehring, C., Hehl, U., Kubo, M., Diesmann, M., and Aertsen, A. (2003). Activity dynamics and propagation of synchronous spiking in locally connected random networks. *Biol. Cybern.* 88, 395–408. doi: 10.1007/s00422-002-0384-4

Memmesheimer, R.-M. (2010). Quantitative prediction of intermittent high-frequency oscillations in neural networks with supralinear dendritic interactions. *Proc. Natl. Acad. Sci. U.S.A.* 107, 11092–11097. doi: 10.1073/pnas.0909615107

Memmesheimer, R.-M., and Timme, M. (2012). Non-additive coupling enables propagation of synchronous spiking activity in purely random networks. *PLoS Comput. Biol.* 8:e1002384. doi: 10.1371/journal.pcbi.1002384

Müller, C., Beck, H., Coulter, D., and Remy, S. (2012). Inhibitory control of linear and supralinear dendritic excitation in CA1 pyramidal neurons. *Neuron* 75, 851–864. doi: 10.1016/j.neuron.2012.06.025

Nadasdy, Z., Hirase, H., Czurko, A., Csicsvari, J., and Buzsaki, G. (1999). Replay and time compression of recurring spike sequences in the Hippocampus. *J. Neurosci.* 19, 9497–9507.

Nowotny, T., and Huerta, R. (2003). Explaining synchrony in feed-forward networks: are McCulloch-Pitts neurons good enough? *Biol. Cybern.* 89, 237–241. doi: 10.1007/s00422-003-0431-9

Polsky, A., Mel, B. W., and Schiller, J. (2004). Computational subunits in thin dendrites of pyramidal cells. *Nat. Neurosci.* 7, 621–627. doi: 10.1038/nn1253

Putrino, D., Brown, E. N., Mastaglia, F. L., and Ghosh, S. (2010). Differential involvement of excitatory and inhibitory neurons of cat motor cortex in coincident spike activity related to behavioral context. *J. Neurosci.* 30, 8048–8056. doi: 10.1523/JNEUROSCI.0770-10.2010

Remy, S., and Spruston, N. (2007). Dendritic spikes induce single-burst long-term potentiation. *Proc. Natl. Acad. Sci. U.S.A.* 104, 17192–17197. doi: 10.1073/pnas.0707919104

Reyes, A. D. (2003). Synchrony-dependent propagation of firing rate in iteratively constructed networks *in vitro*. *Nat. Neurosci.* 6, 593–599. doi: 10.1038/nn1056

Riehle, A., Grün, S., Diesmann, M., and Aertsen, A. (1997). Spike synchronization and rate modulation differentially involved in motor cortical function. *Science* 278, 1950–1953. doi: 10.1126/science.278.5345.1950

Rosenbaum, R. J., Trousdale, J., and Josic, K. (2010). Pooling and correlated neural activity. *Front. Comput. Neurosci.* 4:9. doi: 10.3389/fncom.2010.00009

Rosenbaum, R., Trousdale, J., and Josic, K. (2011). The effect of pooling on spike train correlations. *Front. Neurosci.* 5:58. doi: 10.3389/fnins.2011.00058

Scannell, J. W., Burns, G. A., Hilgetag, C. C., O'Neil, M. A., and Young, M. P. (1999). The connectional organization of the cortico-thalamic system of the cat. *Cereb. Cortex* 9, 277–299. doi: 10.1093/cercor/9.3.277

Tuckwell, H. (1988). *Introduction to Theoretical Neurobiology*. Cambridge: Cambridge University Press. doi: 10.1017/CBO9780511623202

van Vreeswijk, C., and Sompolinsky, H. (1996). Chaos in neuronal networks with balanced excitatory and inhibitory activity. *Science* 274, 1724–1726. doi: 10.1126/science.274.5293.1724

van Vreeswijk, C., and Sompolinsky, H. (1998). Chaotic balanced state in a model of cortical circuits. *Neural Comp.* 10, 1321–1371. doi: 10.1162/089976698300017214

Vogels, T. P., and Abbott, L. F. (2005). Signal propagation and logic gating in networks of integrate-and-fire neurons. *J. Neurosci.* 25, 10786–10795. doi: 10.1523/JNEUROSCI.3508-05.2005

Xu, S., Jiang, W., Poo, M.-M., and Dan, Y. (2012). Activity recall in a visual cortical ensemble. *Nat. Neurosci.* 15, 449–455. doi: 10.1038/nn.3036

Conflict of Interest Statement: The authors declare that the research was conducted in the absence of any commercial or financial relationships that could be construed as a potential conflict of interest.

Received: 23 June 2013; accepted: 11 October 2013; published online: 15 November 2013.

Citation: Jahnke S, Memmesheimer R-M and Timme M (2013) Propagating synchrony in feed-forward networks. Front. Comput. Neurosci. 7:153. doi: 10.3389/fncom.2013.00153

This article was submitted to the journal Frontiers in Computational Neuroscience.

A. APPENDIX

A.1 PROOF OF EXISTENCE OF A GLOBAL MINIMUM OF $p_{NL}(n)$

We will show that $p_{NL}(n)$ as derived in Equation (59),

$$p_{NL}(n) = \frac{n^2\epsilon + 2\Theta_b + n\sqrt{n^2\epsilon^2 + 4\Theta_b\left(\epsilon - \frac{\Theta_b}{\omega}\right)}}{p_f(\kappa)\epsilon(n^2+\omega)\left(1+\mathrm{Erf}\left(\frac{n}{\sqrt{2}}\right)\right)} \tag{A.1}$$

$$= \frac{1}{p_f(\kappa)}\frac{2\Theta_b + n^2\epsilon\left(1+\sqrt{1+\frac{\alpha}{n^2}}\right)}{\left(1+\mathrm{Erf}\left(\frac{n}{\sqrt{2}}\right)\right)\left(n^2\epsilon+\omega\epsilon\right)}, \tag{A.2}$$

has a global minimum for $\epsilon\omega > \Theta_b$. In Equation (A.2) we defined

$$\alpha := \frac{4\Theta_b}{\epsilon}\left(1 - \frac{\Theta_b}{\epsilon\omega}\right). \tag{A.3}$$

For $\epsilon\omega > \Theta_b$, p_{NL} is positive and continuous, and approaches

$$\lim_{n\to-\infty}\left(p_{NL}(n)\right) = \infty, \tag{A.4}$$

$$\lim_{n\to\infty}\left(p_{NL}(n)\right) = \frac{1}{p_f(\kappa)}, \tag{A.5}$$

in the limit of large/small n. Further, the derivative of p_{NL} can be written as

$$\frac{d}{dn}p_{NL}(n) = (2 - h_1(n))\,h_2(n), \tag{A.6}$$

where we defined the functions

$$h_1(n) = \frac{1}{\epsilon\omega}\left(\frac{\sqrt{\frac{2}{\pi}}e^{-\frac{n^2}{2}}\left(n^2+\omega\right)\left(\frac{2\Theta_b}{\sqrt{\alpha+n^2}+n}+n\epsilon\right)}{1+\mathrm{Erf}\left(\frac{n}{\sqrt{2}}\right)}\right.$$
$$\left. + \frac{4\Theta_b n}{\sqrt{\alpha+n^2}+n} + \frac{\alpha\epsilon\left(n^2+\omega\right)}{\alpha+n\left(\sqrt{\alpha+n^2}+n\right)}\right), \tag{A.7}$$

$$h_2(n) = \frac{\omega\left(\sqrt{\alpha+n^2}+n\right)}{p_f(\kappa)\left(\mathrm{Erf}\left(\frac{n}{\sqrt{2}}\right)+1\right)\left(n^2+\omega\right)^2}. \tag{A.8}$$

For $n > 0$ and $\epsilon\omega > \Theta_b$,

$$\alpha > 0, \tag{A.9}$$

$$h_1(n) > 0, \tag{A.10}$$

$$h_2(n) > 0, \tag{A.11}$$

and in the limit of large n,

$$\lim_{n\to\infty} h_1(n) = \frac{1}{\epsilon\omega}\left(0 + 2\Theta_b + \frac{\alpha\epsilon}{2}\right) \tag{A.12}$$

$$= 2\frac{2\Theta_b\omega\epsilon - \Theta_b^2}{\omega^2\epsilon^2} \tag{A.13}$$

$$\lim_{n\to\infty} h_2(n) = 0. \tag{A.14}$$

For $\epsilon\omega > \Theta_b$, $h_1(n)$ is smaller than two for sufficiently large n (cf. Equation A.13) and thus the derivative of $p_{NL}(n)$ becomes positive (cf. Equation A.6). Consequently p_{NL} approaches $1/p_f(\kappa)$ from below for large n (cf. also Equation A.5). This proves the existence of a global minimum of $p_{NL}(n)$, because $p_{NL} > 1/p_f(\kappa)$ for sufficiently small n (cf. Equation A.4).

A.2 BIOLOGICAL MORE DETAILED NEURON MODELS

In section 3.3.3 we consider biologically more detailed neuron models. In this appendix we present descriptions of these models including the parameters used for the numerical simulations in **Figure 13**. These simulations were done using NEST (Gewaltig and Diesmann, 2007), a simulator for spiking neural network models (available at http://www.nest-initiative.org). We implemented new model classes within the NEST framework to handle conductance-based leaky integrate-and-fire neurons with double exponential input conductances as well as non-linear dendritic interactions (source code available from Sven Jahnke).

A.2.1 CB-type model

The CB-type model is a leaky integrate-and-fire neuron with conductance based synapses, augmented with a mechanism for the generation of current pulses mimicking the effect of a dendritic spike (see also Memmesheimer, 2010; Jahnke et al., 2012). The subthreshold dynamics of the membrane potential V_l of neuron l obeys the differential equation

$$C_l^{\mathrm{m}}\frac{dV_l(t)}{dt} = g_l^L\left(V_l^{\mathrm{rest}} - V_l(t)\right) + g_l^A(t)\left(E^{\mathrm{Ex}} - V_l(t)\right)$$
$$+ g_l^G(t)\left(E^{\mathrm{In}} - V_l(t)\right) + I_l^{\mathrm{DS}}(t) + I_l^0. \tag{A.15}$$

Here, C_l^{m} is the membrane capacity, g_l^L is the resting conductance, V_l^{rest} is the resting membrane potential, E^{Ex} and E^{In} are the reversal potentials, and $g_l^A(t)$ and $g_l^G(t)$ are the conductances of excitatory and inhibitory synaptic populations, respectively. $I_l^{\mathrm{DS}}(t)$ models the current pulses caused by dendritic spikes and I_l^0 is a constant current gathering slow external and internal currents. The time course of single synaptic conductances contributing to $g_l^A(t)$ and $g_l^G(t)$ is given by the difference between two exponential functions (e.g., Dayan and Abbott, 2001) with time constants $\tau^{A,1}$ and $\tau^{A,2}$ for the excitatory and $\tau^{G,1}$ and $\tau^{G,2}$ for the inhibitory conductances. Whenever the membrane potential reaches the spike threshold Θ_l, the neuron sends a spike to its postsynaptic neurons, is reset to V_l^{reset} and becomes refractory for a period t_l^{ref}. Additionally to inputs from the preceding layer each neuron receives excitatory and inhibitory Poissonian input spike trains with rates ν^{ex} and ν^{in}; single inputs have coupling strength ϵ^{ex} and ϵ^{in}, respectively.

To account for dendritic spike generation, we consider the sum $g_{l,\Delta t}$ of excitatory input strengths (characterized by the coupling strengths), arriving at an excitatory neuron l within the time window Δt for non-linear dendritic interactions,

$$g_{l,\Delta t}(t) = \sum_j \sum_k \epsilon_{lj}\chi_{[t-\Delta t,\,t]}(t_{jk}^f + \tau), \tag{A.16}$$

where $\chi_{[t-\Delta t,\,t]}$ is the characteristic function of the interval $[t-\Delta t, t]$, t_{jk}^{f} is the kth firing time of neuron j and τ denotes the synaptic delay. We denote the peak conductance (coupling strength) for a connection from neuron j to neuron l by $g_{lj}^{\max}$. If $g_{l,\,\Delta t}$ exceeds a threshold g_Θ, a dendritic spike is initiated and the dendrite becomes refractory for a time window $t^{\mathrm{DS,ref}}$. The effect of the dendritic spike is incorporated into the model by the current pulse that reaches the soma a time τ^{DS} thereafter. This current pulse is modeled as the sum of three exponential functions,

$$I_l^{\mathrm{DS}}(t) = c(g_{\Delta t})\left[-Ae^{-\frac{t}{\tau^{\mathrm{DS},1}}} + Be^{-\frac{t}{\tau^{\mathrm{DS},2}}} - Ce^{-\frac{t}{\tau^{\mathrm{DS},3}}}\right], \quad (A.17)$$

with prefactors $A > 0$, $B > 0$, $C > 0$, decay time constants $\tau^{\mathrm{DS},1}$, $\tau^{\mathrm{DS},2}$, $\tau^{\mathrm{DS},3}$ and a dimensionless correction factor $c\left(g_{\Delta t}\right)$, where $g_{\Delta t}$ is the summed excitatory input at the initiation time of the dendritic spike as given by Equation (A.16). The factor $c\left(g_{\Delta t}\right)$ modulates the pulse strength, ensuring that the peak of the excitatory postsynaptic potential (pEPSP) reaches the experimentally observed region of saturation. At very high excitatory inputs, the conventionally generated depolarization exceeds the level of saturation, $c\left(g_{\Delta t}\right)$ is zero and the pEPSP increases (cf. inset of **Figure 13A**).

Parameters for Figure 13

The single neuron parameters for the numerical simulations are $C_l^{\mathrm{m}} = C^{\mathrm{m}} = 400\,\mathrm{pF}$, $g_l^L = g^L = 25\,\mathrm{nS}$, $V_l^{\mathrm{rest}} = V^{\mathrm{rest}} = -65\,\mathrm{mV}$, $\Theta_l = \Theta = -50\,\mathrm{mV}$, $t_l^{\mathrm{ref}} = t^{\mathrm{ref}} = 3\,\mathrm{ms}$ and $V_l^{\mathrm{reset}} = V^{\mathrm{reset}} = -65\,\mathrm{mV}$. The reversal potentials are $E^{\mathrm{Ex}} = 0\,\mathrm{mV}$ and $E^{\mathrm{In}} = -75\,\mathrm{mV}$ and the time constants for the excitatory and inhibitory conductances are $\tau^{A,1} = \tau^{G,1} = 2.5\,\mathrm{ms}$ and $\tau^{A,2} = \tau^{G,2} = 0.5\,\mathrm{ms}$. The parameters of the dendritic spike current are $\Delta t = 2\,\mathrm{ms}$, $g^\Theta = 8.65\,\mathrm{nS}$, $\tau^{\mathrm{DS}} = 2.7\,\mathrm{ms}$, $A = 55\,\mathrm{nA}$, $B = 64\,\mathrm{nA}$, $C = 9\,\mathrm{nA}$, $\tau^{\mathrm{DS},1} = 0.2\,\mathrm{ms}$, $\tau^{\mathrm{DS},2} = 0.3\,\mathrm{ms}$, $\tau^{\mathrm{DS},3} = 0.7\,\mathrm{ms}$ and $t^{\mathrm{ref,\,DS}} = 5.2\,\mathrm{ms}$ and the dimensionless correction factor is given by $c(g) = \max\left\{1.5 - g \cdot 0.053\mathrm{nS}^{-1}, 0\right\}$. For the first setup ($p^f \approx 0.97$) we set $I_l^0 = I^0 = 250\,\mathrm{pA}$, $\nu^{\mathrm{ex}} = 2.4\,\mathrm{kHz}$, $\nu^{\mathrm{in}} = 0.6\,\mathrm{kHz}$, $\epsilon^{\mathrm{ex}} = 0.6\,\mathrm{nS}$ and $\epsilon^{\mathrm{in}} = 6.6\,\mathrm{nS}$; for the second setup ($p^f \approx 0.67$) we set $I_l^0 = I^0 = 0\,\mathrm{pA}$, $\nu^{\mathrm{ex}} = 20\,\mathrm{kHz}$, $\nu^{\mathrm{in}} = 5\,\mathrm{kHz}$, $\epsilon^{\mathrm{ex}} = 0.6\,\mathrm{nS}$ and $\epsilon^{\mathrm{in}} = -6.6\,\mathrm{nS}$.

A.2.2 HH-type model

We employ a standard model provided by NEST ("hh_psc_alpha"; Hodgkin–Huxley type neuron with alpha-function shaped postsynaptic currents) and incorporated a dendritic spike current as in the CB-Model. The membrane potential V_l of neuron l obeys the differential equation

$$C_l^{\mathrm{m}}\frac{dV_l(t)}{dt} = I_l^{\mathrm{Na}}(t) + I_l^{\mathrm{K}}(t) + I_l^{\mathrm{L}}(t) + I_l^0 + I_l^{\mathrm{ex}}(t) + I_l^{\mathrm{in}}(t) + I_l^{\mathrm{DS}}(t). \quad (A.18)$$

For clarity we drop the index l in the following; all quantities refer to some neuron l. In Equation (A.18),

$$I^{\mathrm{Na}}(t) = g^{\mathrm{Na}}m(t)^3h(t)\left[E^{\mathrm{Na}} - V(t)\right] \quad (A.19)$$

$$I^{\mathrm{K}}(t) = g^{\mathrm{K}}n(t)^4\left[E^{\mathrm{K}} - V(t)\right] \quad (A.20)$$

$$I^{\mathrm{L}}(t) = g^{\mathrm{L}}\left[E^{\mathrm{L}} - V(t)\right] \quad (A.21)$$

specify the Na^+current, the K^+ current and leak current. The dynamics of the gating variables m, n and h are governed by

$$\frac{dm(t)}{dt} = \alpha_{\mathrm{m}}(t)\,[1 - m(t)] - \beta_{\mathrm{m}}(t)m(t) \quad (A.22)$$

$$\frac{dh(t)}{dt} = \alpha_{\mathrm{h}}(t)\,[1 - h(t)] - \beta_{\mathrm{h}}(t)h(t) \quad (A.23)$$

$$\frac{dn(t)}{dt} = \alpha_{\mathrm{n}}(t)\,[1 - n(t)] - \beta_{\mathrm{n}}(t)n(t), \quad (A.24)$$

where the voltage dependencies are given by

$$\alpha_n(t) = \frac{0.01\left[\tilde{V}(t) + 55\right]}{1 - \exp\left[-\frac{\tilde{V}(t)+55}{10}\right]} \quad (A.25)$$

$$\beta_n(t) = 0.125 \cdot \exp\left[-\frac{\tilde{V}(t)\ +\ 65}{80}\right] \quad (A.26)$$

$$\alpha_m(t) = \frac{0.1\left[\tilde{V}(t) + 40\right]}{1 - \exp\left[-\frac{V(t)+40}{10}\right]} \quad (A.27)$$

$$\beta_m(t) = 4 \cdot \exp\left[-\frac{\tilde{V}(t) + 65}{18}\right] \quad (A.28)$$

$$\alpha_h(t) = 0.07 \cdot \exp\left[-\frac{\tilde{V}(t) + 65}{20}\right] \quad (A.29)$$

$$\beta_h(t) = \left(1 + \exp\left[-\frac{\tilde{V}(t) + 35}{10}\right]\right)^{-1}. \quad (A.30)$$

In Equations (A.25–A.30) $\tilde{V}(t) := \frac{V(t)}{1\mathrm{mV}}$ is the value of membrane potential normalized by 1 mV. Spikes are detected by a combined threshold-and-local-maximum search, if there is a local maximum above a certain threshold of the membrane potential, $U_\Theta = 0\,\mathrm{mV}$, it is considered a spike (for more details see the NEST manual and the model implementation available at http://www.nest-initiative.org). After a synaptic delay time τ a spike initiates an alpha-function shaped current pulse at the postsynaptic neurons. The total excitatory and inhibitory input to neuron l is given by

$$I^{\mathrm{ex}}(t) = \sum_k \epsilon_k^{\mathrm{ex}}\frac{e}{\tau^{\mathrm{ex}}}\exp\left[-\frac{t}{\tau^{\mathrm{ex}}}\right]\Theta\left[t - t_k^{\mathrm{ex}}\right] \quad (A.31)$$

$$I^{\mathrm{in}}(t) = \sum_k \epsilon_k^{\mathrm{in}}\frac{e}{\tau^{\mathrm{in}}}\exp\left[-\frac{t}{\tau^{\mathrm{in}}}\right]\Theta\left[t - t_k^{\mathrm{in}}\right], \quad (A.32)$$

where $\epsilon_k^{\mathrm{ex}} > 0$ $\left(\epsilon_k^{\mathrm{in}} < 0\right)$ is the strength of the kth arriving excitatory (inhibitory) spike at neuron l, t_k^{ex} $\left(t_k^{\mathrm{in}}\right)$ denotes the reception time of that spike and e is the Euler constant [the currents $I^{\mathrm{ex}}(t)$ and $I^{\mathrm{in}}(t)$ are normalized such that an input of strength $\epsilon = 1\,\mathrm{pA}$

causes a peak current of 1 pA]. The time constants τ^{ex} and τ^{in} are the synaptic time constants. As before, we account for dendritic spike generation by considering the sum of excitatory input strengths received by neuron l within the time window Δt,

$$\epsilon_{\Delta t}(t) = \sum_k \epsilon_k^{ex} \chi_{[t-\Delta t,t]}(t_k^f + \tau). \tag{A.33}$$

If this sum exceeds the dendritic threshold I^{Θ}, a dendritic spike is initiated and we model its effect is by the current pulse

$$I^{DS}(t) = c(\epsilon_{\Delta t})\left[-Ae^{-\frac{t}{\tau^{DS,1}}} + Be^{-\frac{t}{\tau^{DS,2}}} - Ce^{-\frac{t}{\tau^{DS,3}}}\right], \tag{A.34}$$

starting after a delay time τ^{DS} after the initiation time of the dendritic spike. The correction factor $c(\epsilon_{\Delta t})$ modulates the pulse strength such that the depolarization saturates for suprathreshold inputs until the effects of linearly summed input exceed the effects of the dendritic spike (cf. inset of **Figure 13B**).

A.2.3 Parameters for Figure 13

As before, we consider homogeneous neuronal properties. The single neuron parameters for the numerical simulations are $C^m = 200\,\text{pF}$, $E^K = -77\,\text{mV}$, $E^L = -70\,\text{mV}$, $E^{Na} = 50\,\text{mV}$, $g^K = 3600\,\text{nS}$, $g^L = 30\,\text{nS}$, $g^{Na} = 12000\,\text{nS}$, $\tau^{ex} = 2\,\text{ms}$ and $\tau^{in} = 2\,\text{ms}$. The parameters of the dendritic spike current are $\Delta t = 3.5\,\text{ms}$, $I^{\Theta} = 270\,\text{pA}$, $\tau^{DS} = 2.7\,\text{ms}$, $A = 27.5\,\text{nA}$, $B = 32\,\text{nA}$, $C = 4.5\,\text{nA}$, $\tau^{DS,1} = 0.2\,\text{ms}$, $\tau^{DS,2} = 0.3\,\text{ms}$, $\tau^{DS,3} = 0.7\,\text{ms}$ and $t^{ref,DS} = 5.2\,\text{ms}$ and the dimensionless correction factor is given by $c(\epsilon) = \max\left\{1.54 - \epsilon \cdot 0.002\,\text{pA}^{-1}, 0\right\}$. For the first setup ($p^f \approx 0.97$) we set $I^0 = 500\,\text{pA}$, $\nu^{ex} = 3\,\text{kHz}$, $\nu^{in} = 3\,\text{kHz}$, $\epsilon^{ex} = 20\,\text{pA}$ and $\epsilon^{in} = -20\,\text{pA}$; and for the second setup ($p^f \approx 0.67$) we set $I^0 = 250\,\text{pA}$, $\nu^{ex} = 10\,\text{kHz}$, $\nu^{in} = 10\,\text{kHz}$, $\epsilon^{ex} = 20\,\text{pA}$ and $\epsilon^{in} = -20\,\text{pA}$.

Chapter 4

Original Manuscript: Guiding synchrony through random networks

Citation

Jahnke, S., Timme, M. and Memmesheimer, R.-M. (2012), Guiding Synchrony through Random Networks, *Phys. Rev. X*, **2**, 041016, DOI:10.1103/PhysRevX.2.041016

Original contribution

Conception and design of the study together with M. Timme and R.-M. Memmesheimer. I performed the analytical calculations and numerical simulations. For the simulations I wrote own code (C++ and python modules) and implementated neuron models within the NEST simulation environment (www.nest-initiative.org). I analyzed the data and prepared all figures. I wrote main parts of the manuscript supported by M. Timme and R.-M. Memmesheimer.

Göttingen, 31.03.2014
Place, Date

Sven Jahnke

PHYSICAL REVIEW X 2, 041016 (2012)

Guiding Synchrony through Random Networks

Sven Jahnke,[1,2,3] Marc Timme,[1,2,3] and Raoul-Martin Memmesheimer[4]

[1]*Network Dynamics Group, Max Planck Institute for Dynamics & Self-Organization (MPIDS), Göttingen, Germany*
[2]*Bernstein Center for Computational Neuroscience (BCCN), Göttingen, Germany*
[3]*Fakultät für Physik, Georg-August-Universität Göttingen, Göttingen, Germany*
[4]*Donders Institute, Department for Neuroinformatics, Radboud University, Nijmegen, Netherlands*

(Received 9 August 2011; revised manuscript received 18 June 2012; published 13 December 2012)

Sparse random networks contain structures that can be considered as diluted feed-forward networks. Modeling of cortical circuits has shown that feed-forward structures, if strongly pronounced compared to the embedding random network, enable reliable signal transmission by propagating localized (subnetwork) synchrony. This assumed prominence, however, is not experimentally observed in local cortical circuits. Here, we show that nonlinear dendritic interactions, as discovered in recent single-neuron experiments, naturally enable guided synchrony propagation already in random recurrent neural networks that exhibit mildly enhanced, biologically plausible substructures.

DOI: 10.1103/PhysRevX.2.041016 Subject Areas: Biological Physics, Complex Systems

I. INTRODUCTION

Cortical neural networks generate a ground state of highly irregular spiking activity whose dynamics is sensitive to small perturbations such as missing or additional spikes [1–4]. A robust, reliable transmission of information in the presence of such perturbations and noise is nonetheless assumed to be essential for neural computation. It has been hypothesized that this reliable transmission might be achieved by propagation of pulses of synchronous spikes along feed-forward chains [5]. In current models, functionally relevant chains require a dense connectivity between the neuronal layers of the network [6] or strongly enhanced synapses and specifically modified response properties of neurons within the chain [7]. Such highly distinguished large-scale structures are not observed experimentally, however.

Can less-structured networks also guide synchrony? Recently, single-neuron experiments have revealed a mechanism that nonlinearly promotes synchronous inputs. On synchronous dendritic stimulation, neurons are capable of generating fast dendritic spikes. In the soma, these spikes induce rapid, strong depolarizations [8] that are nonlinearly enhanced compared to depolarizations expected from linear summation of single inputs. If the dendritic spike induces an action potential in the soma, the potential occurs at a fixed time after the stimulation, with submillisecond precision. Other experiments have found slow dendritic spikes that are comparably insensitive to input synchrony [9]. These slow dendritic spikes endow single neurons with computational capabilities comparable to multilayered feed-forward networks of simple-rate neurons [10]. Furthermore, they provide a possible mechanism underlying neural bursting and its propagation, which have been shown to enhance reliability and temporal precision of signal propagation [11,12]. The impact on collective circuit dynamics of fast dendritic spikes that induce nonadditive coupling has not been systematically investigated in a general setting so far.

In this article, we show that and describe how fast dendritic nonlinearities may support guided-synchrony propagation in neural circuits. First, we develop an analytical approach to describe such propagation in linearly and nonlinearly coupled networks. In particular, we derive expressions for the critical connectivity above which propagation occurs and for the size of the propagating pulse. We quantify how dendritic nonlinearities compensate for dense anatomical connections and thereby promote propagation of synchrony. Finally, using large-scale simulations of more detailed recurrent network models, we show that feed-forward networks that occur naturally as part of random circuits enable persistent guided synchrony propagation due to dendritic nonlinearities.

II. MODELS AND METHODS

A. Analytically tractable model

Model with linear summation of inputs. As a basis model, we consider networks of conventional leaky integrate-and-fire neurons that interact by sending and receiving spikes via directed connections. The membrane potential V_l of a neuron l satisfies

$$\dot{V}_l(t) = -\gamma_l V_l(t) + I_l(t), \tag{1}$$

where γ_l is the inverse membrane time constant and $I_l(t)$ is the total input current at time t. In addition to inputs from the network, the neurons receive excitatory and inhibitory random inputs that emulate an embedding network, i.e.,

$$I_l(t) = I_l^0 + I_l^{\mathrm{ext,ex}}(t) + I_l^{\mathrm{ext,in}}(t) + I_l^{\mathrm{net}}(t), \tag{2}$$

where I_l^0 is a constant input current modeling slow external (from outside the chain) and internal (from the chain) currents; $I_l^{\mathrm{ext,ex}}(t)$ and $I_l^{\mathrm{ext,in}}(t)$ are the contributions due to arriving external excitatory and inhibitory spikes [which are modeled as independent random (Poissonian) spike trains with rate $\nu^{\mathrm{ext,ex}}$ and $\nu^{\mathrm{ext,in}}$, respectively]; and $I_l^{\mathrm{net}}(t)$ are the contributions originating from spikes of neurons of the network. In the absence of any spiking activity, the membrane potential exponentially converges toward its asymptotic value $V_l^\infty := I_l^0/\gamma_l$. When the neuron's membrane potential reaches or exceeds its threshold Θ_l, its membrane potential is reset to V_l^{reset} and a spike is emitted, which arrives at the postsynaptic neuron j after a delay time τ_{jl}. For a refractory period t_l^{ref} after the reset, all incoming spikes to neuron l are ignored, and the membrane potential is kept at V_l^{reset}.

We model the fast rise of the membrane potential on the arrival of a presynaptic spike by an instantaneous jump, such that the contributions of the arriving external spikes to the total input current are given by

$$I_l^{\mathrm{ext,ex}}(t) = \sum_{k\in\mathbb{Z}} \epsilon^{\mathrm{ext,ex}}\,\delta(t - t_{l,k}^{\mathrm{ext,ex}}), \tag{3}$$

$$I_l^{\mathrm{ext,in}}(t) = \sum_{k\in\mathbb{Z}} \epsilon^{\mathrm{ext,in}}\,\delta(t - t_{l,k}^{\mathrm{ext,in}}), \tag{4}$$

where $t_{l,k}^{\mathrm{ext,ex}}$ ($t_{l,k}^{\mathrm{ext,in}}$) are the arrival times of the kth excitatory (inhibitory) external spike at neuron l, $\epsilon^{\mathrm{ext,ex}} > 0$ or $\epsilon^{\mathrm{ext,in}} < 0$ are the strengths of single external spikes, and $\delta(\cdot)$ is the Dirac δ distribution. Analogously, the contribution of spikes received from neurons of the network is given by

$$I_l^{\mathrm{net}}(t) = \sum_j \sum_k \epsilon_{lj}\,\delta(t - t_{j,k}^f - \tau_{lj}), \tag{5}$$

where ϵ_{lj} is the coupling strength from neuron j to l and $t_{j,k}^f$ is the kth spike time of neuron j.

Model with nonlinear summation of inputs. In the above model without nonlinear dendrites, the strengths of synchronous inputs are summed up linearly [cf. Eq. (5)]. We incorporate nonlinear dendrites by modulating this sum for excitatory inputs by a nonlinear function σ that can be directly read off from experimental results [8]: σ equals the identity for small excitatory input, increases steeply when the input exceeds a threshold Θ_b, and saturates for larger inputs. We define the dendritic modulation function as

$$\sigma(\epsilon) = \begin{cases} \epsilon & \text{for } \epsilon \le \Theta_b \\ \kappa & \text{otherwise.} \end{cases} \tag{6}$$

For simplicity, we consider only exactly simultaneous spikes as synchronous. Accordingly, conduction delays are chosen homogeneously, $\tau_{ij} \equiv \tau$, so that synchronous presynaptic spiking can be amplified. In this scenario, the detection of synchronous events is straightforward. However, systems with heterogeneous delays and a finite dendritic integration window exhibit qualitatively the same phenomena [13]. The contribution of spikes received from the network is then given by

$$I_l^{\mathrm{net}}(t) = \sum_{t^f}\Big[\sigma\Big(\sum_{j\in M_{\mathrm{ex}}(t^f)} \epsilon_{lj}\Big) + \sum_{j\in M_{\mathrm{in}}(t^f)} \epsilon_{lj}\Big]\delta(t - t^f - \tau), \tag{7}$$

where t^f are all firing times in the network. The sets $M_{\mathrm{ex}}(t^f)$ and $M_{\mathrm{in}}(t^f)$ denote the sets of indices of neurons sending an excitatory or inhibitory spike at time t^f, respectively. Networks with linear dendrites can be described by setting $\sigma(\epsilon) = \epsilon$.

B. Biologically more detailed model

Conductance-based model. In the last part of this article, we employ a biologically more detailed neuron model to highlight the generality of our findings on propagation enhancement. The neuron model is a conductance-based, leaky integrate-and-fire neuron that is augmented by terms introducing the impact of dendritic spikes (see also [14]). The subthreshold dynamics of the membrane potential V_l of neuron l obeys the differential equation

$$C_l^{\mathrm{m}}\frac{dV_l(t)}{dt} = g_l^L[V_l^{\mathrm{rest}} - V_l(t)] + g_l^A(t)[E^{\mathrm{Ex}} - V_l(t)] + g_l^G(t)[E^{\mathrm{In}} - V_l(t)] + I_l^{\mathrm{DS}}(t) + I_l^0. \tag{8}$$

Here, C_l^{m} is the membrane capacity, g_l^L is the resting conductance, V_l^{rest} is the resting membrane potential, E^{Ex} and E^{In} are the reversal potentials, and $g_l^A(t)$ and $g_l^G(t)$ are the conductances of excitatory and inhibitory synaptic populations, respectively. $I_l^{\mathrm{DS}}(t)$ models the current pulses caused by dendritic spikes, and I_l^0 is a constant current gathering slow external and internal currents. The time course of single synaptic conductances contributing to $g_l^A(t)$ and $g_l^G(t)$ is given by the difference between two exponential functions (e.g., [15]). Whenever the membrane potential reaches the spike threshold Θ_l, the neuron sends a spike to its postsynaptic neurons, is reset to V_l^{reset}, and becomes refractory for a period t_l^{ref}.

To account for dendritic spike generation, we consider the sum $g_{l,\Delta t}$ of excitatory input strengths (characterized by the coupling strengths) arriving at an excitatory neuron l within the time window Δt for nonlinear dendritic interactions,

$$g_{l,\Delta t}(t) = \sum_j \sum_k g_{lj}^{\max}\chi_{[t,t-\Delta t]}(t_{j,k}^f + \tau), \tag{9}$$

where $\chi_{[t,t-\Delta t]}$ is the characteristic function of the interval $[t, t-\Delta t]$, $t_{j,k}^f$ is the kth firing time of excitatory neuron j, and τ denotes the synaptic delay. We denote the peak conductance (coupling strength) for a connection from

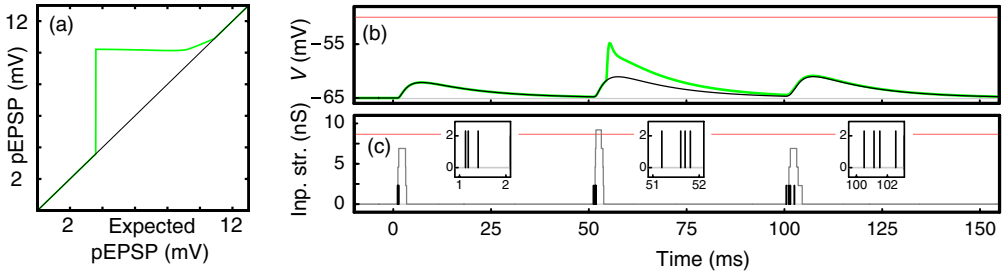

FIG. 1. Example dynamics of a conductance-based, leaky integrate-and-fire neuron with dendritic spike generation. (The neuron is initially at resting membrane potential $V^{\text{rest}} = -65$ mV, there are no external inputs, and $I^0 = 0$.) Panel (a) shows the pEPSP after a stimulation versus the expected pEPSP, i.e., the pEPSP for a neuron without dendritic spike generation. For inputs corresponding to a pEPSP larger than about 3.8 mV, a dendritic spike is generated which leads to a higher depolarization than expected from additive integration. Panel (b) shows the time course of the membrane potential of a neuron with (green) and without (black) nonlinear dendritic interaction in response to different excitatory inputs sequences. (The red horizontal line indicates the somatic spike threshold). Panel (c) shows the input sequences (black lines, strength: $g^{\text{ex}} = 2.3$ nS; close-ups given in insets) and the sum $g_{l,\Delta t}(t)$ of excitatory inputs received within the dendritic integration window $[t - \Delta t, t]$ (gray lines); cf. Eq. (9). At the first spike arrival around $t = 1$ ms, three inputs are received within Δt such that $g_{l,\Delta t}(t)$ reaches 6.9 nS. The sum is smaller than the dendritic threshold $g^{\Theta} = 8.65$ nS [red horizontal line in (c)], so no dendritic spike is generated and there is no difference between the membrane potential for a neuron with and without a mechanism for dendritic spike generation. Around $t = 50$ ms, four spikes arrive within Δt, $g_{l,\Delta t}(t)$ exceeds the dendritic threshold, and a dendritic spike is generated. Around $t = 100$ ms, four spikes arrive at the neuron, but the temporal difference between the last and the first spike is slightly larger than Δt. Consequently, $g_{l,\Delta t}(t)$ does not exceed the dendritic threshold and no dendritic spike is initiated.

neuron j to neuron l by $g_{lj}^{\max}$. If $g_{l,\Delta t}$ exceeds a threshold g_Θ, a dendritic spike is initiated and the dendrite becomes refractory for a time window $t^{\text{DS,ref}}$. The effect of the dendritic spike is incorporated into the model by the current pulse that reaches the soma a time τ^{DS} thereafter. This current pulse is modeled as the sum of three exponential functions,

$$I_l^{\text{DS}}(t) = c(g_{\Delta t})[-Ae^{-(t/\tau^{\text{DS},1})} + Be^{(-t/\tau^{\text{DS},2})} - Ce^{-(t/\tau^{\text{DS},3})}], \tag{10}$$

with prefactors $A > 0$, $B > 0$, $C > 0$, decay time constants $\tau^{\text{DS},1}$, $\tau^{\text{DS},2}$, $\tau^{\text{DS},3}$, and a dimensionless correction factor $c(g_{\Delta t})$, where $g_{\Delta t}$ is the summed excitatory input at the initiation time of the dendritic spike as given by Eq. (9). The factor $c(g_{\Delta t})$ modulates the pulse strength, ensuring that the peak of the excitatory postsynaptic potential (pEPSP) reaches the experimentally observed region of saturation. At very high excitatory inputs, the conventionally generated depolarization exceeds the level of saturation, and the pEPSP increases [cf. Fig. 1(a)].

Detection probability. In the last part of this article, we investigate recurrent networks where a feed-forward subnetwork consisting of a certain number of layers (groups) is created by modifying strengths of existing synaptic connections of the network. To decide whether propagation of synchrony in recurrent networks is successful, we consider the signal-to-noise ratio (SNR): We pick ω neurons, randomly selected from the network, to be a first group. After initiation of synchronous activity in this group, we count the number of spikes from neurons of the ith group, S_i, within a time window $[t_i^{\text{exp}} - \frac{t^w}{2}, t_i^{\text{exp}} + \frac{t^w}{2}]$. (For details on how the ith group is defined, see Sec. III C on recurrent networks.) Here, t_i^{exp} is the expected time for the synchronous pulse to reach layer i, and t^w is the expected width of the synchronous pulse. We consider all spikes within the time window of size t^w centered at t_i^{exp} as part of the synchronous pulse. We assume that $t_i^{\text{exp}} = t_1^{\text{exp}} + (i-1)\Delta t^{\text{exp}}$, where Δt^{exp} itself is chosen after simulation such that $\sum_i S_i$ becomes maximal:

$$S_i = \sum_k \sum_{j \in \text{Gr}(i)} \chi_{[t_i^{\text{exp}} - (t^w/2), t_i^{\text{exp}} + (t^w/2)]}(t_{j,k}^f). \tag{11}$$

Here, $\text{Gr}(i)$ are the indices of neurons of group i, $t_{j,k}^f$ is the kth firing time of neuron j, and χ denotes the characteristic function, as before.

To determine the noise level of group i, we measure the probability $P^i_{\Delta t^{\text{obs}}, t^w}(k)$ of finding k spikes from neurons of group i within time windows t^w over a control time interval during which no synchronous activity is initiated. The noise level N_i of group i is the minimal value satisfying

$$\sum_{k=0}^{N_i} P^i_{\Delta t^{\text{obs}}, t^w}(k) \geq a, \tag{12}$$

with a constant $a \lesssim 1$.

Finally, we denote the propagation of synchrony up to the ith layer as successful if the SNR is larger than b,

$$\text{SNR}_i := \min_{j=1,\ldots,i} \left\{ \frac{S_j}{N_j} \right\} > b, \tag{13}$$

where $b \geq 1$. This means, in particular, that we can distinguish the background (spontaneous) activity from the

signal induced by propagation of synchrony in all layers $1, \ldots, i$.

III. RESULTS

A. Feed-forward chains with linear coupling

How can diluted feed-forward networks (FFNs) propagate synchrony? FFNs consist of a sequence of layers, each composed of ω excitatory neurons; they forward connections to neurons in the subsequent layer randomly present with probability p. Present connections have strength ϵ. Synchronous spiking activity is initiated by exciting neurons of the first layer to spike simultaneously. In the second layer, the synchronous pulse arriving from the first layer excites a certain subgroup of neurons to spike simultaneously which in turn generates a synchronous input to layer three, etc.

To understand the collective dynamics analytically, we consider networks of leaky integrate-and-fire neurons in the limit of fast synaptic currents (cf. Sec. II). In the absence of synchronous activity, each neuron of the FFN receives a large number of inputs from an emulated external network and only very few inputs from the previous layer, such that its dynamics is practically identical to the ground state of balanced networks. If the connections within the FFN are weak and/or the connection probability is low, the spontaneous spiking activity is influenced only weakly by spiking activity of the FFN. Therefore, we assume that the ground-state activity is exclusively governed by the external inputs, effectively setting couplings within the chain to $\epsilon_{ij} = 0$. The external input is balanced, i.e., the mean input is subthreshold, and spontaneous spiking is caused by fluctuations in the input. The network's neurons thus spike in an asynchronous and irregular manner [1,2] and the stationary distribution of membrane potentials $P_V(V)$ can be calculated analytically in diffusion approximation [2,16].

$$p_f(x) := \int_{\Theta - x}^{\Theta} P_V(V) dV \tag{14}$$

is the probability of finding a neuron's membrane potential in the interval $[\Theta - x, \Theta]$. We model the fast rise of the membrane potential on the arrival of (possibly nonlinear enhanced) presynaptic spikes by an instantaneous jump in the membrane potential (cf. Sec. II); thus, $p_f[\sigma(h\epsilon)]$ specifies the spiking probability of a single neuron, after receiving h input spikes of strength ϵ from the preceding layer.

To assess the propagation of synchrony, we consider the average number of neurons that are activated in each layer in response to the initial synchronous pulse (cf. also [17]). When g_i neurons spike synchronously in layer i,

$$p^{\mathrm{sp}}(g_i) := \sum_{h=0}^{g_i} \binom{g_i}{h} p^h (1-p)^{g_i - h} p_f[\sigma(h\epsilon)] \tag{15}$$

is the probability of spiking of a particular neuron in layer $i+1$, where the number of simultaneous inputs h is binomially distributed, $h \sim B(g_i, p)$. Thus, for layers of size ω, the average number of neurons spiking in layer $i+1$ is

$$\langle g_{i+1} \rangle = \omega p^{\mathrm{sp}}(g_i). \tag{16}$$

Substituting the average group size $\langle g_i \rangle$ for the actual size g_i yields the interpolated map $\langle g_{i+1} \rangle = \omega p^{\mathrm{sp}}(\langle g_i \rangle)$, whose fixed points qualitatively determine the propagation of synchronous activity (cf. Fig. 2).

The trivial, absorbing fixed point $G_0 = 0$, defining a state of extinguished activity, always exists. For sufficiently small p, ϵ, and ω, this is the only fixed point. With increasing connectivity and layer size, a pair of fixed

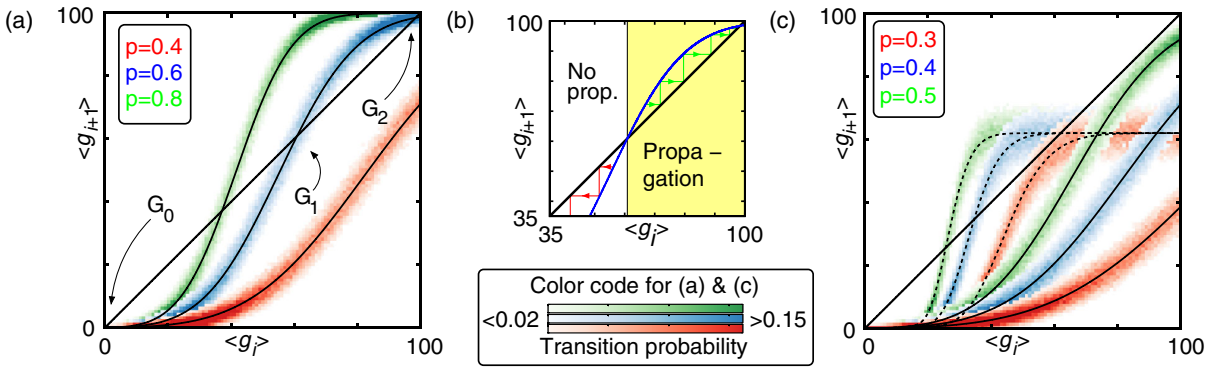

FIG. 2. Emergence of propagation of synchrony. (a) Analytically derived iterated maps approximating the time evolution of the synchronous pulse [solid line, cf. Eq. (16)] and transition probability obtained from network simulations (color code). (b) The basin of attraction of the stable fixed point G_2 is illustrated. Initial pulses within the range $(G_1, \omega]$ propagate with an average pulse size around G_2. (c) Iterated maps for FFNs with linear (solid lines) and nonlinear dendritic interactions (dashed lines). Nonlinear interactions reduce the connectivity required for propagation and allow for smaller fractions of active neurons.

points (G_1, unstable, and G_2, stable) appears via a tangent bifurcation. Initial pulses in the basin of G_2 (i.e., those larger than G_1) typically initiate stable propagation of synchrony with group sizes around G_2. For given layer size ω and connection strength ϵ, the critical connectivity p^* for which $G_1 = G_2$ marks the minimal connectivity that supports stable propagation of synchrony.

To elaborate the influence of nonlinear dendritic interactions, we derive the critical connectivity for FFNs. The mechanisms underlying propagation of synchrony are different for networks with and without nonlinear dendritic interactions and thus require different analytical approaches to derive p^*. We first consider feed-forward chains with conventional, linear coupling, i.e., $\sigma(x) = x$. To obtain p^*, we first expand $p_f(x)$ into a Taylor series up to first order around the mean of the binomial distribution specifying the average number pg_i of active neurons in each layer, such that Eq. (16) simplifies to

$$\langle g_{i+1}\rangle = \omega \sum_{h=0}^{g_i} \binom{g_i}{h} p^h (1-p)^{g_i-h} p_f(h\epsilon) \tag{17}$$

$$\approx \omega \sum_{h=0}^{g_i} \binom{g_i}{h} p^h (1-p)^{g_i-h} \tag{18}$$

$$\times [p_f(g_i p\epsilon) + p_f'(g_i p\epsilon)(h\epsilon - g_i p\epsilon)] \tag{19}$$

$$= \omega p_f(g_i p\epsilon). \tag{20}$$

The linear approximation becomes exact in the limit of large layer sizes ω and small couplings ϵ, where the product $\epsilon\omega$ is kept constant. We obtain an interpolated map from expression (20) by replacing g_i by its mean value $\langle g_i\rangle$. At the fixed point $G := \langle g_{i+1}\rangle = \langle g_i\rangle$, the function

$$F(G, p^\dagger, \omega, \epsilon) := G - \omega p_f(p^\dagger G\epsilon) = 0 \tag{21}$$

vanishes. Here, the values G and $p^\dagger$ are the average group size and the connection probability at the fixed point for given layer size ω and coupling strength ϵ, respectively. Furthermore, F has a double root at the bifurcation point, so the derivative

$$\frac{\partial F(G, p^*, \omega, \epsilon)}{\partial G} = 1 - \omega p^* \epsilon p_f'(p^* G\epsilon) = 0 \tag{22}$$

also vanishes such that the derivative of p_f at the bifurcation point is given by

$$p_f'(p^* G\epsilon) = \frac{1}{\omega p^* \epsilon}. \tag{23}$$

Combining the above equations, we express the derivatives of F at the bifurcation point by

$$\frac{\partial F(G, p^*, \omega, \epsilon)}{\partial p^*} = -\omega G\epsilon p_f'(p^* G\epsilon) = -\frac{G}{p^*}, \tag{24}$$

$$\frac{\partial F(G, p^*, \omega, \epsilon)}{\partial \omega} = -p_f(p^* G\epsilon) = -\frac{G}{\omega}, \tag{25}$$

and

$$\frac{\partial F(G, p^*, \omega, \epsilon)}{\partial \epsilon} = -\omega G p^* p_f'(p^* G\epsilon) = -\frac{G}{\epsilon}. \tag{26}$$

Applying the implicit function theorem yields the set of derivatives of p^*,

$$\frac{\partial p^*(G, \omega, \epsilon)}{\partial G} = -\left(\frac{\partial F(G, p^*, \omega, \epsilon)}{\partial p^*}\right)^{-1}\left(\frac{\partial F(G, p^*, \omega, \epsilon)}{\partial G}\right) = 0, \tag{27}$$

$$\frac{\partial p^*(G, \omega, \epsilon)}{\partial \omega} = -\left(\frac{\partial F(G, p^*, \omega, \epsilon)}{\partial p^*}\right)^{-1}\left(\frac{\partial F(G, p^*, \omega, \epsilon)}{\partial \omega}\right) = -\frac{p^*(G, \omega, \epsilon)}{\omega}, \tag{28}$$

and

$$\frac{\partial p^*(G, \omega, \epsilon)}{\partial \epsilon} = -\left(\frac{\partial F(G, p^*, \omega, \epsilon)}{\partial p^*}\right)^{-1}\left(\frac{\partial F(G, p^*, \omega, \epsilon)}{\partial \epsilon}\right) = -\frac{p^*(G, \omega, \epsilon)}{\epsilon}, \tag{29}$$

which are solved by

$$p_L^* := p^* = \frac{1}{\lambda\epsilon\omega}, \tag{30}$$

where λ is a constant independent of ω and ϵ. We note that we did not make explicit assumptions on the distribution of membrane potentials $P_V(V)$, which is determined by the setup of the external network, i.e., the external input current I^0, the coupling strengths $\epsilon^{\text{ext,ex}}$ and $\epsilon^{\text{ext,in}}$, as well as the firing rates $\nu^{\text{ext,ex}}$ and $\nu^{\text{ext,in}}$. With a different, lengthier approach based on a second-order expansion of p_f, one can derive an analytical estimate of λ [13]. Figure 3(a) displays this analytical approximation for p_L^* and its agreement with numerical simulations. For connectivity larger than p_L^*, there is stable propagation of synchrony even in networks with linear dendritic interactions, and the size of the propagating pulse fluctuates around the stable fixed point G_2 of Eq. (16). (For very large connectivity, pathological high-frequency spiking activity can emerge due to spontaneous chain activation.)

B. Feed-forward chains with nonlinear coupling

We now consider networks incorporating nonlinear dendritic interactions and show that the connectivity and number of active neurons required for propagation of synchrony are smaller. In such networks, the mechanism underlying propagation of synchrony is different, because it is supported predominantly by nonlinearly enhanced inputs. As a consequence, the maximal input is bounded by κ, leading to a saturation in the return map (16)

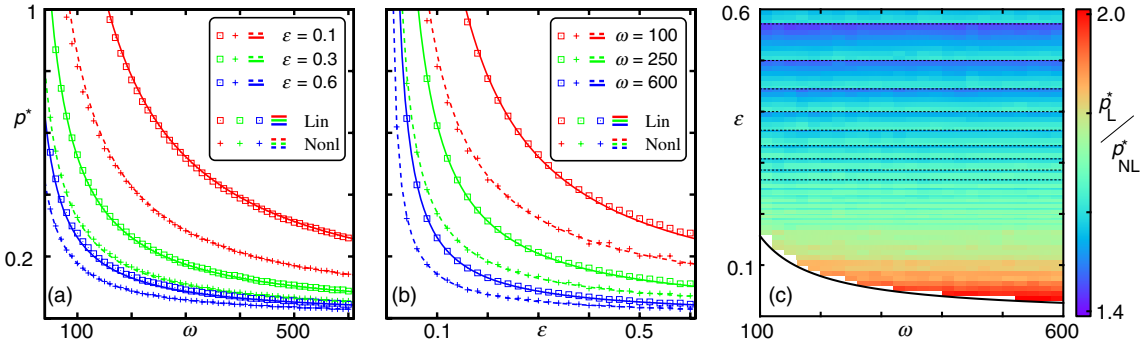

FIG. 3. Critical connectivity in isolated FFNs. (a),(b) Network simulations (symbols) agree well with analytical predictions (solid lines) (30) and (45). The critical connectivity decays with layer size and coupling strength. (c) The reduction factor $c = p^*_{\mathrm{L}}/p^*_{\mathrm{NL}} > 1$ shows that nonlinear dendritic interaction compensates for reduced connectivity. In both scenarios, with linear and nonlinear coupling, we find that $p^* \propto \omega^{-1}$, such that the reduction factor is independent of the layer size. In networks with linear couplings, the critical connectivity is $p^* \propto \epsilon^{-1}$, whereas, in networks with nonlinear coupling, the dependence on ϵ^{-1} is nonlinear. Therefore, the reduction factor increases with decreasing coupling strength. Dashed horizontal lines indicate jumps in the reduction factor at which the number of inputs needed for dendritic spike generation changes.

[cf. Fig. 2(c)]. The saturation enables propagating pulses of a size substantially smaller than ω, in contrast to linearly coupled networks. The discontinuity in the modulation function σ induces a discontinuity in $p_f[\sigma(x)]$, which prevents our previous analytical method. We thus determine the critical connectivity by a self-consistency approach. When a synchronous pulse arrives at a specific layer, the summed excitatory input strength x is either smaller or larger than the dendritic threshold Θ_b. For sufficiently small Θ_b, the spiking probability of a neuron due to a subthreshold input is much smaller than that due to a suprathreshold input, i.e., $p_f(\Theta_b) \ll p_f(\kappa)$. Thus, only a small fraction of neurons receives an input smaller than Θ_b and is elicited to spike. We approximate $p_f(x) = 0$ for $x \leq \Theta_b$. When there is persistent propagation of synchrony, p_γ (which denotes the fraction of neurons that receive sufficiently strong input to reach the dendritic threshold) is constant throughout the layers. The total spiking probability of a single neuron on the arrival of the synchronous pulse is then given by the product $p_\gamma p_f(\kappa)$. The probability

$$p^{\#}(g) = \binom{\omega}{g}[p_\gamma p_f(\kappa)]^g[p_\gamma p_f(\kappa)]^{w-g} \tag{31}$$

for g neurons to spike synchronously follows a binomial distribution. By combining the total spiking probability and the topological connection probability p, we compute the probability

$$P(k) = \sum_{g=k}^{\omega}\binom{g}{k}p^k(1-p)^{g-k}p^{\#}(g) \tag{32}$$

$$= \binom{\omega}{k}[p_\gamma p p_f(\kappa)]^k[1 - p_\gamma p p_f(\kappa)]^{w-k} \tag{33}$$

that a neuron of the subsequent layer receives exactly k synchronous spikes. Thus, k itself is binomially distributed, and we denote its mean value by δ and its standard deviation by σ_δ. Using a Gaussian approximation of the binomial distribution yields the self-consistent equation

$$p_\gamma = \sum_{k=\lceil\Theta_b/\epsilon\rceil}^{\omega} P(k) \tag{34}$$

$$\approx \int_{\Theta_b/\epsilon}^{\infty}\frac{1}{\sqrt{2\pi}\sigma_\delta}\exp\left[-\frac{1}{2}\left(\frac{k-\delta}{\sigma_\delta}\right)^2\right]dk \tag{35}$$

$$= \frac{1}{2}\left[1 - \mathrm{Erf}\left(\frac{\frac{\Theta_b}{\epsilon} - \delta}{\sqrt{2}\sigma_\delta}\right)\right] \tag{36}$$

$$=: \frac{1}{2}\left[1 + \mathrm{Erf}\left(\frac{n}{\sqrt{2}}\right)\right], \tag{37}$$

where we defined

$$n := \frac{\delta - \Theta_b/\epsilon}{\sigma_\delta} \tag{38}$$

$$= \frac{\omega p_\gamma p p_f(\kappa) - \Theta_b/\epsilon}{\sqrt{\omega p_\gamma p_f(\kappa) p[1 - p_\gamma p_f(\kappa) p]}} \tag{39}$$

as the distance between the average number of inputs and the number needed to reach the onset of the nonlinearity, measured in units of σ_δ. Solving definition (38) for p that occurs as an argument of δ and σ_δ and using Eq. (37) yields the connection probability in terms of n,

$$p_{\mathrm{NL}} = \frac{n^2\epsilon + 2\Theta_b + n\sqrt{n^2\epsilon^2 + 4\Theta_b(\epsilon - \frac{\Theta_b}{\omega})}}{p_f(\kappa)\epsilon(n^2+\omega)[1 + \mathrm{Erf}(\frac{n}{\sqrt{2}})]}. \tag{40}$$

For a certain setup of the FFN with variable connectivity, $p_{\mathrm{NL}}(n)$ is the connectivity for which a stationary propagation of synchrony occurs with a certain n. Any p_{NL} above the critical connectivity p^*_{NL} has two preimages n,

corresponding to the group sizes G_1 and G_2, p^*_{NL} has one preimage, and any p_{NL} below p^*_{NL} has none [cf. Fig. 2(c)]. Thus, $p_{\mathrm{NL}}(n)$ has one global minimum at $n = n^*$ where $\frac{dp_{\mathrm{NL}}(n)}{dn}|_{n=n^*} = 0$, and the critical connectivity is $p_{\mathrm{NL}}(n^*) = p^*_{\mathrm{NL}}$.

The comparison of the results for linearly and nonlinearly coupled FFNs is particularly enlightening in the limit of large layer size ($\omega \gg 1$) and small coupling strengths ($\epsilon \ll \Theta - V^{\mathrm{reset}}$). We fix the maximal input to a neuron from the previous layer, $\epsilon\omega = \mathrm{const}$, to preserve the network state and expand Eq. (40) in a power series around $\omega \to \infty$ and $\epsilon \to 0$. Considering the leading terms, we find

$$p_{\mathrm{NL}} \approx 2\frac{\Theta_b + n\sqrt{\Theta_b(\epsilon - \frac{\Theta_b}{\omega})}}{p_f(\kappa)\epsilon\omega[1 + \mathrm{Erf}(\frac{n}{\sqrt{2}})]}. \tag{41}$$

We note that propagation of synchrony mediated by dendritic spikes is enabled if a sufficiently large fraction of neurons of each layer receives a total input larger than or equal to Θ_b, which implies in particular that $\Theta_b < \omega\epsilon$. Moreover, if the connectivity within the FFN is low, stable propagation even requires that $\Theta_b \ll \omega\epsilon$, and p_{NL} further simplifies to

$$p_{\mathrm{NL}} \approx \frac{2\Theta_b}{p_f(\kappa)\epsilon\omega}\frac{1 + n\sqrt{\frac{\epsilon}{\Theta_b}}}{1 + \mathrm{Erf}(\frac{n}{\sqrt{2}})}. \tag{42}$$

As described above, the critical connectivity is given by the minimum of p_{NL} as a function of n, which is assumed at $n = n^*$. $\frac{dp_{\mathrm{NL}}(n)}{dn}|_{n=n^*} = 0$ yields n^* as an implicit function of $\frac{\Theta_b}{\epsilon}$,

$$\sqrt{\frac{\Theta_b}{\epsilon}} = \sqrt{\frac{\pi}{2}}\exp\left(\frac{n^{*2}}{2}\right)\left[1 + \mathrm{Erf}\left(\frac{n^*}{\sqrt{2}}\right)\right] - n^*. \tag{43}$$

For better readability, we define

$$\beta\left(\frac{\Theta_b}{\epsilon}\right) := \frac{1}{2}\left[1 + \mathrm{Erf}\left(\frac{n^*}{\sqrt{2}}\right)\right] - n^*\frac{e^{-(n^{*2}/2)}}{\sqrt{2\pi}}, \tag{44}$$

where $n^* = n^*(\frac{\Theta_b}{\epsilon})$ as given by Eq. (43). Combining Eqs. (42)–(44) enables to simplify the critical connectivity to

$$p^*_{\mathrm{NL}} = \frac{\Theta_b}{p_f(\kappa)\epsilon\omega}\frac{1}{\beta(\Theta_b/\epsilon)}, \tag{45}$$

which depends nonlinearly on the number of spikes needed to reach the dendritic threshold Θ_b/ϵ through the function $1/\beta(\cdot)$. One can show that $\beta(\Theta_b/\epsilon)$ increases with decreasing coupling strength ϵ from $\beta(\Theta_b/\epsilon) = 0.5$ for large ϵ and becomes maximal in the limit of small couplings, $\lim_{\epsilon\to 0}\beta(\Theta_b/\epsilon) = 1$. Figure 3(b) displays the results for p^*_{NL} together with the results of numerical simulations. As in the linearly coupled network, the critical connectivity decays with layer size and coupling strength, but the dependence on $1/\epsilon$ is nonlinear. The factor

$$c := \frac{p^*_{\mathrm{L}}}{p^*_{\mathrm{NL}}} = \frac{p_f(\kappa)}{\lambda\Theta_b}\beta\left(\frac{\Theta_b}{\epsilon}\right), \tag{46}$$

by which the nonlinear dendritic interactions reduce the required network-connectivity, increases with decreasing threshold Θ_b and increasing enhancement κ. Figure 3(c) illustrates the numerically obtained reduction of connectivity: The critical connectivity p^*_{NL} is smaller over the whole parameter range; the reduction is most effective for small ϵ and largely independent of ω.

Nonlinear dendrites thus foster propagation of synchrony. We note that our model still overestimates the capability of linearly coupled networks to propagate synchrony: On synchronous input, linearly coupled groups of neurons generate synchronous output (if they generate output at all). This fact is a consequence of the infinitesimally short synaptic currents. In neurons with extended synaptic currents, the timing of the output strongly depends on the neurons' state and input strength. In contrast, the timing of somatic action potentials elicited by dendritic spikes is largely independent of neuron state and input strength. We therefore expect the effect of nonlinear dendrites to be even stronger in networks of biologically more detailed neurons, as considered in the next section.

C. Recurrent networks

The main findings generalize in two ways: to FFNs occurring in recurrent random networks and to biologically more detailed models. For such systems, we show that, in nonlinearly coupled networks, stable propagation naturally emerges, whereas it is difficult to achieve in linearly coupled networks. In contrast to isolated FFNs studied above, we now account for effects of the FFN on the surrounding network and its feedback. Further, we choose a more detailed neuron model (see Sec. II) to ensure that the main assumptions underlying the analytically tractable model are not crucial for stable propagation of synchrony. In particular, we show that systems with temporally extended postsynaptic responses and a temporally extended nonlinear dendritic interaction window exhibit qualitatively the same phenomena as found above.

We consider networks of randomly connected conductance-based leaky integrate-and-fire neurons [cf. Eqs (8)–(10)]. The networks consist of N^{E} excitatory and N^{I} inhibitory neurons. A directed connection between two neurons is present with probability p. As for the isolated FFNs considered above, we construct the network such that the ground state in the absence of synchronous activity is characterized by balanced excitatory and inhibitory input, which results in an asynchronous irregular spiking activity. For simplicity, all neurons have the same parameters, e.g., $C^{\mathrm{m}}_l = C^{\mathrm{m}}$, $g^L_l = g^L$, etc.

First, we set up a model network in which the total excitation and inhibition to the neurons is balanced such that the spiking activity is asynchronous irregular. The external constant current I^0, together with the leak conductance g^L and the resting potential V^{rest}, determines the asymptotic membrane potential in the absence of incoming spikes:

$$V^\infty = V^{\text{rest}} + \frac{I^0}{g^L}. \tag{47}$$

Additionally, each neuron receives excitatory and inhibitory random Poissonian spike trains. The frequencies are denoted by $\nu^{\text{ext,ex}}$ and $\nu^{\text{ext,in}}$, and the ratio between them is chosen such that it equals the ratio of the number of excitatory and inhibitory neurons in the network:

$$\frac{\nu^{\text{ext,ex}}}{\nu^{\text{ext,in}}} = \frac{N^{\text{E}}}{N^{\text{I}}}. \tag{48}$$

This ensures that each neuron receives the same ratio of excitatory and inhibitory input from both the network and the external sources when neurons in the excitatory and inhibitory network populations spike on average with the same mean rate. All excitatory as well as all inhibitory connections have the same strength, i.e., $g_{lj}^{\max} = g^{\text{ex}}$ for excitatory and $g_{lj}^{\max} = g^{\text{in}}$ for inhibitory connections. The ratio of the peak postsynaptic potentials due to an inhibitory input and an excitatory input at the asymptotic membrane potential V^∞ is approximately given by

$$g^{\text{rat}} := \frac{g^{\text{in}}|V^\infty - E^{\text{in}}|}{g^{\text{ex}}|V^\infty - E^{\text{ex}}|}. \tag{49}$$

We set

$$g^{\text{rat}} \overset{!}{=} \frac{N^{\text{E}}}{N^{\text{I}}} = \frac{\nu^{\text{ext,ex}}}{\nu^{\text{ext,in}}}, \tag{50}$$

$$g^{\text{in}} = \frac{|V^\infty - E^{\text{ex}}|}{|V^\infty - E^{\text{in}}|}\frac{N^{\text{E}}}{N^{\text{I}}}\, g^{\text{ex}} \tag{51}$$

to obtain balanced activity.

In contrast to the model considered in the first sections, now excitatory neurons have a nonzero time window Δt for nonlinear dendritic modulation. When the strength of the excitatory input within Δt exceeds a threshold, a current pulse is injected into the soma, modeling the effect of a dendritic spike. The neuron parameters for this phenomenological model are chosen according to experimental findings to reproduce quantitatively the time course of the membrane potential in response to a dendritic spike. [See Sec. II and Figs. 1(b) and 1(c).]

Considering a random network, we detect naturally occurring weak feed-forward structures suitable for signal transmission in the following way: We randomly choose a group of x neurons to be the first layer. The second layer is composed of x neurons out of those receiving the largest numbers of connections from the initial group. By repeating this selection process l times, we identify a FFN consisting of l layers. In each selection step, we exclude the x neurons of the previous layer, but do not exclude neurons that are members of the layers preceding the previous one. The high-connectivity subnetwork selected from an existing random network as described above by construction has a slightly higher-than-average connection probability. Therefore, this structure is particularly well suited to enable propagation of synchrony. Alternatively, one can assign neurons randomly to the different layers and compensate for smaller connectivity by, e.g., larger layer sizes, according to Eq. (45).

The measurements start after an equilibration phase. (Initially, the network is at rest.) In the ground state, the network generates balanced irregular activity. Propagation of synchrony is initiated by exciting the neurons of the first layer to spike within a short time interval that is smaller than the time window of dendritic integration, Δt. This synchronous spiking leads to an increased input to the second layer after a delay time τ. This input, in turn, may lead to highly synchronous spiking of a certain number of neurons of the second layer (possibly supported by dendritic spikes) and therewith to synchronous spiking after another delay time τ in the third layer, etc. Propagation of synchrony requires (i) that the total input of a layer to its successor within the FFN is sufficiently strong and (ii) that the input to the remaining network is sufficiently weak to avoid excitation of too many neurons to synchronous spiking. Requirement (ii) prevents pathological activity such as "synfire explosions" [6].

After initiating a propagation of synchrony by exciting the neurons of the first group to spike within a short time interval, we measure the probability of detecting a synchronous pulse in the subsequent groups [see Sec. II; cf. Figs. 4(a) and 4(b)]. Although the average connectivity within the identified FFN is significantly larger than the overall connectivity p, it is still small, and propagation of synchronous activity is very unlikely [upper insets of Figs. 4(a) and 4(b)]. We find that it is not sufficient to choose high-connectivity subnetworks as FFNs (as described above) to obtain a stable propagation of synchrony, but that the synapses within the FFN have to be strengthened. To study the transition to propagation, we gradually strengthen the synapses within the FFN. As suggested by the results on isolated chains, we observe a propagation of synchrony over more and more layers for moderate enhancements [Figs. 4(c) and 4(d)]. For very strong enhancements, the feedback from the network becomes important: The synaptic amplification leads to an increased spontaneous activity within the FFN, and this in turn results in an increased background activity. The overall increased spiking activity causes spontaneous synchronous pulses, and a separation of the induced synchronous signal from the

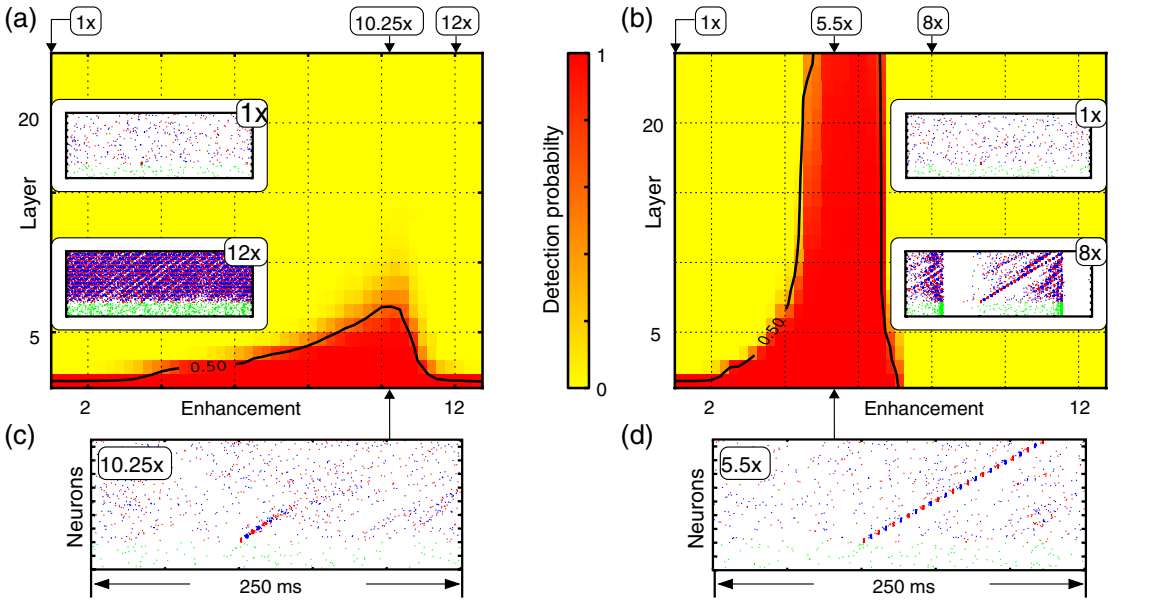

FIG. 4. Nonlinear dendritic interactions enable guided propagation of synchrony in random networks ($N = 10\,000$, $p = 0.03$, $\omega = 30$). (a),(b) Detection probability of induced synchronous activity in (a) conventional networks and (b) in networks with nonlinear dendrites. Insets of (a),(b) and Figs. (c),(d)_Typical examples of network activity for different synaptic-enhancement factors. Red and blue indicate spikes of neurons within the FFN; green indicates spikes of neurons randomly sampled from the remaining neurons.

background activity is not possible anymore [the detection probability decreases; see Figs. 4(a) and 4(b) and lower insets].

In agreement with previous studies (cf. [7]), we find that, in the linearly coupled networks considered, a synchronous pulse propagates only over a few layers, even in the optimal enhancement range [Fig. 4(a)]. In contrast, networks incorporating nonlinear dendrites support stable propagation of synchrony [Fig. 4(b)] in a substantial region of parameter space. In addition, the propagation is enabled for enhancements considerably smaller than the optimal enhancement for networks with linear dendrites.

IV. DISCUSSION

In conclusion, we have analyzed strongly diluted networks with linear and nonlinear dendritic interactions. We have demonstrated how nonlinear dendritic interactions may enhance and stabilize synchrony propagation in both isolated feed-forward chains and recurrent network structures. Moreover, our results show that such local nonlinear interactions support the separation of propagating synchrony and asynchronous background activity. Earlier works [6,7] did not take into account supralinear amplification of synchronous activity. One study [7] used existing connections in recurrent networks to create diluted chains assuming strongly enhanced synapses and at the same time partially decoupling the chain from the rest of the network; still, synchrony could propagate only over a few groups. In contrast, the results presented here indicate that a reliable propagation is achieved by only mildly adapted synapses and without specifically tuning or changing neuron properties or rewiring the network.

The recent study [18] incorporating nonlinear dendrites has shown that synchronous activity can propagate in purely random networks without modified connections. There are no specific propagation paths, but neurons are recruited in a quasirandom manner. Our results described here now indicate that specific feed-forward chains that naturally occur in random neural circuits are capable of persistently propagating synchronous signals if their synaptic strengths are increased. The strengths required in the presence of nonlinear interactions are common in biological neural circuits [19] and may well be generated by learning, e.g., through spike-timing-dependent plasticity.

Dendritic (coupling) nonlinearities therefore offer a viable mechanism for guiding synchrony through weakly structured random topologies.

Recently [12], feed-forward chains with slow dendritic (probably calcium) spikes have been simulated to check the possibility of the occurrence of specific spike patterns that are experimentally observed in the higher vocal center of song birds. Our theoretical work now yields analytic insights about the collective dynamics of circuits with fast dendritic (sodium) spikes. Fast dendritic spikes have been found in the hippocampus and in the neocortex and may thus be involved in hippocampal replay, memory formation, and other computational processes. Experimentally, the influence of fast dendritic spikes could be directly

checked by selectively blocking dendritic sodium channels (see, e.g., [20], which indicates that the types of sodium channels in the dendrite and soma are different) and thereby distinguishing those effects that come from nonadditive coupling via fast dendritic spikes from those induced by other mechanisms. During the last decade, the number of neurons simultaneously accessible has multiplied from a few to the order of 10^2 neurons, with this rapid trend continuing. When recording the activity of a substantial fraction of neurons of a local circuit, synchrony propagation should be clearly detectable and analyzable. Our results suggest that synchrony propagation and thus spike patterns should be influenced if dendritic sodium channels and thus fast dendritic spikes are blocked. Specifically, in the hippocampus, the precision of (replayed) spike patterns decreases or the patterns vanish after blocking. Such experiments would thus provide a direct test of how nonadditive coupling is exploited for the collective dynamics of neural circuits. Once the connectome, i.e., the structural synaptic connectivity, of neural circuits becomes available in the future [21], the relative impact of synaptic, structural to dynamic features of single neurons on circuit dynamics may be well distinguishable.

The basic model of pulse-coupled units considered here is applicable to a range of systems in nature, not only to neural circuits but also, e.g., to earthquakes emerging from abruptly relaxing tectonic plates, and fireflies interacting by exchanging light flashes (e.g., [22]). We have now studied the impact of nonlinear input modulation on collective network dynamics and derived methods for their analysis that may also be useful in a non-neuronal setting. Interestingly, very recent results [23] have shown that fireflies are more prone to respond to synchronous flashes rather than to asynchronous ones, suggesting a direct application of our model.

ACKNOWLEDGMENTS

This work was supported by the BMBF (Grant No. 01GQ1005B), the DFG (Grant No. TI 629/3-1), and the Swartz Foundation. Simulation results were partly obtained using the simulation software NEST [26].

APPENDIX

1. Parameters for Figs. 2 and 3

The single-neuron parameters and the coupling delay are $\tau^{\mathrm{m}} = 1/\gamma = 14$ ms, $\Theta = 15$ mV, $V^{\mathrm{reset}} = 0$ mV, $t^{\mathrm{ref}} = 2$ ms, and $\tau = 10$ ms [15,24]. The external input is characterized by $\epsilon^{\mathrm{ext,ex}} = -\epsilon^{\mathrm{ext,in}} = 0.5$ mV [19,25], $\nu^{\mathrm{ext}} = \nu^{\mathrm{ext,ex}} = \nu^{\mathrm{ext,in}} = 3$ kHz, and $V^{\infty} = 5$ mV. The parameters of the dendritic modulation function were chosen according to single-neuron measurements as $\Theta_b = 4$ mV and $\kappa = 11$ mV [8].

The maps and transition matrices presented in Fig. 2 are derived for $\omega = 100$ and $\epsilon_{ij} = \epsilon = 0.3$ mV. To obtain the distribution of active neurons g_{i+1} in layer $i+1$, we excite g_i neurons of the first layer to spike simultaneously and measure the number of active neurons in the following layer. For each value of g_i, we calculate the distribution for $m = 1000$ different realizations of the FFN and initial conditions.

In Fig. 3, existing connections within the FFN have strengths $\epsilon_{ij} = \epsilon$. We determine the critical connectivity for $\epsilon \in [0.05\ \mathrm{mV}, 0.6\ \mathrm{mV}]$ and layer sizes $\omega \in [50, 600]$ as follows: We construct a FFN consisting of 20 layers, with ω neurons in each layer, and connect neurons of successive layers with probability $p \in [0, 1]$. After an equilibration time t^{init} (initially, the network is at rest), we initiate propagation of synchrony by exciting all neurons of the first layer to spike simultaneously. We then check whether the synchronous pulse propagates up to layer i, i.e., whether there is synchronous activity in layer i at time $t_i^{\mathrm{exp}} = t^{\mathrm{init}} + (i-1)\tau$. We consider the propagation for a certain setup specified by ϵ, ω, and p to be successful if a synchronous pulse propagates along the whole FFN in more than 50% of $o = 31$ realizations of the FFN with different initial conditions. We derive the critical connectivities p_{L}^* and p_{NL}^* up to a resolution of $\frac{\Delta p}{p} = 5 \times 10^{-3}$ by repeatedly bisecting the interval [0,1] and testing the success of propagation.

2. Parameters for Fig. 4

For the network simulations, we employed the simulation software NEST [26]. The networks had a total number of $N = 10\,000$ neurons with $N^{\mathrm{E}} = 8\,000$ and $N^{\mathrm{I}} = 2\,000$. For simplicity, all neurons are considered identical, i.e., $C_l^{\mathrm{m}} = C^{\mathrm{m}}$, $g_l^L = g^L$, $V_l^{\mathrm{rest}} = V^{\mathrm{rest}}$, $I_l^0 = I^0$, $\Theta_l = \Theta$, $t_l^{\mathrm{ref}} = t^{\mathrm{ref}}$, and $V_l^{\mathrm{reset}} = V^{\mathrm{reset}}$. The single-neuron parameters are $C^{\mathrm{m}} = 400$ pF, $V^{\mathrm{rest}} = V^{\mathrm{reset}} = -65$ mV, $g^L = 25$ nS, $\Theta = -50$ mV, $t^{\mathrm{ref}} = 3$ ms [24,27], and $I^0 = 250$ pA, and the frequencies of the external inputs are $\nu^{\mathrm{ext,ex}} = 2.4$ kHz and $\nu^{\mathrm{ext,in}} = 0.6$ kHz. The recurrent connectivity in cortical and hippocampal networks is sparse: Connection probabilities between 1% and 10%, depending on the distance and the region, have been estimated (e.g., [19,24,25]). For our simulations, we choose $p = 0.03$.

The time constants of the excitatory (AMPA) conductances are $\tau^{\mathrm{A},1} = 2.5$ ms and $\tau^{\mathrm{A},2} = 0.5$ ms [28]. For simplicity, we choose the same time constants for the inhibitory ($\mathrm{GABA_A}$) conductances: $\tau^{\mathrm{G},1} = 2.5$ ms and $\tau^{\mathrm{G},2} = 0.5$ ms. The reversal potentials are $E^{\mathrm{ex}} = 0$ mV and $E^{\mathrm{in}} = -75$ mV [15,24]. The strengths of experimentally observed pEPSPs due to single inputs range from small values like 0.1 mV to larger values like 2 mV [19,24,25]. For nonenhanced couplings, we set $g^{\mathrm{ex}} = 0.6$ nS, which corresponds to a pEPSP of approximately 0.3 mV at rest. According to Eq. (51), the coupling strengths of the inhibitory synapses are $g^{\mathrm{in}} = -6.6$ nS to maintain balanced input. This configuration results in an

asynchronous irregular ground state with a spontaneous firing rate $\nu \approx 1.8$ Hz.

The parameters of the dendritic spike current are chosen according to single-neuron measurements in hippocampal cells: $\Delta t = 2$ ms [8], $g^{\Theta} = 8.65$ nS (corresponding to a pEPSP of about 3.8 mV at rest [8]), $\tau^{\mathrm{DS}} = 2.7$ ms (such that $\tau + \tau_{\mathrm{DS}} = 4.7$ ms and the peak of the depolarization is reached approximately 5 ms after presynaptic spiking), $A = 55$ nA, $B = 64$ nA, $C = 9$ nA, $\tau^{\mathrm{DS},1} = 0.2$ ms, $\tau^{\mathrm{DS},2} = 0.3$ ms, $\tau^{\mathrm{DS},3} = 0.7$ ms, and $t^{\mathrm{ref,DS}} = 5.2$ ms. The correction factor, which modulates the strength of the dendritic spike, is found by fitting a linear correction function, $c(g) = \max\{1.5 - g \times 0.053\ \mathrm{nS}^{-1}, 0\}$, such that the experimentally observed region of saturation is obtained. The dynamics of the neuron model incorporating the mechanism for dendritic spike generation is illustrated in Fig. 1.

For calculating the SNR, we use an $a = 0.99$ and $b = 2$ and an expected width of the synchronous pulse $t^{w} = 10$ ms; the result is insensitive to changes in these parameters. The expected interval between successive synchronous active layers, Δt^{exp}, is chosen from the interval [2 ms, 7 ms] such that the signal, $\sum_i S_i$, is maximized (cf. Sec. II). The time interval for the estimation of the noise level is $\Delta t^{\mathrm{obs}} = 15$ s. The detection probability shown in Figs. 4(a) and 4(b) is the fraction of successful propagations obtained from 10 different network realizations, where, for each network setup, propagation of synchrony was tested for 20 initial conditions.

All measurements start after an initial equilibrium phase of $t^{0} = 4000$ ms.

[1] C. v. Vreeswijk and H. Sompolinsky, *Chaos in Neuronal Networks with Balanced Excitatory and Inhibitory Activity*, Science **274**, 1724 (1996).

[2] N. Brunel, *Dynamics of Sparsely Connected Networks of Excitatory and Inhibitory Spiking Neurons*, J. Comput. Neurosci. **8**, 183 (2000).

[3] S. Jahnke, R.-M. Memmesheimer, and M. Timme, *Stable Irregular Dynamics in Complex Neural Networks*, Phys. Rev. Lett. **100**, 048102 (2008); S. Jahnke, R.-M. Memmesheimer, and M. Timme, *How Chaotic Is the Balanced State?*, Front. Comput. Neurosci. **3**, 13 (2009).

[4] M. London, A. Roth, L. Beeren, M. Häusser, and P. Latham, *Sensitivity to Perturbations in vivo Implies High Noise and Suggests Rate Coding in Cortex*, Nature (London) **466**, 123 (2010).

[5] M. Abeles, *Local Cortical Circuits: An Electrophysiological Study* (Springer, Berlin, 1982); M. Diesmann, M.-O. Gewaltig, and A. Aertsen, *Stable Propagation of Synchronous Spiking in Cortical Neural Networks*, Nature (London) **402**, 529 (1999).

[6] C. Mehring, U. Hehl, M. Kubo, M. Diesmann, and A. Aertsen, *Activity Dynamics and Propagation of Synchronous Spiking in Locally Connected Random Networks*, Biol. Cybernet. **88**, 395 (2003); Y. Aviel, C. Mehring, and D. Horn, *On Embedding Synfire Chains in a Balanced Network*, Neural Comput. **15**, 1321 (2003); A. Kumar, S. Rotter, and A. Aertsen, *Conditions for Propagating Synchronous Spiking and Asynchronous Firing Rates in a Cortical Network Model*, J. Neurosci. **28**, 5268 (2008).

[7] T. Vogels and L. Abbott, *Signal Propagation in Networks of Integrate-and-Fire Neurons*, J. Neurosci. **25**, 10786 (2005).

[8] G. Ariav, A. Polsky, and J. Schiller, *Submillisecond Precision of the Input-Output Transformation Function Mediated by Fast Sodium Dendritic Spikes in Basal Dendrites of CA1 Pyramidal Neurons*, J. Neurosci. **23**, 7750 (2003) [http://www.jneurosci.org/content/23/21/7750.full.pdf+html]; S. Gasparini, M. Migliore, and J. C. Magee, *On the Initiation and Propagation of Dendritic Spikes in CA1 Pyramidal Neurons*, J. Neurosci. **24**, 11046 (2004); A. Polsky, B. W. Mel, and J. Schiller, *Computational Subunits in Thin Dendrites of Pyramidal Cells*, Nat. Neurosci. **7**, 621 (2004); S. Gasparini and J. C. Magee, *State-Dependent Dendritic Computation in Hippocampal CA1 Pyramidal Neurons*, J. Neurosci. **26**, 2088 (2006).

[9] M. Häusser, N. Spruston, and G. Stuart, *Diversity and Dynamics of Dendritic Signaling*, Science **290**, 739 (2000).

[10] B. Mel, *The Clusteron: Toward a Simple Abstraction for a Complex Neuron*, Adv. Neural Inf. Process. Syst. **4**, 35 (1991); in *Dendrites*, edited by G. Stuart *et al.* (Oxford University Press, New York, 2007), 2nd ed., pp. 421–440; P. Poirazi, T. Brannon, and B. Mel, *Arithmetic of Subthreshold Synaptic Summation in a Model CA1 Pyramidal Cell*, Neuron **37**, 989 (2003).

[11] R. Traub and R. Wong, *Cellular Mechanism of Neuronal Synchronization in Epilepsy*, Science **216**, 745 (1982); D. Jin, F. Ramazanoglu, and H. Seung, *Intrinsic Bursting Enhances the Robustness of a Neural Network Model of Sequence Generation by Avian Brain Area HVC*, J. Comput. Neurosci. **23**, 283 (2007).

[12] M. Long, D. Jin, and M. Fee, *Support for a Synaptic Chain Model of Neuronal Sequence Generation*, Nature (London) **468**, 394 (2010).

[13] S. Jahnke, R.-M. Memmesheimer, and M. Timme (unpublished).

[14] R.-M. Memmesheimer, *Quantitative Prediction of Intermittent High-Frequency Oscillations in Neural Networks with Supralinear Dendritic Interactions*, Proc. Natl. Acad. Sci. U.S.A. **107**, 11092 (2010).

[15] P. Dayan and L. Abbott, *Theoretical Neuroscience: Computational and Mathematical Modeling of Neural Systems* (MIT Press, Cambridge, Massachusetts, 2001).

[16] N. Brunel and V. Hakim, *Fast Global Oscillations in Networks of Integrate-and-Fire Neurons with Low Firing Rates*, Neural Comput. **11**, 1621 (1999); M. Helias, M. Deger, S. Rotter, and M. Diesmann, *Instantaneous Non-Linear Processing by Pulse-Coupled Threshold Units*, PLoS Comput. Biol. **6**, e1000929 (2010).

[17] M. Abeles, G. Hayon, and D. Lehmann, *Modeling Compositionality by Dynamic Binding of Synfire Chains*, J. Comput. Neurosci. **17**, 179 (2004); S. Goedeke and

M. Diesmann, *The Mechanism of Synchronization in Feed-Forward Neuronal Networks*, New J. Phys. **10**, 015007 (2008).

[18] R.-M. Memmesheimer and M. Timme, *Non-Additive Coupling Enables Propagation of Synchronous Spiking Activity in Purely Random Networks*, PLoS Comput. Biol. **8**, e1002384 (2012).

[19] C. Holmgren, T. Harkany, B. Svennenfors, and Y. Zilberter, *Pyramidal Cell Communication within Local Networks in Layer* 2/3 *of Rat Neocortex*, J. Physiol. **551**, 139 (2003); S. Song, P. Sjöström, M. Reigl, S. Nelson, and D. Chklovskii, *Highly Nonrandom Features of Synaptic Connectivity in Local Cortical Circuits*, PLoS Biol. **3**, e68 (2005).

[20] N. Golding, W. Kath, and N. Spruston, *Dichotomy of Action-Potential Backpropagation in CA1 Pyramidal Neuron Dendrites*, J. Neurophysiol. **86**, 2998 (2001) [http://jn.physiology.org/content/86/6/2998.full]; **87**, a1(E) (2001) [http://jn.physiology.org/content/87/2/a1.short]; V. Menon, N. Spruston, and W. Kath, *A State-Mutating Genetic Algorithm to Design Ion-Channel Models*, Proc. Natl. Acad. Sci. U.S.A. **106**, 16829 (2009).

[21] S. Smith, *Circuit Reconstruction Tools Today*, Curr. Opin. Neurobiol. **17**, 601 (2007); J. Lichtman, J. Livet, and J. Sanes, *A Technicolour Approach to the Connectome*, Nat. Rev. Neurosci. **9**, 417 (2008).

[22] R. Mirollo and S. Strogatz, *Synchronization of Pulse-Coupled Biological Oscillators*, SIAM J. Appl. Math. **50**, 1645 (1990); A. Herz and J. Hopfield, *Earthquake Cycles and Neural Reverberations: Collective Oscillations in Systems with Pulse-Coupled Threshold Elements*, Phys. Rev. Lett. **75**, 1222 (1995).

[23] A. Moiseff and J. Copeland, *Firefly Synchrony: A Behavioral Strategy to Minimize Visual Clutter*, Science **329**, 181 (2010).

[24] P. Andersen, R. Morris, D. Amaral, T. Bliss, and J. O'Keefe, *The Hippocampus Book* (Oxford University Press, New York, 2007).

[25] R. Miles and R. K. Wong, *Excitatory Synaptic Interactions between CA3 Neurones in the Guinea-Pig Hippocampus*, J. Physiol. **373**, 397 (1986) [http://www.ncbi.nlm.nih.gov/pmc/articles/PMC1182545/]; J. Deuchars and A. M. Thomson, *CA1 Pyramid-Pyramid Connections in Rat Hippocampus in vitro: Dual Intracellular Recordings with Biocytin Filling*, Neuroscience (N.Y.) **74**, 1009 (1996).

[26] M.-O. Gewaltig and M. Diesmann, *NEST (Neural Simulation Tool)*, Scholarpedia **2**, 1430 (2007). The software, by the NEST Initiative, is available at www.nest-initiative.org.

[27] N. Staff, H. Jung, T. Thiagarajan, M. Yao, and N. Spruston, *Resting and Active Properties of Pyramidal Neurons in Subiculum and CA1 of Rat Hippocampus*, J. Neurophysiol. **84**, 2398 (2000) [http://jn.physiology.org/content/84/5/2398.long].

[28] P. Jonas, G. Major, and B. Sakmann, *Quantal Components of Unitary EPSCs at the Mossy Fibre Synapse on CA3 Pyramidal Cells of Rat Hippocampus*, J. Physiol. **472**, 615 (1993); G. Liu and R. W. Tsien, *Properties of Synaptic Transmission at Single Hippocampal Synaptic Boutons*, Nature (London) **375**, 404 (1995).

Chapter 5

Original Manuscript: Hub-activated signal transmission in complex networks

Citation

Jahnke, S., Memmesheimer, R.-M. and Timme, M. (2014), Hub-activated signal transmission in complex networks, *Phys. Rev. E (Rapid)*, **89**, 030701, DOI:10.1103/PhysRevE.89.03701

Original contribution

Conception and design of the study together with R.-M. Memmesheimer and M. Timme. I performed the analytical calculations and numerical simulations. For the simulations I implementated neuron models within the NEST simulation environment (www.nest-initiative.org). I analyzed the data and prepared all figures. I wrote main parts of the manuscript and the supplemental material supported by R.-M. Memmesheimer and M. Timme.

Göttingen, 31.03.2014
Place, Date

Sven Jahnke

RAPID COMMUNICATIONS

PHYSICAL REVIEW E **89**, 030701(R) (2014)

Hub-activated signal transmission in complex networks

Sven Jahnke,[1,2,3] Raoul-Martin Memmesheimer,[4] and Marc Timme[1,2,3]

[1]*Network Dynamics, Max Planck Institute for Dynamics and Self-Organization (MPIDS), 37077 Göttingen, Germany*

[2]*Bernstein Center for Computational Neuroscience (BCCN), 37077 Göttingen, Germany*

[3]*Institute for Nonlinear Dynamics, Fakultät für Physik, Georg-August-Universität Göttingen*

[4]*Department for Neuroinformatics, Donders Institute, Radboud University, Nijmegen, Netherlands*

(Received 5 November 2013; published 10 March 2014)

A wide range of networked systems exhibit highly connected nodes (hubs) as prominent structural elements. The functional roles of hubs in the collective nonlinear dynamics of many such networks, however, are not well understood. Here, we propose that hubs in neural circuits may activate local signal transmission along sequences of specific subnetworks. Intriguingly, in contrast to previous suggestions of the functional roles of hubs, here, not the hubs themselves, but nonhub subnetworks transfer the signals. The core mechanism relies on hubs and nonhubs providing activating feedback to each other. It may, thus, induce the propagation of specific pulse and rate signals in neuronal and other communication networks.

DOI: 10.1103/PhysRevE.89.030701 PACS number(s): 87.10.−e, 05.45.Xt, 89.75.Hc

Hubs—nodes that are significantly more highly connected than average—constitute a prominent structural feature of many network dynamical systems, such as infection, transportation, communication, and social networks [1]. The existence of hubs may follow from intentional design to optimize network properties (such as in airline, transportation, and technical communication infrastructure) or may emerge due to self-organization via intrinsic growth rules (World Wide Web and social networks) [1–4]. As hubs can structurally improve the capabilities of networks to transfer signals [5], it is not surprising that they were also found in the brain on different scales: In cortical neuronal circuits, hub regions are assumed to coordinate the activity of other regions and to organize the flow of information between them [6]. On the microscopic level, for instance, the nervous system of *Caenorhabditis elegans* contains single cell hubs [7] involved in the control of pheromone attraction as well as social behavior [8]. Interestingly, Bonifazi *et al*. [9] recently experimentally discovered hub cells also in higher animals where they support synchronous activity in the developing hippocampus. Yet, how exactly hubs dynamically influence information transmission in neural circuits still remains unknown [10].

In this Rapid Communication, we show that hub activity may amplify local signals and may enable their targeted transmission. Specifically, we show how hubs and nonhub subnetworks in neural circuits activate each other to exhibit synchronous pulse emission. Thereby, synchronous pulse activity may robustly propagate along sequences of nonhub subnetworks, thus, enabling directed and specific routing of information across the entire system. The generic mechanism of mutual hub and nonhub activation may equally enable the transmission of pulse-coded as well as rate-coded signals in a wide range of natural and artificial communication networks.

For an example of spiking neural circuits, consider networks of N units randomly connected to each other. Each connection is present with a fixed probability. In the simplest setting, between any pair of neurons, there is an excitatory connection of strength ϵ_+ with probability p_+ and an inhibitory connection of strength ϵ_- with probability $p_- = p_+ =: p$. The dynamics of each unit i is described by a real state variable, its membrane potential $V_i(t)$ in real time t and changes according to leaky integrate-and-fire dynamics. Specifically, V_i integrates excitatory (positive) and inhibitory (negative) pulsed inputs, and when crossing a threshold from below, the potential resets and the unit emits a pulse. This pulse arrives at the postsynaptic neurons after a transmission delay, and its effects are modeled by transient double-exponential conductance changes [11].

Typically, some of the pulse inputs to a neuron are synchronous (i.e., are received within a few milliseconds), and others are asynchronous. Whereas, the neuron integrates all inhibitory and asynchronous excitatory inputs additively, synchronous excitatory inputs are processed nonadditively (nonlinearly). This nonadditive integration takes into account the influence of fast dendritic spikes found in single neuron experiments [12] on the dendritic (input) sites of neurons: Whenever the total excitatory input to a dendrite summed over a short time interval (typically 2 to 3 ms) exceeds a dendritic threshold Θ_d, a dendritic spike is initiated and changes the membrane potential of the neuron after a short delay in a stereotypical way. We model its effect by a stereotypical current pulse causing a rapid strong increase (depolarization) of V_i, which substantially exceeds the level of depolarization expected from linear summation of inputs [11,13,14] and resembles the shape of the depolarization found in experiments [12]. We account for the experimentally observed saturation of the depolarization by inputs exceeding the dendritic threshold Θ_d [12] as well as for the refractory time of ion channels generating dendritic spikes by assuming that the dendrite becomes refractory for a short time period $t^{\mathrm{ref,ds}}$ after a dendritic spike is initiated.

In our numerical simulations, we focus on networks of spiking leaky integrate-and-fire neurons as described above (Simulation results were obtained using the simulation software NEST [15]). To achieve a mechanistic understanding of the observed phenomena, we further derive an analytically tractable description in terms of probabilistic threshold units below.

Motivated by recent anatomical and physiological findings [9], we assume that some $N_\mathrm{h} \geqslant 0$ neurons are hub neurons. They are distinguished (exclusively) by an increased

probability $p_h > p$ to receive input connections from other units in the network.

Following a standard approach for signal transmission in cortical networks [16], we consider signal propagation along weak feed-forward structures: The network contains sequences (chains) of m subnetworks (groups) with N_g neurons each. The neurons in each group are randomly chosen from the nonhub population, and excitatory connection strengths between subsequent subnetworks are increased compared to other coupling strengths in the network, $\epsilon_{sub} > \epsilon_+$.

We consider networks with balanced excitatory and inhibitory connectivities such that, in the absence of external inputs, asynchronous irregular spiking dynamics constitutes their ground state activity [17]. Externally exciting an initial subnetwork to spike synchronously causes synchronous inputs to neurons of the downstream subnetwork and induces synchronous spiking of a fraction of its neurons. This may excite neurons in the ensuing subnetwork to spike, etc., thereby transmitting signals along the chain of subnetworks. However, as the subnetworks are parts of a larger recurrent network, synchronous activity not only may spread from one subnetwork to the next, but also may induce a synchronous spiking response (echo) in the remainder of the network. Depending on the parameters and the number of initially synchronous neurons g_0 in the first subnetwork and r_0 in the remainder of the network, synchronous activity may, in principle, stably propagate, spread across the entire recurrent network, and, thus, may obscure a propagation signal (not shown) or may extinguish after a few subnetworks.

Sample simulations of networks without hubs [$N_h = 0$, Fig. 1(a)] illustrate that spreading and dying out of synchrony dominate state space in agreement with the literature [18] because there is no mechanism keeping the synchronization in the network remainder at a moderate level.

Networks with a substantial number N_h of hub units exhibit qualitatively different dynamics and support signal transmission: As hubs receive more input connections than other units, they have a higher probability of spiking in response to synchronous inputs from a certain subnetwork. Thereby, hubs may establish a synchronous response to propagating synchronous pulses. Due to increased connectivity at hubs only, such an echo is confined to the hub neuron subpopulation and, thus, does not spread over the entire network [cf. Fig. 1(b)].

The increased connectivity towards hubs plays an interesting double role: It ensures that a population of sufficiently many hub neurons exhibits, itself, synchronous activity if supported by synchrony in a (nonhub) subnetwork. At the same time, the fact that the network remainder without hubs has relatively low connectivity prevents spreading of synchronous activity beyond the hub population. This combination enables robust synchrony propagation along sequences of nonhub subnetworks for a range of initially synchronous neurons g_0 in a subnetwork [cf. Fig. 1(b), main panel].

To further understand this coaction mechanism, we consider the dynamics only at the relevant time intervals where synchronous pulses are sent and are received. Observing that

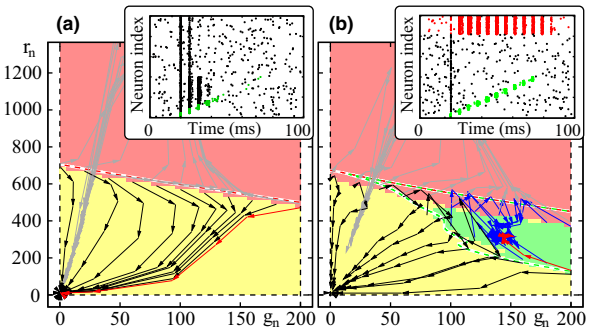

FIG. 1. (Color online) Hubs activate signal transmission in a neural network. Signals consist of localized synchronous spiking activity (times marked green in the insets) transmitted across a sequence of subnetworks (displayed as lowest neuron indices). Spike times of hubs (red) displayed at the top, above those of the remaining neurons (black). Main panels: Joint dynamics of the number of synchronously spiking neurons in the nth subnetwork (g_n) and the total number of synchronously coactivated neurons of the network remainder (r_n) during signal propagation initiated by synchronously stimulating g_0 neurons of the initial subnetwork and r_0 neurons of the network remainder. (a) In networks without hubs, the overall network activity either becomes pathological (large scale synchrony: red shading, gray trajectories) or extinguishes quickly to background activity (yellow shading, black trajectories). Hub neurons in otherwise the same network (b) can induce a persistent signal transmission across nonhubs (green shading, blue trajectories) by generating sustained but bounded synchrony. Red trajectories indicate example dynamics shown in the insets. The dashed lines indicate the borders of activity regions analytically estimated in this Rapid Communication (cf. Eqs. (5) and (6) and Ref. [11]). Parameters: $N = 5000$, $m = 10$, $N_g = 200$, and $p = 0.05$; furthermore, $N_h = 0$ in (a) and $N_h = 900$ and $p_h = 0.12$ in (b).

the neurons effectively act as probabilistic threshold units, we derive an approximate analytic map for the joint response sizes of active hubs and signal carrying (nonhub) units. The spiking probability due to a synchronous input below the dendritic threshold Θ_d is very low [cf. Fig. 2(a)] so that we neglect it against the probability of spiking due to inputs above threshold. The probability $p^{sp}(I_+, I_-)$ of a neuron spiking in response to excitatory and inhibitory inputs I_+ and I_- is a function of the probability distribution of the membrane potentials of that neuron at the time of input reception. We take this dependency into account by assuming that, immediately before every spike reception time, the neuronal state is distributed as in the unperturbed ground state. The function p^{sp}, thus, obeys

$$p^{sp}(I_+, I_-) = \begin{cases} 0 & \text{for} \quad I_+ < \Theta_d, \\ p^0(I_-) & \text{for} \quad I_+ \geqslant \Theta_d, \end{cases} \tag{1}$$

where $p^0(I_-)$ is the spiking probability of a neuron in the ground state receiving a dendritically suprathreshold excitatory input and an inhibitory input of size I_-. In particular, $p^0(0)$ is the spiking probability of a single neuron when a dendritic spike is generated in the absence of inhibition. p^0 depends solely on the inhibitory input I_- because, on one

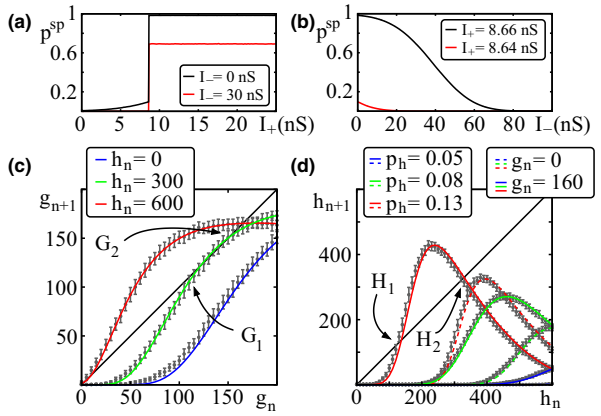

FIG. 2. (Color online) Hubs induce tangent bifurcations towards signal transmission (neuron and network parameters as in Fig. 1). (a) and (b) Firing probability $p^{\rm sp}$ of a neuron in the ground state as a function of synchronous (a) excitatory input I_+ and (b) inhibitory input I_-. (c) and (d) Iterated maps for (c) the number g_n of (synchronously) active neurons in the nth subnetwork (different colors indicate different fixed h_n's) and (d) the number of synchronized hub neurons h_n (different colors: p_h fixed; different line styles: g_n fixed). Analytical predictions [solid and dashed lines; Eqs. (5) and (6)] agree well with numerical simulations of the spiking neural network model (markers). Sufficiently large h_n enables propagation of synchrony (c), and a sufficiently large connection probability $p_{\rm h}$ enables a persistent hub echo for a propagating synchronous pulse (d). Hubs and nonhubs reactivate each other.

hand, only sufficiently strong excitatory inputs exceeding the dendritic threshold elicit a dendritic spike and the effect of a dendritic spike on the postsynaptic neuron saturates, i.e., it remains the same, for stronger excitation [cf. Fig. 2(a)] as found in experiments [12]. On the other hand, inhibition will generally decrease a neuron's spiking probability as it partially compensates the input to the soma due to the dendritic spike (cf. Fig. 2(b) and the experimental findings in Ref. [19]). The precise form of $p^0(I_-)$ depends on the details of the background activity and the properties of neurons and interactions. As will become clear below, all *qualitatively* similar $p^0(I_-)$'s induce the same type of bifurcation relevant for robust signal transmission, and thus, details of $p^0(I_-)$ do not matter.

During robust signal transmission promoted by a hub echo, spikes of hub neurons and neurons of the currently active subnetwork dominate the network dynamics [cf. inset of Fig. 1(b)]. We, thus, focus on these two groups of neurons. The influence of the remaining neurons can be analytically derived analogously [11]. To be specific, assume that $g_n \leqslant N_{\rm g}$ neurons in a given subnetwork n and $h_n \leqslant N_{\rm h}$ hub neurons are active simultaneously, i.e., they spike synchronously. Given the random network topology, for sufficiently large g_n and h_n, the total input to the neurons of the $(n+1)$th subnetwork is approximately Gaussian distributed (approximating the actual binomial distributions) $I_\pm \sim \mathcal{N}(\mu_\pm,\sigma_\pm^2)$ with probability density functions $f_+(I_+)$ and $f_-(I_-)$ and means and variances given by

$$\mu_+ = (\epsilon_+ h_n + \epsilon_{\rm c} g_n)p, \quad \sigma_+^2 = \left(\epsilon_+^2 h_n + \epsilon_{\rm c}^2 g_n\right)p(1-p), \tag{2}$$

$$\mu_- = \epsilon_-(h_n + g_n)p \quad \text{and} \quad \sigma_-^2 = \epsilon_-^2(h_n + g_n)p(1-p). \tag{3}$$

The expected number of neurons that spike synchronously in subnetwork $n+1$ becomes

$$g_{n+1} = N_{\rm g}\int_0^\infty\int_0^\infty p^{\rm sp}(I_+,I_-)f_+(I_+)f_-(I_-)dI_+dI_-. \tag{4}$$

Whereas, $p^{\rm sp}$ discontinuously depends on I_+, it changes smoothly and, thus, locally linearly with I_- [cf. Figs. 2(a) and 2(b)] such that we may set $f_-(I_-) = \delta(I_- - \mu_-)$ to evaluate the integral in Eq. (4), yielding the iterated map,

$$g_{n+1} = N_{\rm g}p^0(\mu_-)\frac{1}{2}\left(1 + {\rm Erf}\left[\frac{\Theta_{\rm d} - \mu_+}{\sqrt{2}\sigma_+}\right]\right) \tag{5}$$

for the number of active signal transferring (nonhub) neurons in the next subnetwork. Note that all three quantities μ_-, μ_+, and σ_+ depend on h_n and g_n through Eqs. (2) and (3).

The iterated map for the number of synchronously active hub neurons h_{n+1} is derived analogously: We discard those h_n neurons that have spiked together with the nth subnetwork because they are unlikely to spike again due to their relative refractoriness such that $N_{\rm h} - h_n$ hub neurons are available to spike. Replacing $N_{\rm g}$ by $N_{\rm h} - h_n$ in Eq. (4) and computing the Gaussian probability densities of the inputs yield the iterated map,

$$h_{n+1} = (N_{\rm h} - h_n)p^0(\tilde{\mu}_-)\frac{1}{2}\left(1 + {\rm Erf}\left[\frac{\Theta_{\rm d} - \tilde{\mu}_+}{\sqrt{2}\tilde{\sigma}_+}\right]\right), \tag{6}$$

where $\tilde{\mu}_+ = \epsilon_+ p_{\rm h}(h_n + g_n)$, $\tilde{\mu}_- = \epsilon_- p_{\rm h}(h_n + g_n)$, and $\tilde{\sigma}_+^2 = \epsilon_+^2 p_{\rm h}(1-p_{\rm h})(h_n + g_n)$.

The joint two-dimensional map (5) and (6) explicates how the hub neurons can enable robust propagation of synchrony [see Figs. 2(c) and 2(d)]: For a given number h_n of active hub neurons, the fixed points of Eq. (5) determine whether robust propagation of synchrony can be initiated in the chain of subnetworks. For networks without (active) hubs $h_n = 0$, there is only one fixed point $G_0 = 0$, and any initial synchronous pulse extinguishes after a small number of subnetworks. With increasing h_n, two additional fixed points G_1 (unstable) and G_2 (stable) appear via a tangent bifurcation at some $h_n = h^*$, and robust signal transmission is enabled for initial synchronous pulses $g_0 \geqslant G_1$ [cf. Fig. 2(c)]. For large numbers of active hubs, even small initial group sizes g_0 are sufficient to generate robust signal transmission across the chain of subnetworks.

Analogously, the fixed points of Eq. (6) determine whether a persistent hub echo for the propagating synchronous pulse establishes for a given hub connectivity $p_{\rm h}$ and group size g_n [cf. Fig. 2(d)]. For small $p_{\rm h}$ and g_n, there is only one fixed point $H_0 = 0$. With increasing $p_{\rm h}$ or g_n, two additional fixed points H_1 (unstable) and H_2 (stable) appear via a tangent bifurcation for some $p_{\rm h}^*$ and g^*. Thus, for sufficiently large hub connectivity $p_{\rm h} \geqslant p_{\rm h}^*$, a persistent echo for a propagating

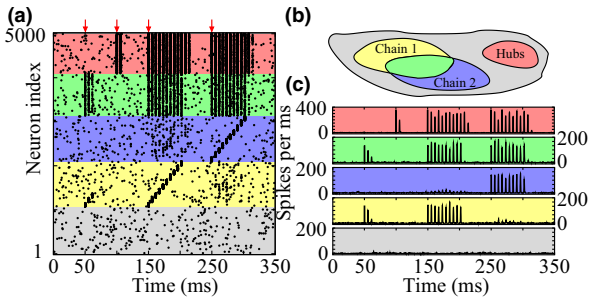

FIG. 3. (Color online) Hub neurons act as a generic signal amplifier and activate different signal routes. The figure shows simulation data for a sparse recurrent spiking neural network [the same network as in Fig. 1(b)] with two chains of subnetworks. (a) Raster plot of the network activity; the background colors indicate whether the neurons are members of one or both chains, hub neurons or remaining neurons, as visualized by (b). (c) Current activity (spikes per bin; bin size 1 ms) of the different neuron populations. If synchronous spiking is initiated either in the initial subnetwork of one chain ($t = 50$ ms) or in the hub neurons ($t = 100$ ms) only, synchronous activity extinguishes quickly. In contrast, if the initial subnetwork of one of the chains as well as the hub neurons are excited ($t = 150$ and 250 ms), robust propagation of synchrony establishes in that specific chain.

synchronous pulse of size g_n can be established; equivalently, for fixed connectivity p_h, sufficiently many synchronously active neurons in the subnetwork maintain a hub echo. The bifurcations resulting from the analytic mapping (5) and (6) approximately predict the numerically found region where robust signal transmission is possible (see the dashed line in Fig. 1 and Ref. [11]).

Having gained this mechanistic understanding, we now illustrate that hubs unspecifically but selectively activate synchrony propagation. Signal propagation becomes possible along any chain of subnetworks that structurally exists in the system if its initial group is excited. In particular, in systems with a second chain of subnetworks embedded, the mutual hub and nonhub feedback can amplify signal transmission along one chain without activating transmission in the other one (cf. Fig. 3).

To summarize, we have demonstrated that hubs may act as amplifiers that enable signal generation and transmission in recurrent networks. So far, hubs were thought to directly distribute various types of signals (e.g., actual information on the World Wide Web, certain infections in disease spreading, and people in travel networks) across a network. We now identified a complementary fundamentally different role of hubs in signal transmission: The hubs studied here do not communicate the specific signal themselves; instead, increased hub activity mirrors the presence of some localized signal in other network parts, and the hubs promote the transmission of any such signal across sequences of nonhub subnetworks.

This mechanism of hub-activated signal propagation essentially relies on: (a) the existence of some highly connected nodes and (b) some sharp thresholdlike processing of incoming inputs by single units (as, for instance, mediated by fast dendritic sodium spikes in neural circuits). Furthermore, the phenomenon is robust against changes in the network topology. As an explicit example, we show that it occurs in scale-free networks [1] where hubs naturally emerge due to the "fat tail" of the degree distribution (cf. Ref. [11] for an example). We, thus, expect that this type of signal transmission may well play a role in biological networks and may even be exploited in self-organized solutions of technical communication networks [20].

It has long been hypothesized that cortical neural networks transmit signals via propagating synchronous spiking activity across subnetworks connected in a feed-forward manner [14,16,18]. The results above now suggest that hubs might enable robust propagation of synchronous signals even in weak embedded feed-forward structures by echoing the synchronous signal propagating along them. In the absence of hubs (and due to the lack of a confining mechanism), the echo cannot contribute in this way as synchronous activity either dies out or spreads across the whole network and causes pathological activity [e.g., Ref. [18] and cf. also Fig. 1(a)]. To reveal the essential mechanisms underlying signal transmission, we disregarded "Dale's law" [21] (stating that each neuron either has only excitatory or has only inhibitory outgoing connections) and considered a simple bimodal degree distribution clearly splitting the system into hub and nonhub neurons. In additional simulations, we verified that the uncovered new type of signal transmission equally emerges in networks with neurons obeying Dale's law and exhibiting natural and broad degree distributions [11].

Interestingly, hubs have recently also been uncovered experimentally in the developing hippocampus [9]. As in the adult hippocampus, synchronized oscillatory activity abounds, and the structural feature of hub neurons might support the directed transmission of specific signals. Such hub-feedback support may provide one reason why hubs emerge in these systems in the first place, cf. also Ref. [22].

Specifically, hub feedback might also be involved in the replay of spike sequences during so-called sharp wave-ripple complexes observed in the hippocampus [23]. Here, during sleep, neurons are activated in the same order as they have been during an exploration phase, accompanied by strong network oscillations. Whereas, most neurons take part in only a few of the different replayed patterns, some are activated in a large fraction of events [24]. Our results suggest that the latter may be unspecific for certain memories and, rather, hub neurons generating a synchronous feedback signal to stabilize signal propagation along a previously learned feed-forward structure of specific neurons.

Finally, our analytical results (5) and (6) for the activity of the hubs and the signal-carrying units clearly demonstrate that the principle of mutual activation underlying the support of signal transmission may act in any network of sharply nonlinear (probabilistic) threshold units as characterizing, e.g., transmission of rate activities in networks of neural populations (McCullogh-Pitts model, e.g., Ref. [25]), (failure) cascades in social, supply, or communication networks (e.g., Ref. [26]), or signaling in gene and protein networks (threshold Boolean networks, e.g., Ref. [27]).

This work was supported by the BMBF (Grant No. 01GQ1005B) and the DFG (Grant No. TI 629/3-1).

[1] M. E. J. Newman, SIAM Rev. **45**, 167 (2003); *Networks, An Introduction* (Oxford University Press, Oxford, 2010).

[2] S. Bornholdt and H. Ebel, Phys. Rev. E **64**, 035104 (2001); H. Ebel, L. I. Mielsch, and S. Bornholdt, *ibid.* **66**, 035103(R) (2002).

[3] P. Kaluza, A. Kölzsch, M. T. Gastner, and B. Blasius, J. R. Soc., Interface **7**, 1093 (2010).

[4] M. Barthelemy, Phys. Rep. **499**, 1 (2011).

[5] F. Liljeros, C. R. Edling, L. A. Amaral, H. E. Stanley, and Y. Aberg, Nature (London) **411**, 907 (2001); S. Riley *et al.*, Science **300**, 1961 (2003); L. Hufnagel, D. Brockmann, and T. Geisel, Proc. Natl. Acad. Sci. USA **101**, 15124 (2004); S. Gonzáles-Bailón, J. Borge-Holthoefer, A. Rivero, and Y. Moreno, Sci. Rep. **1**, 197 (2011).

[6] C. Zhou, L. Zemanova, G. Zamora, C. C. Hilgetag, and J. Kurths, Phys. Rev. Lett. **97**, 238103 (2006); O. Sporns, C. J. Honey, and R. Kötter, PLoS One **2**, e1049 (2007); P. Hagmann *et al.*, PLoS Biol. **6**, e159 (2008); G. Zamora-López, C. Zhou, and J. Kurths, Front. Neuroinform. **4**, 1 (2010).

[7] J. G. White, E. Southgate, J. N. Thomson, and S. Brenner, Philos. Trans. R. Soc., B **314**, 1 (1986); D. H. Hall and R. L. Russell, J. Neurosci. **11**, 1 (1991); L. R. Varshney, B. L. Chen, E. Paniagua, D. H. Hall, and D. B. Chklovskii, PLoS Comput. Biol. **7**, e1001066 (2011).

[8] E. Z. Macosko *et al.*, Nature (London) **458**, 1171 (2009).

[9] P. Bonifazi *et al.*, Science **326**, 1419 (2009).

[10] S. Luccioli, E. Ben-Jacob, A. Barzilai, P. Bonifazi, and A. Torcini (unpublished).

[11] See Supplemental Material at http://link.aps.org/supplemental/10.1103/PhysRevE.89.030701 for further details.

[12] G. Ariav, A. Polsky, and J. Schiller, J. Neurosci. **23**, 7750 (2003); A. Polsky, B. W. Mel, and J. Schiller, Nat. Neurosci. **7**, 621 (2004); S. Gasparini, M. Migliore, and J. C. Magee, J. Neurosci. **24**, 11046 (2004); S. Gasparini and J. C. Magee, *ibid.* **26**, 2088 (2006).

[13] R. M. Memmesheimer, Proc. Natl. Acad. Sci. USA **107**, 11092 (2010).

[14] S. Jahnke, M. Timme, and R. M. Memmesheimer, Phys. Rev. X **2**, 041016 (2012); Front. Comput. Neurosci. **7**, 153 (2013).

[15] M. O. Gewaltig and M. Diesmann, Scholarpedia **2**, 1430 (2007).

[16] M. Abeles, *Corticonics: Neural Circuits of the Cerebral Cortex* (Cambridge University Press, Cambridge, UK, 1991); M. Diesmann, M. O. Gewaltig, and A. Aertsen, Nature (London) **402**, 529 (1999); T. Vogels and L. Abbott, J. Neurosci. **25**, 10786 (2005).

[17] C. V. Vreeswijk and H. Sompolinsky, Science **274**, 1724 (1996); Neural Comput. **10**, 1321 (1998); N. Brunel, J. Comput. Neurosci. **8**, 183 (2000).

[18] C. Mehring, U. Hehl, M. Kubo, M. Diesmann, and A. Aertsen, Biol. Cybern. **88**, 395 (2003); A. Kumar, S. Rotter, and A. Aertsen, J. Neurosci. **28**, 5268 (2008).

[19] C. Müller, H. Beck, D. Coulter, and S. Remy, Neuron **75**, 851 (2012).

[20] J. Klinglmayr, C. Kirst, C. Bettstetter, and M. Timme, New J. Phys. **14**, 073031 (2012).

[21] H. Dale, Proc. R. Soc. Med. **28**, 319 (1935); J. C. Eccles, P. Fatt, and K. Koketsu, J. Physiol. **126**, 524 (1954).

[22] L. Tattini, S. Olmi, and A. Torcini, Chaos **22**, 023133 (2012).

[23] M. A. Wilson and B. L. McNaughton, Science **265**, 676 (1994); W. E. Skaggs and B. L. McNaughton, *ibid.* **271**, 1870 (1996); Z. Nádasdy, H. Hirase, A. Czurkó, J. Csicsvari, and G. Buzsáki, J. Neurosci. **19**, 9497 (1999); A. K. Lee and M. A. Wilson, Neuron **36**, 1183 (2002).

[24] A. Ylinen, A. Bragin, Z. Nádasdy, G. Jandó, I. Szabó, A. Sik, and G. Buzsáki, J. Neurosci. **15**, 30 (1995).

[25] T. Nowotny and R. Huerta, Biol. Cybern. **89**, 237 (2003); N. A. Cayco-Gajic and E. Shea-Brown, Neural Comput. **25**, 1768 (2013).

[26] D. Watts, Proc. Natl. Acad. Sci. USA **99**, 5766 (2002); J. Lorenz, S. Battiston, and F. Schweitzer, Eur. Phys. J. B **71**, 441 (2009).

[27] S. Bornholdt, J. R. Soc., Interface **5**, S85 (2008).

5.1. Supplemental Material

This supplemental material recapitulates further details on the neuron model and single neuron parameters (Section 5.1.1 and 5.1.2) otherwise available in existing literature, it provides additional simulation results for the abstracted threshold model (Section 5.1.3) and bifurcation diagrams complementing the ones of the main article (Section 5.1.4). Further, we demonstrate that hub-activated signal propagation is also found in networks with topologies more natural than the idealized bimodal setting (Section 5.1.5).

5.1.1. Additional information on the neuron models

In the explicit numerical computations supporting and illustrating our theoretical arguments, we employed networks of spiking neurons, more specifically, standard conductance-based leaky integrate-and-fire neurons (e.g., Dayan and Abbott, 2001) endowed with non-additive couplings (cf. also Memmesheimer, 2010; Jahnke et al., 2012)). Here we briefly recapitulate the details of the neuron model.

The state of neuron i is described by its membrane potential V_i and the temporal dynamics are governed by

$$C_i \frac{dV_i(t)}{dt} = g_i^{\mathrm{L}} \left[V_i^{\mathrm{eq}} - V_i(t)\right] + I_i^{\mathrm{ex}}(t) + I_i^{\mathrm{in}}(t), \tag{5.1}$$

where C_i is the membrane capacity, g_i^{L} is the leak conductance and V_i^{eq} is the equilibrium potential. $I_i^{\mathrm{ex}}(t)$ and $I_i^{\mathrm{in}}(t)$ are currents arising from excitatory and inhibitory inputs, respectively. Whenever the membrane potential $V_i(t)$ reaches the spiking threshold V_i^{Θ} at some $t = t^{*-}$, a spike is sent to the post-synaptic neurons j, where it arrives after a delay time τ_{ji}. The sending neuron is reset to $V_i(t^*) = V_i^{\mathrm{reset}}$ and the neuron is refractory for a time period t_i^{ref}. The effect of the synaptic inputs on the postsynaptic neurons is modeled by transient conductance changes. The excitatory and inhibitory input currents to neuron i arising from synaptic inputs from other neurons of the network are given by

$$I_i^{\kappa}(t) \;=\; \sum_{n,j} \epsilon_{ij}^{\kappa} f^{\kappa}\left(t - t_{jn}^{\mathrm{f}} - \tau_{ij}\right) \left[E^{\kappa} - V_i(t)\right], \tag{5.2}$$

where $\kappa \in \{\mathrm{ex}, \mathrm{in}\}$, E^{ex} (E^{in}) denotes the excitatory (inhibitory) reversal potentials, $\epsilon_{ij}^{\mathrm{ex}}$ ($\epsilon_{ij}^{\mathrm{in}}$) the excitatory (inhibitory) coupling strength from neuron j to neuron i, t_{jn}^{f} the nth spike time of neuron j and $f^{\mathrm{ex}}(t)$ ($f^{\mathrm{in}}(t)$) specify the time course of the synaptic conductance given by the difference of two exponentials,

$$f^{\kappa}(t) = (Z^{\kappa})^{-1} \left(e^{-\frac{t}{\tau^{\kappa,1}}} - e^{-\frac{t}{\tau^{\kappa,2}}}\right) \Theta(t). \tag{5.3}$$

In Equation (5.3), $\Theta(\cdot)$ denotes the Heaviside step-function, $\tau^{\kappa,1} > \tau^{\kappa,2}$ are the time constants dominating the rise and decay of the induced conductance change, and

$$Z^{\kappa} = \left(\frac{\tau^{\kappa,2}}{\tau^{\kappa,1}}\right)^{\frac{\tau^{\kappa,2}}{\tau^{\kappa,1}-\tau^{\kappa,2}}} - \left(\frac{\tau^{\kappa,2}}{\tau^{\kappa,1}}\right)^{\frac{\tau^{\kappa,1}}{\tau^{\kappa,1}-\tau^{\kappa,2}}} \tag{5.4}$$

is the normalization factor such that the peak conductance caused by a single input of strength $\epsilon = 1$ equals $\max_t \{f^\kappa(t)\} = 1$.

In addition to linear summation of inputs, we consider nonlinear amplification of synchronous inputs as mediated by fast dendritic spikes in biological circuits. We augment the neurons with a nonlinear dendrite. Inputs that are considered to arrive at a linear dendrite are processed as described above. Inputs on a nonlinear dendrite also cause a conductance change as described above, but additional depolarizations of the membrane potential mimicking the effect of a dendritic spike can be generated. If the total excitatory input to a nonlinear dendrite within a time interval ΔT^s exceeds a certain threshold Θ_d, a current pulse is initiated, which takes effect on the membrane potential after a delay time t^ds. We model the current pulse in a phenomenological approach such that the depolarization caused by a supra-threshold input, $\epsilon \geq \Theta_\mathrm{d}$, resembles the characteristics and time course of the depolarization observed in single neuron experiments (e.g., Ariav et al., 2003). More precisely, the current pulse is described by the sum of three exponential functions,

$$I_\mathrm{ds} = \Theta\left(t - t^\mathrm{ds}\right)\left[-A_1 e^{-\frac{t-t^\mathrm{ds}}{\tau^{\mathrm{ds},1}}} + A_2 e^{-\frac{t-t^\mathrm{ds}}{\tau^{\mathrm{ds},2}}} - A_3 e^{-\frac{t-t^\mathrm{ds}}{\tau^{\mathrm{ds},3}}}\right] \tag{5.5}$$

with positive prefactors A_1, A_2, A_3 and decay time constants $\tau^{\mathrm{ds},1}$, $\tau^{\mathrm{ds},2}$ and $\tau^{\mathrm{ds},3}$. After initiation of such a current pulse the (nonlinear) dendrite becomes refractory for a time period $t^{\mathrm{ref,ds}}$ and does not transmit spikes within the refractory time period.

All simulations were performed using NEST (Gewaltig and Diesmann, 2007), a powerful simulator for spiking neural networks (available at http://ww.nest-intiative.org), augmented by a self-written model class which implements the model described above.

5.1.2. Additional details to Figure 1

In Figure 1 of the main manuscript we demonstrate that hubs can activate signal transmission in spiking neural networks. As stated in the manuscript, the figure displays results from networks of $N = 5000$ neurons, where a sub-population of $N_\mathrm{h} = 900$ neurons is assumed to be hubs. The networks are sparse, neurons are randomly connected with probability $p_- = p_+ = p = 0.05$ and $p_\mathrm{h} = p$ (sub-figure A, i.e., no hubs are present) or $p_\mathrm{h} = 0.12 > p$ (sub-figure B), respectively; single connections have identical coupling strength $\epsilon_{ij}^\mathrm{ex} = \epsilon_+ = 0.2\mathrm{nS}$ (if connection is present) and $\epsilon_{ij}^\mathrm{in} = \epsilon_- = 0.55\mathrm{nS}$ (if connection is present). Feed-forward structures are brought out by randomly selecting $m = 10$ non-overlapping subnetworks of size $N_\mathrm{g} = 200$ and increasing the excitatory coupling strength between neurons of successive subnetworks to $\epsilon_\mathrm{sub} = 1.1\mathrm{nS}$. Additional to inputs from the recurrent network each neuron receives (external) excitatory and inhibitory Poissonian spike trains with rate $\nu^\mathrm{in} = \nu^\mathrm{ex} = 2.4\mathrm{kHz}$, where single inputs have strengths $\epsilon^\mathrm{ex} = 1\mathrm{nS}$ and $\epsilon^\mathrm{in} = 2.75\mathrm{nS}$, respectively. With this choice of parameters the network is in the so-called balanced state (v. Vreeswijk and Sompolinsky, 1996, 1998; Brunel, 2000) and single neurons fire asynchronously with low rate. For each neuron, the recurrent connections are assumed to project on one non-linear dendrite, whereas the external inputs project on linear dendrites, i.e., they do not contribute to the generation of dendritic spikes.

The neurons have identical parameters, $C = 400\text{pF}$, $V^{\text{eq}} = -55\text{mV}$, $E^{\text{ex}} = 0\text{mV}$, $E^{\text{in}} = -75\text{mV}$, $V^{\text{reset}} = -65\text{mV}$, $V^{\Theta} = -50\text{mV}$, $g^{\text{L}} = 25\text{nS}$, $t^{\text{ref}} = 3\text{ms}$, $\tau^{\text{ex},1} = 2.5\text{ms}$, $\tau^{\text{ex},2} = 0.5\text{ms}$, $\tau^{\text{in},1} = 2.5\text{ms}$ and $\tau^{\text{in},2} = 0.5\text{ms}$. The parameters of the dendritic spike current are $A_1 = 55\text{nA}$, $A_2 = 64\text{nA}$, $A_3 = 9\text{nA}$, $\tau^{\text{ds},1} = 0.2\text{ms}$, $\tau^{\text{ds},2} = 0.3\text{ms}$, $\tau^{\text{ds},3} = 0.7\text{ms}$, $\Delta T^{\text{s}} = 2\text{ms}$, $\Theta_{\text{d}} = 8.65\text{nS}$, $t^{\text{ds}} = 2.7\text{ms}$ and $t^{\text{ref,ds}} = 3.5\text{ms}$.

After an equilibration time $t^{\text{init}} = 200\text{ms}$, a randomly selected subset of g_0 neurons of the initial subnetwork as well as a subset of r_0 neurons from the remaining network are excited to spike synchronously. We track the spreading of synchronous activity by counting the number of spiking neurons in the time-interval $\left[t^{\text{init}} + \Delta T_1 - \Delta T^{\text{w}}/2, t^{\text{init}} + \Delta T_1 + \Delta T^{\text{w}}/2\right]$ with $\Delta T^{\text{w}} = 3\text{ms}$ and $\Delta T_1 \in [1\text{ms}, 7\text{ms}]$; the time ΔT_1 (estimated in steps of size 0.1ms) which maximizes this number is assumed to be the temporal difference between the initial and first evoked synchronous pulse. By repeating this procedure we obtain the time-intervals ΔT_n for $n \in \{1, m-1\}$ between successive synchronous pulses and denote the number of spiking neurons of the nth subnetwork ($n = 1$ is referring to the first subnetwork following the initial one) within $\left[t^{\text{init}} + \Delta T_n - \Delta T^{\text{w}}/2, t^{\text{init}} + \Delta T_n + \Delta T^{\text{w}}/2\right]$ by g_n and the number of spiking neurons in the remaining network by r_n. If the total activity, i.e., $g_n + r_n$, exceeds a threshold $\Theta^{\text{path}} = 900$ (we verified that different threshold values do not change the result) for some n the activity is classified as "pathological"; non-pathological trials are classified as "propagating" if $g_{m-1} \geq 100$ (i.e., there is sufficient synchronous activity detected in the final subnetwork) and as "non-propagating" otherwise. For each pair (g_0, r_0) we repeated the experiment $n^{\text{rep}} = 300$ times, and mark the initial conditions in Figure 1 in *red*, if in at least 50% of the trials the activity is pathological, in *green*, if in at least 50% of the trials the activity is non-pathological and in 50% of the non-pathological trials the activity is propagating, and in *yellow* otherwise. The arrows depicted in Figure 1 are sequences of (g_n, r_n). To indicate a dominating direction of flow, they are averaged over all trials that are pathological, propagating or non-propagating, respectively, depending on the classified type of the corresponding initial conditions.

5.1.3. Deriving an iterated map for the remaining neurons

In the main article we demonstrated that hub neurons can enable robust signal propagation. We considered the number of simultaneously active hub neurons, h_n, and the number of synchronously active neurons in a given layer of a sequence of (non-hub) subnetworks, g_n. The co-action of these two populations is sufficient to understand the emergence of echo-promoted propagation of synchrony (cf. Figure 2).

To reproduce the full dynamics, in particular the emergence of pathological activity states (cf. Figure 1; red area), we extend the analysis to the subset of neurons which are neither members of the currently active subnetwork or hub neurons. This extension is analogous to the derivation of the iterated maps Equations (5,6). For the reader's convenience we briefly present the extension below.

We denote the number of remaining neurons by

$$N_{\text{x}} = N - N_{\text{h}} - N_{\text{g}}, \tag{5.6}$$

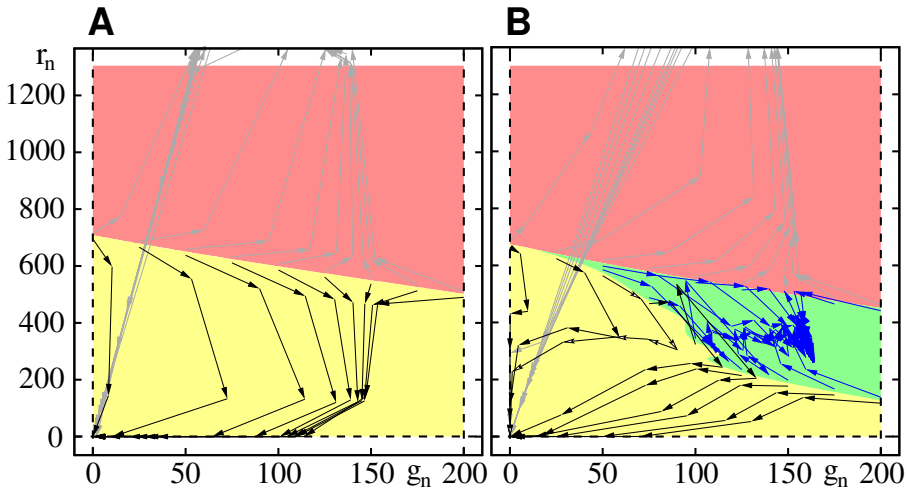

Figure 5.1: Same experiment as shown in Figure 1 but with threshold units as defined by Equation (1). The trajectories indicating the temporal development of synchronous activity and the areas marking the type of the initial conditions are derived from the iterated maps (5.23) and (5.24). Model parameters such as coupling strengths and connection probability, are the same as in the original figure.

where N is the total number of neurons, N_{h} the number of hub neurons and N_{g} the size of the subnetworks as specified in the main article. We note that in this section we consider the subset of neurons which are neither hubs nor members of the currently active subnetwork as the "remaining neurons" and therefore use a slightly different notation than in the main article (where all neurons which do not belong to the currently active subnetwork were denoted as the remaining set of neurons).

The average excitatory coupling strength of connections between the remaining neurons is slightly larger than the average coupling strength ϵ_+, because this subset contains also neurons which are part of some other (currently non-active) subnetwork and therefore some of the connections are strengthened to ϵ_{sub}. The fraction of strengthened connections,

$$p^{\mathrm{frac}} = \frac{pN_{\mathrm{g}}^2\,(m-1)}{pN_{\mathrm{x}}^2}, \tag{5.7}$$

is given by the quotient of the number of enhanced connections and the total number of connections and thus the average (excitatory) coupling between two remaining neurons is

$$\epsilon_{\mathrm{x}} = p^{\mathrm{frac}}\epsilon_{\mathrm{sub}} + \left(1 - p^{\mathrm{frac}}\right)\epsilon_+. \tag{5.8}$$

As before, we denote the number of simultaneously active neurons in the nth subnetwork by g_n and the number of synchronously active hub neurons by h_n. The number of active neurons out of the remaining neurons is denoted by x_n. In the $(n+1)$th time step, the number of synchronously active neurons of each population is given by the product of the number of available neurons of that population (pool) and the spiking probability of a single neuron out of the particular pool

due to the input from the active neurons in the nth time step. The number of available neurons is

$$N_{\mathrm{h}} - h_n \text{ for the hub neurons,} \tag{5.9}$$

$$N_x - x_n \text{ for the remaining neurons and} \tag{5.10}$$

$$N_{\mathrm{g}} - \frac{x_n}{N_{\mathrm{x}}} N_{\mathrm{g}} \text{ for members of the next subnetwork.} \tag{5.11}$$

We note that by considering the remaining neurons, in Equation (5.11) we were able to estimate the fraction, x_n/N_x, of refractory neurons in the $(n+1)$th subnetwork. As before, the spiking probability of the single neurons of each sub-population is derived by calculating the probability density function of the total excitatory and inhibitory input, which can be approximated by Gaussian distributions. The mean inputs and the standard deviations are (cf. also Equations (2,3))

$$\mu_+^{\mathrm{h}} = \epsilon_+ p_{\mathrm{h}} \left(h_n + g_n + x_n\right) \tag{5.12}$$

$$\mu_-^{\mathrm{h}} = \epsilon_- p_{\mathrm{h}} \left(h_n + g_n + x_n\right) \tag{5.13}$$

$$\sigma_+^{\mathrm{h}} = \sqrt{\epsilon_+^2 p_{\mathrm{h}} \left(1 - p_{\mathrm{h}}\right) \left(h_n + g_n + x_n\right)} \tag{5.14}$$

$$\mu_+^{\mathrm{x}} = \epsilon_+ p \left(h_n + g_n\right) + \epsilon_{\mathrm{x}} p x_n \tag{5.15}$$

$$\mu_-^{\mathrm{x}} = \epsilon_- p \left(h_n + g_n + x_n\right) \tag{5.16}$$

$$\sigma_+^{\mathrm{x}} = \sqrt{\epsilon_+^2 p \left(1 - p\right) \left(h_n + g_n\right) + \epsilon_{\mathrm{x}}^2 p \left(1 - p\right) x_n} \tag{5.17}$$

$$\mu_+^{\mathrm{g}} = \epsilon_+ p \left(h_n + x_n\right) + \epsilon_{\mathrm{sub}} p g_n \tag{5.18}$$

$$\mu_-^{\mathrm{g}} = \epsilon_- p \left(h_n + g_n + x_n\right) \tag{5.19}$$

$$\sigma_+^{\mathrm{g}} = \sqrt{\epsilon_+^2 p \left(1 - p\right) \left(h_n + x_n\right) + \epsilon_{\mathrm{sub}}^2 p \left(1 - p\right) g_n} \tag{5.20}$$

which yield the iterated maps

$$h_{n+1} = \left(N_{\mathrm{h}} - h_n\right) \cdot \frac{p^0\left(\mu_-^{\mathrm{h}}\right)}{2} \left(1 + \mathrm{Erf}\left[\frac{\Theta_{\mathrm{d}} - \mu_+^{\mathrm{h}}}{\sqrt{2}\sigma_+^{\mathrm{h}}}\right]\right), \tag{5.21}$$

$$x_{n+1} = \left(N_x - x_n\right) \cdot \frac{p^0\left(\mu_-^{\mathrm{x}}\right)}{2} \left(1 + \mathrm{Erf}\left[\frac{\Theta_{\mathrm{d}} - \mu_+^{\mathrm{x}}}{\sqrt{2}\sigma_+^{\mathrm{x}}}\right]\right), \tag{5.22}$$

$$g_{n+1} = \left(N_{\mathrm{g}} - \frac{x_n}{N_{\mathrm{x}}} N_{\mathrm{g}}\right) \cdot \frac{p^0\left(\mu_-^{\mathrm{g}}\right)}{2} \left(1 + \mathrm{Erf}\left[\frac{\Theta_{\mathrm{d}} - \mu_+^{\mathrm{g}}}{\sqrt{2}\sigma_+^{\mathrm{g}}}\right]\right). \tag{5.23}$$

The iterated maps (5.21-5.23) are a good deterministic approximation for the full dynamics of the system: Figure 1 shows the number of *all* remaining neurons which are synchronously active,

$$r_n = h_n + x_n, \tag{5.24}$$

versus the number of synchronously active neurons in the nth subnetwork. The trajectories derived from the maps (5.23) and (5.24) are displayed in Figure 5.1 and agree well with direct numerical simulations as shown in Figure 1.

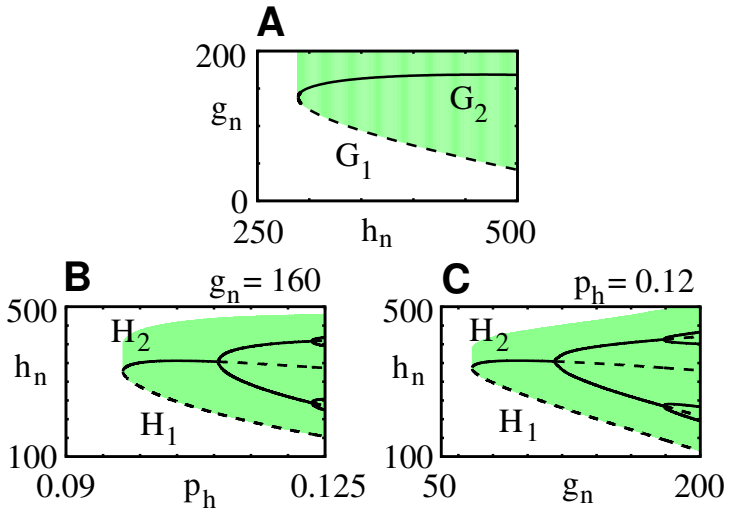

Figure 5.2: Bifurcation diagrams derived from the iterated maps depicted in Figure 1C,D. The dashed lines depict unstable fixed points/periodic orbits (F/POs), the solid lines stable F/POs, and the green areas the basins of attraction of the stable F/POs. (A) Bifurcation diagram for the number of active neurons g_n in the chain of subnetworks as a function of the number of active hub neurons h_n. (B,C) Bifurcation diagram for the number of active hub neurons h_n as a function of (B) the hub-connectivity p_h and (C) the number of synchronously active neurons in the chain of subnetworks g_n. For further explanation see Section 5.1.4.

In the propagating state, we typically have $x_n \ll h_n, g_n$, such that the approximation $x_n = 0$ made within the main article is justified.

5.1.4. Bifurcation diagrams for the iterated maps (5) and (6)

In the main text we derived iterated maps for g_n and h_n, cf. Equations (5,6), and discussed the transition from non-propagating to propagating regime, cf. 2. For completeness, in Figure 5.2, we provide the bifurcation diagrams derived from the iterated maps (5) and (6).

As discussed in the main text, the number of synchronously active neurons g_n undergoes a tangent bifurcation at some $h_n = h^*$ and two fixed points G_1 (unstable) and G_2 (stable) emerge (cf. Figure 5.2A and also Figure 2C). The bifurcation point h^* defines the minimal size of the echo to a propagating synchronous pulse (i.e. the minimal number of synchronously active hub neurons) which is required to enable robust propagation of synchrony.

Likewise, the fixed points of Equation (6) determine whether a persistent echo to propagating synchronous pulses can be established. Starting with only one stable fixed point $H_0 = 0$, with increasing connectivity p_h and/or increasing g_n two additional fixed points H_1 (unstable) and H_2 (stable) appear by a tangent bifurcation for some p_h^* and g^* (cf. Figure 5.2B,C and see also Figure 2D). Interestingly, upon further increasing p_h and/or g_n the second fixed point H_2 becomes unstable by a period doubling bifurcation and a stable orbit of period two emerges, followed by further period doubling bifurcations for larger parameter values (cf. Figure 5.2B,C).

For fixed g_n, if the connectivity towards the hub neurons is sufficiently large, i.e. $p_\mathrm{h} \geq p_\mathrm{h}^*$, a persistent echo to the propagating synchronous pulse can be established. If the connectivity p_h is fixed, at least g^* synchronously active neurons in the chain of subnetworks are required to maintain an echo within the hub neuron population. The approximate size of the echo is either given by the value of the stable fixed point H_2 or by the stable periodic orbit around the unstable fixed point H_2.

5.1.5. Generalizations regarding inhibitory and excitatory neurons as well as network topology

In this section we discuss generalizations of the network topology. We first show that hub-activated propagation of synchrony can be found in networks respecting "Dale's Law" and as a second generalization, we consider scale-free networks, where hubs emerge due to the "fat-tail" of the degree distribution.

Networks respecting Dale's Law

"Dale's Law" (Dale, 1935; Eccles et al., 1954) states that a neuron releases the same set of neuro-transmitters at all its post synaptic terminals. In particular, its commonly assumed that cortical neurons can be classified as either excitatory or inhibitory depending on their main effect on postsynaptic cells.

Experimental data (Haider et al., 2006; Okun and Lampl, 2008; Atallah and Scanziani, 2009) suggests that there is a detailed balance between excitatory and inhibitory input to single neurons in cortical networks during spontaneous and sensory-evoked activity. We consider such balanced state networks (v. Vreeswijk and Sompolinsky, 1996, 1998; Brunel, 2000), where excitatory and inhibitory inputs are of the same order of magnitude and cancel each other on average. Thus, in the ground state spikes are generated by fluctuations of the input and result in irregular asynchronous spiking activity.

A balance between excitatory and inhibitory inputs can be established in networks obeying or disregarding "Dale's Law", thus we expect that the mechanism of hub-activated signal propagation is found in both types of networks. In the previous sections we have considered "hybrid networks" (disregarding Dale's Law). It has been shown that such networks have reduced correlations and fluctuations in the network activity (Kriener et al., 2008) and therefore a reduced tendency to develop (pathological) large scale synchronization. This may raise the question whether the observed phenomenon of hub-activated propagation of synchrony is indeed also found in networks respecting Dale's law. In the following we show that it is the case.

We construct a network similar to the network used for generating the data in Figure 1 (cf. also Section 5.1.2): We take the base population of $N = 5000$ neurons as excitatory and augment it by a population of $N/4 = 1250$ inhibitory neurons. Connections between any pair of neurons are realized with probability $p = 0.05$. In contrast to the simplified model, all connections originating from excitatory neurons are excitatory with strength $\epsilon^{\mathrm{exex}} = 0.2\mathrm{nS}$, if targeting another

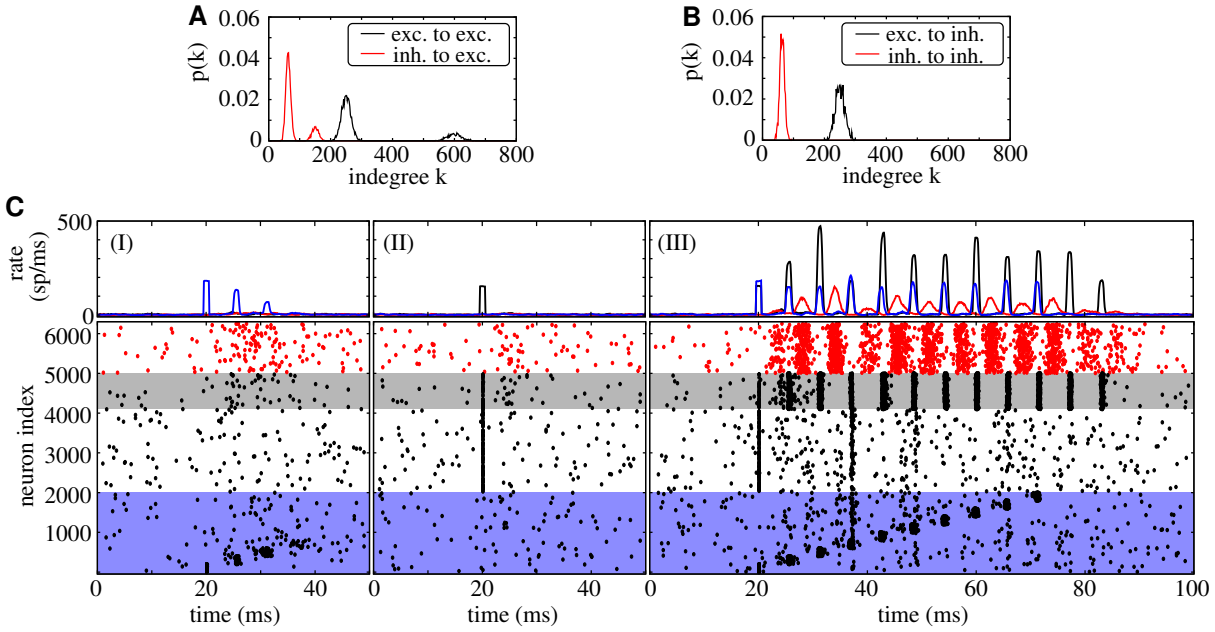

Figure 5.3: Hub-activated propagation of synchrony in networks respecting Dale's Law. In-degree distribution for (A) excitatory neurons and (B) inhibitory neurons. The bimodal distributions in (A) reflect the fact that the network ($N = 5000$ excitatory and $N/4 = 1250$ inhibitory neurons) contains a subset of $N_{\mathrm{h}} = 900$ highly connected excitatory nodes ($p_{\mathrm{h}} = 0.12$). Panel (C) depicts the spiking dynamics of the network after an initial stimulation of (I) the initial subnetwork ($g_0 = 180$) only, (II) a fraction of the remaining excitatory population ($r_0 = 150$) only, and (III) simultaneous stimulation of the initial network and a fraction of the remaining excitatory poulation. In the main panels the dots indicate spikes of excitatory neurons (black) and inhibitory neurons (red), respectively. The colored area highlights the population of hubs (gray) and the fraction of neurons that are members of the chain of subnetworks (blue). The upper panels show the current spiking rate of the different subpopulations (red: inhibitory neurons, blue: excitatory neurons which are members of the chain of subnetworks, black: remaining excitatory neurons). A synchronous pulse propagates only if the initial sub-network as well as a fraction of the network remainder is initially stimulated (III). The propagation is maintained by mutual re-activation of hubs and chain neurons (cf. also Figure 1 and Figure 3 in the main article).

excitatory cell, and strength $\epsilon^{\text{inex}} = 0.38\text{nS}$, if targeting an inhibitory neuron. Connections starting from inhibitory neurons have strength $\epsilon^{\text{exin}} = 1.32\text{nS}$ and $\epsilon^{\text{inin}} = 1.1\text{nS}$ for excitatory or inhibitory target cells, respectively, and are exclusively inhibitory. A subset of the excitatory neurons, $N_h = 900$, is considered to have a higher than average probability, $p_{\text{h}} = 0.12$, to receive inputs from other neurons.

The conduction delays between the neurons are

$$\tau^{\text{exex}} = 2.0\text{ms},\ \tau^{\text{inex}} = 1.0\text{ms}, \tag{5.25}$$

$$\tau^{\text{exin}} = 1.2\text{ms and } \tau^{\text{inin}} = 1.2\text{ms}, \tag{5.26}$$

where τ^{XY} with $X, Y \in \{\text{ex,in}\}$ refers to the conduction delays from neurons of type Y to neurons of type X. The conductions delays for connections to and from the inhbitory neurons (compared to recurrent excitatory connections), are reduced to account for the experimentally observed fast response properties of interneurons (Geiger et al., 1997).

Fast dendritic sodium spikes have been prominently found for excitatory (pyramidal) neurons (Ariav et al., 2003), thus we only equip excitatory neurons with non-linear dendrites. All other neuron parameters as well as the external random inputs stay unchanged (cf. Section 5.1.2). The chain of subnetworks is constructed from the set of (non-hub) excitatory neurons as before and also its parameters are unchanged ($m = 10$, $N_{\text{g}} = 200$ and $\epsilon_{\text{sub}} = 1.1\text{nS}$).

Figure 5.3 shows that this network exhibits the same behavior as the original network. Whereas the activity quickly decays to the level of spontaneous activity after synchronous stimulation of the initial subnetwork only, a simultaneous co-stimulation of a random subset of the remaining network results in persistent propagation of synchrony. As before, the propagating pulse activates the hub neurons and the hub neurons at the same time activate the chain of subnetworks. During propagation of synchrony a large fraction of inhibitory neurons is active and provides stabilizing inhibitory feed-back to the excitatory neurons.

Scale-free networks

So far we assumed that hubs are a distinct sub-population of the excitatory neurons, i.e., we assumed a bimodal degree distribution (cf. Figure 5.3A,B for an illustration). However, the existence of hubs is an intrinsic feature of networks with "fat-tailed" degree distribution, in particular of the prominent class of scale-free networks (Newman, 2003, 2010). These networks, where the degree distribution obeys a power-law, are found in a plethora of network dynamical systems, ranging from social, information or technology to biological networks (Newman, 2003, 2010). In particular, also the link distribution of neurons in some cortical networks, e.g., in developing hippocampus, has been shown to be scale-free (Bonifazi et al., 2009).

Given that the main prerequisite for its underlying mechanism is the existence of highly connected nodes, we expect that hub-activated propagation of synchrony is also found in such scale-free networks. To test this hypothesis, we modify the network topology by drawing the number of incoming excitatory connections to excitatory neurons from a truncated power-law

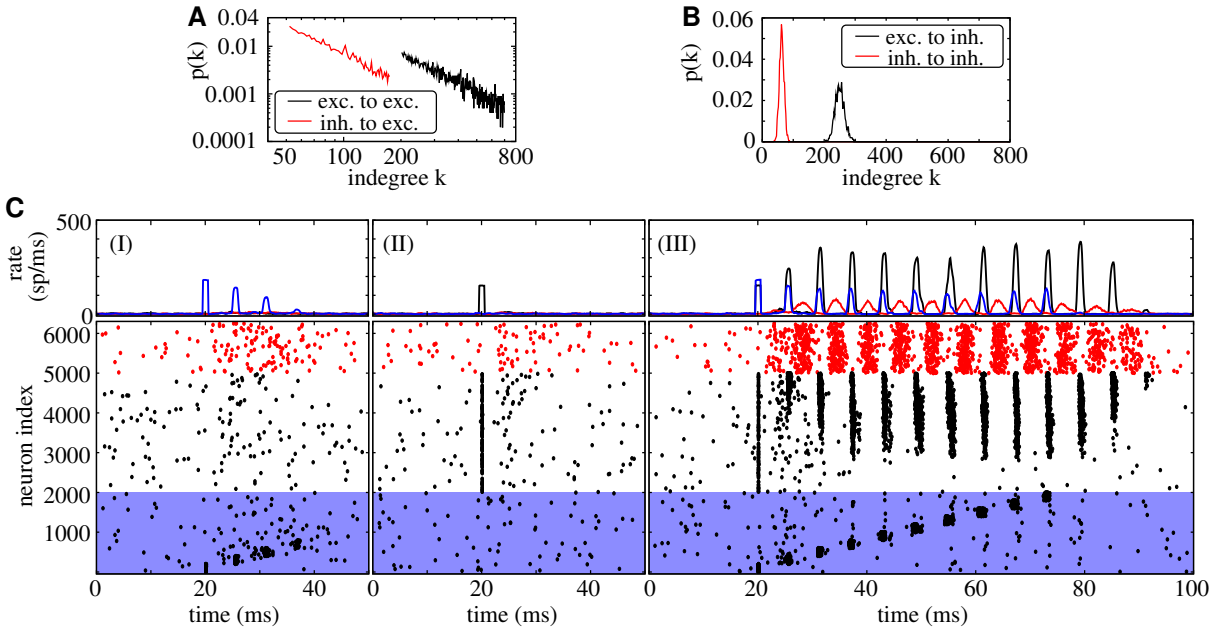

Figure 5.4: Hub-activated propagation of synchrony in scale-free networks. The network is almost identical to the network employed in Figure 5.3, but instead of assuming a distinct population of hubs, the indegree distribution of the excitatory neurons obeys a power-law (exponent $\gamma = 2$) truncated at $k_{\min} = 200$ and $k_{\max} = 700$; cf. panel (A). The indegree distribution of the inhibitory neurons remains unchanged; cf. panel (B). The chain of subnetworks is constructed from the subset of neurons with a low indegree $k \leq 350$. (C) Network activity for the same stimulation protocol as in Figure 5.3C. In the main panels, the blue area indicates the subset of neurons which are members of the chain of subnetworks, the remaining neurons are sorted by their indegree k from down to top. As before, only a simultaneous stimulation of the initial subnetwork and a fraction of the remianing excitatory population results in propagation of synchrony (III).

distribution, i.e., the probability that a single neuron receives k incoming excitatory connections is given by

$$p(k) = \begin{cases} A_{\text{norm}} \cdot k^{-\gamma} & k_{\min} \leq k_{\max} \\ 0 & \text{otherwise,} \end{cases} \tag{5.27}$$

with the normalization factor

$$A_{\text{norm}} := \left(\sum_{k=k_{\min}}^{k_{\max}} k^{-\gamma} \right)^{-1} \tag{5.28}$$

and $k_{\min}$ ($k_{\max}$) denoting the minimal (maximal) indegree. To keep the network balanced, for each neuron the number of incoming inhibitory inputs is assumed to be proportional to the number of excitatory inputs with a proportionality factor λ which equals the ratio of the sizes of the inhibitory and excitatory neuron populations, $\lambda = 1/4$. An example of the indegree distributions is shown in Figure 5.4A. The network setup in Figure 5.4 is almost identical to the setup in Figure 5.3. However, besides the modified degree distribution, to avoid pathological activity we enlarged the weights of single connections between inhibitory and excitatory neurons to $\epsilon^{\text{exin}} = 2.2\text{nS}$. All other network parameters are left unchanged. To keep the network dynamics comparable to the dynamics of the network with bimodal degree distribution, we construct the chain of subnetworks from the neurons with low or moderate indegree (i.e., we draw the subnetworks from the subset of neurons with $k \leq 350$).

The network with scale-free degree distribution as described above exhibits the same dynamics as the network with bimodal degree distribution (cf. Figure 5.3C and Figure 5.4C). A successful propagation of synchrony can be established only, if the initial subnetwork and a fraction of the network remainder are initially stimulated. This propagation is maintained by the mutual activation of neurons with a large number of incoming connections and the neurons propagating the synchronous signal.

Chapter 6

Oscillation-induced signal transmission and gating in neural circuits

Citation

Jahnke, S., Memmesheimer, R.-M. and Timme, M. (2014), Oscillation-induced signal transmission and gating in neural circuits. ©2014 Jahnke, Memmesheimer and Timme.

This chapter is the original submitted version of the article:
Jahnke, S., Memmesheimer, R.-M. and Timme, M. (2014), Oscillation-Induced Signal Transmission and Gating in Neural Circuits, *PLoS Comput. Biol.*, **10**, e1003940,
DOI:10.1371/journal.pcbi.1003940.

Original contribution

Conception and design of the study together with R.-M. Memmesheimer and M. Timme. I performed the analytical calculations and numerical simulations. For the simulations I implementated neuron models within the NEST simulation environment (www.nest-initiative.org). I analyzed the data and prepared all figures. I wrote main parts of the manuscript supported by R.-M. Memmesheimer and M. Timme.

Göttingen, 31.03.2014
Place, Date

Sven Jahnke

Abstract

Reliable signal transmission constitutes a key requirement for neural circuit function. The propagation of synchronous pulse packets through recurrent circuits is hypothesized to be one robust form of signal transmission and has been extensively studied in computational and theoretical works. Yet, although external or internally generated oscillations are ubiquitous across neural systems, their influence on signal propagation remains partly unclear. Here we systematically investigate the impact of oscillations on propagating synchrony. We find that for standard, additive couplings and a net excitatory effect of oscillations, robust propagation of synchrony is enabled in less prominent feed-forward structures than in systems without oscillations. In the presence of non-additive coupling (as mediated by fast dendritic spikes), even balanced oscillatory inputs may enable robust propagation. Here, emerging resonances create complex locking patterns between oscillations and spike synchrony. Interestingly, these resonances make the circuits capable of selecting specific pathways for signal transmission. Oscillations may thus promote reliable transmission and, in co-action with dendritic nonlinearities, provide a mechanism for information processing by selectively gating and routing of signals.

6.1. Introduction

The ground state of cortical networks is characterized by irregular and asynchronous spiking activity (Softky and Koch, 1993; v. Vreeswijk and Sompolinsky, 1996, 1998; Brunel, 2000) and its dynamics are highly sensitive to perturbations, e.g., missing or additional spikes (v. Vreeswijk and Sompolinsky, 1996, 1998; Denker et al., 2004; Jahnke et al., 2009; London et al., 2010; Monteforte and Wolf, 2012). Yet, reliable transmission of information in the presence of such perturbations is assumed to be essential for neural computation. A common hypothesis states that such transmission might be achieved by propagating signals along subnetworks (layers) connected in a feed-forward manner. Indeed, propagation of synchronous and rate signals in feed-forward networks (FFNs) has been demonstrated *in vitro* (e.g., Reyes, 2003; Feinerman et al., 2005; Feinerman and Moses, 2006) and recent experiments suggest that, e.g., the generation of bird-songs relies on activity propagation in feed-forward structures (Long et al., 2010). Moreover, sequential replay observed in hippocampal and neocortical areas also suggest such an underlying feed-forward structure (August and Levy, 1999; Nadasdy et al., 1999; Lee and Wilson, 2002; Leibold and Kempter, 2006; Xu et al., 2012; Eagleman and Dragoi, 2012).

Layered feed-forward networks that support propagation of synchrony are termed synfire chains (e.g., Abeles, 1982, 1991; Diesmann et al., 1999; Gewaltig et al., 2001; Kumar et al., 2010). The propagated signal is a synchronous pulse-packet (Aertsen et al., 1996; Diesmann et al., 1999), i.e., a fraction of synchronously active neurons of one layer which induces synchronous activity in the following, postsynaptic, layer and so on. Robust signal transmission in synfire chains embedded in larger recurrent networks is usually obtained by an increased connectivity (compared to the embedding network) between the neurons of successive layers of the FFN (e.g., Aviel et al., 2003; Mehring et al., 2003; Kumar et al., 2008a). Alternatively, increased synaptic efficiencies (Vogels and Abbott, 2005), or the combination of enhanced synaptic weights and

non-additive coupling (mediated by fast dendritic spikes, cf. Ariav et al., 2003) can enable such a robust propagation (e.g., Jahnke et al., 2012, 2013).

Whereas the neuronal background in cortical networks is asynchronous and irregular, during behavior and cognitive tasks more correlated activity, in particular, oscillations of various frequencies prevail. A plethora of experimental studies links oscillations in, e.g., delta- $(0.1-4\text{Hz})$, alpha- $(10-25\text{Hz})$ or gamma-band $(25-100\text{Hz})$, to attentional states and sensory stimulus selection (e.g., Fries et al., 2002; Fries, 2005; Palva and Palva, 2007; Womelsdorf et al., 2007; Womelsdorf and Fries, 2007; Lakatos et al., 2008; Kopell et al., 2010; Buschman et al., 2012).

In this article we investigate how background oscillations influence the transmission of synchronous activity in feed-forward networks. More precisely, we consider sparse feed-forward structures that emerge as part of a random network and that exhibit moderately enhanced synaptic efficiencies (cf. also Jahnke et al., 2012, 2014a). In particular, the feed-forward structures considered are too weak (in the sense of connectivity and coupling strength) to propagate synchronous signals on top of asynchronous background activity. However, we demonstrate that additional oscillatory input, excitatory and inhibitory spike trains generated by an external oscillating neuronal population, can enable robust propagation of synchrony.

We consider both conventional additive couplings, mediated by transient conductance changes on the dendritic input site, and non-additive couplings that take nonlinear processing of inputs by fast dendritic spikes (e.g., Ariav et al., 2003; Polsky et al., 2004; Gasparini et al., 2004; Gasparini and Magee, 2006) into account. These dendritic spikes are evoked by highly synchronous inputs (i.e., inputs arriving within a time window of less than a few milliseconds) and cause strong, rapid depolarization in the soma of the postsynaptic neuron, exceeding the depolarization expected from additive processing of inputs. Thereby they may foster directed (Jahnke et al., 2012, 2013) and undirected (Memmesheimer and Timme, 2012) propagation of synchrony.

We show that for additively coupled networks, external oscillations support propagation of synchrony only if the (average) excitatory input exceeds the inhibitory input. This exceed causes a net depolarization of the neurons which in turn enables propagation of synchrony. However, there is no resonance between the propagating synchronous signal and the oscillatory stimulation, and temporally distributed external inputs would have the same effect. In contrast, for non-additively coupled networks the sensitivity of dendritic spike elicitation to synchronous inputs yields resonances to oscillations, i.e., there is a specific stimulation frequency range which enables propagation of synchrony. Dendritic spikes are not suppressed by inhibition (cf. Müller et al., 2012) such that they support synchrony propagation also if the inputs are balanced, i.e., if the (average) inhibitory input equals (or even exceeds) the excitatory input. Interestingly, the existence of resonance frequencies provides the possibility to guide synchronous activity along different pathways with distinct resonance frequencies.

6.2. Material & Methods

In this section we briefly introduce the neuron model and system setup. A complete list of standard neuron and model parameters is given in Appendix 6.5.1.

6.2.1. Neuron model

We consider networks of neurons of the integrate-and-fire type (Dayan and Abbott, 2001). Single neurons interact by sending and receiving action potentials (spikes). The state of neuron i is described by its membrane potential V_i and its temporal dynamics are determined by

$$C_i \frac{dV_i(t)}{dt} = g_i^{\mathrm{L}} \left[V_i^{\mathrm{eq}} - V_i(t)\right] + I_i^{\mathrm{ex}}(t) + I_i^{\mathrm{in}}(t), \tag{6.1}$$

where C_i is the membrane capacity, g_i^{L} is the leak conductance and V_i^{eq} is the equilibrium potential. $I_i^{\mathrm{ex}}(t)$ and $I_i^{\mathrm{in}}(t)$ are currents arising from excitatory and inhibitory inputs, respectively. Whenever the membrane potential $V_i(t)$ exceeds the spiking threshold V_i^{Θ} at some time $t = t^*$, a spike is sent to the post-synaptic neurons j, where it arrives after a delay time τ_{ji}. The sending neuron's potential is reset to $V_i(t^*) = V_i^{\mathrm{reset}}$, and the neuron is refractory for a time period t_i^{ref}, i.e., $V_i(t) \equiv V_i^{\mathrm{reset}}$ for $t \in \left[t^*, t^* + t_i^{\mathrm{ref}}\right]$.

6.2.2. Linear (additive) coupling

The effects of the synaptic inputs on postsynaptic neurons are modeled by transient conductance changes. Denoting the reversal potentials of excitatory and inhibitory currents by E^{ex} and E^{in}, the input currents to neuron i arising from synaptic inputs from other neurons of the network are given by

$$I_i^{\mathrm{ex}}(t) = g_i^{\mathrm{ex}}(t)\left[E^{\mathrm{ex}} - V_i(t)\right], \tag{6.2}$$

$$I_i^{\mathrm{in}}(t) = g_i^{\mathrm{in}}(t)\left[E^{\mathrm{in}} - V_i(t)\right]. \tag{6.3}$$

$g_i^{\mathrm{ex}}(t)$ and $g_i^{\mathrm{in}}(t)$ are linear superpositions of single responses,

$$g_i^{\mathrm{ex}}(t) = \sum_{n,j} \varepsilon_{ij}^{\mathrm{ex}} f^{\mathrm{ex}}\left(t - t_{j,n}^{\mathrm{f}} - \tau_{ij}\right), \tag{6.4}$$

$$g_i^{\mathrm{in}}(t) = \sum_{n,j} \varepsilon_{ij}^{\mathrm{in}} f^{\mathrm{in}}\left(t - t_{j,n}^{\mathrm{f}} - \tau_{ij}\right), \tag{6.5}$$

where $\varepsilon_{ij}^{\mathrm{ex}}$ and $\varepsilon_{ij}^{\mathrm{in}}$ denote the excitatory and inhibitory coupling strength from neuron j to neuron i and $t_{j,n}^{\mathrm{f}}$ is the nth spiking time of neuron j. f^{ex} and f^{in} specify the time course of the synaptic

conductance change given by the difference of two exponentials (Dayan and Abbott, 2001) with time constants $\tau^{k,1}$ and $\tau^{k,2}$,

$$f^k(t) = \begin{cases} \left(A^k\right)^{-1} \left(e^{-\frac{t}{\tau^{k,1}}} - e^{-\frac{t}{\tau^{k,2}}}\right) & \text{for } t \geq 0 \\ 0 & \text{for } t < 0 \end{cases}, \tag{6.6}$$

for $k \in \{\text{ex,in}\}$ describing the effect of an excitatory and inhibitory input, respectively, that is received at time $t_0 = 0$. The normalization constant

$$A^k = \left(\frac{\tau^{k,2}}{\tau^{k,1}}\right)^{\frac{\tau^{k,2}}{\tau^{k,1}-\tau^{k,2}}} - \left(\frac{\tau^{k,2}}{\tau^{k,1}}\right)^{\frac{\tau^{k,1}}{\tau^{k,1}-\tau^{k,2}}}. \tag{6.7}$$

is chosen such that the peak conductance $\max_{t \geq t_0} \left\{f^k(t)\right\} = 1$. Throughout this article, we denote the strength of a synaptic connection by the value of the peak conductance, i.e., a single input of strength ε causes a conductance change $\varepsilon \cdot f^k(t)$.

6.2.3. Non-linear (non-additive) coupling

Besides linear summation of inputs (as described above), we consider nonlinear amplification of synchronous inputs mediated by fast dendritic spikes. These have been found in single neuron experiments (e.g., Ariav et al., 2003; Polsky et al., 2004; Gasparini et al., 2004; Gasparini and Magee, 2006) and introduced in recent models of neural networks (Memmesheimer, 2010; Memmesheimer and Timme, 2012; Jahnke et al., 2012, 2014a; Breuer et al., 2014). The amplification is based upon dendritic action potentials which generate a strong depolarization in the soma. Here, three properties are of particular interest: (i) The amplification is very sensitive to input synchrony (relevant time window $\lessapprox 3$ milliseconds), (ii) the peak of the depolarization in the postsynaptic neuron (pEPSP) is reached a certain time interval after stimulation with only sub-millisecond jitter and (iii) with increasing stimulation strength the amplitude of the pEPSP saturates.

We model the contribution of such dendritic spikes to the neuronal input as follows (see also Memmesheimer, 2010; Jahnke et al., 2012): We augment the neurons with an additional nonlinear dendrite. Inputs that arrive at the linear dendrite are processed as described in Section 6.2.2. Inputs on the nonlinear dendrite also cause a conductance change as described above, but additional depolarizations of the membrane potential mimicking the effect of a dendritic spike may be generated. If the total excitatory input to a nonlinear dendrite within a time interval ΔT^{s} exceeds a certain threshold Θ_{b}, a current pulse is initiated which takes effect on the membrane potential after a delay time t^{ds}. We model the current pulse in a phenomenological approach such that the depolarization caused by a suprathreshold input, $\varepsilon \geq \Theta_{\text{b}}$, resembles the characteristics and time course of the depolarization observed in single neuron experiments (cf. Ariav et al., 2003). More precisely, the current pulse is described by the sum of three exponential functions,

$$I_{\mathrm{ds}}(t) = \Theta\left(t - t^{\mathrm{ds}}\right)\left[-A\exp\left(-\frac{t-t^{\mathrm{ds}}}{\tau^{\mathrm{ds},1}}\right) + B\exp\left(-\frac{t-t^{\mathrm{ds}}}{\tau^{\mathrm{ds},2}}\right) - C\exp\left(-\frac{t-t^{\mathrm{ds}}}{\tau^{\mathrm{ds},3}}\right)\right], \quad (6.8)$$

with positive prefactors A,B,C and decay time constants $\tau^{\mathrm{ds},1}$, $\tau^{\mathrm{ds},2}$ and $\tau^{\mathrm{ds},3}$ which are chosen such that the somatic depolarization fits experimental data. After initiation of such a current pulse the (nonlinear) dendrite becomes refractory for a time period $t^{\mathrm{ref,ds}}$ and does not transmit spikes within the refractory time period.

We note that for the generation of a dendritic spike only the excitatory inputs are considered. Consequently, in accordance with recent experimental findings, inhibition fails to suppress fast dendritic sodium spikes. However, the probability that a somatic spike is initiated by a dendritic one might be reduced by hyperpolarization of the soma (Müller et al., 2012; cf. also Jahnke et al., 2014a).

6.2.4. Network setup

We investigate sparsely, randomly connected recurrent networks and study the propagation of synchrony in naturally occurring feed-forward subnetworks (FFNs). "Naturally occurring" here means that the feed-forward structures are present as part of a recurrent network and are not generated by, e.g., adding feed-forward connections. However, they are highlighted by moderately increased excitatory connections.

We denote the total number of neurons in the recurrent network by N. The network itself constitutes an Erdös-Rényi random graph: A directed excitatory synaptic connection between any pair of neurons exists with probability p_{ex}. Inhibition in recurrent networks is usually assumed to be mediated by a population of inhibitory neurons (interneurons). Spiking of excitatory neurons causes a response of inhibitory neurons which in turn project an inhibitory input to the excitatory neurons. Here, we simplify this inhibitory feed-back mechanism and assume that the spiking of neurons, additionally to the excitatory input on the postsynaptic neurons, have an inhibitory effect: An inhibitory connection between any pair of neurons exists with probability p_{in}. We remark that there might exist an inhibitory and excitatory connection between two neurons. However, these cases are rare due to the sparsity of the considered networks (typically $p_{\mathrm{ex}}, p_{\mathrm{in}} \approx 0.05$). The simplification of the inhibitory feed-back loop eases the analytical treatment, but is not crucial for the effect of oscillation induced propagation of synchrony as discussed later on (cf. also Jahnke et al., 2014a).

For clarity of presentation coupling strengths are assumed homogeneous; excitatory connections have strength $\varepsilon_{ij}^{\mathrm{ex}} = \varepsilon_{\mathrm{p}}$, the strength of inhibitory connections is denoted by $\varepsilon_{ij}^{\mathrm{in}} = \varepsilon_{\mathrm{m}}$. We choose the ratio between inhibitory and excitatory connection strengths, $\gamma = \varepsilon_{\mathrm{m}}/\varepsilon_{\mathrm{p}}$, such that the peaks of single excitatory and inhibitory postsynaptic potentials measured at resting membrane potential are of equal amplitude.

We define FFNs by assigning neurons randomly to m groups of ω neurons each, where each neuron belongs to one group at most. These groups constitute the layers of the FFN. By construction, the connectivity between neurons of successive groups of the FFN statistically equals the overall connectivity. To enable propagation of synchrony, we increase the strengths of the already existing excitatory connections between neurons of successive layers; this connection strength is denoted by ε_{c}.

For clarity of presentation, in the first part of the article we investigate the influence of oscillations on propagating synchrony in isolated FFNs (Section 6.3.1-6.3.4). Here, only excitatory connections between neurons of successive layers are present, i.e., $\varepsilon_{\mathrm{p}} = \varepsilon_{\mathrm{m}} = 0$, but $\varepsilon_{\mathrm{c}} > 0$. However, recurrent connections ($\varepsilon_{\mathrm{p}}, \varepsilon_{\mathrm{m}} > 0$) do not change the results qualitatively. We comprehensively study recurrent FFNs and discuss differences to isolated FFNs in Appendix 6.5.3.

6.2.5. Homogeneous neuronal background

In the ground state of balanced networks (v. Vreeswijk and Sompolinsky, 1996, 1998) single neurons fire irregularly and their spiking activity is approximately described by Poissonian spike trains (Tuckwell, 1988; Brunel and Hakim, 1999; Brunel, 2000). In addition to inputs from the recurrent network each neuron receives inputs from remote networks, and we emulate this influence by independent excitatory and inhibitory (Poissonian) spike trains. We denote the rates by $\nu^{\mathrm{ext,ex}}$ and $\nu^{\mathrm{ext,in}}$ and the strength of single spikes (peak conductances) by $\varepsilon^{\mathrm{ext,ex}}$ and $\varepsilon^{\mathrm{ext,in}}$, respectively. Similarly to the recurrent connections, we assume the external input to be balanced, such that the total input is balanced as well. As a consequence, the neurons are in a fluctuation-driven regime, and in the absence of synchrony the neurons spike asynchronously and irregularly and their output spike trains resemble Poissonian spike trains themselves.

6.2.6. Background oscillations

In this article we study the impact of neuronal oscillations on the ability of recurrent networks to propagate synchronous signals. Oscillatory input may arise from oscillations in other circuits or within the local network itself.

To systematically investigate the influence of oscillations on synchrony propagation in a controlled way, we emulate such oscillations by excitatory and inhibitory inputs generated by a 'virtual' population of N_{e} neurons that spike with a mean frequency ν^{s}. Within each oscillation period $T^{\mathrm{s}} = 1/\nu^{\mathrm{s}}$, N_{e} spike times are drawn from a Gaussian distribution centered at $t_n := n/\nu^{\mathrm{s}}$ (for the nth oscillation, $n \in \mathbb{Z}$) with standard deviation σ^{s}. Each of these spikes causes an excitatory input of strength $\varepsilon_{\mathrm{p}}^{\mathrm{ext}}$ with probability $p_{\mathrm{ex}}^{\mathrm{ext}}$ and an inhibitory input of strength $\varepsilon_{\mathrm{m}}^{\mathrm{ext}}$ with probability $p_{\mathrm{in}}^{\mathrm{ext}}$ to each neuron of the recurrent network (cf. Figure 6.1).

Here and in the following the term "balanced oscillations" refers to oscillatory input for which excitatory inputs and inhibitory inputs cause postsynaptic potentials of equal amplitude (cf. also Section 6.2.4); if the average excitatory inputs exceed the inhibitory inputs or vice versa, we denote such inputs as "unbalanced oscillations".

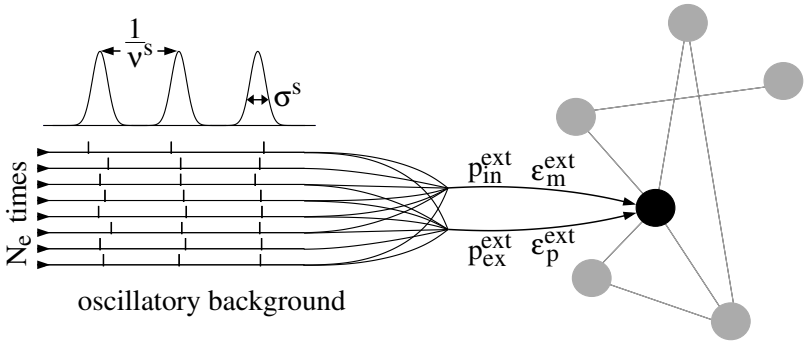

Figure 6.1: Schematic illustration of oscillatory inputs. Oscillatory input is generated by a (virtual) population of N_e neurons which spike once during each oscillation period of length $1/\nu^s$. The actual spiking times are drawn from a Gaussian distribution. At each neuron in the network, each spike causes an excitatory input of strength ε_p^{ext} with probability p_{ex}^{ext} and an inhibitory input of strength ε_m^{ext} with probability p_{in}^{ext}.

Whereas unbalanced oscillations induce a net depolarization or hyperpolarization of the neurons in the network, balanced oscillations maintain the balance between excitation and inhibition, and are thus expected to change the average membrane potential in the ground state only weakly. However, they may influence the effective time constant of the neurons as discussed below in, e.g., Section 6.3.2 (cf. also Destexhe et al., 2003; Kuhn et al., 2004).

The aim of the article is to understand the influence of the oscillatory nature of the input on propagating synchrony, and resonances between signal propagation and input oscillations. We discuss balanced oscillations (Section 6.3.2) and unbalanced oscillations (Section 6.3.3) separately.

6.3. Results

Synchrony propagation through feed-forward structures has been demonstrated for additive and non-additive coupling, and non-oscillatory network background activity (e.g., Diesmann et al., 1999; Gewaltig et al., 2001; Aviel et al., 2003; Vogels and Abbott, 2005; Kumar et al., 2008a; Jahnke et al., 2012). In general, if synaptic coupling is additive (i.e., in the absence of dendritic spikes), the connection strength within the structure, i.e., synaptic efficiencies and/or connectivity, need to be much stronger (perhaps outside the biological plausible range) than for non-additive coupling (Figure 6.2a,d and Jahnke et al., 2012, 2013). With too small coupling strength a synchronous signal fails to propagate, the synchronous activity dies out after a small number of layers (Figure 6.2b,e).

Interestingly, even balanced oscillatory inputs (cf. Section 6.2.6) may stabilize synchrony propagation if the coupling is non-additive (Figure 6.2f), but do not influence or even suppress synchrony propagation in circuits with additive couplings (Fig. 6.2c). With too strong coupling

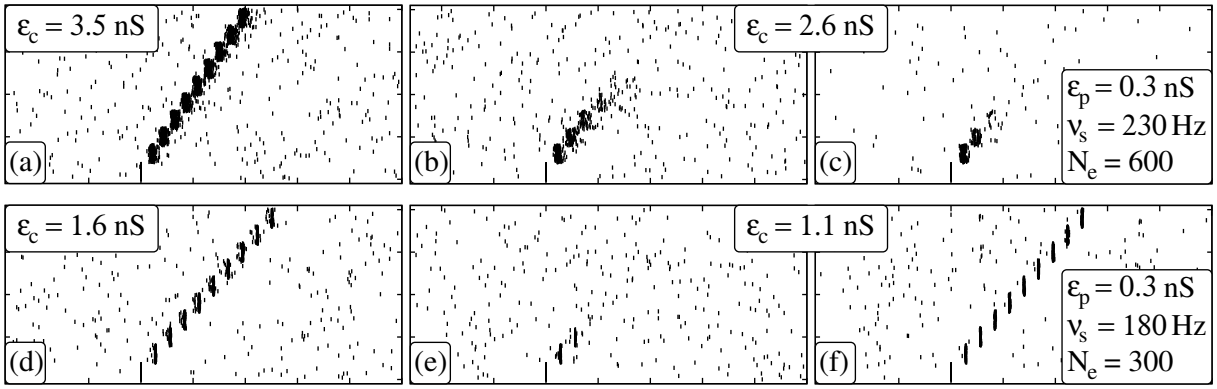

Figure 6.2: Signal transmission in isolated FFNs ($m = 10$, $\omega = 200$, $p_{\mathbf{ex}} = 0.05$) with linear (a-c) and nonlinear (d-f) dendritic interactions. For each dendritic interaction type, raster plots for two different coupling strengths ε_c are shown. Panels (a), (b), (d) and (e) display the network activity in the absence of oscillations; in panels (c) and (f) balanced oscillatory input is present (parameters see inset). The stimulation frequency ν^s equals the propagation frequency ν^p of the stable propagation shown in (a) and (d).

strength spontaneous propagation of synchrony might be initiated causing pathological activity (not shown; cf. Litvak et al., 2003; Rosenbaum et al., 2010, 2011).

Whether synchrony propagation is stabilized or enabled depends on features of neurons, network and oscillatory input, e.g., stimulation frequency or synaptic coupling strength. We investigate the mechanism underlying this stabilization numerically (Section 6.3.2-6.3.4) and analytically (Section 6.5.2). We identify parameter regions for which synchrony propagation is facilitated by oscillations. In particular, we demonstrate that nonlinearly coupled FFNs show resonance to (balanced and unbalanced) oscillations. Interestingly, such resonances provide a gating mechanism for information flow across the network: Different stimulation frequencies may selectively activate different FFNs (with corresponding resonance frequencies) embedded in a recurrent network (Section 6.3.5).

6.3.1. Synchrony Propagation

As a starting point, we investigate isolated FFNs and briefly describe the mechanism underlying propagation of synchrony in networks with and without dendritic nonlinearities.

Each neuron of the FFN receives much more input from the external homogeneous background than from the preceding layer. Therefore, in the absence of synchrony, the FFN's dynamics in the ground state is mainly determined by this external background input, and the neurons of the FFN fire asynchronously with a low rate. However, exciting a fraction of neurons of the first layer of the FFN to spike synchronously causes a synchronous input to the second layer, a fraction of which subsequently spikes synchronously. This process continues from layer to layer and thus can induce persistent propagation of synchrony.

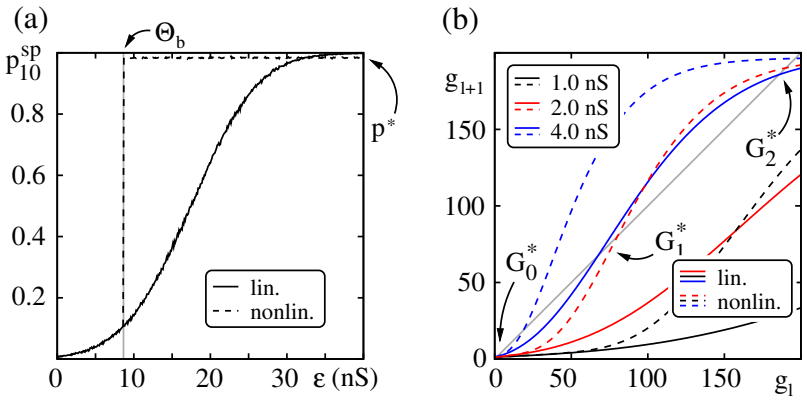

Figure 6.3: Transition from non-propagating to propagating regime. (a) The probability $p_{10}^{\mathrm{sp}}(\varepsilon)$ that a single neuron in the ground state (receiving homogenous background inputs) spikes within 10ms after stimulation by a synchronous input pulse of strength ε. For neurons with linear dendritic interactions (additive coupling; solid line) the spiking probability increases continuously with increasing input ε. For neurons with nonlinear dendritic interactions (non-additive coupling; dashed line), inputs larger than the dendritic threshold Θ_{b} elicit a dendritic spike and therefore the spiking probability jumps to a constant value, $p_{10}^{\mathrm{sp}}(\varepsilon) =: p^*$, for $\varepsilon \geq \Theta_{\mathrm{b}}$. The probabilities are estimated from averaging over 10.000 single trials per connection strength. (b) Map (6.10) specifying the average number of synchronously spiking neurons g_{l+1} in one layer given that in the previous layer g_l neurons have spiked synchronously; derived from the single neuron response probability in (a) for an isolated FFN (here $\omega = 200$, $p_{\mathrm{ex}} = 0.05$). Different colors indicate different strengths of feed-forward connections ($\varepsilon_{\mathrm{c}} \in \{1.0, 2.0, 4.0\}$nS), continuous and dashed lines indicate additive and non-additive coupling.

One can derive an iterated map (cf. also Jahnke et al., 2012, 2013) that specifies the average number of neurons $\bar{g}$ which spike synchronously, i.e., within a certain time interval, given that in the preceding layer g^{in} neurons have spiked synchronously. We denote the probability for a neuron in the asynchronous ground state to spike within a time interval of x milliseconds after receiving an input of strength ε by $p_x^{\mathrm{sp}}(\varepsilon)$. Say that in some layer, g^{in} neurons spike synchronously, then each neuron of the following layer will receive some number $k \in \{0, 1, \ldots, g^{\mathrm{in}}\}$ of synchronous inputs of strength ε_{c}. As each of the g^{in} spikes sent is received by every neuron of the postsynaptic layer with probability p_{ex}, k follows a binomial distribution, $k \sim B\left(g^{\mathrm{in}}, p_{\mathrm{ex}}\right)$, such that on average

$$\bar{g} = \omega \sum_{k=0}^{g^{\mathrm{in}}} \binom{g^{\mathrm{in}}}{k} p_{\mathrm{ex}}^k \left(1 - p_{\mathrm{ex}}\right)^{\omega - k} p_x^{\mathrm{sp}}\left(k\varepsilon_{\mathrm{c}}\right) \tag{6.9}$$

neurons spike within a time interval of x milliseconds.

We asses the temporal development of the size of the synchronous pulse in every layer by considering g_{l+1} the average number of neurons spiking synchronously in layer $l+1$ as a function of g_l the average number synchronous spiking neurons in the preceding layer l. Thus, replacing

$\bar{g}$ by g_{l+1} and g^{in} by g_l in Equation (6.9) we obtain the map

$$g_{l+1} = F(g_l) \tag{6.10}$$

where $F(\cdot)$ is the continuous interpolation of the right hand-side of Equation (6.9) for continuous $g_l \in \mathbb{R}$. The fixed points of the map (6.10) determine the stability region for the propagation of synchrony (cf. Figure 6.3). For small coupling strength ε_{c}, there is only one fixed point $G_0^* \approx 0$ and any synchrony propagation will extinguish within few layers (cf. also Figure 6.2b,e). For sufficiently large layer size ω and coupling strengths ε_{c}, stable propagation of synchrony can be achieved, the size and temporal spread of the synchronous pulse are stable throughout the layers (for an extensive analysis see Jahnke et al., 2013): This is due to the appearance of two additional fixed points, G_1^* (unstable) and G_2^* (stable), which emerge via a tangent bifurcation in the map (6.10) upon increasing ε_c. A synchronous pulse $g_0 \geq G_1^*$ will propagate with a typical group size $g^* \approx G_2^*$.

In a given network, persistent propagation is possible if the connection strengths are larger than some critical value. We denote the critical connection strength, i.e., the bifurcation point at which the fixed points G_1^* and G_2^* emerge, by $\varepsilon_{\text{c}} = \varepsilon_{\text{L}}^*$ for FFNs with linear dendrites and by $\varepsilon_{\text{c}} = \varepsilon_{\text{NL}}^* < \varepsilon_{\text{L}}^*$ for FFNs with nonlinear dendritic interactions.

Stable propagation of synchrony occurs with a certain propagation frequency ν^{p}, which is defined as the inverse of the average time interval between two consecutive synchronous pulses. ν^{p} is governed by (i) the synaptic delay and (ii) the average time t^{sp} that an arriving input needs to trigger a spike in the postsynaptic neuron (if it does so). The synaptic delay is fixed for a given setup, but t^{sp} in general depends on the strength of the input and thereby on the connection strength ε_{c}.

For networks with linear dendrites, t^{sp} decreases with increasing input strength (cf. Figure 6.4a): The increase of the input causes a steeper and steeper rise of the evoked postsynaptic potential, and therefore reduces the (average) time the neuron needs to reach the threshold V^{Θ}. In contrast, t^{sp} is constant for networks with nonlinear dendritic interactions: The spiking of the neuron is triggered by the additional current pulse mimicking the dendritic spike. This current pulse (and with it the resulting depolarization) is independent of the actual input strength (see Section 6.2.3), and the rise of the postsynaptic potential is so steep that $t^{\text{sp}}(\varepsilon)$ is practically constant for $\varepsilon \geq \Theta_{\text{b}}$.

As a consequence, for FFNs with non-additive couplings the propagation frequency ν^{p} depends only weakly on the connection strength ε_{c}. If a propagation of synchrony is enabled for $\varepsilon_{\text{c}} \approx \varepsilon_{\text{NL}}^*$, this propagation occurs with a certain 'natural' propagation frequency $\nu^{\text{p}} = \nu^{\text{nat}}$. In contrast to linearly coupled FFNs, the propagation frequency remains approximately constant for connection strengths above the critical connection strength, $\varepsilon_{\text{c}} > \varepsilon_{\text{NL}}^*$ (Figure 6.4b). For connection strengths satisfying $\Theta_{\text{b}}/\varepsilon_{\text{c}} \in \mathbb{N}$ the propagation frequency ν^{p} jumps: If ε_{c} is increased above Θ_{b}/i for some i, a smaller number i of spikes can trigger a dendritic spike, i.e., a reduced fraction of the synchronous pulse packet is sufficient to trigger dendritic spikes, such that the neurons in each layer tend to spike earlier. This shortens the (average) responding time to the synchronous pulse packet and the propagation frequency increases.

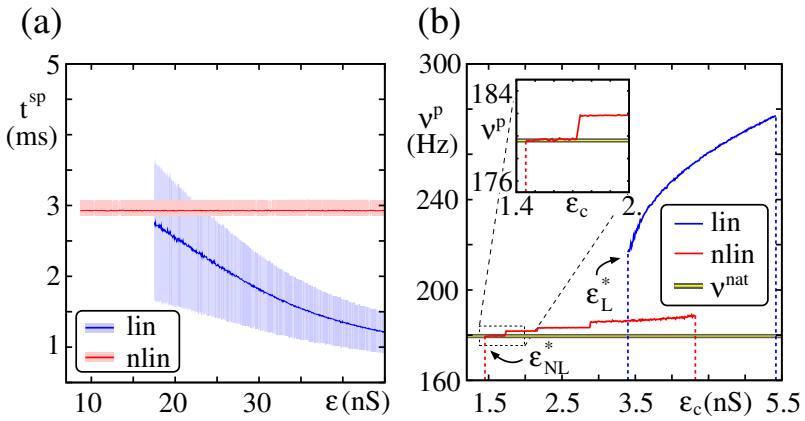

Figure 6.4: Propagation frequency of a synchronous pulse. (a) Mean spiking time t^{sp} of a neuron after stimulation with an input of strength ε (shaded areas indicate the regions between the 0.2 and 0.8 quantiles; only data for $p_{10}^{\mathrm{sp}}(\varepsilon) \geq 0.5$ are shown). For neurons with nonlinear dendritic interactions t^{sp} is constant, whereas for neurons with linear dendritic interactions t^{sp} decreases with increasing stimulation strength ε. (b) Propagation frequency ν^{p} of a synchronous pulse versus strength of the feed-forward connections ε_{c} in the absence of external oscillations ($\omega = 200$, $p_{\mathrm{ex}} = 0.05$); the inset shows a zoomed view of the propagation frequency in FFNs with non-additive couplings for $\varepsilon_{\mathrm{c}} \approx \varepsilon^*_{\mathrm{NL}}$. The yellow line indicates the natural propagation frequency ν^{nat}.

We remark that for large connection strengths ε_{c}, the FFN enters a pathological state of activity: Neurons of one particular layer share inputs from the preceding layer and this causes correlations in their spiking activity. If the single connections become stronger (i.e., only a few inputs are needed to generate a dendritic spike and a somatic output spike) also these correlations become stronger. They may accumulate over the layers of the FFN and lead to spontaneous synchronous spiking activity propagating along the later layers of the FFN (Litvak et al., 2003; Rosenbaum et al., 2010, 2011). Thus, there exist cutoff-connection strengths $\varepsilon_{\mathrm{L}}^{\mathrm{path}}$ and $\varepsilon_{\mathrm{NL}}^{\mathrm{path}}$ for networks with linear and nonlinear dendritic interactions, above which the global spiking activity is characterized by network oscillations and a meaningful propagation of synchronous activity is not possible anymore.

Whereas signal transmission is possible in FFNs with and without dendritic nonlinearities, the underlying mechanism is different: In linearly coupled networks transmission is achieved by eliciting somatic spikes directly, thus also asynchronous inputs and depolarizing constant external currents may contribute to spike propagation. In nonlinearly coupled networks transmission is mediated by dendritic spikes (all-or-none events), and therefore only highly synchronized spiking input contributes.

6.3.2. Synchrony propagation in the presence of balanced oscillations

Depending on the coupling strength FFNs may or may not be capable of propagating synchronous signals. But how do external oscillations influence the propagation of synchrony? Do

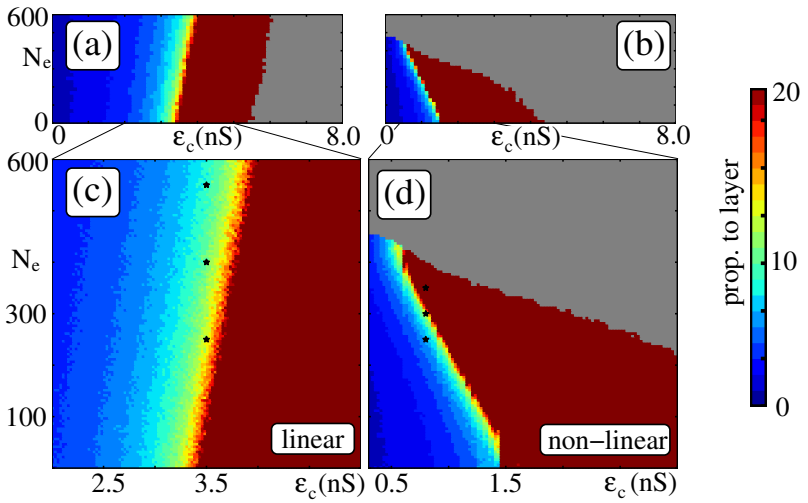

Figure 6.5: Balanced oscillations can support signal transmission in isolated FFNs ($m = 20$, $\omega = 200$, $p_{\mathbf{ex}} = 0.05$). The panels show up to which layer the propagating synchronous pulse (initiated in the first layer in-phase with the external oscillations) is detectable (color-coded) as a function of the coupling strength ε_c and the amplitude of the external network oscillations, measured by N_e. Configurations, where the system enters a pathological activity state (i.e., ongoing spontaneous propagation of synchrony) are marked in gray. Panels (a,c) show simulation results for networks with linear dendritic interactions ($\nu^s = 230$Hz, $\sigma^s = 0.3$ms) and (b,d) for networks with nonlinear dendritic interactions ($\nu^s = 180$Hz, $\sigma^s = 0.3$ms); panels (c) and (d) are close up views of (a) and (b). The black stars indicate the values of ε_c and N_e used in Figure 6.7a,c. Whereas balanced oscillations hinder signal propagation in additively coupled networks (i.e., require compensation by stronger coupling), they can support it in non-additively coupled ones. Other parameters are $p_{ex}^{ext} = p_{in}^{ext} = 0.05$, $\varepsilon_p^{ext} = 0.3$nS, $\varepsilon_m^{ext} = 0.825$nS.

systems with and without dendritic nonlinearities exhibit qualitatively the same behavior?

To answer this question, we first consider isolated FFNs, which receive balanced oscillatory stimulation with frequencies ν^s equal to the propagation frequencies ν^p observed for the onset of propagation of synchrony in unstimulated FFNs (see Section 6.3.1). Thus we expect the stimulation to be in resonance with the propagating synchronous pulse in the FFN. The impact of different stimulation frequencies and the possibility of complex locking patterns between oscillations and propagating synchrony is investigated in Section 6.3.4 below.

How does the amplitude of the oscillatory input as controlled by the number N_e of oscillating (virtual) neurons (see Section 6.2.6 for details) influences signal propagation?

For networks with additive couplings we find that the critical connection strength (i.e., the minimal connection strength which enables propagation of synchrony) increases with increasing oscillation amplitude N_e as illustrated in Figure 6.5a,c: The additional input is balanced, so that the mean input to each neuron is constant (for all N_e), but both the mean excitatory and inhibitory conductances are increased. In this high-conductance state the effective membrane time constant decreases and consequently the amplitude and the width of postsynaptic potentials

decrease (Destexhe et al., 2003; Kuhn et al., 2004). In other words, the additional inputs arising from oscillations decrease the excitability of the neurons. Thus, stronger inputs (in terms of conductances) are needed to generate the same depolarization as in networks without external oscillations and the critical connectivity, $\varepsilon_{\mathrm{L}}^{*}$, increases. This is the same phenomenon that hinders synfire-explosions (Hehl, 2001; Mehring et al., 2003) in networks with conductance-based synapses as described in Kumar et al. (2008a).

In contrast, in networks with non-additive couplings, the critical connection strength decreases with increasing oscillation amplitude N_{e} (see Figure 6.5b,d). In such networks the propagation of synchrony is mainly mediated by dendritic spikes. Dendritic spikes are elicited if the excitatory input on a dendrite within a certain time-window, ΔT^{s}, is larger than the dendritic threshold Θ_{b} (see Section 6.2.3). Inhibition fails to suppress dendritic spikes (Müller et al., 2012) and thus its increase does not hinder signal propagation. If the frequency ν^{s} of network oscillations is in the range of the natural propagation frequency $\nu^{\mathrm{nat}} \approx \nu^{\mathrm{s}}$, and the oscillations are in phase with the propagating signal, the synchronous pulse from the preceding group arrives at each layer synchronously with the oscillatory inputs. Thus, less input from the preceding layer is needed to reach the dendritic threshold. Taken together, by effectively lowering the dendritic threshold Θ_{b} the external inputs reduce the critical connectivity $\varepsilon_{\mathrm{NL}}^{*}$. In Figure 6.5b,d we show that this reduction can yield propagation of synchrony at drastically reduced synaptic efficiencies within the FFN; in the given example the critical connection strength $\varepsilon_{\mathrm{NL}}^{*}$ is reduced by a factor of two to three (from 1.45nS to 0.6nS).

The downside of the robustness of dendritic spikes to inhibition is that even balanced oscillations may cause pathological activity if oscillation amplitude becomes too strong: With increasing amplitude N_{e} the neurons of the FFN become more and more sensitive to inputs from the previous layer. Thus, similar to the regime of overly strong feed-forward connections (cf. remark at the end of the previous Section 6.3.1), correlations in their spiking activity accumulate along the layers of the FFN (Litvak et al., 2003; Rosenbaum et al., 2010, 2011) and induce spontaneous propagation of synchrony (gray areas in Figure 6.5).

6.3.3. Synchrony propagation in the presence of unbalanced oscillations

Like balanced oscillations also unbalanced oscillations may be expected to alter the propagation efficiencies of FFNs: The average external excitatory input is larger or smaller than the inhibitory input, and thus the average ground state membrane potential of the neurons is shifted which influences the neurons' excitability. As we show below this shift clearly influences propagation of synchrony in additively coupled networks, but has only a weak effect in non-additively coupled systems.

For a given excitatory coupling strength $\varepsilon_{\mathrm{p}}^{\mathrm{ext}}$ we denote the corresponding balanced inhibitory coupling strength by

$$\varepsilon_{\mathrm{m}}^{0} := \gamma \varepsilon_{\mathrm{p}}^{\mathrm{ext}}, \tag{6.11}$$

where γ is chosen such that the peaks of the excitatory and inhibitory postsynaptic potentials are of equal amplitude when the input is received at resting potential (cf. Section 6.2.6). We

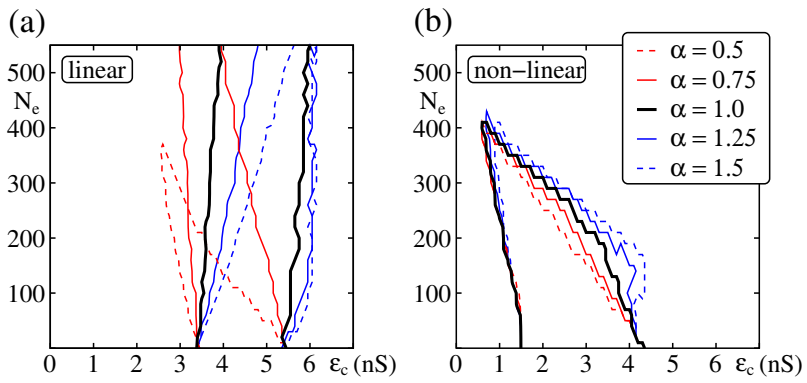

Figure 6.6: Support of propagation of synchrony by unbalanced oscillations. Same setup as in Figure 6.5, but with altered inhibitory coupling strength $\varepsilon_{\mathrm{m}}^{\mathrm{ext}} = \alpha\varepsilon_{\mathrm{m}}^{0}$ as indicated in (b). The lines inclose the parameter regions for which an initial synchronous pulse is detectable up to the final layer. (a) For FFNs with linear dendritic interactions unbalanced oscillations may foster propagation of synchrony, if the excitation exceeds the inhibition ($\alpha < 1$, i.e., $\varepsilon_{\mathrm{m}}^{\mathrm{ext}} < \varepsilon_{\mathrm{m}}^{0}$; red lines) or impede it, if the inhibition exceeds the excitation, respectively ($\alpha > 1$, i.e., $\varepsilon_{\mathrm{m}}^{\mathrm{ext}} > \varepsilon_{\mathrm{m}}^{0}$; blue lines). (b) In contrast, in FFNs with nonlinear dendritic interactions the balance between excitation and inhibition has only a weak effect on the parameter region in which robust propagation of synchrony is possible. For further explanations see Section 6.3.3.

consider isolated FFNs stimulated by oscillations as in the previous section, but we decrease or increase the strength of the inhibitory inputs by a factor α compared to the balanced regime, i.e.,

$$\varepsilon_{\mathrm{m}}^{\mathrm{ext}} = \alpha\varepsilon_{\mathrm{m}}^{0}. \tag{6.12}$$

For additively coupled networks and $\alpha < 1$ such input indeed promotes synchrony propagation (cf. Figure 6.6a, red lines): The oscillatory input depolarizes the neurons of the FFN and thus less synaptic input is needed to elicit a somatic spike; the critical connectivity $\varepsilon_{\mathrm{L}}^{*}$ decreases. At the same time, the increased excitability of the neurons lowers the threshold for pathological activity, $\varepsilon_{\mathrm{L}}^{\mathrm{path}}$. Likewise, for $\alpha > 1$ the neurons are hyperpolarized by the oscillatory input which impedes the generation of somatic spikes; the critical connectivity $\varepsilon_{\mathrm{L}}^{*}$ increases (cf. Figure 6.6a, blue lines).

In contrast, in non-additively coupled networks, the critical connectivity $\varepsilon_{\mathrm{NL}}^{*}$ is largely unaffected by changing the balance of inhibition and excitation (cf. Figure 6.6b). Here, propagation of synchrony is mediated mainly by dendritic spikes, and their generation is not influenced by inhibition (cf. Section 6.2.3 and Müller et al., 2012). Pathological activity is induced if correlations in spontaneous spiking activity accumulate over the layers. Because inhibition reduces the overall spiking activity (and also the probability that a dendritic spike triggers a somatic one), with increasing α (and thus increasing inhibition) the pathological threshold $\varepsilon_{\mathrm{NL}}^{\mathrm{path}}$ increases.

We note that although unbalanced oscillations may promote propagation of synchrony in additively coupled networks, the mechanism underlying this support differs from propagation of

synchrony in non-additively coupled networks. The effect is attributed to the increase of the (average) ground state membrane potential and, as we demonstrate in the next Section 6.3.4, could as well be obtained by additional constant (over time) input currents with the same strength as the mean input due to the oscillations.

6.3.4. Network Resonance

Oscillations may support propagation of synchrony (if in resonance), but how does their actual impact depends on system features such as frequency and amplitude of external oscillations. In the following, we investigate which frequency ranges support or hinder synchrony propagation. In particular, we show that networks with non-additive coupling exhibit resonance to stimulations where the frequency ν^{s} is rationally related to the natural propagation frequency ν^{nat}. In networks with additive couplings, we do not find such a resonance effect, even if the stimulation is unbalanced and therefore supports signal propagation.

First, we consider networks with linear couplings: As pointed out in the previous section, balanced oscillatory inputs decrease the excitability of the neurons of the FFN. Thereby it decreases the capability of the network to propagate synchronous signals for all stimulation frequencies ν^{s}. With increasing ν^{s}, the total number of input spikes per unit time increases and the effective time constant decreases further such that the propagation becomes more and more difficult. Figure 6.7a illustrates that the presence of balanced oscillations indeed inhibits synchrony propagation increasingly, the stronger and the more prominent the oscillations are (i.e., larger N_{e} and ν^{s}).

The support of signal transmission by unbalanced input (cf. Figure 6.6) is caused by an increase of the ground state's membrane potential. With increasing N_{e} and ν^{s} this depolarization increases (increased net excitation) and thus facilitates synchrony propagation more and more. Likewise, the propagation frequency ν^{p} increases until the stimulation gets too strong and the system enters a pathological activity state. We do not observe resonance to the oscillatory stimulation, and the promotion of propagation of synchrony can equally well be obtained by an additional constant (over time) excitatory input I^{s} which is proportional to the stimulation frequency ν^{s} (cf. Figure 6.7b).

In contrast, networks with non-additive couplings show resonance, and even balanced oscillations enable propagation of synchrony for configurations where signal propagation fails for homogeneous external background (i.e., in the absence of external oscillations, cf. Figure 6.5b,d). For stimulation frequencies $\nu^{\mathrm{s}} \approx \nu^{\mathrm{nat}}$, we observe a locking of the propagating signal to the external stimulus: The input from a preceding layer is not sufficient to excite sufficiently many neurons to spike synchronously and to enable persistent propagation. It can, however, take place if there is additional input. An oscillatory external input then influences the timing of the propagating pulse-packet and the propagation frequency ν^{p} locks to the stimulation frequency ν^{s} (cf. Figure 6.7c,d).

With changing ν^{s}, we observe multiple resonance peaks for setups where the ratio of ν^{s} and ν^{nat} is rational, $\nu^{\mathrm{nat}} : \nu^{\mathrm{s}} = n : m$ for some small integers n, m. The arrival of the input from every

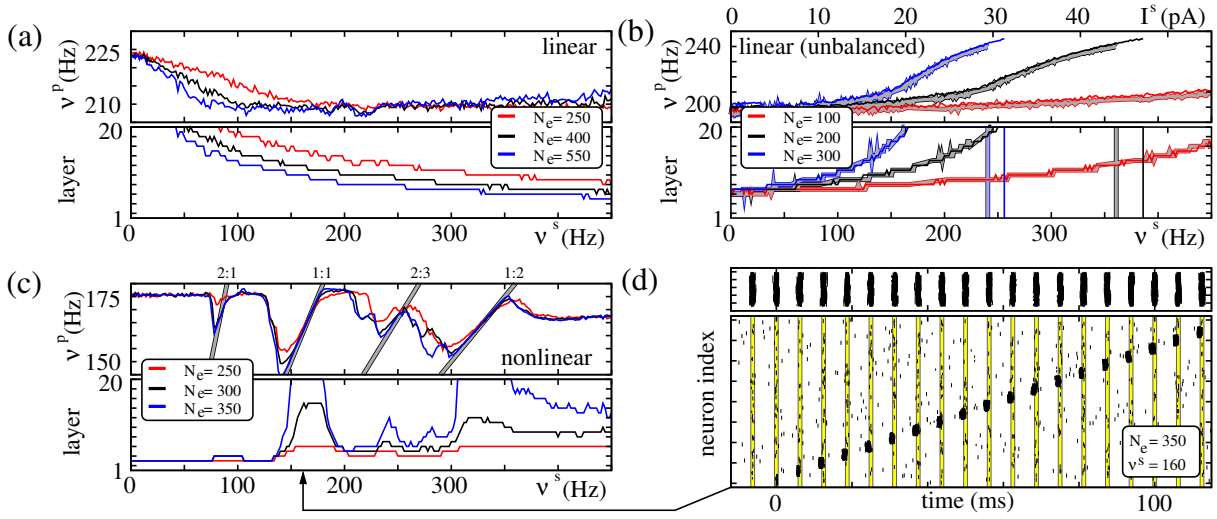

Figure 6.7: FFNs with nonlinear dendritic interactions show resonance. Same network setup as in Figure 6.4; coupling strengths are (a) $\varepsilon_c = 3.5$nS, (b) $\varepsilon_c = 2.8$nS and (c,d) $\varepsilon_c = 0.8$nS. (a-c) The upper panels display the propagation frequency ν^p of the synchronous signal, the lower panels show the layer up to which propagation occurs, as a function of the stimulation frequency ν^s for FFNs with (a,b) linear and (c) nonlinear dendritic interactions. Different colors represent different amplitudes N_e of external oscillations as indicated by insets. In additively coupled FFNs (a) balanced oscillations hinder synchrony propagation, whereas (b) unbalanced oscillations ($\alpha = 0.5$, i.e., excitation exceeds inhibition, cf. Equation 6.12) support it. This support, however, might be equally well achieved by temporally constant additional excitatory inputs: The thick gray filled lines indicate the propagation properties of an FFN, where single neurons receive constant additional current I^s (red; upper vertical axis), $2I^s$ (black) or $3I^s$(blue). In non-additively coupled FFNs even (c) balanced oscillations foster synchrony propagation and, in contrast to additively coupled FFNs, the propagating signal may lock to the oscillatory stimulation if the ratio $\nu^{nat} : \nu^s$ is rational; the gray lines indicate $\nu^p : \nu^s = \{2:1, 1:1, 2:3, 1:2\}$. This locking is illustrated in (d): Raster plots of spikes of the external oscillating population (upper panel) and of the FFN (lower panel). The yellow lines indicate the time intervals $[n/\nu^s - \sigma^s, n/\nu^s + \sigma^s]$ for $n \in \mathbb{N}$, containing $\approx 68\%$ of the spikes of the external oscillatory population (cf. also Figure 6.8).

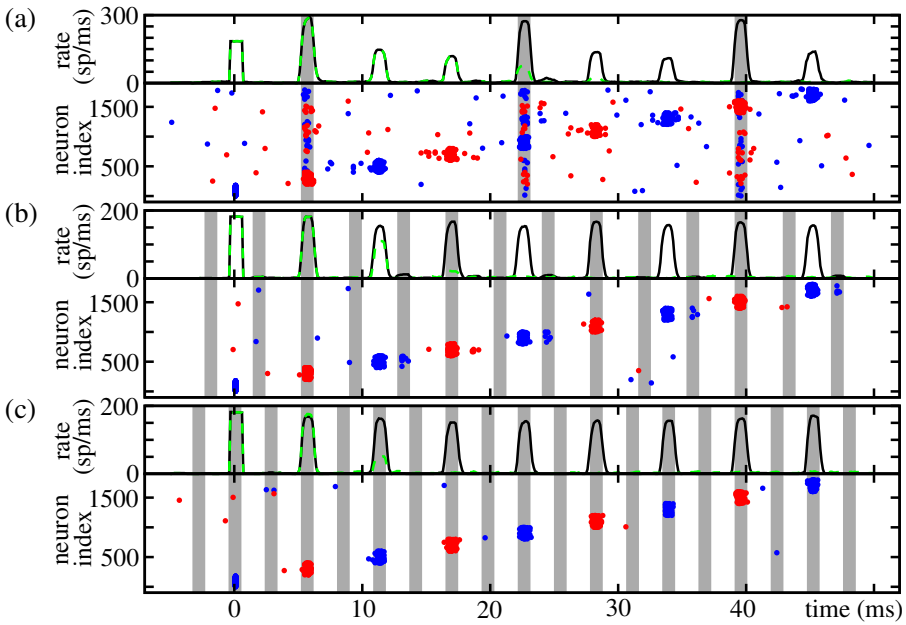

Figure 6.8: Examples of resonance in isolated FFNs with non-additive coupling ($m = 20$, $p_{\rm ex} = p_{\rm in} = 0.05$, $\omega = 200$). The ratio between the stimulation frequency $\nu^{\rm s}$ and the natural propagation frequency $\nu^{\rm nat}$ is rational: (a) $\nu^{\rm s} = \frac{1}{3}\nu^{\rm nat} = 59$Hz, (b) $\nu^{\rm s} = \frac{3}{2}\nu^{\rm nat} = 265.5$Hz and (c) $\nu^{\rm s} = 2\nu^{\rm nat} = 354$Hz. The gray areas indicate the time interval in which the external oscillations may contribute to the generation of somatic spikes. At $t = 0$ synchronous activity is induced in the first layer. The upper panels show the spiking rate of neurons of the FFN in the presence of external oscillations (black solid). The firing rates for identical networks, where the oscillatory input stops at $t = 0$ are shown for comparison (green dashed). The lower panels show the spiking activity of the first nine layers (odd layers: red, even layers: blue). Other parameters are (a-c) $p_{\rm ex}^{\rm ext} = p_{\rm in}^{\rm ext} = 0.05$, $\sigma^{\rm s} = 0$ms, $\varepsilon_{\rm p}^{\rm ext} = 0.15$nS, $\varepsilon_{\rm m}^{\rm ext} = 0.4125$ and (a) $\varepsilon_{\rm c} = 1.3$nS, $N_{\rm e} = 900$, (b) $\varepsilon_{\rm c} = 1.0$nS, $N_{\rm e} = 600$ and (c) $\varepsilon_{\rm c} = 0.8$nS, $N_{\rm e} = 700$.

mth external oscillation coincides with the arrival of the synchronous pulse from the preceding layer at every nth group. Examples are shown in Figure 6.8 for frequency ratios $n : m = 3 : 1$ (the propagation at every third layer is supported by the external input), $n : m = 2 : 3$ (the propagation at every second layer is supported by the external input from every third oscillation) and $n : m = 1 : 2$ (every second oscillatory input coincides with the arrival of the synchronous pulse from the preceding layer).

Near the resonance frequencies the propagation frequency ν^{p} locks to the stimulation frequency ν^{s} (cf. Figure 6.7c gray areas). If the stimulation frequency increases above the resonance frequencies, synchrony propagation breaks down: Due to non-zero synaptic delay, initiation time of a dendritic spike and rise-time of the excitatory postsynaptic potential, there is a minimal time interval a signal needs to propagate from one layer to another. Thus, if the external stimulation frequency becomes too large, the inputs from the preceding layer arrive too late, i.e., outside the dendritic integration window ΔT^{s}, and therefore the additional inputs do not support propagation of synchrony as described above.

We only observe frequency lockings for small integers n, m. The number n counts the (minimal) number of layers a signal has to propagate in the absence of external simulations as the propagation of synchrony is supported by the oscillatory input only for every nth layer. For large n, however, the signal either propagates even in the absence of additional inputs (i.e., there is no need for supporting the signal propagation) or it has decayed after n layers and cannot be stabilized by external inputs. Large m imply high stimulation frequencies, and with increasing stimulation frequency the external input becomes more and more stationary in the sense that additional (oscillatory) inputs are delivered to the neurons of the FFN all the time. A propagation of synchrony may be enabled, but the signal does not lock to the stimulation frequency anymore (cf. Figure 6.7c).

Finally, we remark that we can describe the emergence of oscillation supported propagation of synchrony using methods introduced in Jahnke et al. (2012, 2013). In Appendix 6.5.2 we derive an analytical expression for the minimal amplitude of the oscillatory input, N_{e}^*, for which robust signal propagation is possible and compare the analytical predictions with numerical simulations (cf. Appendix 6.5.3).

6.3.5. Selecting transmission pathways by resonance

Networks with non-additive coupling exhibit resonance to oscillatory signals and this provides the possibility of specifically activating FFNs with different resonance frequencies. As we demonstrate below such resonant signal transmission establishes a mechanism to read out signals encoded in the structure of a recurrent network.

In how far do the results for pure feed-forward structures without recurrent connectivity can be generalized to recurrent systems as relevant for biological neural circuits? The main difference between isolated FFNs and recurrent FFNs is the emergence of a projection of the synchronous activity to all neurons of the network, not only to the neurons of the layer following the currently

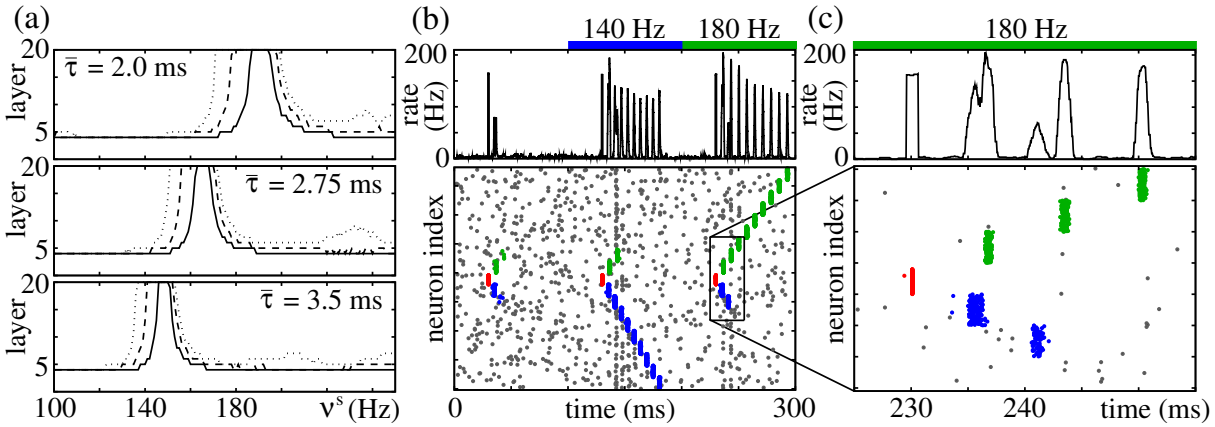

Figure 6.9: Activation of specific signal transmissions in FFNs with different resonance frequencies. (a) With increasing average coupling delays $\bar{\tau}$ (distribution width $\Delta\tau = 0.3$ms) resonance peaks (isolated FFN; $m = 20$, $\omega = 200$, $p_{\mathrm{ex}} = 0.05$, $\varepsilon_{\mathrm{c}} = 1.0$nS) are shifted to lower frequencies (cf. Equation 6.14). The panels show up to which layer a synchronous pulse propagates in the presence of balanced oscillations ($p_{\mathrm{ex}}^{\mathrm{ext}} = p_{\mathrm{in}}^{\mathrm{ext}} = 0.05$, $N_{\mathrm{e}} = 250$, $\varepsilon_{\mathrm{ex}}^{\mathrm{ext}} = 0.3$nS, $\varepsilon_{\mathrm{in}}^{\mathrm{ext}} = 0.825$nS, $\sigma^{\mathrm{s}} = 0.3$ms). The width of the resonance peaks increases with increasing size of the dendritic integration window (solid: $\Delta T^{\mathrm{s}} = 1.0$ms, dashed: $\Delta T^{\mathrm{s}} = 1.5$ms, dotted: $\Delta T^{\mathrm{s}} = 2.0$ms). (b) Raster plot of the spiking activity of a recurrent network ($N = 3800$, $p_{\mathrm{ex}} = p_{\mathrm{in}} = 0.05$, $\varepsilon_{\mathrm{ex}} = 0.2$nS, $\varepsilon_{\mathrm{in}} = 0.55$nS) which contains two FFNs ($m = 10$, $\omega = 200$, $\varepsilon_{\mathrm{c}} = 1.0$nS) which share the initial layer. Both FFNs have different average coupling delays ($\bar{\tau}_1 = 2.0$ms and $\bar{\tau}_2 = 3.5$ms; $\Delta\tau = 0.3$ms) and thus different resonance frequencies (cf. panel a); for the remaining connections the average coupling delays is $\bar{\tau} = 2.75$ms. Whereas a synchronous pulse extinguishes after a few layers in the absence of oscillations ($t = 30$ms), it may propagate along the layers of one FFN or the other depending on the stimulation frequency ($t = 130$ms and $t = 230$ms; $N_{\mathrm{e}} = 250$, $\varepsilon_{\mathrm{ex}}^{\mathrm{ext}} = 0.3$nS, $\varepsilon_{\mathrm{in}}^{\mathrm{ext}} = 0.825$nS, $\sigma^{\mathrm{s}} = 0.3$ms). Panel (c) is a close-up view of the raster plot shown in (b).

active one. For additively coupled networks this projection (similar to balanced oscillatory input) shifts the range of coupling strengths

$$\varepsilon_{\mathrm{c}} \in \left[\varepsilon_{\mathrm{L}}^{*}, \varepsilon_{\mathrm{L}}^{\mathrm{path}}\right] \tag{6.13}$$

for which a persistent propagation of synchrony is possible to larger connection strengths. The length of the interval, however, is unchanged (cf. Figure 6.11 in Appendix 6.5.3). For non-additively coupled networks, the critical connectivity $\varepsilon_{\mathrm{NL}}^{*}$ is largely unaffected, but with more and more prominent recurrent connections the pathological threshold $\varepsilon_{\mathrm{NL}}^{\mathrm{path}}$ decreases. For moderate recurrent connection strengths propagation of synchrony can be induced by oscillations also in recurrent networks without causing pathological activity; though if the connections are too large activity might spread not only from one layer to the next, but might propagate over the whole network ("synfire explosion" activity, Hehl, 2001; Mehring et al., 2003; Aviel et al., 2003). We investigate and discuss such recurrent systems in detail in Appendix 6.5.3

The main resonance frequency in non-additively coupled FFNs is given by the natural propagation frequency ν^{nat}. This frequency, however, is determined by the average time t^{sp} an arriving synchronous input at a given layer needs to trigger a somatic spike (cf. Section 6.3.1) and the average synaptic delay $\bar{\tau}$,

$$\nu^{\mathrm{nat}} \approx \frac{1}{t^{\mathrm{sp}} + \bar{\tau}}. \tag{6.14}$$

We illustrate this dependency in Figure 6.9a indicating the resonance peaks for different $\bar{\tau}$. Here, the coupling delays τ_{ij} between neurons of successive layers are drawn uniformly from an interval of length $\Delta\tau$ centered at $\bar{\tau}$,

$$\tau_{ij} \in \left[\bar{\tau} - \frac{\Delta\tau}{2}, \bar{\tau} + \frac{\Delta\tau}{2}\right]. \tag{6.15}$$

With increasing $\bar{\tau}$, the natural propagation frequency and thus the resonance peaks are shifted to smaller frequencies.

The width of the resonance peak is determined by the temporal spread of the propagating synchronous pulse itself, the temporal spread of the oscillatory inputs (σ^{s}; cf. also Appendix 6.5.2) and the width of the dendritic integration window ΔT^{s}. In particular, the width of the resonance peaks increases with increasing ΔT^{s} as shown in Figure 6.9a.

The existence of separated resonance peaks provides the possibility to specifically activate different signal transmission routes by oscillations of suitable frequencies. As a simple example consider a recurrent network containing two FFNs (cf. Figure 6.9b,c). The coupling delays between neurons of successive layers of the first FFN are centered at $\bar{\tau}_1 = 2.0\mathrm{ms}$, the coupling delays between neurons of successive layers of the second FFN are centered at $\bar{\tau}_2 = 3.5\mathrm{ms} > \bar{\tau}_1$. As before, the feed-forward couplings ε_{c} in both FFNs are too weak to enable a robust propagation of synchrony in the absence of external oscillations (cf. Figure 6.9b). Yet, external oscillations fitting to the resonance frequencies of the FFNs may enable robust propagation in one of the FFNs without activating the other. The close-up view in Figure 6.9c shows that indeed the propagation in both FFNs occur with different propagating frequencies.

6.4. Summary and discussion

Reliable and controlled transmission of signals is considered essential for computation in cortical networks. Propagation of synchronous activity along layered feed-forward networks may be one important way to realize such transmissions (Abeles, 1982; Diesmann et al., 1999; Kumar et al., 2010). Starting with a random recurrent network, feed-forward structures are assumed to be formed in a "training phase" previous to the recall of the learned sequences by, e.g., spike time dependent plasticity (Jun and Jin, 2007; Fiete et al., 2010; Waddington et al., 2012). Moreover, propagating synchronous pulse are also a candidate for generating precisely timed spike patterns in the millisecond range as observed in various neurophysiological studies (e.g., Abeles et al., 1993; Riehle et al., 1997; Johansson and Birznieks, 2004; Putrino et al., 2010).

Robust propagation, however, typically requires a highly prominent feed-forward anatomy, either in the sense of densely connected layers of neurons (Aviel et al., 2003; Mehring et al., 2003; Kumar et al., 2008a) or strongly increased connection strengths between neurons of successive layers (compared to remaining connections of the network) (Vogels and Abbott, 2005). Such prominent structures are experimentally not observed.

In this article we demonstrated that the presence of background oscillations can relax this requirement by supporting the propagating signal by additional external inputs. These additional inputs excite the neurons of the network (including the current target layer of the propagating synchronous pulse) and therefore enable a robust propagation with less inputs from the preceding layer. As a consequence robust signal transmission may emerge in networks with weaker couplings between the layers of the feed-forward network.

Such weaker structures, where the differences between feed-forward connections and remaining recurrent couplings are smaller, can be formed faster by synaptic plasticity (assuming a constant plasticity rate), i.e., the process of creating (and reconfiguring) information pathways is simplified. Alternatively, the background oscillations can enable robust signal transmission in feed-forward networks with reduced layer size (while keeping the coupling strengths fixed). We thus expect that this leads to an increase in the storage capacity of recurrent networks, because a reduced number of "memory-encoding" neurons is required for reliable signal propagation.

Experimental data suggests that there is a balance between excitatory and inhibitory input to single neurons in cortical networks during spontaneous and sensory-evoked activity (Haider et al., 2006; Okun and Lampl, 2008; Atallah and Scanziani, 2009). We therefore considered external oscillatory input, which is composed of an excitatory as well as an inhibitory component.

We find that for additively coupled networks only unbalanced external inputs that cause a net depolarization, support propagation of synchrony. Further, this support does not depend on the oscillatory nature of the input and could equally well be established by a temporally constant input current with the strength of the temporal mean input.

In contrast, for networks with non-additive couplings the ratio of the excitatory and inhibitory input is less important. In these networks propagation of synchrony is mainly mediated by dendritic spikes, which are elicited if the excitatory input within a short time interval exceeds

the dendritic threshold (Ariav et al., 2003; Polsky et al., 2004; Gasparini et al., 2004; Gasparini and Magee, 2006). Further, inhibition fails to suppress the generation of such dendritic spikes (Müller et al., 2012) and thus even inputs with a net hyperpolarizating effect support signal propagation. Due to the short dendritic integration window the timing of the external input is important, and thus only oscillatory inputs of a suitable frequency range can facilitate the propagation of synchrony. Whenever the ratio of the stimulating frequency and the "natural" propagation frequency of the feed-forward network is rational, resonances and locking patterns emerge. The resonance frequencies themselves are determined by the average conduction delays between the neurons of the FFN. This provides a mechanism to selectively activate different signaling pathways by oscillations of suitable frequency.

We conclude that fast dendritic spikes can support signal transmission in the form of propagation of synchrony in several ways: They specifically amplify activity that is synchronous, and thus enable a robust propagation in networks with moderate feed-forward anatomy even in the absence of oscillations (Jahnke et al., 2012, 2013). The amplification (i.e., the eliciting of dendritic spikes) itself depends on the excitatory inputs only. The propagation can be additionally supported by external oscillatory inputs independent of the balance of excitation and inhibition and their relative phase. Thus the occurrence of resonances enables specific information routing through recurrent networks.

Oscillations may arise from external sources (i.e., spatially separated oscillating networks), but also from the embedding network itself provided the network has a suitable topology (e.g., broad distribution of the number of synaptic connections, cf. Jahnke et al., 2014a). In the latter scenario, so-called hub-neurons can echo the propagating synchronous signal, start to oscillate and therefore provide an oscillatory (feed-back) input to the embedded feed-forward structure.

Dendritic spikes are prominently found in, e.g., the hippocampus (cf. Ariav et al., 2003; Gasparini et al., 2004; Müller et al., 2012; Makara and Magee, 2013, and others). In this cortical area spike patterns observed during spatial exploration are replayed during sleep or resting phases (e.g., Nadasdy et al., 1999; Lee and Wilson, 2002; Ji and Wilson, 2007; Davidson et al., 2009). Interestingly, this replay is accompanied by high frequency oscillations up to 200Hz (e.g., Ylinen et al., 1995; Csicsvari et al., 1999a; Maier et al., 2003). Our results suggest that the high-frequency oscillations may contribute to the stabilization of the replay of spike patterns.

Finally, we remark that the mechanism of signal transmission in terms of oscillation induced propagation of synchrony is not restricted to information processing by dendritic spikes in neural networks. As our analytical analysis reveals, the main prerequisite is the threshold-like processing of inputs of the single units of the network. We therefore expect that it may also be found in other networks of sharply nonlinear threshold units, which have been successfully applied to describe a variety of real-world phenomena, like the transmission of rate activities in neural networks (McCullogh-Pitts model, e.g., Nowotny and Huerta, 2003; Cayco-Gajic and Shea-Brown, 2013), (failure) cascades in social, supply or communication networks (e.g., Watts, 2002; Lorenz et al., 2009), or signaling in gene and protein networks (threshold Boolean networks, e.g., Bornholdt, 2008).

Acknowledgments

This work was supported by grants of the BMBF (Grant No. 01GQ1005B) [SJ, MT], the DFG (Grant No. TI 629/3-1) [SJ] and the Max Planck Society [MT]. Simulation results were obtained using the simulation software NEST Gewaltig and Diesmann (2007). We thank Harold Gutch, Hinrich Arnoldt, Paul Tiesinga, Elian Moritz and Jonna Jahnke for stimulating discussions.

6.5. Appendix

6.5.1. Standard neuron parameters

Throughout the article (for simplicity) we consider a homogeneous neuron population. The single neuron parameters are $C_i \equiv C = 400\text{pF}$, $V_i^{\text{reset}} \equiv V^{\text{reset}} = -65\text{mV}$, $V_i^{\Theta} \equiv V^{\Theta} = -50\text{mV}$, $g_i^{\text{L}} \equiv g^{\text{L}} = 25\text{nS}$, $V_i^{\text{eq}} \equiv V^{\text{eq}} = -55\text{mV}$ and $t_i^{\text{ref}} \equiv t^{\text{ref}} = 3\text{ms}$ (Andersen et al., 2007; Staff et al., 2000) for all i.

The time constants of the excitatory conductances (AMPA) are $\tau^{\text{ex},1} = 2.5\text{ms}$ and $\tau^{\text{ex},2} = 0.5\text{ms}$ (Jonas et al., 1993; Liu and Tsien, 1995). For simplicity we assume the same time constants for inhibitory conductances (GABA_A), $\tau^{\text{in},1} = \tau^{\text{ex},1} = 2.5\text{ms}$ and $\tau^{\text{in},2} = \tau^{\text{ex},2} = 0.5\text{ms}$. The reversal potentials are $E^{\text{ex}} = 0\text{mV}$ and $E^{\text{in}} = -75\text{mV}$ (Dayan and Abbott, 2001; Andersen et al., 2007). To obtain balanced recurrent (and external oscillatory) inputs, the ratio γ between excitatory and inhibitory couplings is chosen such that the peaks of single excitatory and inhibitory postsynaptic potentials equal each other when the inputs are received at resting membrane potential, i.e.,

$$\gamma = \frac{|V^{\text{eq}} - E^{\text{ex}}|}{|V^{\text{eq}} - E^{\text{in}}|} = 2.75 \tag{6.16}$$

for standard neuron parameters.

We consider sparsely connected networks (standard connection probability $p_{\text{ex}} = p_{\text{in}} = 0.05$) with homogenous coupling delays $\tau_{ij} \equiv \bar{\tau} = 2.5\text{ms}$ in Section 6.3.1-6.3.4 and with inhomogeneous coupling delay distribution in Section 6.3.5. Each neuron receives excitatory and inhibitory Poissonian spike trains with rates $\nu^{\text{ext,ex}} = \nu^{\text{ext,in}} = 2.4\text{kHz}$. Single inputs have strength $\varepsilon^{\text{ext,ex}} = 1\text{nS}$ and $\varepsilon^{\text{ext,in}} = 2.75\text{nS}$, respectively.

The parameters of the dendritic spike current are chosen according to single neuron experiments (e.g., Ariav et al., 2003; Polsky et al., 2004; Gasparini et al., 2004; Gasparini and Magee, 2006), $\Theta_b = 8.65\text{nS}$, $A = 55\text{nA}$, $B = 64\text{nA}$, $C = 9\text{nA}$, $\tau^{\text{ds},1} = 0.2\text{ms}$, $\tau^{\text{ds},2} = 0.3\text{ms}$, $\tau^{\text{ds},3} = 0.7\text{ms}$ and $t^{\text{ref,ds}} = 5\text{ms}$ (cf. also Memmesheimer, 2010; Jahnke et al., 2012). The standard value for the length of the dendritic integration window is $\Delta T^{\text{s}} = 2\text{ms}$; in Section 6.3.5 it is varied as indicated.

6.5.2. Analytical considerations

Under which conditions do oscillations induce a transition from a regime of non-robust to robust synchrony propagation? In particular, what is the (minimal) amplitude or the degree of synchrony required that allow for robust signal propagation?

To answer this question, we investigate the emergence of oscillation-supported propagation in FFNs with non-additive couplings analytically. We employ a self-consistency approach (cf. also methods introduced in Memmesheimer and Timme, 2012; Jahnke et al., 2012, 2013) to derive an

approximation of the iterated map for the average size of a synchronous pulse that propagates along the layers of an FFN. In particular, we find a scaling law for the amplitude of the external oscillations that enable stable propagation as a function of the system parameters and the dendritic nonlinearity.

Synchronous spiking of neurons in some layer causes a synchronous input to the neurons of the next layer. In the presence of oscillations of suitable frequency, e.g., $\nu^{\mathrm{s}} \approx \nu^{\mathrm{nat}}$, this input may be supported by inputs from the external oscillations. Then the total excitatory input

$$I = I_{\mathrm{e}} + I_{\mathrm{c}} \tag{6.17}$$

is the sum of inputs arising from external oscillations, I_{e}, and from the preceding layer, I_{c}. In networks with non-additive coupling, the spiking probability p^{sp} due to a synchronous input I below the dendritic threshold Θ_{b} is typically much smaller than due to a suprathreshold input (cf. Figure 6.3a). We thus assume that only neurons that receive a suprathreshold input ($I > \Theta_{\mathrm{b}}$) generate a spike with fixed probability p^*, i.e.,

$$p^{\mathrm{sp}}(I) := \begin{cases} p^* & \text{if } I \geq \Theta_{\mathrm{b}} \\ 0 & \text{if } I < \Theta_{\mathrm{b}} \end{cases}. \tag{6.18}$$

Thus, neurons process synchronous signals like simple threshold units, i.e., they generate no response for subthreshold inputs and a fixed response for suprathreshold inputs. For clarity of presentation, we assume that the firing probability p^* is fixed. In general it might be reduced by inhibitory input, but the extension is straightforward and leads to similar results (cf. also Jahnke et al., 2014a).

The timing of somatic spikes initiated by dendritic spikes is highly precise, i.e., the temporal distribution of somatic spikes triggered by dendritic ones is very narrow (cf. Figure 6.4a), in the sub-millisecond range (cf. also Ariav et al., 2003). In particular, the jitter in time is typically much smaller than the dendritic integration window ΔT^{s}. This let us assume that a synchronous pulse packet in one layer causes synchronous spiking within a time interval smaller than ΔT^{s} in the next layer and so on.

In the following we calculate the probability density function $f_I(I)$ for the total excitatory input I to the neurons of a given layer conditioned on (i) the number of synchronously spiking neurons in the previous layer, g^{in}, and (ii) the amplitude of external oscillations, N_{e}. Then, the average number of synchronously spiking neurons in the considered layer is

$$g^{\mathrm{out}} = \omega \int_0^\infty p^{\mathrm{sp}}(I) f_I(I|g^{\mathrm{in}}, N_{\mathrm{e}}) dI \tag{6.19}$$

$$= \omega p^* \int_{\Theta_{\mathrm{b}}}^\infty f_I(I|g^{\mathrm{in}}, N_{\mathrm{e}}) dI. \tag{6.20}$$

First we consider the input from the previous layer. Given the random topology of the FFN, the probability that a neuron receives exactly k (out of the maximal number g^{in}) inputs is binomially distributed,

$$p(k) = \binom{g^{\mathrm{in}}}{k} (p_{\mathrm{ex}})^k (1 - p_{\mathrm{ex}})^{g^{\mathrm{in}} - k}. \tag{6.21}$$

For a sufficiently large number g^{in} of neurons participating in the synchronous pulses, we can approximate the binomial distribution (6.21) by a Gaussian distribution and thus the excitatory synchronous input follows

$$I_{\text{c}} = k\varepsilon_{\text{c}} \sim \mathcal{N}\left(\mu_{\text{c}}, \sigma_{\text{c}}^2\right) \tag{6.22}$$

with mean

$$\mu_{\text{c}} = \varepsilon_{\text{c}} g^{\text{in}} p_{\text{ex}} \tag{6.23}$$

and standard deviation

$$\sigma_{\text{c}} = \varepsilon_{\text{c}} \sqrt{g^{\text{in}} p_{\text{ex}} \left(1 - p_{\text{ex}}\right)}. \tag{6.24}$$

Likewise, the number of excitatory inputs l each neuron receives within one oscillation period from the external (virtual) neuron population is binomially distributed, $l \sim B\left(N_{\text{e}}, p_{\text{ex}}^{\text{ext}}\right)$ (cf. Section 6.2.6). The arrival times are drawn from a Gaussian distribution with standard deviation σ^{s}. We assume that propagation of synchrony in the FFN and the external oscillations are in-phase. Then for $\sigma^{\text{s}} > 0$ the fraction

$$p_{\Delta T^{\text{s}}} = \int_{-\frac{\Delta T^{\text{s}}}{2}}^{\frac{\Delta T^{\text{s}}}{2}} \frac{1}{\sqrt{2\pi}\sigma^{\text{s}}} \exp\left[-\frac{1}{2}\left(\frac{\tau}{\sigma^{\text{s}}}\right)^2\right] d\tau \tag{6.25}$$

$$= \text{Erf}\left(\frac{\Delta T^{\text{s}}}{\sqrt{8}\sigma^{\text{s}}}\right) \tag{6.26}$$

of the additional inputs arrive within the dendritic integration window ΔT^{s} and can support the generation of dendritic spikes. For $\sigma^{\text{s}} = 0$, all inputs are received synchronously and thus $p_{\Delta T^{\text{s}}} = 1$; for non-zero σ^{s} the effective size of the external oscillation (i.e., the effective average number of neurons that may contribute to the generation of dendritic spikes) is

$$N_{\text{e}}^{\text{eff}} = p_{\Delta T^{\text{s}}} N_{\text{e}}, \tag{6.27}$$

and the number of excitatory inputs from the oscillatory neuron population is distributed according to $l \sim B\left(N_e^{\text{eff}}, p_{\text{ex}}^{\text{ext}}\right)$.

For sufficiently large $N_{\text{e}}^{\text{eff}}$, one can again use a Gaussian approximation which yields

$$I_{\text{e}} \sim \mathcal{N}\left(\mu_{\text{e}}, \sigma_{\text{e}}^2\right) \tag{6.28}$$

with

$$\mu_{\text{e}} = \varepsilon_{\text{p}}^{\text{ext}} N_{\text{e}}^{\text{eff}} p_{\text{ex}}^{\text{ext}} \quad \text{and} \quad \sigma_{\text{e}} = \varepsilon_{\text{p}}^{\text{ext}} \sqrt{N_{\text{e}}^{\text{eff}} p_{\text{ex}}^{\text{ext}} \left(1 - p_{\text{ex}}^{\text{ext}}\right)}. \tag{6.29}$$

The sum of the inputs I_{e} and I_{c} is then also approximately Gaussian distributed,

$$I = I_{\text{e}} + I_{\text{c}} \sim \mathcal{N}\left(\mu, \sigma^2\right), \tag{6.30}$$

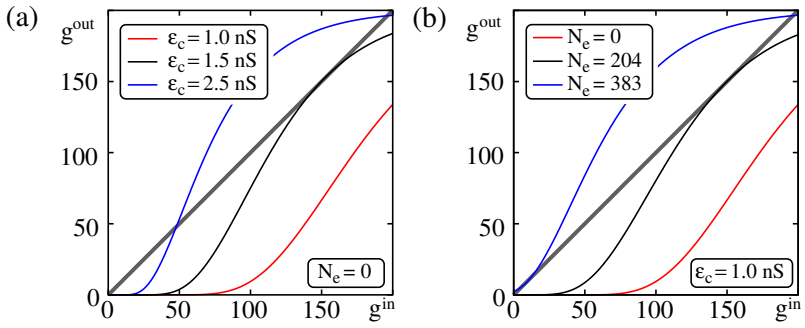

Figure 6.10: Map yielding the temporal evolution of the average size of a synchronous pulse in an FFN with non-additive coupling (cf. Equation 6.33; $\omega = 200$, $p_{\mathrm{ex}} = 0.05$, $\Theta_{\mathrm{b}} = 8.65$nS). (a) N_e =0 (absence of external oscillations), different colors indicate different coupling strength ε_{c}. (b) The coupling strength $\varepsilon_{\mathrm{c}} = 1.0$nS is fixed and external oscillations ($p_{\mathrm{ex}}^{\mathrm{ext}} = 0.05$, $\varepsilon_{\mathrm{p}}^{\mathrm{ext}} = 0.3$nS, $\sigma^{\mathrm{s}} = 0$ms) are present, different colors indicate different N_{e}. With increasing (a) connection strength ε_{c} or increasing (b) oscillation amplitude N_{e}, two fixed points emerge by a tangent bifurcation. This bifurcation point marks the transition from a regime where no propagation is possible to a regime where persistent propagation of synchrony can be achieved (cf. also Figure 6.3b).

with mean $\mu = \mu_{\mathrm{e}} + \mu_{\mathrm{c}}$ and variance $\sigma^2 = \sigma_{\mathrm{e}}^2 + \sigma_{\mathrm{c}}^2$, i.e.,

$$\mu = \varepsilon_{\mathrm{p}}^{\mathrm{ext}} N_{\mathrm{e}}^{\mathrm{eff}} p_{\mathrm{ex}}^{\mathrm{ext}} + \varepsilon_{\mathrm{c}} g^{\mathrm{in}} p_{\mathrm{ex}} \tag{6.31}$$

and

$$\sigma = \sqrt{\left(\varepsilon_{\mathrm{p}}^{\mathrm{ext}}\right)^2 N_{\mathrm{e}}^{\mathrm{eff}} p_{\mathrm{ex}}^{\mathrm{ext}} \left(1 - p_{\mathrm{ex}}^{\mathrm{ext}}\right) + \varepsilon_{\mathrm{c}}^2 g^{\mathrm{in}} p_{\mathrm{ex}} \left(1 - p_{\mathrm{ex}}\right)}. \tag{6.32}$$

Using the distribution (6.30) of I allows us to specify the iterated map for the average size of a synchronous pulse according to Equation (6.20),

$$g^{\mathrm{out}} = \frac{\omega p^*}{2} \left(1 + \mathrm{Erf}\left[\frac{\mu - \Theta_{\mathrm{b}}}{\sqrt{2}\sigma}\right]\right), \tag{6.33}$$

where the size of the initial pulse packet g^{in} appears as argument of μ and σ (see Equations 6.31 and 6.32).

As explained in Section 6.3.1 (cf. Equation 6.10), the fixed points $G^* = g^{\mathrm{out}} = g^{\mathrm{in}}$ of Equation (6.33) determine the stability of the propagation of a synchronous pulse. With increasing coupling strength two fixed points emerge via a tangent bifurcation (Figure 6.10a; cf. also Figure 6.3b), and external oscillations have a similar effect (Figure 6.10b). This transition enables robust propagation of synchrony, and the external oscillations thus reduce the critical connection strength $\varepsilon_{\mathrm{NL}}^*$ (i.e., the minimal coupling strength for which robust signal propagation is possible).

For a given network setup, $N_{\mathrm{e}} = N_{\mathrm{e}}^*$ specifies the minimal size of the external oscillation which enables stable propagation of synchrony. It can be found by numerically determining the bifurcation point of Equation (6.33). Additionally, one can derive a scaling law for N_{e}^* based on two observations:

1. In the absence of external oscillations ($N_\mathrm{e} = 0$), the position of the bifurcation point of Equation (6.33) depends on the coupling strength ε_c and the dendritic threshold Θ_b only via the quotient

$$\kappa := \frac{\Theta_\mathrm{b}}{\varepsilon_\mathrm{c}}, \tag{6.34}$$

which is the number of spikes from the preceding layer that are needed to elicit a dendritic spike. Equation (6.33) reads

$$g^\mathrm{out} = \frac{\omega p^*}{2}\left(1 + \mathrm{Erf}\left[\frac{g^\mathrm{in} p_\mathrm{ex} - \kappa}{\sqrt{2 g^\mathrm{in} p_\mathrm{ex}\left(1 - p_\mathrm{ex}\right)}}\right]\right). \tag{6.35}$$

For a given network setup, the connection probability p_ex, group size ω and spiking probability p^* (which is determined by the ground state and the parameters of the dendritic spike) are fixed. Thus the bifurcation point where the fixed points $G_1^* = G_2^* = g^\mathrm{out} = g^\mathrm{in}$ appear by a tangent bifurcation, depends solely on κ (the only unknown quantity). Consequently, there is some $\kappa^* = \kappa$ specifying this bifurcation point, i.e., the transition point from non-propagating to propagating regime depends just on the number of spikes necessary to elicit a dendritic spike. The actual value κ^* can be found either by numerical simulation of the system, numerical solution of Equation (6.35) or by the analytical methods introduced in Jahnke et al. (2012, 2013).

2. The main influence of external oscillatory inputs is an effective reduction of the dendritic threshold Θ_b, such that the properties of the system described above can be approximated by a network without external oscillatory input, but with a reduced dendritic threshold $\Theta_\mathrm{b}^\mathrm{eff} < \Theta_\mathrm{b}$: In the setups considered the additional oscillatory input contributes to the generation of dendritic spikes, but the main contribution arises from the input arriving from the previous layer (the signal to be propagated), i.e., $\mu_\mathrm{e} < \mu_\mathrm{c}$. Moreover, the feed-forward connections ε_c are enhanced compared to the remaining excitatory couplings, $\varepsilon_\mathrm{p}^\mathrm{ext} < \varepsilon_\mathrm{c}$. Thus the total variation of the input $\sigma = \sigma_\mathrm{e}^2 + \sigma_\mathrm{c}^2$ (cf. Equation 6.32) is dominated by the contribution σ_c^2 of the input from the previous layer,

$$\varepsilon_\mathrm{p}^\mathrm{ext}\mu_e\left(1 - p_\mathrm{ex}^\mathrm{ext}\right) < \varepsilon_\mathrm{p}\mu_\mathrm{c}\left(1 - p_\mathrm{ex}\right) \tag{6.36}$$

$$\sigma_e^2 < \sigma_\mathrm{c}^2. \tag{6.37}$$

In particular for $\varepsilon_\mathrm{p}^\mathrm{ext} \ll \varepsilon_\mathrm{c}$ the contribution of the external inputs to the total variation of the input becomes negligible, i.e., $\sigma_\mathrm{e}^2 \ll \sigma_\mathrm{c}^2$, and the argument of the error function in Equation (6.33) simplifies to

$$\frac{\mu - \Theta_\mathrm{b}}{\sqrt{2}\sigma} = \frac{\mu_\mathrm{c} + \mu_\mathrm{e} - \Theta_\mathrm{b}}{\sqrt{2\left(\sigma_\mathrm{c}^2 + \sigma_\mathrm{e}^2\right)}} \tag{6.38}$$

$$\approx \frac{\mu_\mathrm{c} - \Theta_\mathrm{b}^\mathrm{eff}}{\sqrt{2}\sigma_\mathrm{c}} \tag{6.39}$$

where we defined the effective dendritic threshold

$$\Theta_\mathrm{b}^\mathrm{eff} := \Theta_\mathrm{b} - \mu_\mathrm{e}. \tag{6.40}$$

The above observations indicate that the bifurcation point is found for some constant

$$\kappa^* = \frac{\Theta_{\mathrm{b}}^{\mathrm{eff}}}{\varepsilon_{\mathrm{c}}} = \frac{\Theta_{\mathrm{b}} - \mu_{\mathrm{e}}}{\varepsilon_{\mathrm{c}}}, \tag{6.41}$$

such that the minimal size of the external oscillations N_{e}^*, which enables propagation of synchrony, is given by (using Equations 6.29, 6.27 and 6.26)

$$N_e^* = \mathrm{Erf}\left[\frac{\Delta T^{\mathrm{s}}}{\sqrt{8}\sigma^{\mathrm{s}}}\right]^{-1} \frac{\Theta_b - \varepsilon_{\mathrm{c}}\kappa^*}{\varepsilon_{\mathrm{p}}^{\mathrm{ext}} p_{\mathrm{ex}}^{\mathrm{ext}}}. \tag{6.42}$$

Equation (6.42) indicates that N_{e}^* changes linearly with the coupling strength ε_{c} (cf. Figure 6.5 and 6.6). Further it is inversely proportional to the coupling strength between the external oscillatory population and the neurons of the FFN, $N_{\mathrm{e}}^* \propto 1/\varepsilon_{\mathrm{p}}^{\mathrm{ext}}$, and the dependence of N_{e}^* on the temporal spread σ^{s} of the external oscillations is determined by the prefactor $1/p_{\Delta T^{\mathrm{s}}}$.

The above results are derived for isolated FFNs. However, we will show and discuss in the following Appendix 6.5.3 that the results hold in good approximation also for FFNs that are part of recurrent networks.

6.5.3. Synchrony propagation in recurrent FFNs

For clarity of presentation, in this article we focus mainly on isolated FFNs (i.e., $\varepsilon_{\mathrm{m}} = \varepsilon_{\mathrm{p}} = 0$; only feed-forward connection are present; cf. Sections 6.3.1-6.3.4). However, FFNs which are part of a random recurrent network show qualitatively the same dynamics as isolated ones as we demonstrate in this section. We consider recurrent FFNs where all neurons of the network are assigned to be a member of exactly one layer, i.e., $N = m\omega$ (cf. Figure 6.11a). In the first subsection we consider propagation of synchrony in front of a homogeneous background activity, and afterwards, in the second subsection, we study the impact of external oscillations. We investigate the influence of network parameters, discuss the differences to isolated FFNs and compare the results of network simulations with the analytical predictions presented in Appendix 6.5.2.

Homogenous background activity

What is the impact of recurrent connections on propagation of synchrony? Do recurrent connections within the FFN alter its propagation efficiency?

To gain some insight into the dynamics of recurrent FFNs, we start with isolated FFNs ($\varepsilon_{\mathrm{p}} = \varepsilon_{\mathrm{m}} = 0$, as before) and gradually increase the recurrent coupling strengths ε_{p} and ε_{m}. We keep the ratio of the coupling strengths ε_{p} and ε_{m} balanced (i.e., $\varepsilon_{\mathrm{m}} = \gamma \cdot \varepsilon_{\mathrm{p}}$, cf. Section 6.2.4), such that the mean additional input to each neuron arising from recurrent connections is approximately zero and the network remains in the balanced state (v. Vreeswijk and Sompolinsky, 1996, 1998; Brunel, 2000).

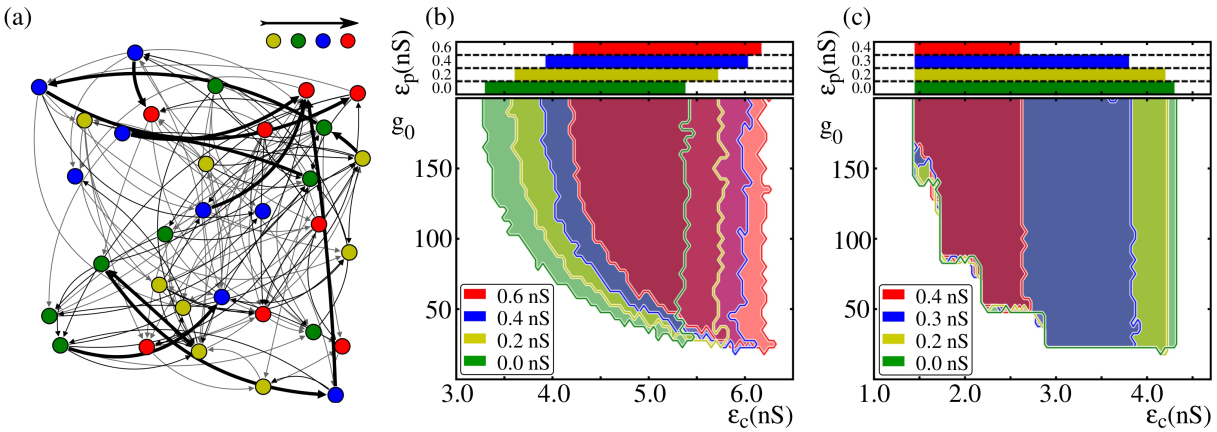

Figure 6.11: Propagation of synchrony in embedded FFNs. (a) Scheme of the network setup: We show an example network of 32 neurons that are assigned to 4 consecutive layers (yellow→green→blue→red). The arrows indicate connections between neurons (excitatory: black; inhibitory: gray), their thickness highlights the connection strength (thin arrows: ε_p and ε_m; thick arrows: feed-forward couplings ε_c, with increased strength). The connectivity between neurons of successive layers equals the overall connectivity. (b,c) Upper panel: Illustration of the range of coupling strengths ε_c between the layers of the FFN that allow for a robust and non-pathological propagation of synchrony in recurrent networks ($N = 3000$, $m = 15$, $\omega = 200$, $p_{ex} = p_{in} = 0.05$) with (b) linear and (c) nonlinear dendritic interactions for different recurrent connection strengths ε_p (color coded; $\varepsilon_m = 2.75\varepsilon_p$). The lower panel shows the region of successful propagation (horizontal axis: size of the initial synchronous pulse, g_0; vertical axis: feed-forward coupling strength ε_c).

For networks with linear dendritic interactions, the critical connection strength ε_L^* (the minimal coupling strength ε_c for which a robust propagation of synchrony is possible) as well as the pathological connection strength ε_L^{path} (the maximal coupling strength ε_c for which a non-pathological propagation of synchrony is possible) increases with increasing recurrent connection strength ε_p and ε_m. However, the length of the interval $\left[\varepsilon_L^*, \varepsilon_L^{path}\right]$ is only weakly affected (cf. Figure 6.11b).We note that the additional input arising from the projection of the synchronous pulse in one layer to the whole network (instead of only to the following layer) is similar to the input originating from balanced external oscillations (cf. also Figure 6.5) and this additional balanced inputs decrease the excitability of the neurons by lowering the effective membrane time constant (cf. Section 6.3.2 and Destexhe et al., 2003; Kuhn et al., 2004).

In contrast, in networks with nonlinear dendritic interactions, where propagation of synchrony is mainly mediated by dendritic spikes, recurrent connections influence the critical connection strength ε_{NL}^* only weakly (cf. Figure 6.11c): In principle, the additional inputs arising from recurrent connections support the generation of dendritic spikes as additional excitatory inputs effectively lower the dendritic threshold Θ_b, and therewith decrease ε_{NL}^* (compare also the analytical considerations in Appendix 6.5.2). However, in the ground-state the neurons of the recurrent network spike asynchronously with a low rate and therefore the additional excitatory input to each neuron within the dendritic integration window ΔT^s is small compared to the

dendritic threshold Θ_b.

However, recurrent connections decrease the pathological connection strength $\varepsilon_\mathrm{NL}^\mathrm{path}$, above which propagation of synchrony causes pathological network states: In recurrent FFNs all neurons, not only the neurons belonging to one specific layer, receive synchronous inputs if a synchronous pulse packet propagates along the layers of an FFN. Thus each neuron which is not member of the currently active layer receives an additional (compared to the isolated FFN) input, the projection of the synchronous activity. The average strength of the excitatory part of the input during persistent propagation is given by

$$I^\mathrm{add} = g^* p_\mathrm{ex} \varepsilon_\mathrm{p} \lessapprox \omega p_\mathrm{ex} \varepsilon_\mathrm{p}, \tag{6.43}$$

where g^* denotes the average size of the propagating pulse and $g^* \approx G_2^*$ with the stable fixed point G_2^* of the iterated map (6.33) (cf. also Equation 6.10). I^add effectively decreases the dendritic threshold, i.e., even for neurons that do not belong to the next layer the amount of synaptic input needed to elicit a dendritic spike is reduced by propagation of synchrony. This can become detrimental for information processing: In combination with inputs arising from spontaneous activity the additional input may induce synchronous spiking in currently non-active layers and the synchronous pulse starts to spread over the whole network causing pathological activity ('synfire explosion', cf. Mehring et al., 2003). Thus recurrent connections within the FFN decrease the length of the interval $\left[\varepsilon_\mathrm{NL}^*, \varepsilon_\mathrm{NL}^\mathrm{path}\right]$ of coupling strengths for which a non-pathological propagation of synchrony is possible (cf. Figure 6.11c).

Background oscillations

External oscillations can induce robust synchrony propagation in networks with recurrent connections. The underlying mechanism is the same as in isolated chains. The amplitude $N_\mathrm{e}^\mathrm{path}$ of external oscillation above which the system enters pathological dynamics is reduced by recurrent connections. The critical amplitude N_e^* for which the transition from non-propagating to oscillation induced propagation of synchrony occurs, however, is largely unaffected. Moreover, the analytical considerations for N_e^* derived in Appendix 6.5.2 are in good approximations also for recurrent FFNs.

In this section we consider recurrent FFNs as introduced above and assume that the connectivity between the external oscillating (virtual) neuron population and the neurons of the network is statistically identical to the recurrent connectivity in the network itself, i.e., $\varepsilon_\mathrm{p} = \varepsilon_\mathrm{p}^\mathrm{ext}$, $\varepsilon_\mathrm{m} = \varepsilon_\mathrm{m}^\mathrm{ext}$, $p_\mathrm{ex} = p_\mathrm{ex}^\mathrm{ext}$ and $p_\mathrm{in} = p_\mathrm{in}^\mathrm{ext}$.

According to Equation (6.42) we expect a linear relationship between the excitatory feed-forward coupling strength ε_c and the amplitude N_e^*. Indeed, we observe such a relation in isolated (Figure 6.5b,d) as well as in recurrent FFNs (Figure 6.12a). The impact of recurrent connections on N_e^* is negligible (as discussed above) and Equation (6.42) well predicts the scaling of N_e^* (dashed line in Figure 6.12a).

However, the presence of recurrent connections lowers the threshold for pathological activity, N_e^path: In absence of recurrent connections ($\varepsilon_\mathrm{p} = \varepsilon_\mathrm{m} = 0$) an external oscillation of size

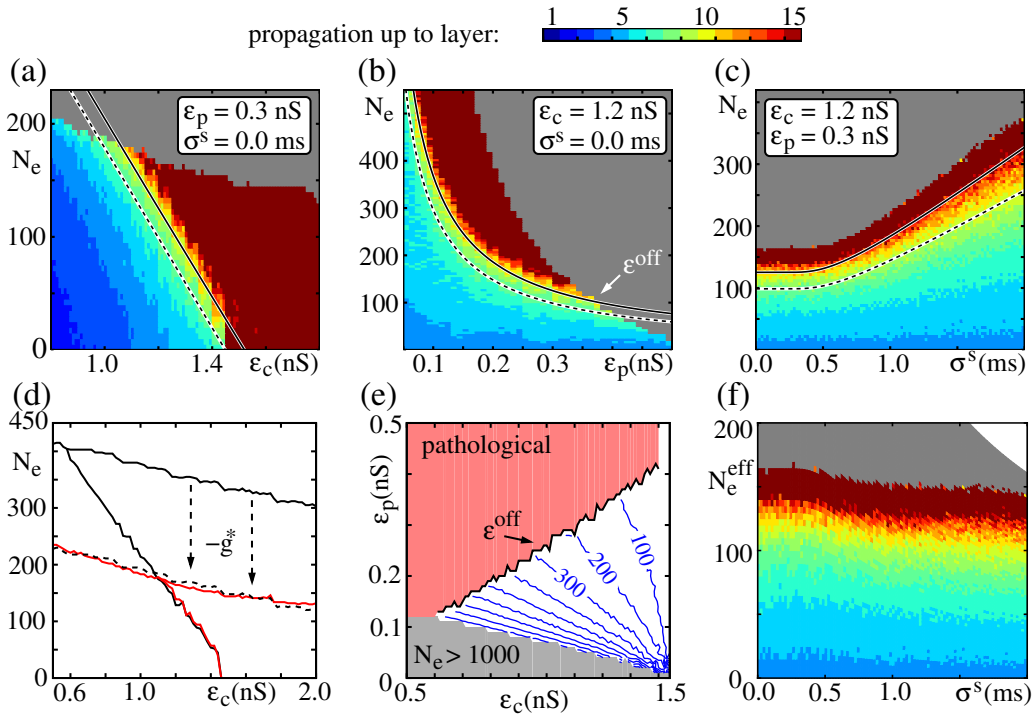

Figure 6.12: Oscillation induced propagation of synchrony in recurrent FFNs ($m = 15$, $\omega = 200$, $p_{ex} = p_{in} = 0.05$). Panels (a-c) show up to which layer a synchronous pulse propagates in the presence of external network oscillations (cf. also Fig. 6.5d). The lines indicate the estimated critical amplitude N_e^*, above which propagation of synchrony is enabled, derived from Equation (6.33) (solid; numerical solution of the fixed point equation) and Equation (6.42) (dashed). Gray areas indicate parameter sets causing pathological activity. The individual panels show the amplitude of the external oscillations vs. (a) the feed-forward connectivity ε_c, (b) the recurrent connectivity $\varepsilon_p = \varepsilon_p^{ext}$ and (c) the width of the external oscillations ν^s (other parameters are fixed with values displayed in the insets). In panel (d) we compare N_e^* and N_e^{path} for recurrent FFNs (red solid line; same data as in panel a) and isolated FFNs (black solid line, $\varepsilon_p^{ext} = \varepsilon_m^{ext} = 0$). The black dashed line indicates the pathological threshold N_e^{path} for isolated FFNs reduced by the average size g^* of a (stable) propagating synchronous pulse. Panel (e) shows the region of recurrent coupling strengths, $\varepsilon_p = \varepsilon_p^{ext}$, and feed-forward coupling strengths, ε_c, for which propagation of synchrony is possible (white area) or causes pathological activity (red area). The separation line is denoted by ε^{off} (cf. panel b). The blue lines indicate the contour lines of $N_e^* = \{100, 200, \ldots, 900\}$. For setups where $N_e^* > 1000$ due to limitations of computing capabilities no simulations are performed (gray area). (f) Same data as in panel (c), but with rescaled (effective) size N_e^{eff} of external oscillations (cf. Equation 6.27).

$N_e \geq N_e^{\text{path}}$ causes pathological activity (cf. Figure 6.5b,d). Here, in the presence of recurrent connections all neurons 'feel' the propagating synchronous signal through recurrent projections. The recurrent input resembles an external oscillatory input of size g^* (where g^* is the average size of the propagating synchronous pulse packet) with coupling strengths $\varepsilon_{\text{p}}^{\text{ext}} = \varepsilon_{\text{p}}$ and $\varepsilon_{\text{m}}^{\text{ext}} = \varepsilon_{\text{m}}$. Thus, the threshold for pathological activity N_e^{path} is reduced by the average size of the propagation pulse packet g^*, $N_e^{\text{path}} \to N_e^{\text{path}} - g^*$ as illustrated in Figure 6.12d.

Further, Equation (6.42) indicates that N_e^* is inversely proportional to the excitatory coupling strength $\varepsilon_{\text{p}}^{\text{ext}}$. Indeed, for small $\varepsilon_{\text{p}}^{\text{ext}}$ large amplitudes N_{e} of oscillations are required to enable propagation of synchrony and with increasing $\varepsilon_{\text{p}}^{\text{ext}}$ smaller and smaller amplitudes of oscillations are sufficient (cf. Figure 6.12b). At the same time the threshold for pathological activity decreases: By increasing the excitatory connection strengths ε_{p} and $\varepsilon_{\text{p}}^{\text{ext}}$ both (i) the impact of the projection of the propagating synchronous pulse and (ii) the impact of external oscillations increase. For sufficiently large recurrent coupling strengths the threshold for pathological activity, N_e^{path}, decreases below the critical oscillation amplitude, $N_e^{\text{path}} \leq N_e^*$. The sum of the projection of the propagating synchronous signal and the external oscillation becomes large and even spontaneous spiking activity is sufficient to trigger more and more spikes in the network and thus cause pathological activity ('synfire-explosion'). For given coupling strength ε_{c} between the layers of the FFN there is a maximal recurrent coupling strength ε^{off}, such that for $\varepsilon_{\text{p}} = \varepsilon_{\text{p}}^{\text{ext}} \geq \varepsilon^{\text{off}}$, no meaningful, i.e., non-pathological, propagation of synchrony is possible (cf. Figure 6.12b). In Figure 6.12e we illustrate the region of coupling strengths ($\varepsilon_{\text{p}} = \varepsilon_{\text{p}}^{\text{ext}}$ and ε_{c}) for which a robust propagation of synchrony can be achieved given that an external oscillation of suitable size is present. In particular, it turns out that the maximal recurrent coupling strength ε^{off} depends linearly on the feed-forward coupling strength ε_{c} between the layers of the FFN.

Finally, Equation (6.42) predicts that N_{e}^* is related to the temporal width σ^{s} of the external oscillations via the factor $p_{\Delta T^{\text{s}}}$ (cf. Equation 6.26). As discussed in Appendix 6.5.2, the effective size N_e^{eff} of the external oscillation decreases with increasing σ^{s} (cf. Equation 6.27). Consequently, the critical size N_e^* and the pathological threshold N_e^{path} increase. However, the length of the interval $\left[N_e^*, N_e^{\text{path}}\right]$, i.e., the size of the interval of oscillation amplitudes that enable persistent propagation of synchrony, stays almost constant (Fig. 6.12c,f).

Chapter 7

Towards a unified model for Sharp-Wave-Ripples and replay

Citation

Jahnke, S., Timme, M. and Memmesheimer, R.-M. (2014), Towards a unified model for Sharp-Wave-Ripples and replay.

This chapter is an earlier version of the article:
Jahnke, S., Timme, M. and Memmesheimer, R.-M. (2015), A Unified Dynamic Model for Learning, Replay and Sharp-Wave/Ripples, which is currently under review at *J. Neurosci.*

Original contribution

Conception and design of the study together with M. Timme and R.-M. Memmesheimer. I performed the analytical calculations and numerical simulations. For the simulations I implementated neuron models within the NEST simulation environment (www.nest-initiative.org). I analyzed the data and prepared all figures. I wrote main parts of the manuscript supported by M. Timme and R.-M. Memmesheimer.

Göttingen, 31.03.2014
Place, Date

Sven Jahnke

Abstract

The hippocampus is crucially involved in episodic memory formation and consolidation. Consolidation takes place during Sharp-Wave-Ripple complexes (SPW/Rs) which are short episodes of highly increased hippocampal activity with superimposed high-frequency oscillations. Additionally, previously learned spike sequences reflecting behavior, e.g., traversed trajectories in space, are replayed. The neurophysiological mechanisms underlying this activity patterns are not yet well understood. In the present article, we derive a unifying model showing how experience may be stored and thereafter be replayed in conjunction with SPW/Rs. In the proposed model, the generation of the sharp wave activity itself, the ripples and the replay are all based on dendritic sodium spikes and therefore are intimately interrelated. These spikes, prominently found in the basal dendrites of pyramidal neurons, selectively amplify highly synchronous presynaptic inputs, and thus enable replay of spike sequences even in very sparsely connected networks like the CA1. Somatic spikes elicited by dendritic ones are very precise, and the typical time difference between presynaptic spiking and postsynaptic spiking caused by dendritically amplified inputs predicts the ripple frequency of about 200Hz. The wave-form of the SPW/Rs is determined by an initial increase of synchronous activity supported by dendritic spike generation, and a subsequent decrease of activity by inhibitory feed-back, which eventually terminates the event.

7.1. Introduction

The interest in spatial processing and memory in the hippocampus, has been driven to a large extent by the observation of hippocampal "place cells": During exploratory behavior they signal by their spiking the position of an animal in the environment (O'Keefe and Dostrovsky, 1971; O'Keefe, 1976; Ekstrom et al., 2003; Kjelstrup et al., 2008; Harvey et al., 2009). Exploration is accompanied by theta oscillations, rhythmic modulations in neural population activity and in the local field potential (LFP) with frequencies of $4 - 10$Hz. When several places are visited, sequences of spiking activity emerge within the theta cycles due to preferred place cell firing relative to the phase of the theta oscillation (O'Keefe and Recce, 1993; Skaggs et al., 1996; Maurer and McNaughton, 2007; Gupta et al., 2012). These reflect the recent past and future place field traversing, compressed in time. The sequences of activity are replayed in a further compressed manner, while the animal rests and sleeps (Wilson and McNaughton, 1994; Nadasdy et al., 1999; Lee and Wilson, 2002; Pastalkova et al., 2008; Davidson et al., 2009). This happens during so-called sharp-wave-ripple events (SPW/Rs), short phases of strongly enhanced activity ("sharp waves", durations of about 50-100ms) with highly synchronous spiking at about 120-200Hz ("ripples") (Buzsáki et al., 1992; Ylinen et al., 1995; Maier et al., 2003).

SPW/Rs and the associated replay are assumed to be crucial for memory consolidation (Buzsáki, 1989). Indeed, the replay reflects activity from exploration phases (Wilson and McNaughton, 1994; Nadasdy et al., 1999; Lee and Wilson, 2002; Pastalkova et al., 2008; Davidson et al., 2009), the inter-ripple-interval of 5ms is in the optimal range for the induction of synaptic modifications (Markram et al., 1997; Bi and Poo, 1998), SPW/Rs occur coordinated with activation across neocortical brain regions (Ji and Wilson, 2007; O'Neill et al., 2010; Logothetis et al., 2012), and

suppression of SPW/Rs impairs memory consolidation (Girardeau et al., 2009; Ego-Stengel and Wilson, 2010; Jadhav et al., 2012). The "two-stage model" for memory (Marr, 1971; Willshaw and Buckingham, 1990), assumes that SPW/Rs and replay lead to the consolidation of memory content by transferring it from preliminary storage in the hippocampus to long-term storage in the neocortex (Buzsáki, 1989). It has also been suggested that SPW/Rs and replay are involved in incorporation of new information into existing contexts, associating and processing previous experiences, planning of future behavior and deleting memories from hippocampal storage (O'Keefe and Nadel, 1978; Buzsáki, 2006; Tse et al., 2007; Mehta, 2007; Gupta et al., 2010; Pfeiffer and Foster, 2013). To assess whether and how the different assumed tasks can be fulfilled, it is essential to understand the mechanisms underlying SPW/R patterns and the replay.

Sequence learning and sequence generation

Previous modeling studies mainly focused on the encoding part of sequence generation and did not consider biological plausible SPW/R-like activity. In a series of articles, W. Levy and coworkers have explored characteristics of sequence learning and later, time compressed recall, on different levels of abstraction (Levy, 1996; August and Levy, 1999; Sullivan and Levy, 2004). Most related to our study, August and Levy (1999) consider a population of spiking, leaky integrate-and-fire neurons with excitatory connections and overall averaged inhibition. In an exploration phase, part of the neuron population is sequentially stimulated, and as a consequence of learning also the unstimulated neurons become sensitive to a specific stimulation period: The entire network dynamics organize into one activity sequence. In a subsequent recall phase, synaptic plasticity is switched off, the level of inhibition is lowered and random or targeted external stimulation are applied to the network. This evokes compressed replay of the activity sequence observed during exploration. The model was modified to learn multiple sequences of subsequently active neuron groups with a multiplicative learning rule including an additional synaptic competition term (Samura et al., 2008).

Molter et al. (2007) describe place cell populations as coupled phase oscillators, which possess an intrinsic theta oscillation frequency during exploration. The model incorporates theta phase precession by assuming that the intrinsic frequency increases with progress in the place field such that the activity in different place cell populations peaks sequentially within the theta cycle. During exploration, recurrent connections are functionally inactivated but learned. This allows later recall of the sequence when recurrent connectivity is switched on.

Bush et al. (2010) have implemented the theta phase precession by a modulation of the external input current that depends on the position relative to the place field center and the theta phase. The study employs a spiking network of one hundred excitatory neurons to show that different additive spike- and spike/rate-dependent learning rules are suitable to learn activity sequences: The network organizes into a feed-forward chain, where the weights between subsequently activated groups of neurons have weights saturated at the maximal weight, while background weights that are not part of the chain have weights close to zero.

Cutsuridis and Hasselmo (2011) have used a CA1 microcircuit of four pyramidal cells and four interneurons of different types to study how the experimentally found distinct firing patterns of the involved neuron types may be relevant for encoding and replay. The generation of a short activity sequence is imposed on the CA1 microcircuit model by a CA3 network that is not explicitly modeled.

Very recently, Scarpetta and coworkers have estimated the ability of networks to store multiple precisely timed, simple periodic spike sequences (every neuron contributes one spike) in networks of leaky integrate-and-fire neurons endowed with additive Hebbian learning (Scarpetta and Giacco, 2013; Scarpetta et al., 2013). Further studies used two-state neurons to assess the network capacity for activity sequences (Leibold and Kempter, 2006; Scarpetta et al., 2011) or rate units to model learning of sequential activation of neuron populations (Verduzco-Flores et al., 2012).

Only one study has considered the replay of spike sequences in conjunction with SPW/R-like activity (Vladimirov et al., 2013): The model assumes that the plexus of proximal axon collaterals is connected by axo-axonic gap junctions. In this plexus, spikes multiply in avalanche-like manner, overall generating a continuous ripple-frequency oscillation. The spikes enter the main axon and the soma only if the soma receives a (subthreshold) dendritic depolarization. By this mechanism weak dendritic inputs are amplified and somatic spiking was observed to be propagated over short chains of mono-synaptically connected single neurons.

Activity propagation along feed-forward structures has also been investigated as a model for reliable information transmission in noisy networks, largely independently from hippocampal sequence learning (Abeles, 1982; Diesmann et al., 1999; Kumar et al., 2010). These studies on "synfire chains" have mostly considered feed-forward networks with a dense, often all-to-all connectivity between subsequent layers (Aviel et al., 2003; Mehring et al., 2003; Kumar et al., 2008b). However, since cortical neural networks are overall sparse (Braitenberg and Schüz, 1998; Holmgren et al., 2003)), we may also expect some level of dilution for embedded feed-forward chains. Such chains created from existing connections in sparse recurrent networks require strong synaptic efficiencies and specifically modified neuron properties to enable synchrony propagation (Vogels and Abbott, 2005). Very recently, we have shown that the nonlinear dendritic interactions which have been suggested to underlie generation of SPW/Rs (Memmesheimer, 2010), promote propagation of activity along biologically plausible, comparably weak and highly diluted synfire chains (Jahnke et al., 2012, 2013).

Synopsis and structure of this article

In the present article, we derive a unifying model showing how experience may be stored and thereafter be replayed in conjunction with SPW/Rs. We model spatial exploration accompanied by place cell activity and theta oscillations in the hippocampus, followed by a resting or slow-wave-sleep phase in which the network generates SPW/Rs and replay. We first consider the encoding phase and model learning of network structures reflecting place cell sequences during exploration of an environment. These structures are part of a large, sparse, spiking neural network. Thereafter, we consider the recall and show that the sequences are replayed in conjunction with emergent SPW/R-like global network activity. The third part assesses the quality

of the replay as well as different ways of its initiation. Finally, we consider storage and recall of multiple sequences. We conclude the main part of the article with a comprehensive discussion of the biological plausibility of the model.

7.2. Results

7.2.1. Spatial exploration phase

Location tuning and phase precession

In a given environment, a large fraction of pyramidal cells ("place cells") in hippocampal regions CA3 and CA1 display well-defined sensitivity to spatial positions (Mizuseki et al., 2012), and therewith form a cognitive map of the environment. In different environments, the same neurons encode different places (e.g., Muller and Kubie, 1987; Quirk et al., 1990; Bostock et al., 1991; Colgin et al., 2008). Place cells encode position by spike rate and by spike timing. They fire at increased rate when the current position of an animal is within their receptive (place) fields (O'Keefe and Dostrovsky, 1971; O'Keefe, 1976; Ekstrom et al., 2003; Kjelstrup et al., 2008; Harvey et al., 2009). The preferred timing of single spikes depends on the position relative to the place field center and on the phase of the background theta oscillation (O'Keefe and Recce, 1993; Skaggs et al., 1996; Maurer and McNaughton, 2007; Gupta et al., 2012): When the animal enters a place field, single cells spike late in the theta-cycle. While traversing the place field, spiking occurs at earlier and earlier times ("phase precession") and when the animal leaves the place field, the place cell preferably spikes at the beginning of the cycle.

The neuronal mechanisms underlying phase precession and location tuning is still under debate. It has been proposed that phase precession may arise from interference between two oscillatory inputs with slightly different frequencies (O'Keefe and Recce, 1993; Lengyel et al., 2003). Spikes are elicited if the summed input exceeds a certain threshold and thus timing of single spikes is determined by the high-frequency wave of the interference pattern, which progressively advances relative to the lower frequency input which is in synchrony with the background theta oscillation. Alternatively, phase precession may arise from interaction of theta-modulated inhibition with external excitation of increasing strength (Magee, 2001; Mehta et al., 2002; Harris et al., 2002; Thurley et al., 2008). Spikes are triggered, if the excitation exceeds the inhibition and thus spikes are shifted to earlier and earlier times in the theta cycle. As a third option, it has been proposed that phase precession is caused by asymmetric recurrent connections between place cells which have been learned in earlier training sessions on the same track and predict the animal's path (Jensen and Lisman, 1996; Tsodyks et al., 1996). At the beginning of each theta cycle, location specific excitation activates some place cells and initiate a wave of activity that spreads towards cells with place fields shortly ahead of the current position along the path.

In this article, we implement a phenomenological approach which is compatible with all three models: Phase precession is established by adding an external excitatory input current (to each activated cell) that peaks near the time of preferred firing (cf. Figure 7.1). For simplicity, we

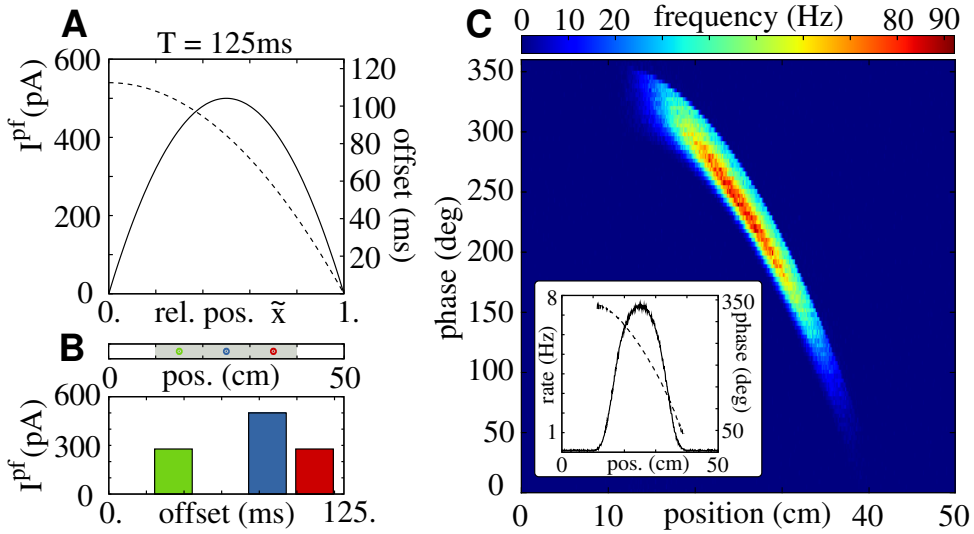

Figure 7.1: Place tuning and phase precession of single cells. (A) When the actual position x is within the place field of a neuron, rectangular current pulses are injected to the neuron. Their amplitudes I^{pf} (solid, left vertical axis; Equation 7.21) and temporal offsets (DT) with respect to the background theta rhythm (dashed line, right vertical axis; Equation 7.22) are functions of the relative position $\tilde{x}$ in the place field (cf. Equation 7.20). In panel (B) we show examples of the current pulses for a place field $\mathcal{P} = [10, 40]$ cm and the positions $x = \{15, 25, 35\}$ cm. The positions in the place field are shown in the upper subpanel, the resulting input currents in the lower subpanel. (C) The main panel displays the resulting spatio-temporal receptive field. The inset shows the average firing rate (solid; left vertical axis) and average phase shift against the theta rhythm (dashed; right vertical axis) as a function of the current position. The neuron increases firing rate for positions within the place field and shows phase precession. For further details see methods section.

assume that the current takes the form of a short, rectangular pulse which is shifted relative to the beginning of the theta cycle by a temporal offset DT. DT is almost equal to a full period when the place field is entered and decreases while traversing it. The amplitude increases with proximity to the place field center, incorporating the experimentally observed increase in firing rate (or firing probability). As a result, the neurons show both, phase precession and an increase in firing rate for positions nearer to the place field center (cf. Figure 7.1C and detailed description in methods section).

Learning of feed-forward sub-structures

During spatial exploration, sequences of visited places are reflected by sequences of increased activity of place cells. Independent of the exact underlying mechanism, the phenomenon of phase precession yields a compressed version of such sequences: During one theta cycle, neurons with overlapping place fields spike in the same order as the place fields of the single neurons have been or will be traversed. The (average) time difference between spikes of neurons with nearby receptive fields is in the range of tens of milliseconds, i.e., in the range of spike timing dependent plasticity (STDP; cf. Caporale and Dan, 2008, for a review) where dependent on the exact timing of presynaptic and postsynaptic spikes changes of connection strengths between neurons are induced. For hippocampal pyramidal neurons in culture it has been demonstrated that causal spiking results in potentiation and anti-causal spiking results in depression of synaptic efficiencies (Bi and Poo, 1998). The combination of compressed representation of sequences by phase precession and potentiation of synaptic efficiencies by causal spiking favors the emergence of feed-forward structures (Skaggs et al., 1996; Mehta et al., 1997; Buzsáki, 2006; Bush et al., 2010).

Network setup and equilibrium phase

We consider sparsely connected random networks with a biological plausible STDP update rule, where theta phase precession and background dynamics generate spiking that resembles the activity during a run along a linear track. By numerical simulations we show that feed-forward substructures are formed which enable the guided propagation of synchronous activity, and thus replay of the previously experienced spike patterns, in a subsequent recall phase.

We consider networks of N^{ex} excitatory and N^{in} inhibitory neurons of leaky integrate-and-fire type. The neurons are globally, but sparsely connected, with heterogeneous connection strengths and coupling delays. Single spikes induce transient conductance changes on the postsynaptic neurons. Motivated by recent neurophysiological experiments (Ariav et al., 2003; Gasparini et al., 2004; Polsky et al., 2004; Gasparini and Magee, 2006), we integrate nonlinear dendritic interactions, modeling the ability of (basal) dendrites of hippocampal pyramidal cells to initiate dendritic sodium spikes (cf. also Memmesheimer, 2010; Jahnke et al., 2012, 2014a). Highly synchronized excitatory input can elicit such a dendritic spike (modeled by a stereotypical current pulse) which causes a stronger depolarization in the soma of the postsynaptic neuron than expected from linear summation of single inputs.

Recurrent connections between excitatory neurons are plastic and updated according to a "power-law" update rule (Morrison et al., 2007; Standage et al., 2007), i.e., the dependence of potentiation/depression on the weight before this increase or decrease obeys a power-law. All other connections are considered static. It has been shown that the power-law update rule yields an unimodal weight distribution (Morrison et al., 2007) for the asynchronous irregular background activity of balanced networks (v. Vreeswijk and Sompolinsky, 1996, 1998; Brunel, 2000). Due to the fact that dendritic spikes are elicited by highly synchronous input only, this still holds in the presence of nonlinear dendritic interactions as considered in this article (data not shown). Further details on the neuron model, network setup and STDP update rule are given in the methods section.

Running along a linear track

After an equilibration phase where the recurrent network weights have assumed the stationary weight distribution, we consider the movement along a linear track of length L. A subset of $N^{\mathrm{pf}} < N^{\mathrm{ex}}$ excitatory neurons is assumed to have an active place field on the track. Without loss of generality, we consider the first N^{pf} neurons with the index $i \in \left\{1, \ldots, N^{\mathrm{pf}}\right\}$ as neurons with an active place field. For simplicity, we assume that the place fields $\mathcal{P}_i$ have identical widths $\Delta w_i \equiv \Delta w$ and their centers

$$x_i^{\mathrm{ctr}} = \frac{L}{N^{\mathrm{pf}} - 1} \cdot (i - 1) \tag{7.1}$$

are distributed homogeneously along the track (cf. also methods section). To prevent boundary effects, we extend the track by $\Delta w/2$ at the beginning and at the end (i.e., total track length $L^{\mathrm{tot}} = L + \Delta w$), such that during the movement all place fields are completely traversed (cf. gray shaded area in Figure 7.2A). Further, we discretize the movement along the linear track: We assume that the position is fixed during each theta cycle with period T, and that the position increases in jump-like manner between consecutive cycles. Starting initially with $x_0 = 0$, the position during the jth oscillation is given by

$$x_{j+1} = x_j + \Delta x \tag{7.2}$$

and the jump-size Δx is drawn uniformly from the interval

$$\Delta x \in [0, 2\bar{v}T] \tag{7.3}$$

where $\bar{v}$ specifies the average running velocity (cf. inset of Figure 7.2A).

During the run single neurons with overlapping place fields spike in an order approximately reflecting the order in which the place fields are traversed during the run (examples are shown in Figure 7.2B,C). As discussed above, this ordered spiking in combination with plastic synapses results in the formation of a feed-forward structure. In Figure 7.2D, we show the distribution of synaptic weights as a function of the distance between the place field centers of the postsynaptic and the presynaptic neuron. Its shape and development can be understood as follows. With repeating traversals of the track, the feed-forward structure becomes more and more prominent.

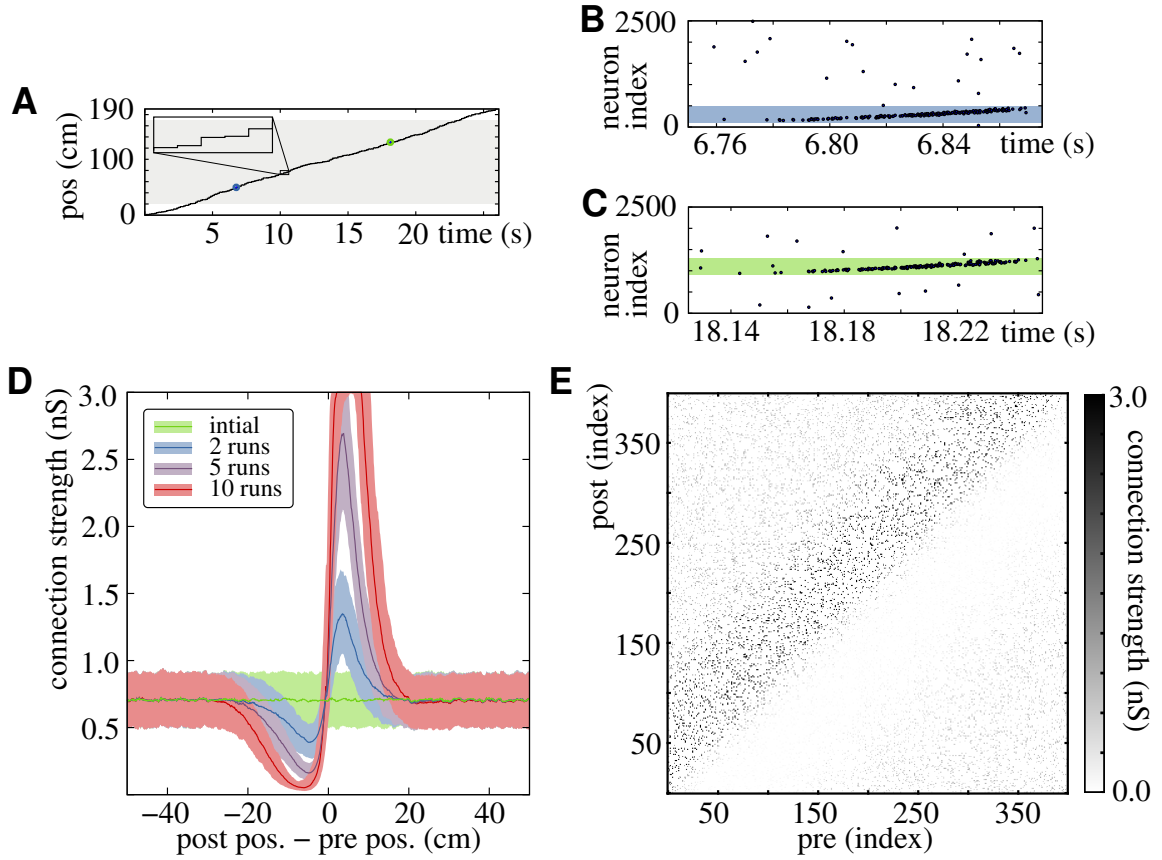

Figure 7.2: Learning of feed-forward structures. (A) Example trajectory of a modeled run along a linear track of a total length of $L^{\text{tot}} = 190\text{cm}$ with average velocity $\bar{v} = 8\text{cm/s}$. For simplicity, we assume that the position is fixed for the short period of one theta cycle ($T = 125\text{ms}$). Between consecutive theta cycles the position increases randomly in jump-like manner, here on average by one centimeter (cf. zoomed view of the trajectory presented in the inset). Place fields are assigned to $N^{\text{pf}} = 1500$ of $N^{\text{ex}} = 2500$ excitatory neurons and the centers are distributed homogeneously in the interval $\left[\frac{\Delta w}{2}, L^{\text{tot}} - \frac{\Delta w}{2}\right]$ (indicated by the gray shaded area). (B,C) Spiking activity of the excitatory neuron population for the period of one theta cycle at different positions (indicated by the blue and green circle in A). The colored area indicates the fraction of neurons with place fields containing the current position. (D) Distribution of synaptic weights as a function of the distance between the place field centers of the postsynaptic and the presynaptic neuron. The solid line indicates the mean weight and the colored area the interval containing 80% of the weights (0.1 to 0.9 percentile). Different colors show the distribution after different numbers of runs as indicated by the inset. (E) Connectivity matrix for connections between the first 400 neurons after 10 runs (red curve in D).

Strengths of connections between neurons with similar place fields are altered only weakly: During the run such neurons spike at similar times and therefore the order of spiking of these neurons (and with it the potentiation or depression of synaptic weights) is approximately random. Consequently, even after multiple runs along the same track, the weight distribution is similar to the equilibrium weight distribution. With increasing distance between the centers of the place fields, the average temporal distance between spiking times increases, and the order of spiking is more reliably preserved. Accordingly, also the average weight change increases. However, the amplitude of weight changes induced by a single spike pairing decreases exponentially with temporal difference between spikes. Therefore, the average weight assumes a maximum (minimum) for moderate distances between place field centers and converges to the equilibrium weight distribution for large distances.

7.2.2. Replay of spike patterns

Replay and emergence of SPW/R-like events

As discussed above, during the exploration phase a "stripe-like" feed-forward structure is formed (cf. Figure 7.2D,E). In the following we show that such a structure enables replay of spike patterns experienced during the run. Importantly, the observed replay resembles the replay observed during SPW/Rs in the hippocampus in several aspects: It occurs together with high frequency oscillations (Buzsáki et al., 1992; Ylinen et al., 1995; Maier et al., 2003), it is strongly stochastic, i.e., has a high trial-to-trial variability (Wilson and McNaughton, 1994; Nadasdy et al., 1999; Lee and Wilson, 2002; Pastalkova et al., 2008; Davidson et al., 2009), the replay is a short intermittent activity pattern in front of asynchronous low rate activity, and the wave-form of the total activity increases in the beginning of the replay event and decreases towards the end of the event (Buzsáki et al., 1992; Ylinen et al., 1995; Maier et al., 2003).

In the ground state the neurons spike asynchronously and irregular. To keep the ground state activity of networks after different number of runs comparable (and to account for possible homeostatic effects), we adjust an external constant input current I^0 to the neurons such that the average spiking rate of the neurons equals $\nu = 1\text{Hz}$. Replay events are initiated in a target manner by eliciting a group of g_0 neurons with adjacent place fields to spike synchronously. This spiking causes a synchronous input to the postsynaptic neurons after some delay time and therefore might induce synchronous spiking of a fraction of these neurons. Due to the feed-forward structure, neurons with place fields subsequent to place fields of the initially synchronous subset of neurons receive stronger total input than other neurons of the network, and therefore have a higher probability to spike. In particular, in these neurons more dendritic spikes are initiated which elicit a subsequent somatic spike with high probability and high temporal precision (Ariav et al., 2003; Müller et al., 2012 and cf. also Jahnke et al., 2012, 2013). As a consequence the spikes of the postsynaptic neurons remain synchronized even if the synaptic delays are moderately heterogeneous: Only spikes received within the dendritic integration window ΔT^{s} can contribute to the initiation of a dendritic spike, and inputs which arrive outside a small window around the peak of an input pulse (consisting of multiple input spikes) are unlikely to generate

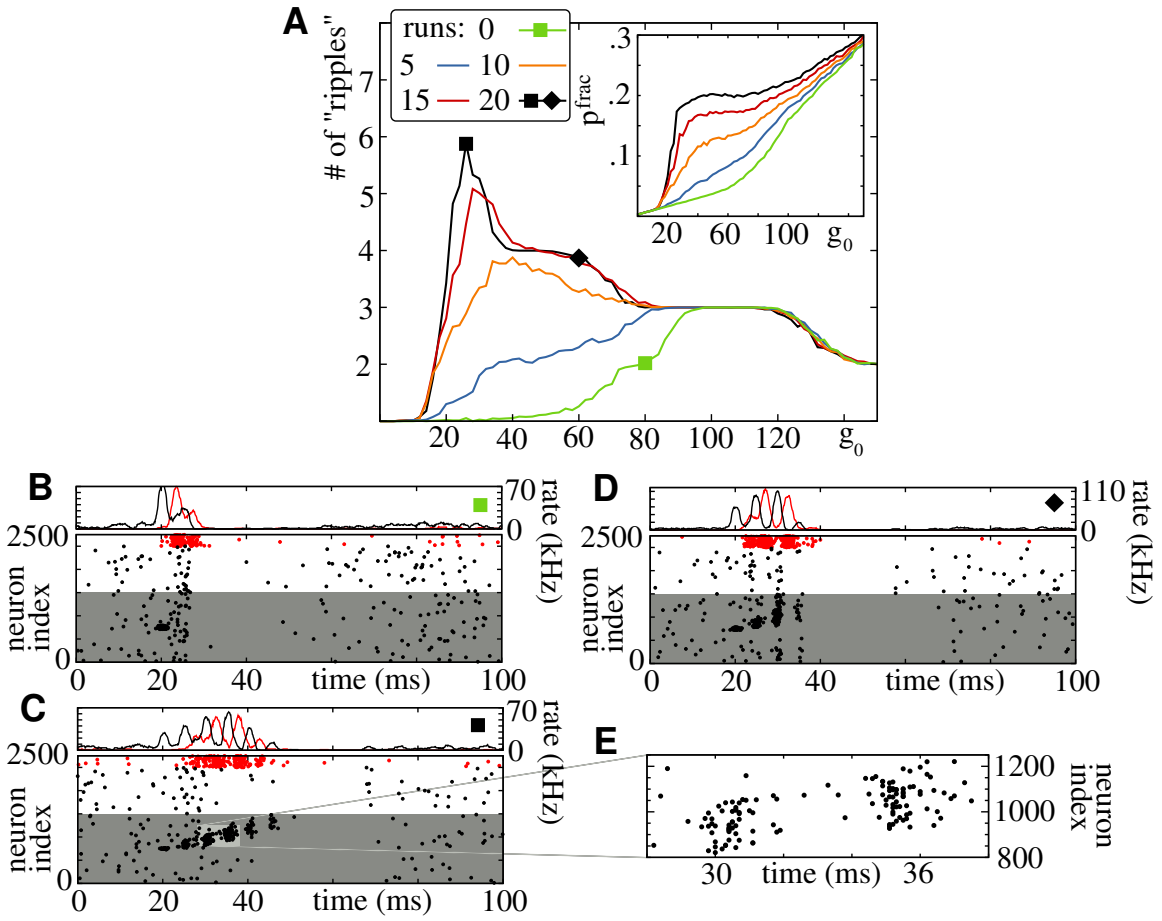

Figure 7.3: Replay of spike patterns during Sharp-Wave-Ripple-like events induced by synchronous stimulation. (A) Average number of consecutive synchronous groups ("ripples") versus the number of initially synchronously stimulated neurons g_0. Different colors correspond to different number of runs along the linear track. The inset shows the average fraction p^{frac} of place cells that spike at least once during the replay events. The data are derived by averaging over $n = 10000$ replay events. (B-D) Examples of network activity: In the upper panels we show the firing rate, in the lower panels the spiking activity of the excitatory (black) and the inhibitory (red) neuron population. The size of the initial stimulation and number of runs along the linear track are indicted by the markers (upper panels and A). The gray shaded area in the lower panels indicate the subset of neurons which have a active place field on the track. (E) Closeup view of the spike data shown in (C) which illustrates that successive synchronous groups overlap. For further explanations see main text.

dendritic spikes and somatic output. This keeps the propagating activity confined to highly synchronous pulses.

For small g_0 only a small number g_1 of the postsynaptic neurons spike in response to the initial synchronous pulse. With increasing g_0 also the size g_1 of the secondary synchronous pulse increases, and at some point g_1 exceeds g_0, i.e., more than initially synchronized neurons are excited to spike synchronously. This secondary synchronous pulse induce a third one, for which similar rules hold, etc. The synchronous activity can propagate across the network reflecting the previously learned feed-forward structure.

In contrast to layered feed-forward networks (e.g., Diesmann et al., 1999; Vogels and Abbott, 2005; Jahnke et al., 2012), where the size of each synchronous pulse is bounded from above by the layer size, here the sizes of the synchronous pulses may be expected to grow, and potentially lead to epileptic-like pathological activity. Such pathological activity, however, is prevented by the inhibitory feed-back loop: Increasing activity of excitatory neurons cause increasing activity of the inhibitory neuron population. The resulting inhibitory feed-back does not hinder the generation of dendritic spikes, but it decreases the probability that a somatic spike is initiated by hyperpolarization of the postsynaptic neurons (cf. Müller et al., 2012). As a consequence, for very large synchronous pulses the inhibitory feed-back overwhelms the excitation, the pulse does not spread further across the network, and the overall activity decays to the level of spontaneous activity. Pathological activity in the form of global synchrony is prevented.

In Figure 7.3 we illustrate typical replay events after the exploration phase on a linear track (cf. Figure 7.2). If the initial synchronous pulse is too small, insufficiently many neurons respond to the initial pulse and the activity decreases quickly. If the initial stimulation is too large, the size of the synchronous pulse grows too fast and the replay event is terminated almost immediately by recurrent inhibition. In between there is a broad range of initial stimulations for which synchronous activity propagates along the feed-forward structure lasting for a moderate number of synchronous pulses (ripples): There is an optimal stimulation size g^*, where the number of ripples becomes maximal (cf., e.g., black square in Figure 7.3A, and Figure 7.3C). g^* separates the regime, where the sizes of the synchronous groups decays from the beginning and the regime, where the sizes of the synchronous groups initially grow (cf. also Jahnke et al., 2012, 2014a).

A replay event is also elicited by initial stimulations g_0 exceeding g^* (cf. Figure 7.3D for an example). However, with increasing g_0 the sizes of subsequent synchronous groups as well as the inhibitory feed-back increase, and thus the event is terminated by recurrent inhibition after a shorter number of ripples. The moderate number of ripples is consistent with the low number of ripples observed in neurophysiological experiments (e.g. Maier et al., 2003). The mechanism described above is thus suitable to "read-out" finite sequences of the previously learned feed-forward structure. The wave-form of the total activity resembles the wave-form observed during SPW/Rs in the hippocampus.

Characteristics of replay events

In the following we quantitatively analyze the replay events. In particular, we focus on the propagation frequency and the quality of the ordering of single spikes during replay events compared to the ordering of the place field centers in the track.

Replay events are mainly mediated by dendritic spikes and the propagation frequency is determined by the average temporal difference t^{diff} between presynaptic spikes and postsynaptic spikes elicited by dendritic ones. The expected propagation frequency can thus be calculated taking the axonal delay τ^{ax}, the synaptic delay τ^{ex}, the latency of the dendritic spike τ^{DS}, and the average time difference t^{ds} between the onset of the response to the dendritic spike and the spiking of the postsynaptic neurons into account. Considering quantitative neurophysiological measurements we estimate the expected temporal difference t^{diff} to be in the range of $3.7 - 6.4$ms (cf. methods section for more details). Therefore, the expected propagation frequency (approximately $150 - 270$Hz) is consistent with the frequencies observed during SPW/Rs in the hippocampus (Buzsáki et al., 1992; Ylinen et al., 1995; Maier et al., 2003 and cf. also Memmesheimer, 2010). Indeed, for the standard parameters employed in the article (chosen to be approximately centered within the biologically plausible parameter range), the propagation frequency is approximately 200Hz as illustrated in Figure 7.4A.

To quantify the quality of ordering of spikes in a replay event we calculate the matching index I (Ji and Wilson, 2007) with respect to the original ordering of place field centers for each event: We consider all neurons with an active place field that take part in the replay events. We count the total number of spike pairs where the spikes are sent in the same order as in the original sequence, subtract the number of pairs with reverse ordering, and normalize by the total number of spike pairs occurring in the replay event. Thus the matching index I is a real number in the interval $[-1, 1]$, which is $I = 1$ for perfect replay of the original sequence, $I = -1$ for reverse replay, and $I \approx 0$ for random replay sequences. In Figure 7.4B we show the average matching index for replay events induced after different number of runs along the linear track. The matching index increases with the number of ripples, i.e., the number of successive synchronous groups (cf. Figure 7.3A) and becomes maximal for the same initial stimulations for which the number of ripples is maximal.

However, even for the optimal parameter range, we find $I < 1$, i.e., the replay is not perfect (the sequence is not perfectly ordered). In contrast to layered feed-forward networks (e.g., Diesmann et al., 1999; Vogels and Abbott, 2005; Kumar et al., 2010; Jahnke et al., 2012), there are no separated subsets of neurons (layers) which constitute the potentially members of each synchronous pulse. Instead, the neurons participating in subsequent synchronous pulses are recruited from the set of neurons with place field centers following the place field centers of the neurons of the preceding synchronous pulse. Thus the synchronous pulse propagates along the previously learned feed-forward structure, yet, the range of place field centers of neurons of consecutive synchronous pulses overlap (cf. Figure 7.3E). Additionally, the ordering of spikes within one synchronous pulse depends strongly on the current state of the neurons upon reception of the synchronous input, and thus the spiking order within one of these pulses is approximately random. Both effects mentioned above cause deviations between the order of

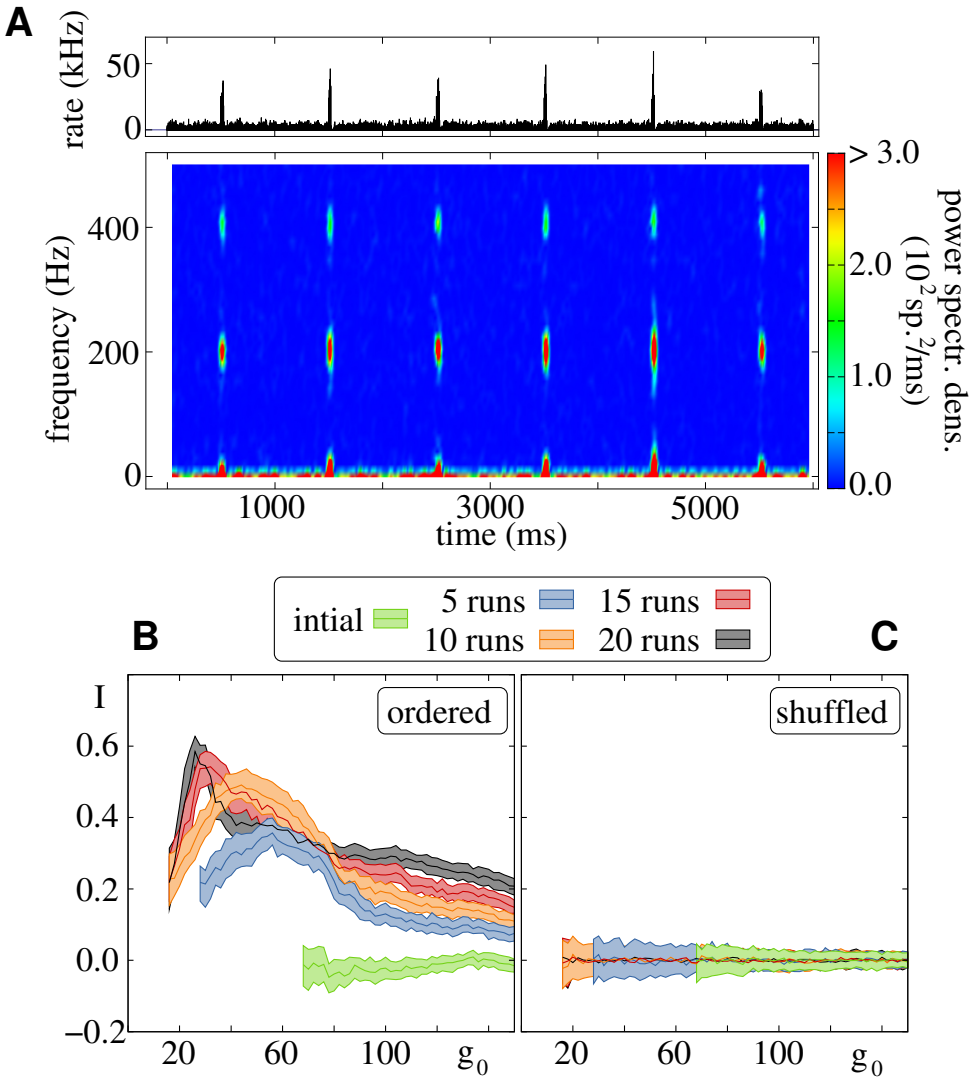

Figure 7.4: Characteristics of replay events. (A) The lower panel shows the spectrogram of the dynamics of the excitatory neuron population displayed in Figure 7.3C, and the upper panel shows the corresponding network rate. There are clear maxima at a frequency of about 200Hz during replay events. (B) Average matching index I (solid lines) versus the number of initially synchronously spiking neurons g_0 after different numbers of runs along a linear track (same data and color-code as in Figure 7.3A). Only runs where at least two "ripples" are initiated are considered for the analysis, therefore the curves are truncated at the left side. The shaded areas indicate the value range containing 50% of the values (0.25 to 0.75 quantiles). With increasing number of ripples (cf. Figure 7.3A) the quality of the ordering within replay events increases. (C) As a control experiment we shuffled the neuron indices and calculated the matching index. As expected, the matching index index fluctuates around zero, highlighting that the sequence is randomly ordered.

spikes in the replay event and the order of the place field centers, and they therefore reduce the matching index I below the maximal value $I^{\max} = 1$. Nonetheless, after a few number of runs along the linear track, the average matching index is substantially larger compared to a control scenario where the neuron indices are shuffled (cf. Figure 7.4B,C). The "center of place field centers" of neurons participating in subsequent synchronous pulses propagate along the feed-forward structure (cf. Figure 7.3C,D).

Robustness of the occurrence of replay events

Besides the number of runs along the linear track, also the widths Δw of the place fields, the maximal synaptic modification, and the strength of the excitatory-inhibitory feedback loop influence the properties and quality of replay events. In the following we show that the emergence of replay and SPW/R-like activity is robust against changes of the network setup.

With increasing place field width Δw, the range of positions

$$x \in \left[x_i^{\mathrm{ctr}} - \Delta w/2, x_i^{\mathrm{ctr}} + \Delta w/2\right] \tag{7.4}$$

where a single (place encoding) neuron i becomes active increases. Assuming a fixed running velocity $\bar{v}$ and learning rate λ, this increase implies that each neuron is activated for a longer time interval during one run. Thus also the total number of spike pairings between place encoding neurons increases resulting in a faster formation of the feed-forward structure. Indeed, with increasing Δw, the average number of ripples per replay event (cf. Figure 7.5A) as well as the ordering (cf. Figure 7.5B) increase for fixed number of runs. This increase is similiar to the increase achieved by an increasing number of runs for fixed Δw (cf. Figure 7.3A and Figure 7.4B).

As argued above, the excitatory-to-inhibitory and inhibitory-to-excitatory coupling controls the number of ripples and the length of replay events. To illustrate the influence of this feed-back loop, we scale the relevant coupling strengths by a factor γ, i.e.,

$$\epsilon'_{\mathrm{inex}} = \gamma \cdot \epsilon_{\mathrm{inex}} \text{ and } \epsilon'_{\mathrm{exin}} = \gamma \cdot \epsilon_{\mathrm{exin}}, \tag{7.5}$$

where ϵ_{inex} ($\epsilon'_{\mathrm{inex}}$) denotes the (modified) excitatory-to-inhibitory, and ϵ_{exin} ($\epsilon'_{\mathrm{exin}}$) the (modified) inhibitory-to-excitatory coupling strengths. With decreasing γ (i.e., less prominent feed-back loop), we observe more and more ripples (cf. Figure 7.5C), and replay events become longer and longer. However, the quality of the ordering within the replay events do not increase (cf. Figure 7.5D). Synchronous activity propagates along the learned feed-forward structure (see previous subsection), but additionally the synchronous activity might also spread to other neurons with place fields not subsequent to the currently active synchronous group. Such spreading is hindered by an increase of γ. Here only the strongest signals (i.e., the projection of the propagating signal on the neurons with subsequent place fields) are sufficiently strong to overcome the inhibitory feed-back which yields more ordered replay sequences (cf. Figure 7.5D).

We conclude that the occurrence of induced replay events is robust against variations of initial stimulation size, number of runs along the linear track, place field width and strength of inhibitory feed-back loop.

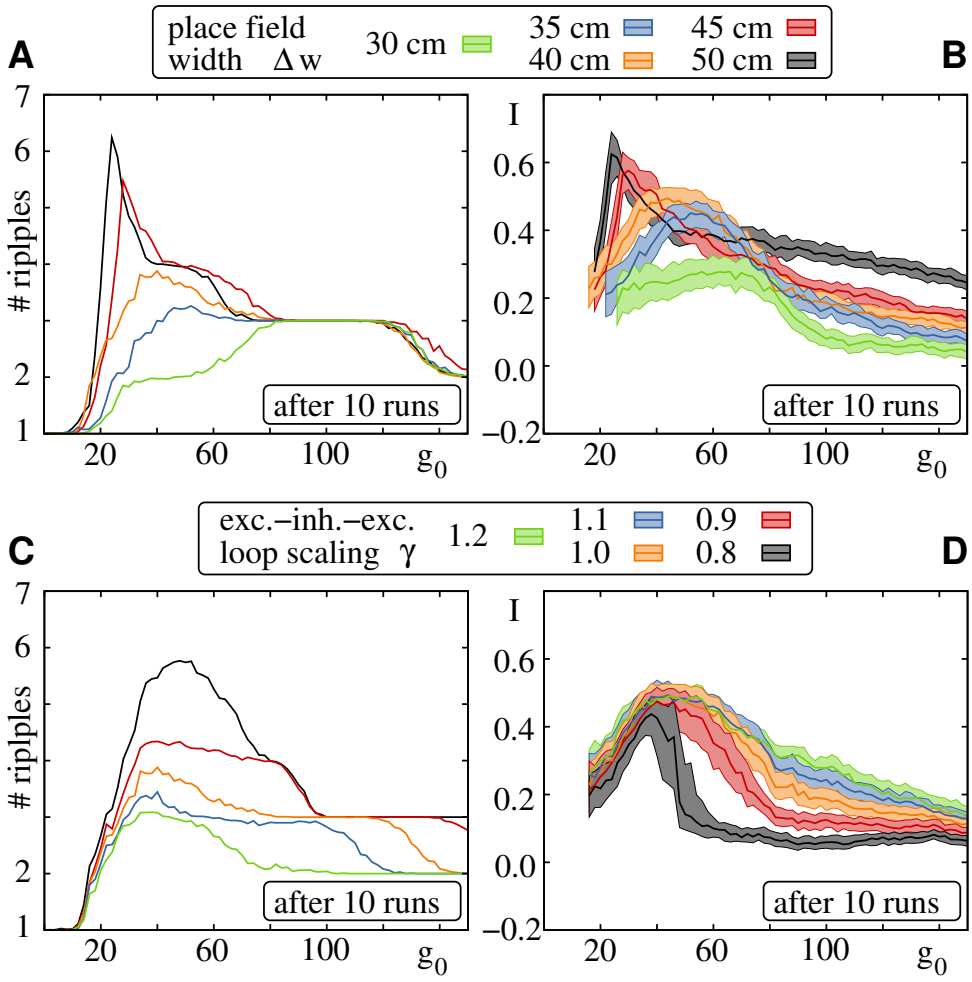

Figure 7.5: Impact of place field width and strength of inhibitory feed-back loop on replay events. Number of ripples (A,C) and matching index (B,D) versus the number g_0 of initially synchronous neurons after a fixed number of runs (averaged over $n = 10000$ replay events). In (A,B) different colors indicate different place field widths Δw and in (C,D) different colors correspond to different scaling γ of the inhibitory feed-back loop (cf. Equation 7.5) as indicated above the panels. Increasing Δw yields a faster learning of feed-forward structure, and thus increase the ordering of replay events. The inhibitory feed-back controls the number of ripples per replay event: With decreasing γ more and more ripples (i.e., longer events) emerge. However, longer replay events do not lead to more ordered sequences as the synchronous signal might spread out over larger parts of the recurrent network. For more detailed discussion see main text.

Unspecific stimulation

So far we considered replay events triggered by a specific (read-out) stimulation, i.e., events are started by synchronous spiking of a subset of neurons with neighboring place field centers. However, with more and more prominent feed-forward structures (achieved, e.g., by increasing number of runs) the minimal number of initially synchronized neurons which are sufficient to elicit a replay event decreases. This decrease suggest that replay events might also be triggered by unspecific stimulation of a random subset of neurons which contain subsets of neurons with nearby place field centers by chance, and thus might induce replay events.

We test this conjecture, by stimulating a small subset of g_0 randomly selected neurons out of the total population of N^{ex} neurons to spike synchronously. If the formed feed-forward structure is sufficiently prominent (i.e., after sufficiently many runs along the track and/or for sufficiently large place field widths Δw) this random stimulation indeed elicit SPW/Rs-like events with a moderate number of consecutive synchronous groups (ripples).

To evaluate if this events contain information about the order of the place field centers, we calculate the matching index I with respect to the original order of place field centers as before. Furthermore, we test whether the information about the order can already be inferred from the activity of a limited number of neurons (as it is the case in experimental setups where only spike data from a very limited number of neurons are available). We calculate the matching index from a randomly selected subset of S neurons out of all place-encoding neurons: Indeed, the distribution of matching indices (Figure 7.6A) clearly shows that the order within the replay events is non-random and reflects the original order of place field centers along the linear track (examples of spiking activity of the subset S of selected neurons are shown in Figure 7.6B-D).

Storing and recall of multiple sequences

The hippocampus is assumed to serve as a preliminary storage device for information (Buzsáki, 1989; Willshaw and Buckingham, 1990) and simultaneous storage (and recall) of multiple memory contents is essential for its function. In the following, we demonstrate that multiple sequences can be simultaneously stored and successfully recalled in a single network.

We consider the encoding of n^{tr} different linear tracks. For each track, we assume that a number N^{pf} randomly selected neurons out of the total set of N^{ex} excitatory neurons encodes a position on the specific track. As before, the encoded positions (i.e., the place field centers) are distributed homogeneously along the corresponding track and randomly assigned to the selected place-encoding neurons. In the exploration phase all n^{tr} tracks are traversed one after each other, and thus multiple stripe-like feed-forward substructures are formed. For the recall phase we selectively stimulate replay events corresponding to one of the traversed tracks: g_0 neurons with neighboring place field centers with respect to one of the tracks are stimulated synchronously. We analyze the elicited replay events, by calculating the matching index with respect to order of place field centers for each of the trained tracks. The distributions of this matching indices clearly show, that the different feed-forward structures can be selectively activated (cf. Figure

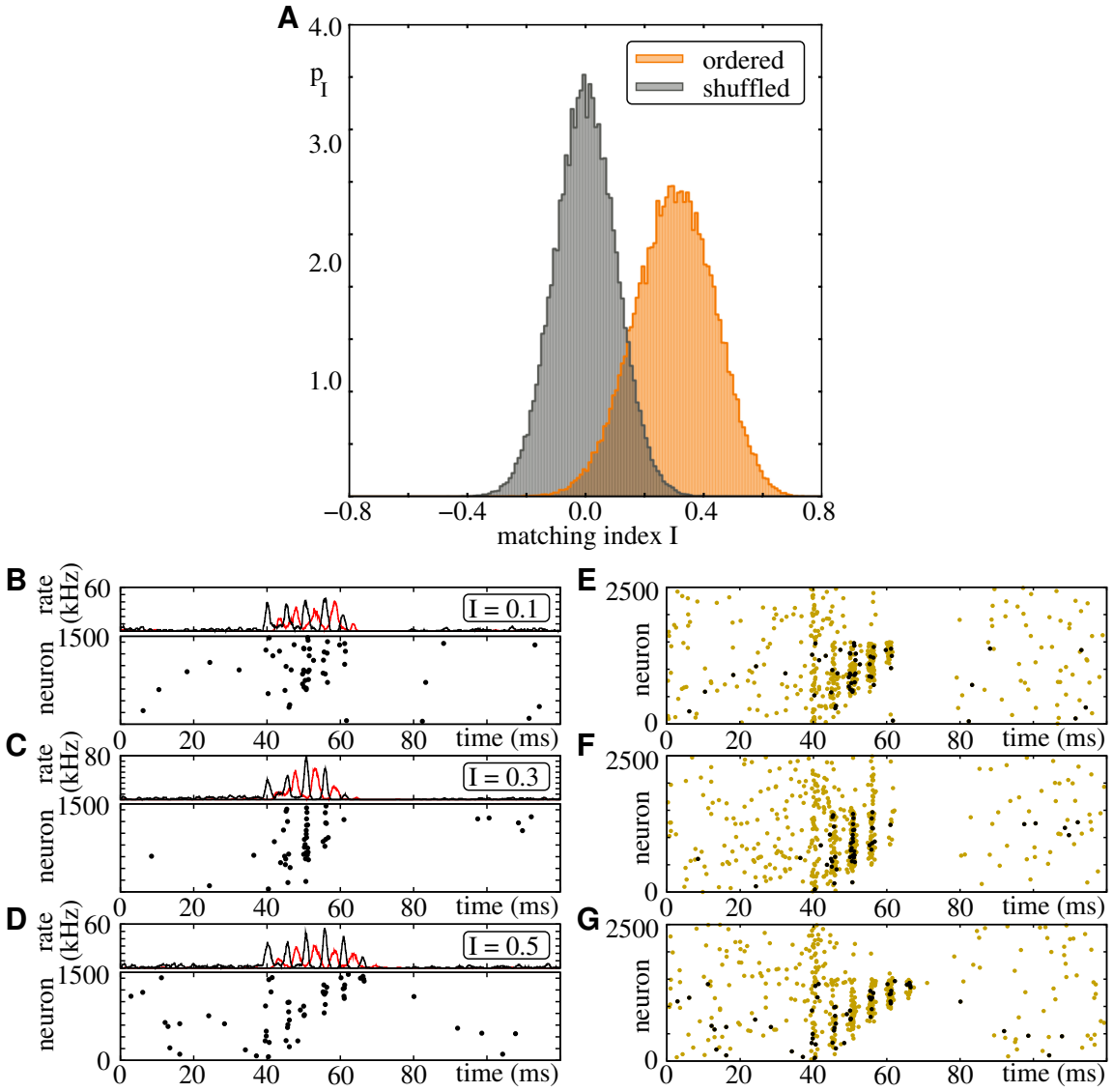

Figure 7.6: Replay events elicited by unspecific (random) stimulation. After an initial exploration phase (15 runs, $\Delta w = 50$cm, other parameters as before) a random subset of $g_0 = 50$ excitatory neurons ($N^{\text{ex}} = 2500$) is stimulated to spike synchronously. We consider all events with at least 5 ripples, i.e., 5 consecutive synchronous groups (3273 out of 10000 events). For each of this events we draw $S = 200$ neurons out of the $N^{\text{pf}} = 1500$ place-encoding neurons and calculate the matching index I with respect to the ordering of the place fields centers along the linear track (to gain better statistics we repeated the drawing 100 times for each event). The resulting distribution of matching index (A, orange) is shifted to positive values, compared to the control setting where the neuron indices are shuffled before calculation of the matching indices (A, black): The spikes within the events are ordered according to the order of place fields centers along the linear track. (B-C) Examples of spiking dynamics of a subset of S neurons (main panels) and the population activity (upper panels, excitatory neurons: black, inhibitory neurons: red) for different matching indices I as indicated in the upper panels. Panels (E-G) display the activity of all excitatory neurons (the selected subset S in (B-D) is indicated by black symbols, other neurons yellow symbols).

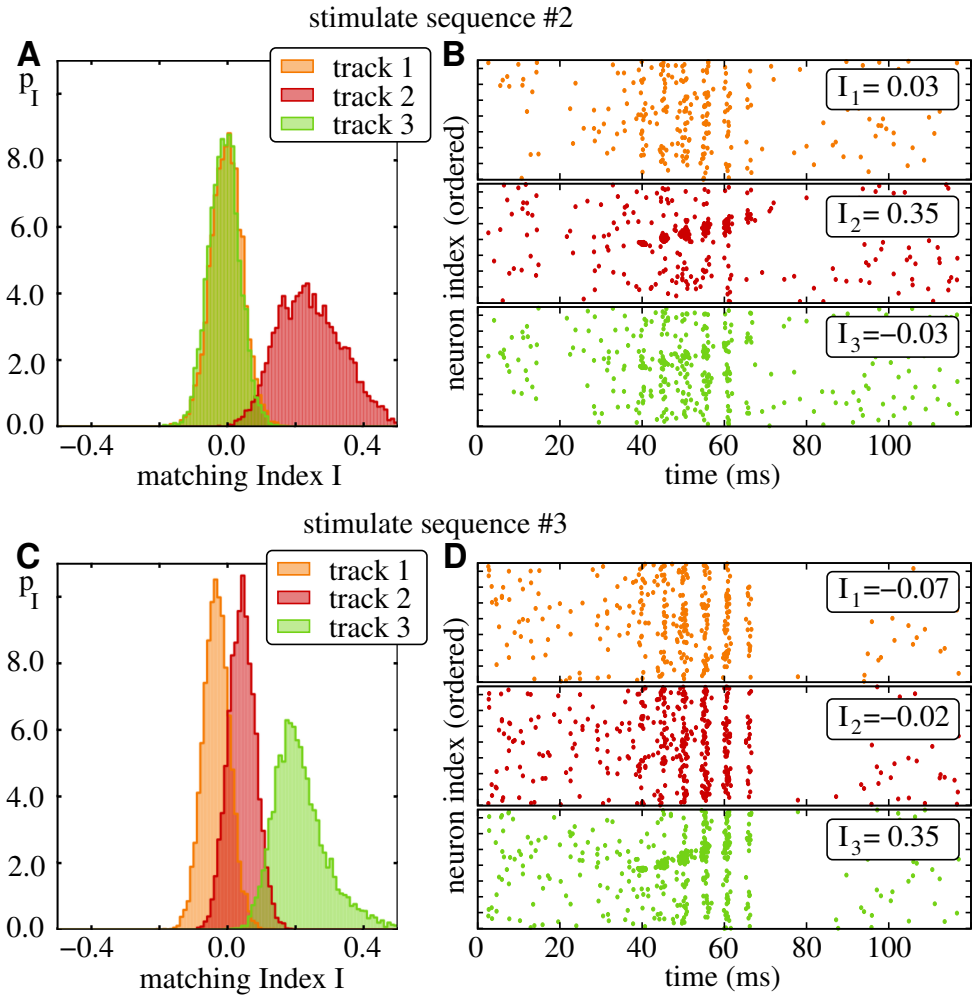

Figure 7.7: Recall of multiple sequences. Before recall the network is trained in an exploration phase on $n^{\mathrm{tr}} = 3$ different linear tracks ($\Delta w = 40$cm, 30 total number of runs; other parameters as before) which are traversed one after another. The set of neurons ($N^{\mathrm{pf}} = 1500$ neurons per track) which encode places on each track are drawn randomly. In the recall phase, $g_0 = 40$ neurons with neighboring place fields are stimulated synchronously (cf. also Figure 7.3). (A,C) Distribution of matching indices ($n = 100000$ events) with respect to the order of place field centers of different tracks (color code). The set of initial stimulated neurons is taken from place-encoding neurons of (A) track 2 or (C) track 3, respectively. (B,D) Example rasterplots of all place-encoding neurons of different tracks (same color code as in A and C). The neurons are ordered according to the ordering of place field centers.

7.7A,C). We conclude that even relatively small networks with simple (global) connectivity, as considered in the article, enable a storage of multiple sequences and a successful recall is possible, although the single feed-forward substructures have a substantial overlap.

7.2.3. Biological plausibility of SPW/R and replay model

In our article we have derived a unifying model to understand learning of activity during exploratory phases and its recall together with emergent Sharp-Wave-Ripples. So far, studies have investigated either learning and recall, or mechanisms of emergent network phenomena. Studies on the former often use abstract neuron models and/or consider small neuron populations with dense, often all-to-all coupling. Investigating emergent phenomena requires larger systems. Neural networks are usually taken to be spiking and have very sparse topology to be compatible with experimental findings. Further, they often incorporate specific, experimentally established single neuron properties which are not covered by standard neuron models.

Our study has bridged the gap between the previously separated fields of research on learning and on emergent neural network activity. In the remainder of the article, we review proposed mechanisms for generation of SPW/Rs, underlying sequence learning and recall. We further discuss the plausibility of our model with respect to recent experimental observations.

Models for SPW/Rs

So far, mainly three mechanisms have been suggested to underlie SPW/R events. The sharp wave may depend on short term plasticity leading to population bursts (Deuchars and Thomson, 1996; Loebel and Tsodyks, 2002; Memmesheimer, 2010), on recurrent excitation enhanced by nonlinear dendrites and inhibition (Memmesheimer, 2010), and/or on recurrent excitation and inhibition only (Taxidis et al., 2012).

For the ripple oscillations, three models exist: The first one assumes that the presence of excitatory input due to a sharp wave input excites the interneuron networks to oscillate. The inhibition from the interneurons entrains the phasic spiking of the pyramidal cells (Buzsáki and Chrobak, 1995; Ylinen et al., 1995) and thereby yields network oscillations in the ripple frequency range in response to both constant (Brunel and Wang, 2003; Geisler et al., 2005) and sharp wave-like transient input (Taxidis et al., 2012, 2013). The second model is based on the assumption that axo-axonal gap junctions (Schmitz et al., 2001; Hamzei-Sichani et al., 2007) connect pyramidal cell axons to a network where spikes can propagate and multiply in the presence of an external depolarizing input (Traub et al., 1999; Traub and Bibbig, 2000; Maex and Schutter, 2007). Rhythmic generation of bursts of axonal spiking are generated, which excite pyramidal cell and interneuron somata to spike after antidromic and orthodromic spike propagation. The third model is based on nonlinear dendrites which enable propagation of synchronous activity (Memmesheimer, 2010; Memmesheimer and Timme, 2012; Jahnke et al., 2013) and thereby generate sharp-wave-like events with high-frequency ripples. The ripple frequency

range is determined by experimentally measured characteristics of nonlinear dendrites (Ariav et al., 2003; Müller et al., 2012) and agrees with the experimentally found one.

The models are not mutually exclusive and, in view of current experimental knowledge on SPW/Rs, all three are plausible (for a more detailed discussion, see Memmesheimer, 2010). We note that the oscillations might also depend on the excitatory-inhibitory loop, like in the gamma "PING"-mechanism (Börgers and Kopell, 2003; Bartos et al., 2007; Tiesinga and Sejnowski, 2009): This feed-back loop can generate oscillations in the ripple frequency range and the fast response properties of the involved interneurons (cf. Geiger et al., 1997; Csicsvari et al., 1998; Jonas et al., 2004) allow for the experimentally observed phase differences between the preferred spiking of the pyramidal and the interneuron populations (Geisler et al., 2005; Memmesheimer, 2010).

The choice of the SPW/R-model in our article

As basis of our article, we have chosen the model established by Memmesheimer (2010) for several reasons: The events generated in the model networks resemble the experimentally measured ones in their shape, duration, firing and current input characteristics. The model explains the ripple frequencies based on data from single neuron measurements (Ariav et al., 2003; Müller et al., 2012). This also holds for the lower frequency, less pronounced ripples in CA3 *in vivo* (Memmesheimer, 2010). The model explains sharp wave and ripples as one event and does not require the assumption of an external sharp wave input for region CA1, consistent with the experimental observation of SPW/Rs in the functionally disconnected or partially deafferented CA1 *in vitro* and *in vivo* (Maier et al., 2003; Nimmrich et al., 2005; Nakashiba et al., 2009; Maier et al., 2011). Our model is based on the assumption that excitatory input mediated by recurrent connections generates strong, fast dendritic sodium spikes in regions CA3 and in CA1. Indeed, recent experiments show ripple-locked excitatory input currents even in the functionally disconnected region CA1 (Maier et al., 2011), suggesting a role of recurrent excitatory connectivity in generating ripples. While recurrent and feed-forward inhibition, as prevalent during SPW/Rs, severely affects responses to non- or weakly-dendritically amplified excitatory input (Müller et al., 2012), strong dendritic spikes and their triggering of action potentials are robust against it (Kamondi et al., 1998; Müller et al., 2012). Further, it has recently been shown that the frequency of ripple oscillations *in vitro* is insensitive against changes in strength and duration of inhibitory interactions (Viereckel et al., 2013). In contrast, *in vitro* experiments on (gamma) oscillations that depend on recurrent inhibition or the excitatory-inhibitory loop, as well as several modeling studies found a decrease of oscillation frequency with increasing inhibition strength and duration (Whittington et al., 1995; Wang and Buzsáki, 1996; Fisahn et al., 1998; Tiesinga and José, 2000; Tiesinga et al., 2001; Bartos et al., 2007). This may indicate that ripples do not depend on inhibition or that they obey a low firing rate oscillation mechanism (Brunel and Wang, 2003; Donoso et al., 2013) despite the high fraction of participating neurons (Csicsvari et al., 1999a; Klausberger et al., 2003). Finally, a functional connection between the fast dendritic sodium-based spikes and SPW/Rs may be suggested by the fact that SPW/Rs occur exclusively in the hippocampus (Buzsáki and Silva, 2012), the only structure where also

fast dendritic sodium spikes have been found to dominate (Ariav et al., 2003; Nevian et al., 2007; Müller et al., 2012; Major et al., 2013).

Recurrent connectivity may be expected to induce dendritic spiking

To further stress the plausibility of our model, we highlight a rough computation that shows that recurrent connectivity may be expected to be sufficient to generate dendritic spiking during SPW/Rs. We show that the strength of input which a pyramidal neuron receives during SPW/Rs from recurrent connectivity is comparable to the input a CA1 neuron receives from Schaffer collaterals. The latter has been experimentally directly shown to generate dendritic spikes (Kamondi et al., 1998).

Recurrent connectivity in both hippocampal regions CA3 and CA1 is sparse, but individual connections are strong. The estimates for the connection probability are about 5% for CA3 (Amaral et al., 1990; Traub and Miles, 1991), and 1% for CA1 in a distance of 200μm (Deuchars and Thomson, 1996). Anatomical data and comparison with other brain areas may suggest a more localized coupling in CA1, such as an increase of connectivity with greater proximity due to a local axonal plexus (Knowles and Schwartzkroin, 1981; Holmgren et al., 2003; Orman et al., 2008). We first consider CA1 recurrent connections and assume that the connectivity is unstructured and that a possible coupling is present with probability 1%. The fraction of CA1 pyramidal neurons sending a spike within a window of 5ms around the peak of a SPW is 5% (Csicsvari et al., 2000), and the total number of pyramidal neurons within CA1 is about 3×10^5 (Andersen et al., 2007; Ascoli and Atkeson, 2005). So, about 150 recurrent inputs per neuron are generated around the peak of a SPW, while a few synchronous recurrent inputs are sufficient to generate a dendritic spike (about 6 for the mean coupling strength measured by Deuchars and Thomson, 1996). Additionally, the presence of several dendrites can lead to a further increase in the effect of the supra-linearity, because more than one dendrite can generate spikes (Breuer et al., 2014).

The estimated number of inputs can now be compared to a similarly estimated number of inputs from CA3 neurons. The connectivity from CA3 to CA1 pyramidal neurons is also sparse, it was estimated to 6% (Sayer et al., 1990). In a window of 5ms around the peak of a SPW, 1% of the CA3 pyramidal neurons send a spike (Csicsvari et al., 2000), and the total number of pyramidal neurons within CA3 is about 2×10^5 (Ascoli and Atkeson, 2005; Andersen et al., 2007). This estimation yields a number of 120 inputs to each CA1 pyramidal neuron. The input strength of CA3 to CA1 connections is smaller than the strength of CA1 recurrent inputs (mean somatic EPSP 0.1mV for CA3→CA1, Sayer et al., 1990, vs. 0.7mV for CA1→CA1 connections, Deuchars and Thomson, 1996), and the complexity of the basal and apical dendrites (such as the number of branches) is similar (e.g., Andersen et al., 2007).

We conclude that the total excitatory input received by a basal dendritic branch within SPW/Rs due to recurrent CA1→CA1 connections is at least comparable to the input an apical dendritic branch receives through CA3→CA1 Schaffer collaterals. However, inputs from CA3 are known to generate dendritic spikes during SPW/Rs in the apical dendrites of CA1 neurons (Kamondi et al., 1998). Thus, the comparison indicates that inputs from recurrent connections are likely

to generate dendritic spikes in CA1 basal dendrites. For CA3 recurrent connections, a similar argument holds with 5% recurrent connectivity, so 100 inputs per neuron around the peak of the SPW and a strength of $0.6 - 1.3$mV for individual inputs (Traub and Miles, 1991).

7.3. Discussion

In the present article, we have suggested a unifying model for learning, replay, sharp wave generation, and ripple generation. In our model, all four experimentally observed abilities of hippocampal networks are intimately interrelated. They are enhanced or enabled by nonlinear dendritic interactions mediated by fast dendritic spikes: The nonlinear dendrites promote replay directly and via the generation of sharp waves and ripples. The replay can take place on underlying networks that are only weakly structured and sparse, therewith the nonlinear dendrites indirectly simplify learning.

We introduced learning during an exploration phase by incorporating a standard type of network plasticity; changes of synaptic strengths depend on the timing of presynaptic and postsynaptic somatic spikes. We have incorporated a learning rule which possesses a power-law dependence on the synaptic weight before modification, in agreement with experimental findings (Bi and Poo, 1998; Morrison et al., 2007). It leads to a biologically plausible, stable, unimodal synaptic weight distribution. Our work shows that despite the tendency of the synapses to converge to the same equilibrium value, and the persistence of non-negligible background weights, the network structures established during exploration are strong enough to generate replay. We emphasize that our networks do not organize into a single feed-forward structure to enable replay, and that they allow learning of multiple sequences.

Besides synaptic weight modification also other forms of network plasticity have been experimentally found (Mozzachiodi and Byrne, 2010). Our network model suggest that especially the activity-dependent change of coupling between nonlinear dendritic branches and the soma (branch strength potentiation) may play a prominent role during learning of activity patterns in the hippocampus: When dendritic spike initiation occurs together with somatic action potentials, the strength of the dendritic spikes and their impact on the soma increase (Losonczy et al., 2008; Müller et al., 2012). This leads to strong dendritic spikes that support the reproduction of input-output relations from exploration phases, and may thus be expected to enhance dendritic spike based replay of activity during SPW/Rs.

We find that supported by nonlinear dendrites, activity propagates along comparably weakly enhanced, sparse, biologically plausible network structures. This generates a recall of the original sequence, which is noisy in the sense that the spike order is only roughly preserved and not every neuron of the sequence participates in every recall, in agreement with the experimental findings (Wilson and McNaughton, 1994; Nadasdy et al., 1999; Lee and Wilson, 2002; Pastalkova et al., 2008; Davidson et al., 2009).

Our model suggests that replay in hippocampal region CA1 may proceed dependent on its own recurrent connectivity and does not need to be directly imposed by replay in CA3. This is

consistent with experimental observations of replay in CA1 which is deafferented from CA3 (Nakashiba et al., 2009). It may support the different functionality of cells in CA3 and CA1 (Mizuseki et al., 2012), and allow for a more complex impact of replay within CA3 (and perhaps further regions such as the enthorinal cortex) and replay in CA1.

A common question is why replay is absent during exploration phases, while similar network structures generate replay during recall phases. This is usually explained by a strengthening of effective recurrent excitation by neuromodulators during recall (Hasselmo, 2006). In contrast to previous models, we do not have to assume such a strengthening. In our model, replay requires synchronous spiking, due to the sensitivity of nonlinear dendrites to it. To evoke the common targeted recall starting from a salient location, in our model a group of neurons with a subgroup encoding the location is activated to spike synchronously. For spontaneous, random recall, the spiking activity may be overall increased such that also a high level of synchronous spiking is present which at times evokes spontaneous recall. Since sufficient synchronous spiking is not present during exploration, replay will not be generated.

The learned network structures are "stripe-like" , they do not possess segmented, distinct groups of neurons like synfire chains (cf. Abeles, 1982, 1991). Importantly, we nevertheless observe that the propagation of activity proceeds in synchronous pulses, and thus "ripples" as experimentally found superimposed to sharp waves are generated. The occurrence of the pulses can be understood as follows: Replay is initiated by a synchronous stimulation of a few neurons partially sensitive to places near the same position in a trained sequence. This increases synchronous input and thus dendritic spiking in postsynaptic excitatory neurons, especially in such postsynaptic neurons which receive stronger synaptic input from many of the stimulated neurons. Due to the previous learning phase, these are neurons which signal places in the near future relative to the original position within the trained sequence. The dendritic spikes promote somatic spikes or directly generate them, with high temporal precision after the experimentally measured delay time of about 5ms (Ariav et al., 2003; Müller et al., 2012). Together with conventional inputs, this evokes a better synchronized, larger pulse of response spikes, in which neurons signaling the near future of the learned sequence are overrepresented. The pulse evokes a third one, with neurons farer in the future of the sequence being particularly prevalent and so on. Our simulations show that the pulses do not broaden despite the lack of underlying group structure in the network; they stay narrow and precise, due to the high precision of dendritic spike triggered somatic output spikes. In turn, the temporal structuring of propagating activity and the consequent input synchronization allow dendritic amplification of many inputs and thus promote the underlying replay.

Our model explains the experimentally found "sharp wave" in the hippocampus by an initially increase in the size of the synchronous pulses, and a subsequent decrease by inhibitory feedback. The amplitude of the increase is determined by the broadness of the learned network structure, by the amount of recurrent excitation and by the limiting action of accumulating overall recurrent inhibition in the network. We have recently shown that synchronous activity does not only affect neurons within the feed-forward structure, but induces a broader increase in network spiking activity (Jahnke et al., 2014a). The unspecific overall increase in activity supports replay by providing additional input to the neurons and the dendrites, thus making

them more ready to generate spikes in response to recurrent input which generates the replay. The event terminates when the overall inhibition overcomes recurrent excitation.

Taken together, our model suggests that ripple oscillations are generated by propagating activity and in turn enhance it. This idea of ripples supporting replay does not necessarily require that either of them depends on nonlinear dendrites. Indeed, we have recently shown that externally imposed high-frequency oscillations support propagation of synchrony along synfire chains both in presence and absence of nonlinear dendrites (Jahnke et al., 2014b). We expect that propagation along non-segmented network structures may equally well be supported. Further, we expect that also intrinsic ripple oscillations that are not dependent on nonlinear dendrites may be able to serve this purpose.

Our study clears the path for investigating the role of replay and SPW/Rs in learning and memory. An important direction of future research is how replay and SPW/Rs act back to restructure hippocampal networks. In particular it has been hypothesized that SPW/Rs may consolidate (Nadasdy et al., 1999) or erase (Buzsáki, 2006; Mehta, 2007) memory content in the hippocampus, and that they may lead to associative processes (Buzsáki, 2006; Andersen et al., 2007). The plasticity rules responsible for such restructuring may be different from those in exploration phases, due to the high level of inhibition during SPW/Rs (Nishiyama et al., 2000; Aihara et al., 2007; Cutsuridis, 2013) and it may be necessary to account for the prevalence of dendritic spikes (Remy and Spruston, 2007; Losonczy et al., 2008; Müller et al., 2012). Another important question is how replay and SPW/Rs shape neocortical networks. In particular, future research will clarify whether and how highly noisy, scarce replay in conjunction with SPW/R-activity and neocortical sleep spindles can imprint and consolidate memory content, as assumed by the two-stage memory hypothesis.

7.4. Acknowledgments

This work was supported by the BMBF (Grant No. 01GQ1005B) and the DFG (Grant No. TI 629/3-1). All simulation results were obtained using the simulation software NEST (Gewaltig and Diesmann, 2007). We thank Francesco Battaglia, Harold Gutch and Paul Tiesinga for stimulating discussions.

7.5. Methods

In this section we introduce the neuron model and system setup, provide a complete list of standard neuron and model parameters and derive a quantitative estimate for the average propagation frequency during induced replay events.

7.5.1. Neuron model

We consider networks of leaky integrate-and-fire neurons. The state of neuron i is described by its membrane potential V_i and the temporal dynamics of the membrane potential obey

$$C_i \frac{dV_i(t)}{dt} = g_i^{\mathrm{L}} \left[V_i^{\mathrm{eq}} - V_i(t)\right] + I_i^{\mathrm{ex}}(t) + I_i^{\mathrm{in}}(t) + I_i^0, \tag{7.6}$$

where C_i is the membrane capacity, g_i^{L} is the resting conductance and V_i^{eq} is the equilibrium potential. I_i^0 is a constant input current to neuron i and $I_i^{\mathrm{ex}}(t)$ and $I_i^{\mathrm{in}}(t)$ are currents arising from excitatory and inhibitory inputs, respectively. Whenever the membrane potential $V_i(t)$ exceeds the spiking threshold V_i^{Θ} at some $t = t^*$, a spike is sent to the postsynaptic neurons j, where it arrives after a delay time τ_{ji}. The sending neuron is reset to $V_i(t^*) = V_i^{\mathrm{reset}}$ and the neuron is refractory for a time period t_i^{ref}, i.e. $V_i(t) \equiv V_i^{\mathrm{reset}}$ for $t \in \left[t^*, t^* + t_i^{\mathrm{ref}}\right]$.

7.5.2. Synapses and dendrite models

Synapses

The effects of the synaptic inputs on the postsynaptic neurons are modeled by transient conductance changes. The time course of the synaptic conductance is given by the difference of two exponentials with time constants $\tau^{k,1}$ and $\tau^{k,2}$,

$$f^k(t) = \begin{cases} \left(A^k\right)^{-1} \left(e^{-\frac{t}{\tau^{k,1}}} - e^{-\frac{t}{\tau^{k,2}}}\right) & \text{for } t \geq 0 \\ 0 & \text{for } t < 0 \end{cases}, \tag{7.7}$$

for $k \in \{\mathrm{ex,in}\}$ describing the effect of an excitatory and inhibitory input, respectively, that is received at time $t_0 = 0$. The normalization constant A^k is chosen such that the peak conductance $\max_{t \geq t_0} \left\{f^k(t)\right\} = 1$,

$$A^k = \left(\frac{\tau^{k,2}}{\tau^{k,1}}\right)^{\frac{\tau^{k,2}}{\tau^{k,1} - \tau^{k,2}}} - \left(\frac{\tau^{k,2}}{\tau^{k,1}}\right)^{\frac{\tau^{k,1}}{\tau^{k,1} - \tau^{k,2}}}. \tag{7.8}$$

Throughout this article, we denote the strength of a synaptic connection by the value of the peak conductance, i.e., a single input from a connection of strength ϵ causes a conductance change $\epsilon \cdot f^k(t)$. Denoting the reversal potentials of excitatory and inhibitory currents by E^{ex} and E^{in}, the input currents to neuron i arising from synaptic inputs from other neurons of the network are given by

$$I_i^{\mathrm{ex}}(t) = g_i^{\mathrm{ex}}(t) \left[E^{\mathrm{ex}} - V_i(t)\right], \tag{7.9}$$

$$I_i^{\mathrm{in}}(t) = g_i^{\mathrm{in}}(t) \left[E^{\mathrm{in}} - V_i(t)\right]. \tag{7.10}$$

$g_i^{\mathrm{ex}}(t)$ and $g_i^{\mathrm{in}}(t)$ are linear superpositions of single responses (cf. Equation 7.7),

$$g_i^{\mathrm{ex}}(t) = \sum_{n,j} \epsilon_{ij}^{\mathrm{ex}} f^{\mathrm{ex}}\left(t - t_{j,n}^{\mathrm{f}} - \tau_{ij}\right), \tag{7.11}$$

$$g_i^{\mathrm{in}}(t) = \sum_{n,j} \epsilon_{ij}^{\mathrm{in}} f^{\mathrm{in}}\left(t - t_{j,n}^{\mathrm{f}} - \tau_{ij}\right), \tag{7.12}$$

where $\epsilon_{ij}^{\mathrm{ex}}$ (and $\epsilon_{ij}^{\mathrm{in}}$) denote the excitatory (and inhibitory) coupling strength from neuron j to neuron i and $t_{j,n}^{\mathrm{f}}$ is the nth spiking time of neuron j.

Non-linear dendrites

The above model implicitly assumes linear input summation in the dendrites. In addition to this, we incorporate nonlinear amplification of synchronous inputs mediated by fast dendritic spikes which have been found in single neuron experiments (Ariav et al., 2003; Gasparini et al., 2004; Polsky et al., 2004; Gasparini and Magee, 2006) and have been introduced in recent models of neuronal networks (Memmesheimer, 2010; Jahnke et al., 2012, 2013). Whenever the excitatory input to a (nonlinear) dendrite summed over a short time interval (ΔT^{s}) of less than some milliseconds crosses the dendritic threshold Θ_b, a dendritic spike is initiated and causes a depolarization in the some of the postsynaptic neuron, which exceeds the depolarization expected form linear summation of single inputs. We model the effect of a dendritic spike by a stereotypical current pulse, which is injected to the some after a time interval τ^{DS} after the dendritic threshold is crossed. The temporal offset τ^{DS} models the latency between the onset of the (linear) postsynaptic response and the response to the dendritic spike as observed in single neuron experiments (Ariav et al., 2003). The current pulse is described by the sum of three exponential functions,

$$I_{\mathrm{ds}} = \Theta\left(t - \tau^{\mathrm{DS}}\right)\left[-A\exp\left(-\frac{t-\tau^{\mathrm{DS}}}{\tau^{\mathrm{ds},1}}\right) + B\exp-\left(\frac{t-\tau^{\mathrm{DS}}}{\tau^{\mathrm{ds},2}}\right) - C\exp\left(-\frac{t-\tau^{\mathrm{DS}}}{\tau^{\mathrm{ds},3}}\right)\right] \tag{7.13}$$

with positive prefactors A,B,C and decay time constants $\tau^{\mathrm{ds},1}$, $\tau^{\mathrm{ds},2}$ and $\tau^{\mathrm{ds},3}$ which are chosen such that the somatic depolarization fits experimental data. To obtain the experimentally observed saturation of the somatic depolarization for inputs exceeding the dendritic threshold, the nonlinear dendrite becomes refractory for a time period $t^{\mathrm{ref,ds}}$ after generation of such a current pulse and does not transmit spikes within the refractory time period.

Synaptic plasticity

Recurrent excitatory connections are considered to be plastic and their weights are adjusted activity dependent. We employ a pair-based update rule for synaptic connections, i.e., the change of the weight of a synaptic connection depends on the temporal difference between pairs of pre- and post-synaptic spikes. Let Δ be the temporal difference between the spike of a post-

and a pre-synaptic neuron and denote the synaptic weight by ϵ, then this spike pair induces a weight change

$$\Delta\epsilon = \begin{cases} F^+(\epsilon)\exp\left(-\frac{|\Delta t|}{\tau^+}\right) & \text{if } \Delta t > 0 \\ -F^-(\epsilon)\exp\left(-\frac{|\Delta t|}{\tau^-}\right) & \text{if } \Delta t < 0. \end{cases} \tag{7.14}$$

Here $\tau^\pm$ are the time constants of the update window and $F^\pm(\epsilon)$ describes the weight dependence of the update rule. As proposed by Morrison et al. (2007) we use a power-law update rule

$$F^+(\epsilon) = \lambda\epsilon_0^{1-\mu}\epsilon^\mu \tag{7.15}$$

$$F^-(\epsilon) = \lambda\alpha\epsilon \tag{7.16}$$

where λ specifies the learning rate, ϵ_0 is a reference weight, $\mu \in [0,1]$ is the exponent of the synaptic potentiation rule and α is the asymmetry parameter which scales the synaptic depressing with respect to the synaptic potentiation. We choose the power-law update rule, because (i) it can be fitted to experimental data (Bi and Poo, 1998) better than, e.g., pure additive or multiplicative update rules (Morrison et al., 2007), and (ii) it has been shown that this update rule generate an unimodal weight distribution in the presence of uncorrelated Poissonian inputs (Morrison et al., 2007).

7.5.3. Network setup

We consider networks that are composed of N^{ex} excitatory and N^{in} inhibitory neurons. The neurons are randomly connected. Single connections are present with constant probabilities $p^{X,Y}$ (where $X, Y \in \{\text{ex}, \text{in}\}$) which depend on the type of post- and pre-synaptic neurons, e.g., $p^{\text{in,ex}}$ specifies the probability that a connection between an excitatory and inhibitory neuron is realized. The connection strengths are drawn from a Gaussian distribution with mean $\mu^{X,Y}$ and standard deviation $\sigma^{X,Y}$. The recurrent excitatory connections are considered plastic and adjust their weights according to the update rule (7.14-7.16), all other weights are static.

Like the synaptic weights the conduction delays are chosen heterogeneous. The total conduction delay between the presynaptic spiking and the onset of the postsynaptic somatic response can be decomposed into two components: (i) the axonal delay τ^{ax} and (ii) the time between the onset of synaptic transmission and the onset of the somatic response τ^X. We assume that τ^X is constant, but depends of the type of the postsynaptic neuron, whereas τ^{ax} depends on the distance between pre- and post-synaptic neuron and the conduction velocity. All neurons are placed on square patch witch edge length S, and τ^{ax} is computed by dividing the euclidean distance between the neurons by the conduction velocity v^{ax}. The mean distance between two (uniformely distributed) neurons on the quadratic patch is given by (Mathai et al., 1999)

$$\bar{d} = \frac{2 + \sqrt{2} + 5\text{Log}\left(\sqrt{2}+1\right)}{15} \cdot S \approx 0.5214 \cdot S \tag{7.17}$$

and thus the mean axonal delay are

$$\bar{\tau^{\text{ax}}} \approx 0.5214 \cdot \frac{S}{v^{\text{ax}}}. \tag{7.18}$$

To exclude finite size effects all axonal delays are shuffled. Additionally, neurons receive external Poissonian spike trains with rate $\nu^{X,Y}$ and constant input strength $c^{X,Y}$.

7.5.4. Place cell tuning curves

Differrent mechanisms underlying the location tuning and phase precession of hippocampal place cells have been proposed (see, e.g., Maurer and McNaughton, 2007; Moser et al., 2008, for reviews). In this article we adopt the idea that they are caused by the interaction of theta-modulated inhibition and excitation which increases along the place field (Mehta et al., 2002; Harris et al., 2002).

In our simplified model, spiking of place cells is generated by injection of rectangular current pulses whose amplitude and timing is determined by the current position x on a linear track. We assign a place field, centered at x_i^{ctr} with width Δw_i,

$$\mathcal{P}_i = \left[x_i^{\mathrm{ctr}} - \frac{\Delta w_i}{2}, x_i^{\mathrm{ctr}} + \frac{\Delta w_i}{2} \right], \tag{7.19}$$

randomly to some neurons i; we assume that only a fraction, p^{pf}, of the excitatory neurons are place-encoding on a given track. If the current position is within the place field of neuron i, i.e., $x \in \mathcal{P}_i$, additional rectangular current pulses of duration $\Delta\tau$ are injected. The amplitude as well as the timing of this current pulses depend on

$$\tilde{x}_i = \frac{x - \left(x_i^{\mathrm{ctr}} - \frac{\Delta w_i}{2} \right)}{\Delta w_i}, \tag{7.20}$$

the relative position within the place field of that cell.

The current pulses are time locked to an (virtual) oscillating background signal, the theta oscillation. During each oscillation period T, all neuron with a place field that incloses the current position x (i.e., $0 \leq \tilde{x}_i \leq 1$) receives an input of strength

$$I^{\mathrm{pf}}(\tilde{x}_i) = I^{\max} \left[-(2 \cdot \tilde{x}_i - 1)^2 + 1 \right] \tag{7.21}$$

which is shifted against the background oscillation by

$$DT(\tilde{x}_i) = 0.9 \left(1 - \tilde{x}_i^2 \right) T. \tag{7.22}$$

Such the amplitude is maximal at the center ($I^{\mathrm{pf}}(\tilde{x}_i = 0.5) = I^{\max}$) and decays quadratically to zero towards the beginning ($I^{\mathrm{pf}}(\tilde{x}_i = 0) = 0$) and the end ($I^{\mathrm{pf}}(\tilde{x}_i = 1) = 0$) of the place field (cf. Figure 7.1A; solid line). Further, the current pulse is shifted by almost a full oscillation period T against the theta oscillation when the position x is in the beginning of the place field ($DT(\tilde{x}_i = 0) = 0.9T$), and this time shift decreases quadratically to zero with increasing position ($DT(\tilde{x}_i = 1) = 0$) (cf. Figure 7.1A; dashed line).

To quantify the location tuning properties, we measure the spatio-temporal receptive field of a neuron with some place field $\mathcal{P}$: We record the spiking activity for different positions $x = \{x_1, x_2, \ldots, x_n\}$. For each recorded spike we calculate the phase-shift with respect to the theta oscillation,

$$\phi := 360^\circ \cdot \left(\frac{t^{\mathrm{sp}}}{T} - \left\lfloor \frac{t^{\mathrm{sp}}}{T} \right\rfloor \right) \in (0^\circ, 360^\circ] \,. \tag{7.23}$$

where t^{sp} denotes the spiking time and $\lfloor x \rfloor$ is the floor-function which maps a real number x to the largest integer not greater than x. The spatio-temporal receptive field is then a two-dimensional histogram for the location x (binning δx) and the phase shift ϕ (binning$\delta\phi$) normalized by the total time spent in this bin. As illustrated in Figure 7.1C the spiking reflects the characteristic of the rectangular input current: When traversing the place field, the average firing rate increases until it reaches the maximum at the center of the place field, and decreases afterwards. The single spikes are correlated to the theta rhythm: When entering the place field, the neuron spikes late in the theta rhythm and the preferred spiking moves to earlier and earlier times with increasing position.

7.5.5. Standard neuron and model parameter

Throughout the article we consider homogeneous neuron populations. We consider networks with $N^{\mathrm{ex}} = 2500$ excitatory and $N^{\mathrm{in}} = 250$ inhibitory neurons. The single neuron parameters for excitatory cells are $C_i \equiv C = 400\mathrm{pF}$, $V_i^{\mathrm{reset}} \equiv V^{\mathrm{reset}} = -65\mathrm{mV}$, $V_i^{\Theta} \equiv V^{\Theta} = -45\mathrm{mV}$, $g_i^{\mathrm{L}} \equiv g^{\mathrm{L}} = 25\mathrm{nS}$, $V_i^{\mathrm{eq}} \equiv V^{\mathrm{eq}} = -65\mathrm{mV}$ and $t_i^{\mathrm{ref}} \equiv t^{\mathrm{ref}} = 3\mathrm{ms}$ (Andersen et al., 2007; Staff et al., 2000) for all i. For inhibitory neurons we set $C_i \equiv C = 200\mathrm{pF}$, $V_i^{\mathrm{reset}} \equiv V^{\mathrm{reset}} = -65\mathrm{mV}$, $V_i^{\Theta} \equiv V^{\Theta} = -55\mathrm{mV}$, $g_i^{\mathrm{L}} \equiv g^{\mathrm{L}} = 25\mathrm{nS}$, $V_i^{\mathrm{eq}} \equiv V^{\mathrm{eq}} = -65\mathrm{mV}$ and $t_i^{\mathrm{ref}} \equiv t^{\mathrm{ref}} = 3\mathrm{ms}$ (Buhl et al., 1996; Geiger et al., 1997) for all i.

For excitatory neurons, the time constants of the excitatory conductances (AMPA) are $\tau^{\mathrm{ex},1} = 2.5\mathrm{ms}$ and $\tau^{\mathrm{ex},2} = 0.5\mathrm{ms}$ (Jonas et al., 1993; Liu and Tsien, 1995), and the time constants for inhibitory conductances ($\mathrm{GABA_A}$) are $\tau^{\mathrm{in},1} = 4.0\mathrm{ms}$ and $\tau^{\mathrm{in},2} = 0.3\mathrm{ms}$ (Pearce, 1993; Hájos and Mody, 1997; Bartos et al., 2007). For inhibitory neurons, the time constants of the excitatory conductances (AMPA) are $\tau^{\mathrm{ex},1} = 2.0\mathrm{ms}$ and $\tau^{\mathrm{ex},2} = 0.35\mathrm{ms}$ (Geiger et al., 1997; Galarreta and Hestrin, 2001; Angulo et al., 2001), and the time constants for inhibitory conductances ($\mathrm{GABA_A}$) are $\tau^{\mathrm{in},1} = 2.5\mathrm{ms}$ and $\tau^{\mathrm{in},2} = 0.4\mathrm{ms}$.

The connection probability are $p^{\mathrm{ex,ex}} = 0.08$, $p^{\mathrm{ex,in}} = 0.1$, $p^{\mathrm{in,ex}} = 0.1$ and $p^{\mathrm{in,in}} = 0.02$ (Ascoli and Atkeson, 2005; Andersen et al., 2007; Deuchars and Thomson, 1996). Recurrent excitatory neurons are plastic, with $\tau^{+} = 15\mathrm{ms}$, $\tau^{-} = 30\mathrm{ms}$, $\lambda = 0.05$, $\epsilon_0 = 1\mathrm{nS}$, $\mu = 0.4$ and $\alpha = 0.68$ as standard values for the power-law update rule. For this parameters the equilibrium weight distributions is approximately Gaussian with mean $\mu^{\mathrm{ex,ex}} = 0.7\mathrm{nS}$ and standard-deviation $\sigma^{\mathrm{ex,ex}} = 0.16\mathrm{nS}$. All other weights are drawn from Gaussian distributions with $\mu^{\mathrm{ex,in}} = 2.5\mathrm{nS}$, $\mu^{\mathrm{in,ex}} = 1.0\mathrm{nS}$, $\mu^{\mathrm{in,in}} = 2.0\mathrm{nS}$, and $\sigma^{\mathrm{ex,in}} = 0.25\mathrm{nS}$, $\sigma^{\mathrm{in,ex}} = 0.1\mathrm{nS}$, $\sigma^{\mathrm{in,in}} = 0.2$.

The dendritic conduction delays are $\tau^{\mathrm{ex}} = 1\mathrm{ms}$ and $\tau^{\mathrm{in}} = 0.5\mathrm{ms}$; the axonal delays are distance dependent (cf. Section 7.5.3). Neurons are randomly distributed on a square path with edge length $S = 350\mu\mathrm{m}$ and the conduction velocity is $v^{\mathrm{ax}} = 300\mu\mathrm{m/ms}$.

The parameters of the dendritic spike current are chosen according to single neuron experiments (e.g., Ariav et al., 2003; Polsky et al., 2004; Gasparini et al., 2004; Gasparini and Magee, 2006), $\Theta_b = 8.65\text{nS}$, $A = 55\text{nA}$, $B = 64\text{nA}$, $C = 9\text{nA}$, $\tau^{\text{ds},1} = 0.2\text{ms}$, $\tau^{\text{ds},2} = 0.3\text{ms}$, $\tau^{\text{ds},3} = 0.7\text{ms}$, $\tau^{\text{DS}} = 2.7\text{ms}$ and $t^{\text{ref,ds}} = 5\text{ms}$ (cf. also Memmesheimer, 2010; Jahnke et al., 2012). The standard value for the length of the dendritic integration window is $\Delta T^{\text{s}} = 2\text{ms}$.

The neurons receive external Poissonian random inputs with rates $\nu^{\text{ex,ex}} = 1.5\text{kHz}$, $\nu^{\text{ex,in}} = 0.5\text{kHz}$, $\nu^{\text{in,ex}} = 0.3\text{kHz}$ and $\nu^{\text{in,in}} = 0.1\text{kHz}$, and input strengths $c^{\text{ex,ex}} = 1.8\text{nS}$, $c^{\text{ex,in}} = 2.875\text{nS}$, $c^{\text{in,ex}} = 1.875\text{nS}$ and $c^{\text{in,in}} = 2.5\text{nS}$.

7.5.6. Estimating the propagation frequency of Sharp-Wave-Ripple like events

In our model, the spiking probability of a neuron due to an excitatory input below the dendritic threshold (i.e., no dendritic spike is elicited) is substantially smaller than the spiking probability due to a supra-threshold input (cf., also Jahnke et al., 2012, 2013, 2014a). Therefore replay events (i.e., propagating synchronous pulses) are mainly mediated by nonlinearly dendritically amplified inputs, and thus the propagation frequency is determined by the average time between presynaptic spikes and postsynaptic spikes elicited by dendritic ones.

The relevant neurophysiological quantities to estimate the propagation frequency are the axonal delay τ^{ax}, the synaptic delay τ^{ex}, the latency of the dendritic spike τ^{DS}, and the average time difference t^{ds} between the onset of the response to the dendritic spike and the spiking of the postsynaptic neurons. For hippocampal neurons, the synaptic delay τ^{ex} is typically in the range of $0.5 - 1.5\text{ms}$ (Miles and Wong, 1986; Debanne et al., 1995; Boudkkazi et al., 2007) and the latency of dendritic spikes τ^{DS} is in the order of $2.4 - 2.9\text{ms}$ (Ariav et al., 2003). The average axonal delay τ^{ax} depends on the the distance between presynaptic and postsynaptic neurons and the propagation velocity v^{ax}. The range of local connections in the hippocampus have been measured to be in the order of $300 - 400\mu\text{m}$ (Knowles and Schwartzkroin, 1981; Christian and Dudek, 1988; Oram et al., 1999; Orman et al., 2008). We therefore assume that the neurons are distributed on a quadratic patch width edge length S in the order of $300 - 400\mu m$. Together with the a conduction velocity of $200 - 400\mu m$ (Andersen et al., 2000; Meeks and Mennerick, 2006), the average axonal delay is in the range of $0.3 - 1.3\text{ms}$. The time t^{ds} between the onset of the response to the dendritic spike and the spike of the postsynaptic neuron depends weakly on the parameters of the current mimicking the dendritic spike and the neurons' ground state. For standard parameters it is typically between $0.5 - 0.9\text{ms}$. Combining the above estimations the average temporal difference between a presynaptic and postsynaptic spikes elicited by a dendritic spikes is between $3.7 - 6.4\text{ms}$ and therefore the propagation frequency is expected to be in the range $150 - 250\text{Hz}$.

Chapter 8

Summary and discussion

In this thesis we investigate the impact of dendritic sodium spikes on the dynamics of recurrent networks. These spikes endow neuronal dendrites with a powerful coincidence detection mechanism, and thereby enable them to detect and to nonlinearly amplify highly synchronous inputs (Ariav et al., 2003; London and Häusser, 2005; Spruston, 2008). In particular, we concentrate on signal transmission in the form of synchronous pulse packets in embedded feed-forward substructures. Such structures are hypothesized to underlie the generation of precisely timed spike patterns and signal transmission in recurrent networks (Abeles, 1982, 1991; Diesmann et al., 1999; Kumar et al., 2010).

Isolated feed-forward networks

As a starting point, we analyze signal transmission in isolated feed-forward structures (Chapter 3). We investigate leaky integrate-and-fire neurons in the limit of infinitesimal short interaction pulses. Here, the transmitted signal consists of exactly synchronous pulses. This approach allows to study the propagating of synchrony by considering solely the size of the pulse in terms of the number of synchronous spikes (instead of the size and the temporal spread, cf., e.g., Diesmann et al., 1999; Gewaltig et al., 2001; Goedeke and Diesmann, 2008), such that the analysis becomes analytically tractable. We consider both linearly and nonlinearly coupled networks. We derive scaling laws as well as quantitative estimates for the critical connectivity, marking the bifurcation point between regimes where robust propagation of synchrony is possible and where it is not.

The analytical derivations are based on rather general assumptions: (a) The effect of a synchronous pulse packet is approximated by the summed effect of single inputs, and (b) the spiking probability due to an dendritically enhanced input is substantial larger than due to a non-enhanced input. Therefore the scaling laws can be directly applied to biologically more plausible models, and in particular for networks incorporating nonlinear dendrites, even quantitative predictions for the critical connectivity are obtained.

Dendritic spikes indeed substantially reduce the coupling strength or layer size required for robust signal propagation. We conclude that even highly diluted feed-forward structures with synaptic efficiencies in the biological plausible range may be capable of transmitting synchronous signals if nonlinear dendritic interactions are taken into account.

Feed-forward sub-networks in recurrent networks

We furthermore consider embedded feed-forward substructures that occur naturally as parts of sparse random recurrent networks: The substructures are distinct from the remaining network by increased coupling strengths (Chapter 4 - 6) which might well be generated by learning, e.g., spike-time-dependent plasticity (cf. also Chapter 7).

Robust signal transmission requires a reliable separation of background activity and the transmitted signal. This puts conflicting requirements on the strength of the feed-forward structure: On the one hand it must be sufficiently strong to enable a robust signal propagation, on the other hand it must be sufficiently weak to prevent spontaneous synchrony propagation caused by accumulated correlations (Tetzlaff et al., 2002; Litvak et al., 2003; Rosenbaum et al., 2011). These constraints strongly limit the capability of linearly coupled networks to robustly propagate synchronous signals (Chapter 4, and cf. also Vogels and Abbott, 2005), in particular, if the layer sizes are small.

In nonlinearly coupled networks, propagation of synchrony is mainly mediated by dendritic spikes that are sensitive to synchronous input only, i.e., the effective strength of the synaptic connections changes dynamically with input synchrony. Therefore these spikes support separation of signal and background activity. Robust propagation is enabled (by dendritically enhanced inputs), while the asynchronous background activity does not induce spontaneous synchrony propagation. We conclude that dendritic nonlinearities offer a viable mechanism for robust signal transmission in recurrent networks with weakly (biological plausible) feed-forward substructures.

Network echo

In recurrent networks, the propagating signal also influences the global activity of the embedding network. Propagating synchronous signals induce synchronous spiking in the embedding network that might cause pathological activity states ("Synfire explosions" Mehring et al., 2003; Aviel et al., 2003).

In Chapter 5 we consider the network echo to propagating synchronous signals, and their backreaction to the propagating pulses in nonlinearly coupled networks. We show analytically, supported by direct numerical simulations, that for standard (Erdös-Renyi) random topologies this network echo is either negligible (if the recurrent coupling is weak — the embedded feed-forward network behaves like an isolated structure with appropriate random background inputs), or synchrony spreads over the whole network and cause large scale synchronous events (synfire

explosions). In essence, for such random graphs all neurons have a similar connectivity and thus either none or all neurons of the network echo the synchronous propagating signal.

However, if the degree distribution (i.e., the distribution of incoming and outgoing connections for each neurons) is broader, also moderate — non pathological — network echos can emerge. In particular, we show that in networks that contain a small number of hubs (nodes that are higher-than-average connected), these nodes preferably respond to propagating synchronous signals in the feed-forward substructure. In the presence of a synchronous signal, the population of hubs starts to oscillate (i.e., it echos the transmitted signal) and its feedback in turn stabilizes the propagating pulse. Hub- and signal-carrying populations activate each other and thereby the hub-nodes enable signal transmission through weakly structured networks in which a robust signal propagation is not possible in the absence of hubs.

This mutual activation is in contrast to the function commonly associated with hubs: In our setting the hubs themselves do not spread the relevant signals, but unspecifically activate the signal carrying subnetworks. We show that this phenomenon is generic in networks whose units have some probabilistic threshold character. This character is abundant throughout networks in nature and society, e.g., it occurs in neural networks, in gene and protein networks, in social networks, in supply networks and in communication networks (e.g., Granovetter, 1978; Watts, 2002; Nowotny and Huerta, 2003; Bornholdt, 2008; Lorenz et al., 2009; Cayco-Gajic and Shea-Brown, 2013). Likewise, hubs constitute a prominent structural feature in many real world networks (Bornholdt and Ebel, 2001; Liljeros et al., 2001; Riley et al., 2003; Ebel et al., 2002; Hufnagel et al., 2004; Bonifazi et al., 2009; Kaluza et al., 2010; Newman, 2010; Barthelemy, 2011; Varshney et al., 2011). We conclude that hubs can act as generic (dynamic) signal amplifier in recurrent networks.

It remains to investigate how other prominent features of real world networks, like small-world properties (Watts and Strogatz, 1998; Newman, 2010), or the prevalence of certain small sub-patterns (called “motifs”; Milo et al., 2002; Song et al., 2005; Perin et al., 2011) influence signal transmission. We hypothesize that they might likewise have a selective amplifying effect on synchronous signals.

Neuronal oscillations

Network oscillations of various frequencies are abundant in cortical networks and can be related to attentional states and sensory stimulation (Fries et al., 2002; Fries, 2005; Palva and Palva, 2007; Womelsdorf et al., 2007; Womelsdorf and Fries, 2007; Lakatos et al., 2008; Kopell et al., 2010; Buschman et al., 2012). Moreover, in the hippocampus the occurrence of precise spike patterns is accompanied by high-frequency oscillations of up to 200 Hz (Buzsáki et al., 1992; Ylinen et al., 1995; Maier et al., 2003, 2011; Buzsáki and Silva, 2012, cf. also Chapter 7).

In Chapter 6 we investigate the impact of background oscillations (in particular, high-frequency oscillations) on the capabilities of recurrent networks to transmit synchronous signals. Such oscillations, by exciting the neurons of the network (including the current target layer of a propagating synchronous pulse) and thus contributing to spike generation, may enable a robust signal

propagation in weak feed-forward structures, even if those are too weak to robustly propagate a signal in the absence of this additional stimulation.

We highlight that propagation in networks with and without dendritic nonlinearities differ qualitatively: In linearly coupled networks the time between presynaptic stimulation and postsynaptic spike generation (if the input is sufficiently strong to elicit a spike) decreases with increasing stimulation strength — larger and larger depolarization causes shorter and shorter responding times. In nonlinearly coupled networks, if the postsynaptic spike is caused by a dendritic one (which is an all-or-none event), the time difference between stimulation and postsynaptic spike only weakly depends on stimulation strength. As a consequence, propagation of synchrony in nonlinearly coupled feed-forward networks exhibits a "natural" propagation frequency, while in linearly coupled networks the propagation frequency increases with coupling strength.

The existence of a natural propagation frequency together with the short dendritic integration window (i.e., the sensitivity of dendritic spike generation to highly synchronous stimulation only) yields resonances and locking between (external) oscillations and propagating synchronous signals: The additional (oscillatory) input may contribute to dendritic spike generation only if the ratio between the natural frequency and stimulation frequency is rational. Therefore the emergence of resonance yields a mechanism to selectively activate different signal propagation pathways (i.e., different feed-forward substructure) with appropriate stimulation frequencies.

In linearly coupled networks such resonances are absent. The additional oscillatory input, however, might nonetheless support signal propagation, but this support is caused by a net depolarizing effect which can be equally well obtained by a temporally constant depolarizing input current.

Experimental data suggest that there is a balance between excitatory and inhibitory inputs to single neurons in cortical networks during spontaneous and sensory-evoked activity (Haider et al., 2006; Okun and Lampl, 2008; Atallah and Scanziani, 2009). We therefore consider external inputs composed of inhibitory and excitatory spike trains. In linearly coupled networks, the temporally averaged net depolarization (or hyperpolarization) determines whether a propagation of synchrony is supported or not: Only net depolarizing inputs promote signal transmission. In contrast, in nonlinearly coupled networks, the ratio between excitation and inhibition is less important: Dendritic spikes are elicited by sufficiently strong and synchronous excitatory inputs, and inhibition fails to suppress dendritic spike generation (Müller et al., 2012). Thus, oscillations can support signal transmission even if the net effect of the inputs is hyperpolarizing.

Memory formation

Taken together, in Chapter 3 - 6 we analytically and computationally study synchrony propagation in isolated and embedded feed-forward networks. We show that nonlinear dendrites relax the requirement of prominent feed-forward structures for robust signal transmission, and that this is requirement can be even more relaxed by neuronal oscillations, or by suitable connection topologies of the embedding network.

Mildly prominent feed-forward structures (in contrast to all-to-all coupled synfire chains) are compatible with experimental findings. Further, they can be formed faster by synaptic plasticity (assuming a constant plasticity rate), i.e., the process of formation and reconfiguration of information pathways (memories) is simplified. Alternatively, they allow signal transmission in networks with reduced layer size (assuming constant synaptic efficiencies). We thus expect an increase in storage capacity, as the number of neurons required to represent a certain memory is reduced.

Biological application

An important candidate region for the generation of propagating synchrony is the hippocampus. Here during sleep or rest, previously learned spike patterns are replayed (Wilson and McNaughton, 1994; Lee and Wilson, 2002) in conjunction with globally increased spiking activity and superimposed high-frequency oscillations (Buzsáki et al., 1992; Ylinen et al., 1995; Maier et al., 2003) — the Sharp Wave Ripple complexes (SPW/Rs). Strong dendritic sodium spikes that are capable of generating highly precise output spikes are prominently found in the basal and radial oblique dendrites of hippocampal pyramidal neurons (Ariav et al., 2003; Losonczy et al., 2008; Müller et al., 2012; Makara and Magee, 2013). At these dendritic regions most of the recurrent connections in area CA1/3 terminate (Andersen et al., 2007; Cutsuridis et al., 2010), suggesting that the replay observed in CA1/3 may be mediated by these spikes.

In Chapter 7 we derive a unified model to describe the learning of activity patterns during spatial exploration phases, and its subsequent recall with emergent Sharp Wave Ripples. During the exploration phase, spiking activity resembling the one observed in *in vivo* experiments generates a stripe-like feed-forward structure by spike-time-dependent plasticity and the later recall of the learned spike patterns is enabled by dendritic spikes.

Our model explains the (comparatively) short duration of the events, the form of the Sharp Wave and the high stochasticity of the replay. It even quantitatively predicts the oscillation frequency of the ripples (Memmesheimer, 2010). SPW/R events are started by an initial specific (i.e., targeted to a special "initial" subset of neurons) or unspecific (i.e., targeted to the whole network) synchronous stimulation. Synchronous activity propagates along the stripe-like learned feed-forward structure. In contrast to layered feed-forward networks, where the size of each synchronous pulse is bounded from above by the layer size, here no such confining mechanism is present. The size of subsequent synchronous pulses increases. However, at the same time the activity of the inhibitory interneurons increases. The inhibitory feed-back might not suppress strong dendritic spikes, but if too strong hinder somatic spike generation by strong hyperpolarization of the cell body (Müller et al., 2012). Thus after an initial increase of activity the inhibition overwhelms the excitatory input and terminates the event. This mechanism explains the finite duration and the wave form of the event. Due to the absence of a layered structure, consecutive pulses smear out and overlap each other. Moreover, because of the sparse connectivity only a moderate fraction of neurons take part in a single SPW/R event. These effects explain the trial-to-trial variability of the replayed spike patterns. Finally, the ripple frequency

is determined by the average time interval between a presynaptic stimulation and postsynaptic spike elicited by dendritic ones. We show that for biologically plausible parameter values (including heterogeneous distance-dependent delay distributions and finite activation times for dendritic spike generation), the propagation (i.e., oscillation) frequency is in the experimentally observed range of $150 - 200$ Hz (cf. also Memmesheimer, 2010). In our model and in agreement with recent experimental findings the oscillation frequency does not change with strength and duration of inhibitory interactions (Viereckel et al., 2013).

It is commonly assumed that area CA1 is too sparsely connected to enable a replay based on recurrent connectivity (Andersen et al., 2007; Cutsuridis et al., 2010). Yet, we discuss in Chapter 7 that even the sparse connectivity in CA1 is sufficient to generate local dendritic spikes (during SPW/R events) and therefore render the local generation of replay and SPW/R in that sparsely connected region possible. This is in agreement with experimental observation of replay in CA1 which is deafferented from CA3 (Nakashiba et al., 2009).

Our study clears the path for investigating the role of replay and SPW/Rs in learning and memory. An important direction of future research is how replay and SPW/Rs act back to restructure hippocampal networks. In particular it has been hypothesized that SPW/Rs may consolidate (Nadasdy et al., 1999) or erase (Buzsáki, 2006; Mehta, 2007) memory content in the hippocampus, and that they may lead to associative processes (Buzsáki, 2006; Andersen et al., 2007). The plasticity rules responsible for such restructuring may be different from those in exploration phases, due to the high level of inhibition during SPW/Rs (Nishiyama et al., 2000; Aihara et al., 2007; Cutsuridis, 2013) and it may be necessary to account for the prevalence of dendritic spikes (Remy and Spruston, 2007; Losonczy et al., 2008; Müller et al., 2012). Another important question is how replay and SPW/Rs shape neocortical networks. In particular, future research will clarify whether and how highly noisy, scarce replay in conjunction with SPW/R-activity and neocortical sleep spindles can imprint and consolidate memory content, as assumed by the two-stage memory hypothesis (Marr, 1971; Buzsáki, 1989).

Bibliography

Abbott L.F. and Nelson S.B. (2000). Synaptic plasticity: Taming the beast. *Nat. Neurosci.* **3**:1178.

Abeles M. (1982). *Local Cortical Circuits: An Electrophysiological Study*. Springer, Berlin.

Abeles M. (1991). *Corticonics: Neural Circuits of the Cerebral Cortex*. Cambridge University Press.

Abeles M., Bergman H., Margalit E., and Vaadia E. (1993). Spatiotemporal firing patterns in the frontal cortex of behaving monkeys. *J. Neurophysiol.* **70**:1629.

Aertsen A., Diesmann M., and Gewaltig M.O. (1996). Propagation of synchronous spiking activity in feedforward neural networks. *J. Physiol.* **90**:243.

Agnihotri N.T., Hawkins R.D., Kandel E.R., and Kentros C. (2004). The long-term stability of new hippocampal place fields requires new protein synthesis. *Proc. Natl. Acad. Sci. U. S. A.* **101**:3656.

Aihara T., Abiru Y., Yamazaki Y., Watanabe H., Fukushima Y., and Tsukada M. (2007). The relation between spike-timing dependent plasticity and Ca^{2+} dynamics in the hippocampal CA1 network. *Neuroscience* **145**:80.

Amaral D., Ishizuka N., and Claiborne B. (1990). Neurons, numbers and the hippocampal network. *Prog. Brain Res.* **83**:1.

Andersen P., Morris R., Amaral D., Bliss T., and O'Keefe J. (2007). *The Hippocampus Book*. Oxford University Press, Oxford.

Andersen P., Soleng A., and Raastad M. (2000). The hippocampal lamellar hypothesis revisited. *Brain Res.* **886**:165.

Angulo M., Rossier J., and Audinat E. (2001). Postsynaptic glutamate receptors and integrative properties of fast-spiking interneurons in the rat neocortex. *J. Neurophysiol.* **82**:1295.

Ariav G., Polsky A., and Schiller J. (2003). Submillisecond precision of the input-output transformation function mediated by fast sodium dendritic spikes in basal dendrites of CA1 pyramidal neurons. *J. Neurosci.* **23**:7750.

Ascoli G. and Atkeson J. (2005). Incorporating anatomically realistic cellular-level connectivity in neural network models of the rat hippocampus. *Biosystems* **79**:173.

Atallah B.V. and Scanziani M. (2009). Instantaneous modulation of gamma oscillation frequency by balancing excitation with inhibition. *Neuron* **62**:566.

August D. and Levy W. (1999). Temporal sequence compression by an integrate-and-fire model of hippocampal area CA3. *J. Comput. Neurosci.* **6**:71.

Aviel Y., Mehring C., Abeles M., and Horn D. (2003). On embedding synfire chains in a balanced network. *Neural Comput.* **15**:1321.

Azevedo F.A.C., Carvalho L.R.B., Grinberg L.T., Farfel J.M., Ferretti R.E.L., Leite R.E.P., Jacob Filho W., Lent R., and Herculano-Houzel S. (2009). Equal numbers of neuronal and nonneuronal cells make the human brain an isometrically scaled-up primate brain. *J. Comp. Neurol.* **513**:532.

Bang-Jensen J. and Gutin G. (2002). *Digraphs. Theory, Algorithms and Applications.* Springer, London.

Barthelemy M. (2011). Spatial networks. *Phys. Rep.* **499**:1 .

Bartos M., Vida I., and Jonas P. (2007). Synaptic mechanisms of synchronized gamma oscillations in inhibitory interneuron networks. *Nat. Rev. Neurosci.* **8**:45.

Bean B.P. (2007). The action potential in mammalian central neurons. *Nat. Rev. Neurosci.* **8**:451.

Bear M., Paradiso M., and Connors B. (2006). *Neuroscience: Exploring the Brain.* Lippincott Williams & Wilkins.

Ben-Ari Y., Khazipov R., Leinekugel X., Caillard O., and Gaiarsa J.L. (1997). $GABA_A$, NMDA and AMPA receptors: A developmentally regulated 'ménage à trois'. *Trends Neurosci.* **20**:523.

Bi G. and Poo M. (2001). Synaptic modification by correlated activity: Hebb's postulate revisited. *Annu. Rev. Neurosci.* **24**:139.

Bi G.Q. and Poo M.M. (1998). Synaptic modifications in cultured hippocampal neurons: Dependence on spike timing, synaptic strength, and postsynaptic cell type. *J. Neurosci.* **18**:10464.

Bienenstock E.L., Cooper L.N., and Munro P.W. (1982). Theory for the development of neuron selectivity: Orientation specificity and binocular interaction in visual cortex. *J. Neurosci.* **2**:32.

Birznieks I., Wheat H.E., Redmond S.J., Salo L.M., Lovell N.H., and Goodwin A.W. (2010). Encoding of tangential torque in responses of tactile afferent fibres innervating the fingerpad of the monkey. *J. Physiol.* **588**:1057.

Bonifazi P., Goldin M., Picardo M.A., Jorquera I., Cattani A., Bianconi G., Represa A., Ben-Ari Y., and Cossart R. (2009). GABAergic hub neurons orchestrate synchrony in developing hippocampal networks. *Science* **326**:1419.

Börgers C. and Kopell N. (2003). Synchronization in networks of excitatory and inhibitory neurons with sparse, random connectivity. *Neural Comput.* **15**:509.

Bornholdt S. (2008). Boolean network models of cellular regulation: Prospects and limitations. *J. R. Soc. Interface* **5**:S85.

Bornholdt S. and Ebel H. (2001). World Wide Web scaling exponent from Simon's 1955 model. *Phys. Rev. E* **64**:035104.

Bostock E., Muller R.U., and Kubie J.L. (1991). Experience-dependent modifications of hippocampal place cell firing. *Hippocampus* **1**:193.

Both M., Bähner F., von Bohlen und Halbach O., and Draguhn A. (2008). Propagation of specific network patterns through the mouse hippocampus. *Hippocampus* **18**:899.

Boudkkazi S., Carlier E., Ankri N., Caillard O., Giraud P., Fronzaroli-Molinieres L., and Debanne D. (2007). Release-dependent variations in synaptic latency: A putative code for short- and long-term synaptic dynamics. *Neuron* **56**:1048.

Braitenberg V. and Schüz A. (1998). *Cortex: Statistics and Geometry of Neuronal Connectivity*. Springer, Berlin.

Branco T., Clark B.A., and Häusser M. (2010). Dendritic discrimination of temporal input sequences in cortical neurons. *Science* **329**:1671.

Brette R., Rudolph M., Carnevale T., Hines M., Beeman D., Bower J.M., Diesmann M., Morrison A., Goodman P.H., Harris F.C., Zirpe M., Natschläger T., Pecevski D., Ermentrout B., Djurfeldt M., Lansner A., Rochel O., Vieville T., Muller E., Davison A.P., Boustani S.E., and Destexhe A. (2007). Simulation of networks of spiking neurons: A review of tools and strategies. *J. Comput. Neurosci.* **23**:349.

Breuer D., Timme M., and Memmesheimer R. (2014). Non-additive dendrites in single neurons and associative memory networks. *Phys. Rev. X* **in press**.

Brunel N. (2000). Dynamics of sparsely connected networks of excitatory and inhibitory spiking neurons. *J. Comput. Neurosci.* **8**:183.

Brunel N. and Hakim V. (1999). Fast global oscillations in networks of integrate-and-fire neurons with low firing rate. *Neural Comput.* **11**:1621.

Brunel N. and Wang X.J. (2003). What determines the frequency of fast network oscillations with irregular neural discharges? I. Synaptic dynamics and excitation-inhibition balance. *J. Neurophysiol.* **90**:415.

Buhl E., Szilágyi T., Halasy K., and Somogyi P. (1996). Physiological properties of anatomically identified basket and bistratified cells in the CA1 area of the rat hippocampus in vitro. *Hippocampus* **6**:294.

Burgess N. and O'Keefe J. (2011). Models of place and grid cell firing and theta rhythmicity. *Curr. Opin. Neurobiol.* **21**:734.

Burkitt A. (2006a). A review of the integrate-and-fire neuron model: I. Homogeneous synaptic input. *Biol. Cybern.* **95**:1.

Burkitt A. (2006b). A review of the integrate-and-fire neuron model: II. Inhomogeneous synaptic input and network properties. *Biol. Cybern.* **95**:97.

Buschman T.J., Denovellis E.L., Diogo C., Bullock D., and Miller E.K. (2012). Synchronous oscillatory neural ensembles for rules in the prefrontal cortex. *Neuron* **76**:838.

Bush D., Philippides A., Husbands P., and O'Shea M. (2010). Dual coding with STDP in a spiking recurrent neural network model of the hippocampus. *PLoS Comput. Biol.* **6**:e1000839.

Buzsáki G. (1989). Two-stage model of memory trace formation: A role for "noisy" brain states. *Neuroscience* **31**:551.

Buzsáki G. (2006). *Rhythms of the Brain.* Oxford University Press, Oxford.

Buzsáki G. and Chrobak J. (1995). Temporal structures in spatially organized neuronal ensembles: A role for interneuronal networks. *Curr. Opin. Neurobiol.* **5**:504.

Buzsáki G., Horváth Z., Urioste R., Hetke J., and Wise K. (1992). High frequency network oscillation in the hippocampus. *Science* **256**:1025.

Buzsáki G. and Silva F.L.d. (2012). High frequency oscillations in the intact brain. *Prog. Neurobiol.* **98**:241.

Ramón y Cajal S. (1888a). Estructura de los centros nerviosos de les aves. *Rev. Trim. Histol. Normal Patol.* **1**:1.

Ramón y Cajal S. (1888b). Sobre las fibras nerviosas de la capa granulosa del cerebelo. *Rev. Trim. Histol. Normal Patol.* **1**:107.

Ramón y Cajal S. (1888c). Sobre las fibras nerviosas de la capa molecular del cerebelo. *Rev. Trim. Histol. Normal Patol.* **1**:33.

Caporale N. and Dan Y. (2008). Spike timing-dependent plasticity: A hebbian learning rule. *Annu. Rev. Neurosci.* **31**:25.

Câteau H. and Fukai T. (2001). Fokker-planck approach to the pulse packet propagation in synfire chain. *Neural Netw.* **14**:675.

Cayco-Gajic N.A. and Shea-Brown E. (2013). Neutral stability, rate propagation, and critical branching in feedforward networks. *Neural Comput.* **25**:1768.

Cenquizca L.A. and Swanson L.W. (2007). Spatial organization of direct hippocampal field CA1 axonal projections to the rest of the cerebral cortex. *Brain Res. Rev.* **56**:1.

Chartrand G. and Lesniak L. (2000). *Graphs and Digraphs.* Chapman and Hall, Boca Raton.

Christian E. and Dudek F. (1988). Electrophysiological evidence from glutamate microapplications for local excitatory circuits in the CA1 area of rat hippocampal slices. *J. Neurophysiol.* **59**:110.

Chrobak J. and Buzsáki G. (1996). High-frequency oscillations in the output network of the hippocampal-enthorinal axis of the freely behaving rat. *J. Neurosci.* **16**:3056.

Colgin L.L., Moser E.I., and Moser M.B. (2008). Understanding memory through hippocampal remapping. *Trends Neurosci.* **31**:469.

Connors B. and Long M. (2004). Electrical synapses in the mammalian brain. *Annu. Rev. Neurosci.* **27**:393.

Cook E.P. and Johnston D. (1997). Active dendrites reduce location-dependent variability of synaptic input trains. *J. Neurophysiol.* **78**:2116.

Cook E.P. and Johnston D. (1999). Voltage-dependent properties of dendrites that eliminate

location-dependent variability of synaptic input. *J. Neurophysiol.* **81**:535.

Csicsvari J., Hirase H., Czurko A., and Buzsáki G. (1998). Reliability and state dependence of pyramidal cell-interneuron synapses in the hippocampus: An ensemble approach in the behaving rat. *Neuron* **21**:179.

Csicsvari J., Hirase H., Czurkó A., Mamiya A., and Buzsáki G. (1999a). Fast network oscillations in the hippocampal CA1 region of the behaving rat. *J. Neurosci.* **19:RC20**:1.

Csicsvari J., Hirase H., Czurkó A., Mamiya A., and Buzsáki G. (1999b). Oscillatory coupling of hippocampal pyramidal cells and interneurons in the behaving rat. *J. Neurosci.* **19**:274.

Csicsvari J., Hirase H., Mamiya A., and Buzsáki G. (2000). Ensemble patterns of hippocampal CA3-CA1 neurons during sharp wave-associated population events. *Neuron* **28**:585.

Cutsuridis V. (2013). Interaction of inhibition and triplets of excitatory spikes modulates the NMDA-r-mediated synaptic plasticity in a computational model of spike timing-dependent plasticity. *Hippocampus* **23**:75.

Cutsuridis V., Graham B., Cobb S., and Vida I. (2010). *Hippocampal Microcircuits: A Computational Modeler's Resource Book.* Springer Series in Computational Neuroscience. Springer.

Cutsuridis V. and Hasselmo M. (2011). Spatial memory sequence encoding and replay during modeled theta and ripple oscillations. *Cognitive Computation* **3**:554.

Dale H. (1935). Pharmacology and nerve-endings (Walter Ernest Dixon memorial lecture). *Proc. R. Soc. Med.* **28**:319.

Dave A.S. and Margoliash D. (2000). Song replay during sleep and computational rules for sensorimotor vocal learning. *Science* **290**:812.

Davidson T., Kloosterman F., and Wilson M. (2009). Hippocampal replay of extended experience. *Neuron* **63**:497.

Dayan P. and Abbott L. (2001). *Theoretical Neuroscience: Computational and Mathematical Modeling of Neural Systems.* MIT Press, Cambridge.

Debanne D., Guérineau N., Gähwiler B., and Thompson S. (1995). Physiology and pharmacology of unitary synaptic connections between pairs of cells in areas CA3 and CA1 of rat hippocampal slice cultures. *J. Neurophysiol.* **73**:1282.

Denker M., Timme M., Diesmann M., Wolf F., and Geisel T. (2004). Breaking synchrony by heterogeneity in complex networks. *Phys. Rev. Lett.* **92**:074103.

Dermietzel R. (1998). Gap junction wiring: A 'new' principle in cell-to-cell communication in the nervous system? *Brain Res. Rev.* **26**:176.

Destexhe A., Rudolph M., and ParÃŁ D. (2003). The high-conductance state of neocortical neurons in vivo. *Nat. Rev. Neurosci.* **4**:739.

Deuchars J. and Thomson A. (1996). CA1 pyramid-pyramid connections in rat hippocampus *in vitro*: Dual intracellular recordings with biocytin filling. *Neuroscience* **74**:1009.

Diesmann M., Gewaltig M.O., and Aertsen A. (1999). Stable propagation of synchronous spiking in cortical neural networks. *Nature* **402**:529.

Donoso J., Chenkov N., and Kempter R. (2013). Modeling ripple oscillations in the hippocampus. *BMC Neuroscience* **14**:P208.

Duvernoy H.M. (2005). *The Human Hippocampus: Functional Anatomy, Vascularization and Serial Sections with MRI*. Springer.

Eagleman S.L. and Dragoi V. (2012). Image sequence reactivation in awake V4 networks. *Proc. Natl. Acad. Sci. U. S. A.* **109**:19450.

Ebel H., Mielsch L.I., and Bornholdt S. (2002). Scale-free topology of e-mail networks. *Phys. Rev. E* **66**:035103(R).

Eccles J.C., Fatt P., and Koketsu K. (1954). Cholinergic and inhibitory synapses in a pathway from motor-axon collaterals to motoneurones. *J. Physiol.* **126**:524.

Ego-Stengel V. and Wilson M. (2010). Disruption of ripple-associated hippocampal activity during rest impairs spatial learning in the rat. *Hippocampus* **20**:1.

Eichenbaum H., Dudchenko P., Wood E., Shapiro M., and Tanila H. (1999). The hippocampus, memory, and place cells: Is it spatial memory or a memory space? *Neuron* **23**:209.

Ekstrom A., Kahana M., Caplan J., Fields T., Isham E., Newman E., and Fried I. (2003). Cellular networks underlying human spatial navigation. *Nature* **425**:184.

Engineer C.T., Perez C.A., Chen Y.H., Carraway R.S., Reed A.C., Shetake J.A., Jakkamsetti V., Chang K.Q., and Kilgard M.P. (2008). Cortical activity patterns predict speech discrimination ability. *Nat. Neurosci.* **11**:603.

Ernst U., Pawelzik K., and Geisel T. (1995). Synchronization induced by temporal delays in pulse-coupled oscillators. *Phys. Rev. Lett.* **74**:1570.

Feinerman O. and Moses E. (2006). Transport of information along unidimensional layered networks of dissociated hippocampal neurons and implications for rate coding. *J. Neurosci.* **26**:4526.

Feinerman O., Segal M., and Moses E. (2005). Signal propagation along unidimensional neuronal networks. *J. Neurophysiol.* **94**:3406.

Fiete I.R., Senn W., Wang C.Z.H., and Hahnloser R.H.R. (2010). Spike-time-dependent plasticity and heterosynaptic competition organize networks to produce long scale-free sequences of neural activity. *Neuron* **65**:563.

Filatrella G., Nielsen A.H., and Pedersen N.F. (2008). Analysis of a power grid using a kuramoto-like model. *Eur. Phys. J. B* **61**:485.

Fisahn A., Pike F.G., Buhl E.H., and Paulsen O. (1998). Cholinergic induction of network oscillations at 40 hz in the hippocampus in vitro. *Nature* **394**:186.

Fries P. (2005). A mechanism for cognitive dynamics: Neuronal communication through neuronal coherence. *Trends Cogn. Sci.* **9**:474.

Fries P., Schröder J.H., Roelfsema P.R., Singer W., and Engel A.K. (2002). Oscillatory neuronal synchronization in primary visual cortex as a correlate of stimulus selection. *J. Neurosci.* **22**:3739.

Galarreta M. and Hestrin S. (2001). Spike transmission and synchrony detection in networks of GABAergic interneurons. *Science* **292**:2295.

Galvani L. and Aldini J. (1792). *Aloysii Galvani: De viribus electricitatis in motu musculari.* apud Societatem typographicum.

Gasparini S. and Magee J.C. (2006). State-dependent dendritic computation in hippocampal CA1 pyramidal neurons. *J. Neurosci.* **26**:2088.

Gasparini S., Migliore M., and Magee J.C. (2004). On the initiation and propagation of dendritic spikes in CA1 pyramidal neurons. *J. Neurosci.* **24**:11046.

Geiger J., Lübke J., Roth A., Frotschner M., and Jonas P. (1997). Submillisecond AMPA receptor signaling at a principal neuron-interneuron synapse. *Neuron* **18**:1009.

Geisler C., Brunel N., and Wang X.J. (2005). Contributions of intrinsic membrane dynamics to fast network oscillations with irregular neuronal discharges. *J. Neurophysiol.* **94**:4344.

Gennari F. (1782). *De peculiari structura cerebri.* Parmae ex regio typographeo.

Gerlach J. (1872). über die struktur der grauern substanz des menschlichen gehirns. *Zentralbl. Med. Wissensch.* **10**:273.

Gerstner W. and Kistler W. (2002). *Spiking Neuron Models: Single Neurons, Populations, Plasticity.* Cambridge Univ. Press, Cambridge.

Gewaltig M.O. and Diesmann M. (2007). Nest (neural simulation tool). *Scholarpedia* **2**:1430.

Gewaltig M.O., Diesmann M., and Aertsen A. (2001). Propagation of cortical synfire activity: Survival probability in single trials and stability of the mean. *Neural Netw.* **14**:657.

Girardeau G., Benchenane K., Wiener S., Buzsáki G., and Zugaro M. (2009). Selective suppression of hippocampal ripples impairs spatial memory. *Nat. Neurosci.* **12**:1222.

Girardeau G. and Zugaro M. (2011). Hippocampal ripples and memory consolidation. *Curr. Opin. Neurobiol.* **21**:452.

Gjorgjieva J., Clopath C., Audet J., and Pfister J.P. (2011). A triplet spike-timing-dependent plasticity model generalizes the bienenstock-cooper-munro rule to higher-order spatiotemporal correlations. *Proc. Natl. Acad. Sci. U. S. A.* **108**:19383.

Glickstein M. (2006). Golgi and cajal: The neuron doctrine and the 100th anniversary of the 1906 nobel prize. *Curr. Biol.* **16**:R147.

Glickstein M. and Rizzolatti G. (1984). Francesco gennari and the structure of the cerebral cortex. *Trends Neurosci.* **7**:464 .

Goedeke S. and Diesmann M. (2008). The mechanism of synchronization in feed-forward neuronal networks. *New J. Phys.* **10**:015007.

Golding N.L., Mickus T.J., Katz Y., Kath W.L., and Spruston N. (2005). Factors

mediating powerful voltage attenuation along CA1 pyramidal neuron dendrites. *J. Physiol.* **568**:69.

Golding N.L. and Spruston N. (1998). Dendritic sodium spikes are variable triggers of axonal action potentials in hippocampal CA1 pyramidal neurons. *Neuron* **21**:1189.

Golgi C. (1873). Sulla struttura della sostanza grigia del cervello. *Gazetta Medica Italiana – Lombardia* **33**:244.

Gollo L.L., Kinouchi O., and Copelli M. (2012). Statistical physics approach to dendritic computation: The excitable-wave mean-field approximation. *Phys. Rev. E* **85**:011911.

Gollo L.L., Kinouchi O., and Copelli M. (2013). Single-neuron criticality optimizes analog dendritic computation. *Sci. Rep.* **3**:3222.

Granovetter M. (1978). Threshold models of collective behavio. *Am. J. Sociol.* **83**:1420.

Gupta A.S., van der Meer M.A.A., Touretzky D.S., and Redish A.D. (2010). Hippocampal replay is not a simple function of experience. *Neuron* **65**:695.

Gupta A.S., van der Meer M.A.A., Touretzky D.S., and Redish A.D. (2012). Segmentation of spatial experience by hippocampal Îÿ sequences. *Nat. Neurosci.* **15**:1032.

Gutfreund Y., Zheng W., and Knudsen E.I. (2002). Gated visual input to the central auditory system. *Science* **297**:1556.

Gütig R., Aharonov R., Rotter S., and Sompolinsky H. (2003). Learning input correlations through nonlinear temporally asymmetric hebbian plasticity. *J. Neurosci.* **23**:3697.

Hagmann P., Cammoun L., Gigandet X., Meuli R., Honey C.J., Wedeen V.J., and Sporns O. (2008). Mapping the structural core of human cerebral cortex. *PLoS Biol.* **6**:e159.

Haider B., Duque A., Hasenstaub A.R., and McCormick D.A. (2006). Neocortical network activity in vivo is generated through a dynamic balance of excitation and inhibition. *J. Neurosci.* **26**:4535.

Hájos N. and Mody I. (1997). Synaptic communication among hippocampal interneurons: Properties of spontaneous IPSCs in morphologically identified cells. *J. Neurosci.* **17**:8427.

Hamzei-Sichani F., Kamasawa N., Janssen W., Yasumura T., Davidson K., Hof P., Wearne S., Stewart M., Young S., Whittington M., Rash J., and Traub R. (2007). Gap junctions on hippocampal mossy fiber axons demonstrated by thin-section electron microscopy and freeze fracture replica immunogold labeling. *Proc. Natl. Acad. Sci. U. S. A.* **104**:12548.

Harris K.D., Henze D.A., Hirase H., Leinekugel X., Dragoi G., Czurkó A., and Buzsáki G. (2002). Spike train dynamics predicts theta-related phase precession in hippocampal pyramidal cells. *Nature* **417**:738.

Harvey C.D., Collman F., Dombeck D.A., and Tank D.W. (2009). Intracellular dynamics of hippocampal place cells during virtual navigation. *Nature* **461**:941.

Hasselmo M.E. (2006). The role of acetylcholine in learning and memory. *Curr. Opin. Neurobiol.* **16**:710.

Häusser M. (2001). Synaptic function: Dendritic democracy. *Curr. Biol.* **11**:R10 .

Häusser M. and Mel B. (2003). Dendrites: Bug or feature? *Curr. Opin. Neurobiol.* **13**:372.

Häusser M., Spruston N., and Stuart G. (2000). Diversity and dynamics of dendritic signaling. *Science* **290**:739.

Hebb D.O. (1949). *The Organization of Behavior: A Neuropsychological Theory*. Wiley, New York, new ed edition.

Hehl U. (2001). *Embedding of Synchronous Spike Activity in Cortical Networks*. Ph.D. thesis, Albert-Ludwigs-Universität Freiburg im Breisgau.

Helias M., Deger M., Rotter S., and Diesmann M. (2010). Instantaneous non-linear processing by pulse-coupled threshold units. *PLoS Comput. Biol.* **6**:e1000929.

Hennig M.H. (2013). Theoretical models of synaptic short term plasticity. *Front. Comput. Neurosci.* **7**:45.

Herculano-Houzel S. (2009). The human brain in numbers: A linearly scaled-up primate brain. *Front. Hum. Neurosci.* **3**:31.

Herz A. and Hopfield J. (1995). Earthquake cycles and neural reverberations: Collective oscillations in systems with pulse-coupled threshold elements. *Phys. Rev. Lett.* **75**:1222.

Hodgkin A. and Huxley A. (1952). A quantitative description of membrane current and its application to conduction and excitation in nerve. *J. Physiol.* **117**:500.

Holmgren C., Harkany T., Svennenfors B., and Zilberter Y. (2003). Pyramidal cell communication within local networks in layer 2/3 of rat neocortex. *J. Physiol.* **551**:139.

Hopfield J. (1982). Neural networks and physical systems with emergent collective computational abilities. *Proc. Natl. Acad. Sci. U. S. A.* **79**:2554.

Hufnagel L., Brockmann D., and Geisel T. (2004). Forecast and control of epidemics in a globalized world. *Proc. Natl. Acad. Sci. U. S. A.* **101**:15124.

Iansek R. and Redman S.J. (1973). The amplitude, time course and charge of unitary excitatory post-synaptic potentials evoked in spinal motoneurone dendrites. *J. Physiol.* **234**:665.

Jacobs M.S., McFarland W.L., and Morgane P.J. (1979). The anatomy of the brain of the bottlenose dolphin (tursiops truncatus). rhinic lobe (rhinencephalon): The archicortex. *Brain Res. Bull.* **4 Suppl 1**:1.

Jadhav S.P., Kemere C., German P.W., and Frank L.M. (2012). Awake hippocampal sharp-wave ripples support spatial memory. *Science* **336**:1454.

Jahn R. and Fasshauer D. (2012). Molecular machines governing exocytosis of synaptic vesicles. *Nature* **490**:201.

Jahnke S., Memmesheimer R.M., and Timme M. (2008). Stable irregular dynamics in complex neural networks. *Phys. Rev. Lett.* **100**:048102.

Jahnke S., Memmesheimer R.M., and Timme M. (2009). How chaotic is the balanced state? *Front. Comput. Neurosci.* **3**:13.

Jahnke S., Memmesheimer R.M., and Timme M. (2013). Propagating synchrony in feed-forward networks. *Front. Comput. Neurosci.* **7**:153.

Jahnke S., Memmesheimer R.M., and Timme M. (2014a). Hub-activated signal transmission in complex networks. *Phys. Rev. E* **89**:030701(R).

Jahnke S., Memmesheimer R.M., and Timme M. (2014b). Oscillation induced propagation of synchrony. *PLoS Comput. Biol.* **10**:e1003940.

Jahnke S., Timme M., and Memmesheimer R.M. (2012). Guiding synchrony through random networks. *Phys. Rev. X* **2**:041016.

Jarsky T., Roxin A., Kath W.L., and Spruston N. (2005). Conditional dendritic spike propagation following distal synaptic activation of hippocampal CA1 pyramidal neurons. *Nat. Neurosci.* **8**:1667.

Jensen O. and Lisman J. (1996). Hippocampal CA3 region predicts memory sequences: Accounting for the phase precession of place cells. *Learn. Mem.* **3**:279.

Ji D. and Wilson M.A. (2007). Coordinated memory replay in the visual cortex and hippocampus during sleep. *Nat. Neurosci.* **10**:100.

Johansson R.S. and Birznieks I. (2004). First spikes in ensembles of human tactile afferents code complex spatial fingertip events. *Nat. Neurosci.* **7**:170.

Johnson A. and Alberts J.B. (2002). *Molecular Biology of the Cell, Fourth Edition.* Garland Science, New York, U.S.A.

Jonas P., Bischofberger J., Fricker D., and Miles R. (2004). Interneuron diversity series: Fast in, fast out: Temporal and spatial signal processing in hippocampal interneurons. *Trends Neurosci.* **27**:30.

Jonas P., Major G., and B.Sakmann (1993). Quantal components of unitary EPSCs at the mossy fibre synapse on CA3 pyramidal cells of rat hippocampus. *J. Physiol.* **472**:615.

Jones L.M., Depireux D.A., Simons D.J., and Keller A. (2004). Robust temporal coding in the trigeminal system. *Science* **304**:1986.

Jun J.K. and Jin D.Z. (2007). Development of neural circuitry for precise temporal sequences through spontaneous activity, axon remodeling, and synaptic plasticity. *PLoS ONE* **2**:e723.

Kaluza P., Kölzsch A., Gastner M.T., and Blasius B. (2010). The complex network of global cargo ship movements. *J. R. Soc. Interface* **7**:1093.

Kamondi A., Acsádi L., and Buzsáki G. (1998). Dendritic spikes are enhanced by cooperative network activity in the intact hippocampus. *J. Neurosci.* **18**:3919.

Kandel E.R., Schwartz J.H., and Jessell T.M. (2000). *Principles of Neural Science, Fourth Edition.* McGraw-Hill Companies, Inc., New Yorck, U.S.A.

Katz Y., Kath W., Spruston N., and Hasselmo M. (2007). Coincidence detection of place and temporal context in a network of spiking hippocampal neurons. *PLoS Comput. Biol.* **3**:2432.

Kayser C., Montemurro M.A., Logothetis N.K., and Panzeri S. (2009). Spike-phase coding boosts and stabilizes information carried by spatial and temporal spike patterns. *Neuron* **61**:597.

Kempermann G., Wiskott L., and Gage F.H. (2004). Functional significance of adult neurogenesis. *Curr. Opin. Neurobiol.* **14**:186.

Kilavik B.E., Roux S., Ponce-Alvarez A., Confais J., Grün S., and Riehle A. (2009). Long-term modifications in motor cortical dynamics induced by intensive practice. *J. Neurosci.* **29**:12653.

Kim S., Guzman S.J., Hu H., and Jonas P. (2012). Active dendrites support efficient initiation of dendritic spikes in hippocampal CA3 pyramidal neurons. *Nat. Neurosci.* **15**:600.

Kistler W.M. and Gerstner W. (2002). Stable propagation of activity pulses in populations of spiking neurons. *Neural Comput.* **14**:987.

Kjelstrup K., Solstad T., Brun V., Hafting T., Leutgeb S., Witter M., Moser E., and Moser M. (2008). Finite scale of spatial representation in the hippocampus. *Science* **321**:140.

Klausberger T. (2009). GABAergic interneurons targeting dendrites of pyramidal cells in the CA1 area of the hippocampus. *Eur. J. Neurosci.* **30**:947.

Klausberger T., Magill P., Márton L., J.D.B.Roberts, Cobden P., Buzsáki G., Cobden P., Buzsáki G., and Somogyi P. (2003). Brain-state- and cell-type-specific firing of hippocampal interneurons in vivo. *Nature* **421**:844.

Klausberger T., Márton L.F., Baude A., Roberts J.D.B., Magill P.J., and Somogyi P. (2004). Spike timing of dendrite-targeting bistratified cells during hippocampal network oscillations in vivo. *Nat. Neurosci.* **7**:41.

Klausberger T., Marton L.F., O'Neill J., Huck J.H.J., Dalezios Y., Fuentealba P., Suen W.Y., Papp E., Kaneko T., Watanabe M., Csicsvari J., and Somogyi P. (2005). Complementary roles of cholecystokinin- and parvalbumin-expressing gabaergic neurons in hippocampal network oscillations. *J. Neurosci.* **25**:9782.

Knowles W. and Schwartzkroin P. (1981). Axonal ramifications of hippocampal CA1 pyramidal cells. *J. Neurosci.* **1**:1236.

Kopell N., Kramer M.A., Malerba P., and Whittington M.A. (2010). Are different rhythms good for different functions? *Front. Hum. Neurosci.* **4**:187.

Kremkow J., Perrinet L.U., Masson G.S., and Aertsen A. (2010). Functional consequences of correlated excitatory and inhibitory conductances in cortical networks. *J. Comput. Neurosci.* **28**:579.

Kriener B., Tetzlaff T., Aertsen A., Diesmann M., and Rotter S. (2008). Correlations and population dynamics in cortical networks. *Neural Comput.* **20**:2185.

Kuhn A., Aertsen A., and Rotter S. (2004). Neuronal integration of synaptic input in the fluctuation-driven regime. *J. Neurosci.* **24**:2345.

Kumar A., Rotter S., and Aertsen A. (2008a). Conditions for propagating synchronous spiking and asynchronous firing rates in a cortical network model. *J. Neurosci.* **28**:5268.

Kumar A., Rotter S., and Aertsen A. (2010). Spiking activity propagation in neuronal networks: Reconciling different perspectives on neural coding. *Nat. Rev. Neurosci.* **11**:615.

Kumar A., Schrader S., Aertsen A., and Rotter S. (2008b). The high-conductance state of cortical networks. *Neural Comput.* **20**:1.

Lakatos P., Karmos G., Mehta A.D., Ulbert I., and Schroeder C.E. (2008). Entrainment of neuronal oscillations as a mechanism of attentional selection. *Science* **320**:110.

Lapicque L. (1907). Recherches quantitatives sur l'excitation electrique des nerfs traiteé comme une polarisation. *J. Physiol. Pathol. Gen.* **9**:620.

Larkum M.E., Nevian T., Sandler M., Polsky A., and Schiller J. (2009). Synaptic integration in tuft dendrites of layer 5 pyramidal neurons: A new unifying principle. *Science* **325**:756.

Larkum M.E. and Zhu J.J. (2002). Signaling of layer 1 and whisker-evoked Ca^{2+} and na+ action potentials in distal and terminal dendrites of rat neocortical pyramidal neurons in vitro and in vivo. *J. Neurosci.* **22**:6991.

Larkum M.E., Zhu J.J., and Sakmann B. (2001). Dendritic mechanisms underlying the coupling of the dendritic with the axonal action potential initiation zone of adult rat layer 5 pyramidal neurons. *J. Physiol.* **533**:447.

Lee A.K. and Wilson M.A. (2002). Memory of sequential experience in the hippocampus during slow wave sleep. *Neuron* **36**:1183.

Leibold C. and Kempter R. (2006). Memory capacity for sequences in a recurrent network with biological constraints. *Neural Comput.* **18**:904.

Lengyel M., Szatmáry Z., and Erdi P. (2003). Dynamically detuned oscillations account for the coupled rate and temporal code of place cell firing. *Hippocampus* **13**:700.

Leonardo A. and Fee M.S. (2005). Ensemble coding of vocal control in birdsong. *J. Neurosci.* **25**:652.

Leutgeb S., Leutgeb J.K., Barnes C.A., Moser E.I., McNaughton B.L., and Moser M.B. (2005a). Independent codes for spatial and episodic memory in hippocampal neuronal ensembles. *Science* **309**:619.

Leutgeb S., Leutgeb J.K., Moser M.B., and Moser E.I. (2005b). Place cells, spatial maps and the population code for memory. *Curr. Opin. Neurobiol.* **15**:738.

Levy W.B. (1996). A sequence predicting CA3 is a flexible associator that learns and uses context to solve hippocampal-like tasks. *Hippocampus* **6**:579.

Liljeros F., Edling C.R., Amaral L.A., Stanley H.E., and Aberg Y. (2001). The web of human sexual contacts. *Nature* **411**:907.

Lisman J.E., Fellous J.M., and Wang X.J. (1998). A role for NMDA-receptor channels in working memory. *Nat. Neurosci.* **1**:273.

Litvak V., Sompolinsky H., Segev I., and Abeles M. (2003). On the transmission of rate code in long feedforward networks with excitatory-inhibitory balance. *J. Neurosci.* **23**:3006.

Liu G. and Tsien R. (1995). Properties of synaptic transmission at single hippocampal synaptic boutons. *Nature* **375**:404.

Lledo P.M., Alonso M., and Grubb M.S. (2006). Adult neurogenesis and functional plasticity in neuronal circuits. *Nat. Rev. Neurosci.* **7**:179.

Loebel A. and Tsodyks M. (2002). Computation by ensemble synchronization in recurrent networks with synaptic depression. *J. Comput. Neurosci.* **13**:111.

Logothetis N.K., Eschenko O., Murayama Y., Augath M., Steudel T., Evrard H.C., Besserve M., and Oeltermann A. (2012). Hippocampal-cortical interaction during periods of subcortical silence. *Nature* **491**:547.

London M. and Häusser M. (2005). Dendritic computation. *Annu. Rev. Neurosci.* **28**:503.

London M., Roth A., Beeren L., Häusser M., and Latham P. (2010). Sensitivity to perturbations in vivo implies high noise and suggests rate coding in cortex. *Nature* **466**:123.

Long M.A., Jin D.Z., and Fee M.S. (2010). Support for a synaptic chain model of neuronal sequence generation. *Nature* **468**:394.

Lorenz J., Battiston S., and Schweitzer F. (2009). Systemic risk in a unifying framework for cascading processes on networks. *Eur. Phys. J. B* **71**:441.

Losonczy A. and Magee J. (2006). Integrative properties of radial oblique dendrites in hippocampal CA1 pyramidal neurons. *Neuron* **50**:291.

Losonczy A., Makara J.K., and Magee J.C. (2008). Compartmentalized dendritic plasticity and input feature storage in neurons. *Nature* **452**:436.

Maex R. and Schutter E.D. (2007). Mechanism of spontaneous and self-sustained oscillations in networks connected through axo-axonal gap junctions. *Eur. J. Neurosci.* **25**:3347.

Magee J.C. (2001). Dendritic mechanisms of phase precession in hippocampal CA1 pyramidal neurons. *J. Neurophysiol.* **86**:528.

Magee J.C. and Cook E.P. (2000). Somatic EPSP amplitude is independent of synapse location in hippocampal pyramidal neurons. *Nat. Neurosci.* **3**:895.

Maier N., Nimmrich V., and Draguhn A. (2003). Cellular and network mechanisms underlying spontaneous sharp wave-ripple complexes in mouse hippocampal slices. *J. Physiol.* **550**:873.

Maier N., Tejero-Cantero A., Dorrn A.L., Winterer J., Beed P.S., Morris G., Kempter R., Poulet J.F.A., Leibold C., and Schmitz D. (2011). Coherent phasic excitation during hippocampal ripples. *Neuron* **72**:137.

Mainen Z. and Sejnowski T. (1995). Reliability of spike timing in neocortical neurons. *Science* **268**:1503.

Major G., Larkum M.E., and Schiller J. (2013). Active properties of neocortical pyramidal

neuron dendrites. *Annu. Rev. Neurosci.* **36**:1.

Makara J.K., Losonczy A., Wen Q., and Magee J.C. (2009). Experience-dependent compartmentalized dendritic plasticity in rat hippocampal CA1 pyramidal neurons. *Nat. Neurosci.* **12**:1485.

Makara J.K. and Magee J.C. (2013). Variable dendritic integration in hippocampal CA3 pyramidal neurons. *Neuron* **80**:1438.

Markram H. (2006). The blue brain project. *Nat. Rev. Neurosci.* **7**:153.

Markram H., Lübke J., Frotscher M., and Sakmann B. (1997). Regulation of synaptic efficacy by coincidence of postsynaptic APs und EPSPs. *Science* **275**:213.

Markus E.J., Qin Y.L., Leonard B., Skaggs W.E., McNaughton B.L., and Barnes C.A. (1995). Interactions between location and task affect the spatial and directional firing of hippocampal neurons. *J. Neurosci.* **15**:7079.

Marr D. (1971). Simple memory: A theory for archicortex. *Philos. Trans. R. Soc. Lond. B* **262**:23 .

Mathai A., Moschopoulos P., and Pederzoli G. (1999). Random points associated with rectangles. *Rendiconti del Circolo Matematico di Palermo* **48**:163.

Maurer A.P. and McNaughton B.L. (2007). Network and intrinsic cellular mechanisms underlying theta phase precession of hippocampal neurons. *Trends Neurosci.* **30**:325.

Mazarello P. (1999). Camillo Golgi's scientific biography. *J. Histor. Neurosci.* **8**:132.

Meeks J. and Mennerick S. (2006). Action potential initiation and propagation in CA3 pyramidal axons. *J. Neurophysiol.* **97**:3460.

Mehring C., Hehl U., Kubo M., Diesmann M., and Aertsen A. (2003). Activity dynamics and propagation of synchronous spiking in locally connected random networks. *Biol. Cybern.* **88**:395.

Mehta M. (2007). Cortico-hippocampal interaction during up-down states and memory consolidation. *Nat. Neurosci.* **10**:13.

Mehta M.R., Barnes C.A., and McNaughton B.L. (1997). Experience-dependent, asymmetric expansion of hippocampal place fields. *Proc. Natl. Acad. Sci. U. S. A.* **94**:8918.

Mehta M.R., Lee A.K., and Wilson M.A. (2002). Role of experience and oscillations in transforming a rate code into a temporal code. *Nature* **417**:741.

Mel B.W. (1992). Nmda-based pattern discrimination in a modeled cortical neuron. *Neural Comput.* **4**:502.

Memmesheimer R.M. (2010). Quantitative prediction of intermittent high-frequency oscillations in neural networks with supralinear dendritic interactions. *Proc. Natl. Acad. Sci. U. S. A.* **107**:11092.

Memmesheimer R.M. and Timme M. (2012). Non-additive coupling enables propagation of synchronous spiking activity in purely random networks. *PLoS Comput. Biol.* **8**:e1002384.

Migliore M. and Shepherd G.M. (2002). Emerging rules for the distributions of active dendritic conductances. *Nat. Rev. Neurosci.* **3**:362.

Miles R. and Wong R. (1986). Excitatory synaptic interactions between CA3 neurones in the guinea pig hippocampus. *J. Physiol.* **373**:397.

Milo R., Shen-Orr S., Itzkovitz S., Kashtan N., Chklovskii D., and Alon U. (2002). Network motifs: Simple building blocks of complex networks. *Science* **298**:824.

Milojkovic B.A., Radojicic M.S., Goldman-Rakic P.S., and Antic S.D. (2004). Burst generation in rat pyramidal neurones by regenerative potentials elicited in a restricted part of the basilar dendritic tree. *J. Physiol.* **558**:193.

Mirollo R. and Strogatz S. (1990). Synchronization of pulse-coupled biological oscillators. *SIAM J. Appl. Math.* **50**:1645.

Mizuseki K., Royer S., Diba K., and Buzsáki G. (2012). Activity dynamics and behavioral correlates of CA3 and CA1 hippocampal pyramidal neurons. *Hippocampus* **22**:1659.

Moita M.A.P., Rosis S., Zhou Y., LeDoux J.E., and Blair H.T. (2004). Putting fear in its place: Remapping of hippocampal place cells during fear conditioning. *J. Neurosci.* **24**:7015.

Molter C., Sato N., and Yamaguchi Y. (2007). Reactivation of behavioral activity during sharp waves: A computational model for two stage hippocampal dynamics. *Hippocampus* **17**:201.

Monteforte M. and Wolf F. (2012). Dynamic flux tubes form reservoirs of stability in neuronal circuits. *Phys. Rev. X* **2**:041007.

Moreno Y., Nekovee M., and Pacheco A.F. (2004). Dynamics of rumor spreading in complex networks. *Phys. Rev. E* **69**:066130.

Morrison A., Aertsen A., and Diesmann M. (2007). Spike-timing-dependent plasticity in balanced random networks. *Neural Comput.* **19**:1437.

Morrison A., Diesmann M., and Gerstner W. (2008). Phenomenological models of synaptic plasticity based on spike timing. *Biol. Cybern.* **98**:459.

Morrison A., Mehring C., Geisel T., Aertsen A.D., and Diesmann M. (2005). Advancing the boundaries of high-connectivity network simulation with distributed computing. *Neural Comput.* **17**:1776.

Moser E.I., Kropff E., and Moser M.B. (2008). Place cells, grid cells, and the brain's spatial representation system. *Annu. Rev. Neurosci.* **31**:69.

Mozzachiodi R. and Byrne J.H. (2010). More than synaptic plasticity: Role of nonsynaptic plasticity in learning and memory. *Trends Neurosci.* **33**:17.

Müller C., Beck H., Coulter D., and Remy S. (2012). Inhibitory control of linear and supralinear dendritic excitation in CA1 pyramidal neurons. *Neuron* **75**:851.

Muller R.U. and Kubie J.L. (1987). The effects of changes in the environment on the spatial firing of hippocampal complex-spike cells. *J. Neurosci.* **7**:1951.

Nadasdy Z., Hirase H., Czurko A., Csicsvari J., and Buzsáki G. (1999). Replay and time compression of recurring spike sequences in the hippocampus. *J. Neurosci.* **19**:9479.

Nakashiba T., Buhl D.L., McHugh T.J., and Tonegawa S. (2009). Hippocampal CA3 output is crucial for ripple-associated reactivation and consolidation of memory. *Neuron* **62**:781.

Nakashiba T., Young J.Z., McHugh T.J., Buhl D.L., and Tonegawa S. (2008). Transgenic inhibition of synaptic transmission reveals role of CA3 output in hippocampal learning. *Science* **319**:1260.

Naundorf B., Geisel T., and Wolf F. (2005). Action potential onset dynamics and the response speed of neuronal populations. *J. Comput. Neurosci.* **18**:297.

Naundorf B., Wolf F., and Volgushev M. (2006). Unique features of action potential initiation in cortical neurons. *Nature* **440**:1060.

Neves G., Cooke S.F., and Bliss T.V.P. (2008). Synaptic plasticity, memory and the hippocampus: A neural network approach to causality. *Nat. Rev. Neurosci.* **9**:65.

Nevian T., Larkum M.E., Polsky A., and Schiller J. (2007). Properties of basal dendrites of layer 5 pyramidal neurons: A direct patch-clamp recording study. *Nat. Neurosci.* **10**:206.

Newman M.E.J. (2003). The structure and function of complex networks. *SIAM Review* **45**:167.

Newman M.E.J. (2010). *Networks, An Introduction.* Oxford Univ. Press.

Nimmrich V., Maier N., Schmitz D., and Draguhn A. (2005). Induced sharp wave-ripple complexes in the absence of synaptic inhibition in mouse hippocampal slices. *J. Physiol.* **563.3**:663.

Nishiyama M., Hong K., Mikoshiba K., Poo M.M., and Kato K. (2000). Calcium stores regulate the polarity and input specificity of synaptic modification. *Nature* **408**:584.

Nowak L., Sanchez-Vivez M., and McCormick D. (1997). Influence of low and high frequency inputs on spike timing in visual cortical neurons. *Cereb. Cortex* **7**:487.

Nowotny T. and Huerta R. (2003). Explaining synchrony in feed-forward networks: Are mcculloch-pitts neurons good enough? *Biol. Cybern.* **89**:237.

Oja E. (1982). A simplified neuron model as a principal component analyzer. *J. Math. Biol.* **15**:267.

O'Keefe J. (1976). Place units in the hippocampus of the freely-moving rat. *Exp. Neurol.* **51**:78.

O'Keefe J. and Dostrovsky J. (1971). The hippocampus as a spatial map. Preliminary evidence from unit activity in the freely-moving rat. *Brain Res.* **34**:171.

O'Keefe J. and Nadel L. (1978). *Hippocampus as a Cognitive Map.* Oxford Univ. Press, Oxford.

O'Keefe J. and Recce M. (1993). Phase relationship between hippocampal place units and

the EEG theta rhythm. *Hippocampus* **3**:317.

Okun M. and Lampl I. (2008). Instantaneous correlation of excitation and inhibition during ongoing and sensory-evoked activities. *Nat. Neurosci.* **11**:535.

O'Neill J., Pleydell-Bouverie B., Dupret D., and Csicsvari J. (2010). Play it again: Reactivation of waking experience and memory. *Trends Neurosci.* **33**:220.

O'Neill J., Senior T.J.J., Allen K., Huxter J.R.R., and Csicsvari J. (2008). Reactivation of experience-dependent cell assembly patterns in the hippocampus. *Nat. Neurosci.* **11**:209.

Oram M.W., Wiener M.C., Lestienne R., and Richmond B.J. (1999). Stochastic nature of precisely timed spike patterns in visual system neuronal responses. *J. Neurophysiol.* **81**:3021.

Orman R., von Gizycki H., Lytton W., and Stewart M. (2008). Local axon collaterals of area CA1 support spread of epileptiform discharges within CA1, but propagation is unidirectional. *Hippocampus* **18**:1021.

Palva S. and Palva J.M. (2007). New vistas for alpha-frequency band oscillations. *Trends Neurosci.* **30**:150.

Panzeri S., Brunel N., Logothetis N.K., and Kayser C. (2010). Sensory neural codes using multiplexed temporal scales. *Trends Neurosci.* **33**:111.

Panzeri S., Petersen R.S., Schultz S.R., Lebedev M., and Diamond M.E. (2001). The role of spike timing in the coding of stimulus location in rat somatosensory cortex. *Neuron* **29**:769.

Paoletti P. (2011). Molecular basis of NMDA receptor functional diversity. *Eur. J. Neurosci.* **33**:1351.

Pastalkova E., Itskov V., Amarasingham A., and Buzsáki G. (2008). Internally generated cell assembly sequences in the rat hippocampus. *Science* **5**:1322.

Pathak M.M., Yarov-Yarovoy V., Agarwal G., Roux B., Barth P., Kohout S., Tombola F., and Isacoff E.Y. (2007). Closing in on the resting state of the shaker K^+ channel. *Neuron* **56**:124.

Paxinos G. (2004). *The Rat Nervous System.* Elsevier Science, San Diego.

Payton B.W., Bennett M.V., and Pappas G.D. (1969). Permeability and structure of junctional membranes at an electrotonic synapse. *Science* **166**:1641.

Pearce R. (1993). Physiological evidence for two distinct $GABA_A$ responses in rat hippocampus. *Neuron* **10**:189.

Perin R., Berger T.K., and Markram H. (2011). A synaptic organizing principle for cortical neuronal groups. *Proc. Natl. Acad. Sci. U. S. A.* **108**:5419.

Perkel D. and Bullock T. (1968). *Neural Coding: A Report Based on an NRP Work Session Organized by Theodore Holmes Bullock and Held on January 21-23, 1968.* Neurosciences Research Program bulletin. Neurosciences Research Program.

Pfeiffer B.E. and Foster D.J. (2013). Hippocampal place-cell sequences depict future paths to remembered goals. *Nature* **497**:74.

Poirazi P., Brannon T., and Mel B. (2003a). Arithmetic of subthreshold synaptic summation in a model CA1 pyramidal neuron. *Neuron* **37**:977.

Poirazi P., Brannon T., and Mel B. (2003b). Pyramidal neuron as two-layer network. *Neuron* **37**:989.

Poirazi P. and Mel B.W. (2001). Impact of active dendrites and structural plasticity on the memory capacity of neural tissue. *Neuron* **29**:779.

Polsky A., Mel B., and Schiller J. (2004). Computational subunits in thin dendrites of pyramidal cells. *Nat. Neurosci.* **7**:621.

Polsky A., Mel B., and Schiller J. (2009). Encoding and decoding bursts by NMDA spikes in basal dendrites of layer 5 pyramidal neurons. *J. Neurosci.* **29**:11891.

Purves D., Augustine G., Fitzpatrick D., Hall W., LaMantia A.S., McNamara J., and White L., editors (2008). *Neuroscience, Fourth Edition.* Sinauer Associates, Inc., Sunderland, U.S.A.

Putrino D., Brown E.N., Mastaglia F.L., and Ghosh S. (2010). Differential involvement of excitatory and inhibitory neurons of cat motor cortex in coincident spike activity related to behavioral context. *J. Neurosci.* **30**:8048.

Quirk G.J., Muller R.U., and Kubie J.L. (1990). The firing of hippocampal place cells in the dark depends on the rat's recent experience. *J. Neurosci.* **10**:2008.

Rauch A., LaCamera G., Lüscher H., Senn W., and Fusi S. (2003). Neocortical pyramidal cells respond as integrate-and-fire neurons to in vivo like input currents. *J. Neurophysiol.* **90**:1598.

Raviola E. and Mazzarello P. (2011). The diffuse nervous network of Camillo Golgi: Facts and fiction. *Brain Res. Rev.* **66**:75 . Camillo Golgi and Modern Neuroscience.

Reeves C. and Taylor D. (2004). A history of the optic nerve and its diseases. *Eye (Lond)* **18**:1096.

Remy S., Csicsvari J., and Beck H. (2009). Activity-dependent control of neuronal output by local and global dendritic spike attenuation. *Neuron* **61**:906.

Remy S. and Spruston N. (2007). Dendritic spikes induce single-burst long-term potentiation. *Proc. Natl. Acad. Sci. U. S. A.* **104**:17192.

Renart A., de la Rocha J., Bartho P., Hollender L., Parga N., Reyes A., and Harris K. (2010). The asynchronous state in cortical circuits. *Science* **327**:587.

Reyes A.D. (2003). Synchrony-dependent propagation of firing rate in iteratively constructed networks in vitro. *Nat. Neurosci.* **6**:593.

Rhodes P. (2008). Recoding patterns of sensory input: Higher order features and the function of nonlinear dendritic trees. *Neural Comput.* **20**:2000.

Rice J. (2007). *Mathematical statistics and data analysis*. Statistics Series. Duxbury Press.

Riehle A., Grün S., Diesmann M., and Aertsen A. (1997). Spike synchronization and rate modulation differentially involved in motor cortical function. *Science* **278**:1950.

Rieke F., Warland D., de Ruyter van Stevenick R., and Bialek W. (1997). *Spikes, Exploring the Neural Code*. MIT Press.

Riley S., Fraser C., Donnelly C.A., Ghani A.C., Abu-Raddad L.J., Hedley A.J., Leung G.M., Ho L.M., Lam T.H., Thach T.Q., Chau P., Chan K.P., Lo S.V., Leung P.Y., Tsang T., Ho W., Lee K.H., Lau E.M.C., Ferguson N.M., and Anderson R.M. (2003). Transmission dynamics of the etiological agent of sars in hong kong: impact of public health interventions. *Science* **300**:1961.

Rohden M., Sorge A., Timme M., and Witthaut D. (2012). Self-organized synchronization in decentralized power grids. *Phys. Rev. Lett.* **109**:064101.

Rosenbaum R., Trousdale J., and Josic K. (2011). The effects of pooling on spike train correlations. *Front. Neurosci.* **5**:58.

Rosenbaum R.J., Trousdale J., and Josic K. (2010). Pooling and correlated neural activity. *Front. Comput. Neurosci.* **4**:9.

Rubin J., Lee D.D., and Sompolinsky H. (2001). Equilibrium properties of temporally asymmetric hebbian plasticity. *Phys. Rev. Lett.* **86**:364.

Rudolph M. and Destexhe A. (2007). How much can we trust neural simulation strategies? *Neurocomputing* **70**:1966 . Computational Neuroscience: Trends in Research 2007 Computational Neuroscience 2006.

Sabatini B.L. and Regehr W.G. (1996). Timing of neurotransmission at fast synapses in the mammalian brain. *Nature* **384**:170.

Samura T., Hattori M., and Ishizaki S. (2008). Sequence disambiguation and pattern completion by cooperation between autoassociative and heteroassociative memories of functionally divided hippocampal CA3. *Neurocomputing* **71**:3176. Advances in Neural Information Processing (ICONIP 2006) / Brazilian Symposium on Neural Networks (SBRN 2006).

Sayer R., Friedlander M., and Redman S. (1990). The time course and amplitude of EPSPs evoked at synapses between pairs of CA3/CA1 neurons in the hippocampal slice. *J. Neurosci.* **70**:828.

Scarpetta S. and Giacco F. (2013). Associative memory of phase-coded spatiotemporal patterns in leaky integrate and fire networks. *J. Comput. Neurosci.* **34**:319.

Scarpetta S., Giacco F., and de Candia A. (2011). Storage capacity of phase-coded patterns in sparse neural networks. *Europhys. Lett.* **95**:28006.

Scarpetta S., Giacco F., Lombardi F., and de Candia A. (2013). Effects of poisson noise in a if model with stdp and spontaneous replay of periodic spatiotemporal patterns, in absence of cue stimulation. *Biosystems* **112**:258.

Schiess M., Urbanczik R., and Senn W. (2012). Gradient estimation in dendritic reinforce-

ment learning. *J. Math. Neurosci.* **2**:2.

Schmitz D., Schuchmann S., Fisahn A., Draguhn A., Buhl E., Petrasch-Parwez E., Dermietzel R., Heinemann U., and Traub R. (2001). Axo-axonal coupling: A novel mechanism for ultrafast neuronal communication. *Neuron* **31**:831.

Schnupp J.W.H., Hall T.M., Kokelaar R.F., and Ahmed B. (2006). Plasticity of temporal pattern codes for vocalization stimuli in primary auditory cortex. *J. Neurosci.* **26**:4785.

Shadlen M. and Newsome W. (1998). The variable discharge of cortical neurons: Implications for connectivity, computation, and information coding. *J. Neurosci.* **18**:3870.

Shadlen M.N. and Newsome W.T. (1994). Noise, neural codes and cortical organization. *Curr. Opin. Neurobiol.* **4**:569.

Sjöström P.J., Rancz E.A., Roth A., and Häusser M. (2008). Dendritic excitability and synaptic plasticity. *Physiol. Rev.* **88**:769.

Skaggs W. and McNaughton B. (1996). Replay of neuronal firing sequences in rat hippocampus during sleep following spatial experience. *Science* **29**:1870.

Skaggs W.E., McNaughton B.L., Wilson M.A., and Barnes C.A. (1996). Theta phase precession in hippocampal neuronal populations and the compression of temporal sequences. *Hippocampus* **6**:149.

Softky W. and Koch C. (1993). The highly irregular firing of cortical cells is insonsistent with temporal integration of random EPSPs. *J. Neurosci.* **13**:334.

Song S., Miller K.D., and Abbott L.F. (2000). Competitive hebbian learning through spike-timing-dependent synaptic plasticity. *Nat. Neurosci.* **3**:919.

Song S., Sjöström P., Reigl M., Nelson S., and Chklovskii D. (2005). Highly nonrandom features of synaptic connectivity in local cortical circuits. *PLoS Biol.* **3**:0507.

Sotelo C. (2003). Viewing the brain through the master hand of Ramón y Cajal. *Nat. Rev. Neurosci.* **4**:71.

Spencer W. and Kandel E. (1961). Electrophysiology of hippocampal neurons: Iv. fast prepotentials. *J. Neurophysiol.* **24**:272.

Spruston N. (2008). Pyramidal neurons: Dendritic structure and synaptic integration. *Nat. Rev. Neurosci.* **9**:206.

Staff N., Jung H.Y., Thiagarajan T., Yao M., and Spruston N. (2000). Resting and active properties of pyramidal neurons in subiculum and CA1 of rat hippocampus. *J. Neurophysiol.* **84**:2398.

Standage D., Jalil S., and Trappenberg T. (2007). Computational consequences of experimentally derived spike-time and weight dependent plasticity rules. *Biol. Cybern.* **96**:615.

Stephan H. (1983). Evolutionary trends in limbic structures. *Neurosci. Biobehav. Rev.* **7**:367.

Stephan H. and Manolescu J. (1980). Comparative investigations on hippocampus in insectivores and primates. *Z. Mikrosk. Anat. Forsch.* **94**:1025.

Strogatz S. (2003). *Sync: The Emerging Science of Spontaneous Order*. Hyperion.

Stuart G., Schiller J., and Sakmann B. (1997). Action potential initiation and propagation in rat neocortical pyramidal neurons. *J. Physiol.* **505**:617.

Stuart G.J. and Häusser M. (2001). Dendritic coincidence detection of EPSPs and action potentials. *Nat. Neurosci.* **4**:63.

Sudhof T.C. (2004). The synaptic vesicle cycle. *Annu. Rev. Neurosci.* **27**:509.

Sullivan D., Csicsvari J., Mizuseki K., Montgomery S., Diba K., and Buzsáki G. (2011). Relationships between hippocampal sharp waves, ripples, and fast gamma oscillation: Influence of dentate and entorhinal cortical activity. *J. Neurosci.* **31**:8605.

Sullivan D.W. and Levy W.B. (2004). Quantal synaptic failures enhance performance in a minimal hippocampal model. *Network* **15**:45.

Taxidis J., Coombes S., Mason R., and Owen M.R. (2012). Modeling sharp wave-ripple complexes through a CA3-ca1 network model with chemical synapses. *Hippocampus* **22**:995.

Taxidis J., Mizuseki K., Mason R., and Owen M.R. (2013). Influence of slow oscillation on hippocampal activity and ripples through cortico-hippocampal synaptic interactions, analyzed by a cortical-ca3-ca1 network model. *Front. Comput. Neurosci.* **7**:3.

Tchumatchenko T., Malyshev A., Wolf F., and Volgushev M. (2011). Ultrafast population encoding by cortical neurons. *J. Neurosci.* **31**:12171.

Tetzlaff C., Kolodziejski C., Markelic I., and Wörgötter F. (2012). Time scales of memory, learning, and plasticity. *Biol. Cybern.* **106**:715.

Tetzlaff T., Buschermöhle M., Geisel T., and Diesmann M. (2003). The spread of rate and correlation in stationary cortical networks. *Neurocomputing* **52**:949.

Tetzlaff T., Geisel T., and Diesmann M. (2002). The ground state of cortical feed-forward networks. *Neurocomputing* **44-46**:673.

Thompson L. and Best P. (1990). Long-term stability of the place-field activity of single units recorded from the dorsal hippocampus of freely behaving rats. *Brain Res.* **509**:299 .

Thomson A.M., West D.C., Wang Y., and Bannister A.P. (2002). Synaptic connections and small circuits involving excitatory and inhibitory neurons in layers 2-5 of adult rat and cat neocortex: Triple intracellular recordings and biocytin labelling in vitro. *Cereb. Cortex* **12**:936.

Thurley K., Leibold C., Gundlfinger A., Schmitz D., and Kempter R. (2008). Phase precession through synaptic facilitation. *Neural Comput.* **20**:1285.

Tiesinga P., Fellous J., José J., and Sejnowski T. (2001). Computational model of carbachol-induced delta, theta, and gamma oscillations in the hippocampus. *Hippocampus* **11**:251.

Tiesinga P. and José J. (2000). Robust gamma oscillations in networks of inhibitory hippocampal interneurons. *Network* **11**:1.

Tiesinga P. and Sejnowski T. (2009). Cortical enlightenment: Are attentional gamma oscillations driven by ING or PING? *Neuron* **63**:727.

Timme M. (2002). *Collective Dynamics in Networks of Pulse-Coupled Oscillators.* Ph.D. thesis, Georg-August-Universität zu Göttingen.

Timme M., Wolf F., and Geisel T. (2002). Coexistence of regular and irregular dynamics in complex networks of pulse-coupled oscillators. *Phys. Rev. Lett.* **89**:258701.

Traub R. and Miles R. (1991). *Neuronal Networks of the Hippocampus.* Cambridge University Press, Cambridge.

Traub R. and Wong R. (1982). Cellular mechanism of neuronal synchronization in epilepsy. *Science* **216**:745.

Traub R.D. and Bibbig A. (2000). A model of high-frequency ripples in the hippocampus based on synaptic coupling plus axon-axon gap junctions between pyramidal neurons. *J. Neurosci.* **20**:2086.

Traub R.D., Schmitz D., Jefferys J.G., and Draguhn A. (1999). High-frequency population oscillations are predicted to occur in hippocampal pyramidal neuronal networks interconnected by axoaxonal gap junctions. *Neuroscience* **92**:407.

Tse D., Langston R.F., Kakeyama M., Bethus I., Spooner P.A., Wood E.R., Witter M.P., and Morris R.G.M. (2007). Schemas and memory consolidation. *Science* **316**:76.

Tsodyks M.V., Skaggs W.E., Sejnowski T.J., and McNaughton B.L. (1996). Population dynamics and theta rhythm phase precession of hippocampal place cell firing: A spiking neuron model. *Hippocampus* **6**:271.

Tuckwell H. (1988). *Introduction to theoretical neurobiology.* Cambridge Univ. Press, Cambridge.

Van Leeuwenhoek A. (1719). *Epistolae physiologicae super compluribus naturae arcanis.* Works. A. Beman.

van Strien N.M., Cappaert N.L.M., and Witter M.P. (2009). The anatomy of memory: An interactive overview of the parahippocampal-hippocampal network. *Nat. Rev. Neurosci.* **10**:272.

Varshney L.R., Chen B.L., Paniagua E., Hall D.H., and Chklovskii D.B. (2011). Structural properties of the caenorhabditis elegans neuronal network. *PLoS Comput. Biol.* **7**:e1001066.

Verduzco-Flores S.O., Bodner M., and Ermentrout B. (2012). A model for complex sequence learning and reproduction in neural populations. *J. Comput. Neurosci.* **32**:403.

Vicq-d'Azur F. (1786). *Traité d'anatomie et de physiologie.* Didot l'Aine, Paris.

Viereckel T., Kostic M., Bähner F., Draguhn A., and Both M. (2013). Effects of the GABA-uptake blocker nnc-711 on spontaneous sharp wave-ripple complexes in mouse hippocampal slices. *Hippocampus* **23**:323.

Vladimirov N., Tu Y., and Traub R.D. (2013). Synaptic gating at axonal branches, and

sharp-wave ripples with replay: a simulation study. *Eur. J. Neurosci.* **38**:3435.

Vogels T. and Abbott L. (2005). Signal propagation and logic gating in networks of integrate-and-fire neurons. *J. Neurosci.* **25**:10786.

v. Vreeswijk C. and Sompolinsky H. (1996). Chaos in neuronal networks with balanced excitatory and inhibitory activity. *Science* **274**:1724.

v. Vreeswijk C. and Sompolinsky H. (1998). Chaotic balanced state in a model of cortical circuits. *Neural Comput.* **10**:1321.

Waddington A., Appleby P.A., De Kamps M., and Cohen N. (2012). Triphasic spike-timing-dependent plasticity organizes networks to produce robust sequences of neural activity. *Front. Comput. Neurosci.* **6**:88.

Waldeyer-Hartz H. (1891). über einige neuere forschungen im gebiete der anatomie des centralnervensystems. *Deutsch. Med. Wochnschr.* **17**:1213.

Wang H.X., Gerkin R.C., Nauen D.W., and Bi G.Q. (2005). Coactivation and timing-dependent integration of synaptic potentiation and depression. *Nat. Neurosci.* **8**:187.

Wang X.J. (1999). Synaptic basis of cortical persistent acitivity: The importance of NMDA receptors to working memory. *J. Neurosci.* **19**:9587.

Wang X.J. (2001). Synaptic reverberation underlying mnemonic persistent activity. *Trends Neurosci.* **24**:455.

Wang X.J. and Buzsáki G. (1996). Gamma oscillation by synaptic inhibition in a hippocampal interneuronal network model. *J. Neurosci.* **16**:6402.

Watts D. and Strogatz S. (1998). Collective dynamics of 'small-world' networks. *Nature* **393**:440.

Watts D.J. (2002). A simple model of global cascades on random networks. *Proc. Natl. Acad. Sci. U. S. A.* **99**:5766.

Whittington M., Traub R., and Jefferys J. (1995). Synchronized oscillations in interneuron networks driven by metabotropic glutamate receptor activation. *Nature* **373**:612.

Wikimedia (2007). *Complete neuron cell diagram* by User:Ladyofhats. `http://commons.wikimedia.org/wiki/File:Complete_neuron_cell_diagram_en.svg` (accessed 11.02.2014), public domain.

Wikimedia (2009). *Neuron hand-tuned* by User:Faigl.Iadislav. `http://en.wikipedia.org/wiki/File:Neuron_Hand-tuned.svg` (accessed 15.02.2014), Creative Commons Attribution-Share Alike 3.0.

Wikimedia (2010). *Laszlo Seress' preparation of a human hippocampus alongside a sea horse* by User:Anthonyhcole. `http://en.wikipedia.org/wiki/File:Hippocampus_and_seahorse_cropped.JPG` (accessed 25.02.2014), Creative Commons Attribution-Share Alike 3.0.

Wikimedia (2013). *Chemically gated channel* by User:BruceBlaus. `http://upload.wikimedia.org/wikipedia/commons/c/ce/Blausen_0225_ChemicallyGatedChannel.png` (accessed 13.02.2014), Creative Commons Attribution 3.0.

Williams S.R. and Stuart G.J. (1999). Mechanisms and consequences of action potential burst firing in rat neocortical pyramidal neurons. *J. Physiol.* **521**:467.

Willshaw D.J. and Buckingham J.T. (1990). An assessment of Marr's theory of the hippocampus as a temporary memory store. *Philos. Trans. R. Soc. Lond. B* **329**:205 .

Wilson M. and McNaughton B. (1994). Reactivation of hippocampal ensemble memories during sleep. *Science* **265**:676.

Wilson M.A. and McNaughton B.L. (1993). Dynamics of the hippocampal ensemble code for space. *Science* **261**:1055.

Witter M. and Amaral D. (2004). Hippocampal formation. In G. Paxinos, editor, *The Rat Nervous System*, chapter 21, pages 635–704. Elsevier Science, San Diego.

Womelsdorf T. and Fries P. (2007). The role of neuronal synchronization in selective attention. *Curr. Opin. Neurobiol.* **17**:154.

Womelsdorf T., Schoffelen J.M., Oostenveld R., Singer W., Desimone R., Engel A.K., and Fries P. (2007). Modulation of neuronal interactions through neuronal synchronization. *Science* **316**:1609.

Wood E.R., Dudchenko P.A., and Eichenbaum H. (1999). The global record of memory in hippocampal neuronal activity. *Nature* **397**:613.

Wood E.R., Dudchenko P.A., Robitsek R.J., and Eichenbaum H. (2000). Hippocampal neurons encode information about different types of memory episodes occurring in the same location. *Neuron* **27**:623.

Xu S., Jiang W., Poo M.M., and Dan Y. (2012). Activity recall in a visual cortical ensemble. *Nat. Neurosci.* **15**:449.

Ylinen A., Bragin A., Nádasdy Z., Jandó G., Szabó I., Sik A., and Buzsáki G. (1995). Sharp wave-associated high-frequency oscillation (200Hz) in the intact hippocampus: Network and intracellular mechanisms. *J. Neurosci.* **15**:30.

Yu A.C. and Margoliash D. (1996). Temporal hierarchical control of singing in birds. *Science* **273**:1871.

Zucker R.S. and Regehr W.G. (2002). Short-term synaptic plasticity. *Annu. Rev. Physiol.* **64**:355.

Acknowledgements

First of all, this thesis would never have been possible without the constant support and supervision of Marc. I learned a lot from you, including writing abstracts-summaries-and-discussions (the word "iteration" got a new connotation over the years :)), fighting with referees, and accepting the fact that every (not only working related) task takes at least twice the time than scheduled. At the same time thank you very much for allowing me to handle my scientific work and research flexible, and let me concentrate the projects I wanted to (including the once which never finished :)). Also thanks for the creating the Network Dynamics group (btw.: Why is there no sexy acronym for the group??) and supporting the relaxed atmosphere.

Without Raoul I would most probably have never finished even my first paper. Although you are permanently concerned that the current situation is "katastrophal", and there is always a final, ultimate deadline approaching, we finally found the time to discuss scientific and non-scientific issues. Thanks for all the skype-ing, the poetry and the free food. I really enjoyed the several stays at Radboud University, the sharing of your office, the 45-5-45-15-45-5-lunch-45-5-45-15-45-....-working-scheme, and the walks in the park.

I thank Theo — not only for agreeing being a member of my examination board — but also for creating the wonderful working atmosphere in the *good old times* before Haus 2 became a "Geisterhaus" and the department was still down here.

Thank you Barbara with helping me handling all the administrative stuff, the forms, the contracts, the train tickets — and thanks for the cookies in the office :).

Thank you, Antje and Frauke, for constantly reminding me on deadlines, not beeing angry if I didn't manage to answer all the mails, and helping me with finally gathering all the papers for submitting this thesis. I'm very happy that all the things were handled so flexible in your office.

Many thanks to Denny, Hecke and Yorck for keeping the computers and the servers running, and, in particular, for granting me root access. That has made live much, much easier ...

I thank all the present and past "Network-Dynamic-ers", the NLD-to-Fassberg-evaders, and the remaining folks from *Standort:Bunsenstrasse* for the amazing working atmosphere. In particular, I enjoyed the scientific conversations (well ... to be honest ... most of the chats were rather non-scientific), the pizza, and consuming some million cups of coffee together with Anna, Hecke, Harold, Jose, Jan, Gunter, Lukas, Martin, Sarah. In particular, in the final phase of my PhD time where I stayed in the institute during the late-night hours and the weekends, you helped me very much to survive that time by distracting me .... and now? *Twilight*?

During the years I shared the office with Holger, Max, Harold and Florentia — thanks for the fun (yes, you can have fun in office ;-)). Very special thanks goes also to Dirk, who is my currently

assigned room mate — but due to his permanent absence I was able to fill the room with all the stuff I need, I don't need and I am too lazy to remove.

Tatjana, Christian, Hecke and Hinrich provided me the LaTeX source of their dissertations and granted permissions to pirate their styles — you helped me very much with making my thesis look fancier.

David, Debshanka, Florian, Hecke, Jose, Sarah volunteered (or were forced to volunteer) to proof-read parts of this thesis. Although I don't like criticism that much — you were a great support to bring the thesis into its final version. Moreover, now I have someone to blame for typos and weird, unclear phrases that you didn't uncovered ;-).

Für die Zeit abseits des Büros (auch wenn diese letztlich doch etwas limitiert war) möchte ich vor allem bei Robert, Maria, Tina, Kevin, Matthias, Lilly, Kathleen und Alvaro bedanken. Auch wenn ich es nie zum Volleyball geschafft habe, ich typischerweise eure Geburtstage vergesse und es mit dem Anrufen und der Pünktlichkeit oft nicht so genau genommen habe — Vielen Dank das ihr Göttingen zu einem besonderen Platz gemacht habt.

Vielen, vielen Dank an meine Eltern für die Unterstützung über all die Jahre. Ohne euch hätte ich es nie bis hierher geschafft.

Judith, Jonna, Elian and MiMiMo ohne euch wäre all das hier gar nichts Wert. Es ist so wunderbar, dass es euch gibt (oder geben wird :) — @MiMiMO: Vielen Dank für deine Geduld) und das ich nun wieder viel-viel-viel mehr Zeit mit und für euch haben werde ... Danke das ihr mir das "Lächeln am Morgen" beigebracht habt ...

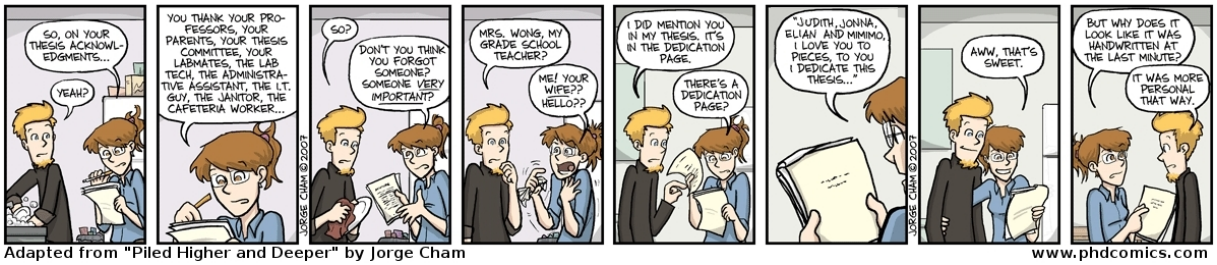

Finally, I am grateful to Tidgituk for not turning of the light in the last minute ;-).